

**The Messinian salinity crisis: chronology and paleoenvironment  
in the (circum-)Mediterranean area**

Erik Snel

**GEOLOGICA ULTRAIECTINA**

Mededelingen van de  
Faculteit Geowetenschappen  
departement Aardwetenschappen  
Universiteit Utrecht

No. 317

Members of the dissertation committee:

Prof. dr. Silvia M. Iaccarino  
Dipartimento di Scienza della Terra, Università degli Studi di Parma  
Parma, Italy

Prof. dr. Francisco J. Sierro Sánchez  
Departamento de Geología, Universidad de Salamanca  
Salamanca, Spain

Prof. dr. Poppe L. de Boer  
Department of Earth Sciences, Utrecht University  
Utrecht, The Netherlands

Prof. dr. Cornelis G. Langereis  
Department of Earth Sciences, Utrecht University  
Utrecht, The Netherlands

This study was supported by the Netherlands Council for Earth and Life Sciences (ALW) with financial aid from the Netherlands Organisation for Scientific Research (NWO).

The research for this thesis was carried out at the Stratigraphy/Paleontology Group, Department of Earth Sciences, Utrecht University, Budapestlaan 4, 3584 CD Utrecht, The Netherlands ([http://www.geo.uu.nl/Research/Strat\\_Paleontology](http://www.geo.uu.nl/Research/Strat_Paleontology)); at the Paleomagnetic Laboratory Fort Hoofddijk, Budapestlaan 17, 3584 CD Utrecht, The Netherlands (<http://www.geo.uu.nl/~forth/>); and at the Palaeoecology Group, Laboratory of Palaeobotany & Palynology, Budapestlaan 4, 3584 CD Utrecht, The Netherlands (<http://www3.bio.uu.nl/palaeo/>).

The author can be reached through e-mail: [snel@geo.uu.nl](mailto:snel@geo.uu.nl)

ISBN/EAN: 978-90-5744-177-6

Graphic design: Geomedia, Faculteit Geowetenschappen, Universiteit Utrecht (7674)

Copyright © Erik Snel, p/a Faculteit Geowetenschappen, Universiteit Utrecht, 2010.

Niets uit deze uitgave mag worden vermenigvuldigd en/of openbaar gemaakt door middel van druk, fotokopie of welke andere wijze dan ook zonder voorafgaande schriftelijke toestemming van de auteur.

All rights reserved. No parts of this publication may be reproduced in any form, by print or photo print, microfilm or other means, without written permission by the author.

Cover pages: Gessoso-Solfifera Formation west of Borgo Tossignano, Italy (front); lignite quarry near Ptolemaida, Greece (back)

# **The Messinian salinity crisis: chronology and paleoenvironment in the (circum-)Mediterranean area**

**De saliniteitscrisis van het Messinien: chronologie en paleomilieu**

**in het (circum-)Mediterrane gebied**

*(met een samenvatting in het Nederlands)*

**PROEFSCHRIFT**

ter verkrijging van de graad van doctor aan de Universiteit Utrecht  
op gezag van de rector magnificus, prof.dr. J.C. Stoof,  
ingevolge het besluit van het college voor promoties  
in het openbaar te verdedigen op  
donderdag 8 april 2010 des middags te 12.45 uur

door

Erik Snel

geboren op 5 april 1974  
te Antwerpen, België

Promotor:  
Prof. dr. G.J. van der Zwaan  
Co-promotor:  
Dr. F.J. Hilgen

# Contents

---

<b>Bibliography</b>	6
<b>Introduction and summary</b>	7
<b>Chapter 1</b> Late Miocene to Early Pliocene chronostratigraphic framework for the Dacic Basin, Romania	13
<b>Chapter 2</b> Calcareous nannofossil biostratigraphy and magnetostratigraphy of the upper Miocene and lower Pliocene of the Northern Aegean (Orphanic Gulf-Strimon Basin areas), Greece	37
<b>Chapter 3</b> Vertical motions in the Aegean volcanic arc: evidence for rapid subsidence preceding volcanic activity on Milos and Aegina	71
<b>Chapter 4</b> No major deglaciation across the Miocene-Pliocene boundary: integrated stratigraphy and astronomical tuning of the Loulja sections (Bou Regreg area, NW Morocco)	95
<b>Chapter 5</b> The Messinian salinity crisis from the Atlantic to the Eastern Paratethys	137
<b>Samenvatting</b>	181
<b>Acknowledgements</b>	186
<b>Curriculum Vitae</b>	187

# Bibliography

---

## Chapter 2:

Snel, E., Mărunțeanu, M., Macaleş, R., Meulenkamp, J.E., Van Vugt, N., 2006. Late Miocene to Early Pliocene chronostratigraphic framework for the Dacic Basin, Romania. *Palaeogeography, Palaeoclimatology, Palaeoecology* 238, 107-124. doi:10.1016/j.palaeo.2006.03.021

## Chapter 3:

Snel, E., Mărunțeanu, M., Meulenkamp, J.E., 2006. Calcareous nannofossil biostratigraphy and magnetostratigraphy of the Upper Miocene and Lower Pliocene of the Northern Aegean (Orphanic Gulf-Strimon Basin areas), Greece. *Palaeogeography, Palaeoclimatology, Palaeoecology* 238, 125-150. doi:10.1016/j.palaeo.2006.03.022

## Chapter 4:

Van Hinsbergen, D.J.J., Snel, E., Garstman, S.A., Mărunțeanu, M., Langereis, C.G., Wortel, M.J.R., Meulenkamp, J.E., 2004. Vertical motions in the Aegean volcanic arc: evidence for rapid subsidence preceding volcanic activity on Milos and Aegina. *Marine Geology* 209, 329-345. doi:10.1016/j.margeo.2004.06.006

## Chapter 5:

Van der Laan, E., Snel, E., De Kaenel, E., Hilgen, F.J., Krijgsman, W., 2006. No major deglaciation across the Miocene-Pliocene boundary: Integrated stratigraphy and astronomical tuning of the Loulja sections (Bou Regreg area, NW Morocco). *Paleoceanography* 21, PA3011, doi:10.1029/2005PA001193

## Chapter 6 (partly based on):

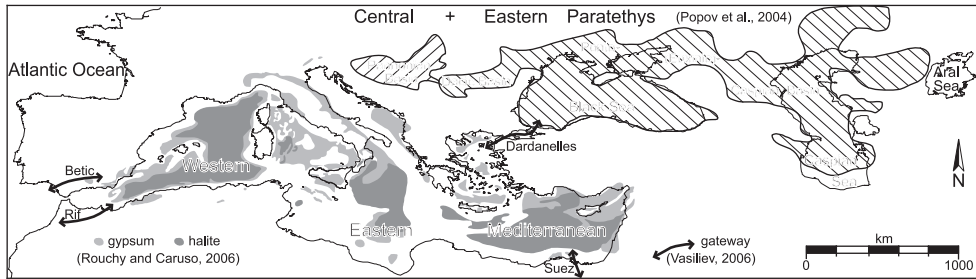
Hilgen, F.J., Kuiper, K.F., Krijgsman, W., Snel, E., Van der Laan, E., 2007. Astronomical tuning as the basis for high resolution chronostratigraphy: the intricate history of the Messinian Salinity Crisis. *Stratigraphy* 4, 231-238

# Introduction and summary

---

During the Messinian stage (7.246–5.332 Ma; Lourens et al., 2004), at the end of the Miocene, the area that is occupied by today's Mediterranean Sea (see map; Krijgsman, 2002) underwent dramatic environmental changes. In this relatively short period connections with the Atlantic Ocean became stepwise restricted and interrupted, massive amounts of evaporites were deposited (an estimated 1 million km<sup>3</sup> in total; Ryan, 2009), and the Mediterranean Basin was partially refilled with non-marine waters after water levels had dropped more than one kilometre. The onset of the Pliocene corresponds to a sudden inflow of oceanic water through the gateway near Gibraltar, restoring fully marine conditions and leading to the modern land–sea configuration. Evidence for these events came from observations of land-based sections, in which a succession of evaporitic limestone, gypsum, salt, and younger clastics with hypohaline fossils is exposed that is wedged in between older and younger sediments containing the remains of open marine micro-organisms (Selli, 1973). To describe the observed sequence of events, Selli (1960) introduced the phrase 'Messinian salinity crisis' (MSC). The concept of an isolated and desiccated Mediterranean gained widespread acceptance following the 1970 cruise of the Deep Sea Drilling Project, which demonstrated the presence of massive gypsum and salt deposits on the Mediterranean Sea floor (see map; Hsü et al., 1973). A comprehensive overview of the various models that tried to explain this phenomenon is discussed by Benson and Rakic-El Bied (1991). The evaporitic strata of the Messinian stage can be subdivided into a lower and an upper part (Decima and Wezel, 1971), the exact timing and depositional setting of which are still being debated (CIESM, 2008). The Lower Evaporites were deposited during the first, (restricted) marine phase of the MSC (5.96–5.59 Ma), whereas the Upper Evaporites represent the shallow water environment that prevailed after the erosional event caused by evaporitic drawdown of the Mediterranean during total isolation from the Atlantic Ocean (Krijgsman et al., 1999). This second interval (~5.50–5.33 Ma) is further characterized by fresh to brackish water faunas in non-marine strata. These strata cover or alternate with gypsum beds of the Upper Evaporites and are referred to as Lago Mare (Ruggieri, 1967). Its character, being fed by precipitation and rivers with deposition below sea level, resembled the environment of the present-day brackish Caspian Sea. In fact, the Caspian Sea is one of the remnants of the vast inland sea, the so-called Paratethys (see map; Laskarev, 1924), that existed to the northeast of the Mediterranean during the MSC. It constituted the other isolated part of the water mass that, together with the Mediterranean, once formed the Tethys Ocean between Eurasia and the African and Indian plates (Meulenkamp and Sissingh, 2003; Popov et al., 2004).

This thesis presents results of the Ph.D. project on 'Mediterranean Gateways', conducted in the context of the multi-disciplinary research programme 'Mediterranean Neogene depositional environments: modelling, validation and perspectives' (Wortel et al., 1998), a joint effort of the Geodynamics Research Institute (GOI) and the Institute of Paleoenvironment and Paleoclimate Utrecht (IPPU) of the Faculty of Earth Sciences at Utrecht University and the Department of Geosciences of Pennsylvania State University. The overall objective of this programme was to understand the origin and spatial/temporal distribution of circum-Mediterranean Miocene black shale (sapropel) and evaporite sequences in terms of the combined effects of geodynamic and environmental (climatic, oceanographic) processes in the African–Eurasian collision zone. Initially, three lines of approach were envisioned, which were translated into a time-stratigraphic



and tectonostratigraphic, a numerical modelling, and an environmental research component. The aim of the latter component involved detailed analyses of the effects of successive tectonically and climate-induced (sealevel) events on basin configuration and sedimentation. The focus of this Ph.D. study, contributing to the environmental component, was on the paleoceanographic and environmental response of the circum-Mediterranean to deteriorating Atlantic-Mediterranean and intra-Mediterranean connections and to recurrent opening of Mediterranean-Paratethys (marine) gateways prior to, during, and after the MSC. For this purpose, research concentrated on integrated stratigraphic analyses of upper Miocene and lower Pliocene sequences in a) the Eastern Paratethys Dacic Basin (Romania), b) the Mediterranean Orphanic Gulf and Strimon Basin areas in the Northern Aegean and Aegina and Milos in the Southern Aegean (Greece), and c) the adjacent North Atlantic Bou Regreg area (Morocco). Further cyclostratigraphic and biostratigraphic analyses focussed on proper MSC units within Spanish, Italian, and Greek marginal basins of the Mediterranean.

In order to constrain the timing of Mediterranean-Paratethys connections spanning the MSC interval, a detailed correlation of upper Neogene Paratethys stages to those in the Mediterranean is indispensable. This can be achieved through establishing chronostratigraphic frameworks on both sides of the northeastern gateway. Previous and concurrent studies in the Eastern Paratethys have demonstrated the potential in this respect of cyclostratigraphy and magnetostratigraphy of the Miocene and Pliocene (Van Vugt, 2000; Vasiliev, 2006). **Chapter 2** presents magnetostratigraphic and biostratigraphic data that resulted from sampling campaigns of upper Miocene and lower Pliocene sediments along the northern margin of the Dacic Basin (Romania) in 1996-1999. Ages between 6.5 and 4.0 Ma are obtained for regional stages of this part of the Eastern Paratethys, which are defined by the appearance and development of fresh to brackish water mollusc taxa. The Maeotian-Pontian boundary can be placed at ~6.15 Ma and the Pontian-Dacian boundary at ~5.3 Ma, so that the Pontian stage becomes coeval with the upper half of the Messinian stage and encompasses the MSC. The Odessian-Portaferrian and Portaferrian-Bosphorian substage boundaries are estimated at ~6.0 Ma and ~5.6 Ma, respectively. The boundary between the lower Dacian (Getian) and the upper Dacian (Parscovian) substages can be dated at ~4.55 Ma, while the Dacian-Romanian boundary is placed at ~4.25 Ma. Alternatively, correlation of normal polarity intervals in the Dacian-Romanian section of Lupoia to older subchrons of the Astronomical Polarity Time Scale may give age estimates for the latter two boundaries of ~4.83 Ma and ~4.58 Ma, respectively. Occurrences of calcareous nannofossils in the middle and upper Pontian and in the lower Dacian, with age estimates of approximately 5.9, 5.6, 5.3, and 5 Ma, are interpreted to indicate intermittent influxes of marine (Atlantic) water into the Paratethys via the Mediterranean, thus limiting the period of isolation of the latter basin during the MSC to the Lago Mare and Upper Evaporite interval. Note that additional data and recent views lead to modified conclusions



with respect to this subject (both here and in the next chapter) and the chronostratigraphy of the Dacic Basin: see chapter 6.

In **chapter 3**, the results are discussed of three field campaigns in the Orphanic Gulf and Strimon Basin areas of the Northern Aegean (Greece) in 1998-2000. This study area is located intermediate between the Mediterranean and the Black Sea along the former margin of the Eastern Paratethys and may have been an integral part of the northeastern gateway. Biostratigraphic, lithostratigraphic, and paleomagnetic data facilitate correlations to Mediterranean Neogene stratigraphic records and suggest that the sediments cover an interval between 7.5 and 5 Ma. The transition from the shallow marine Dafni Formation to the brackish-lacustrine Choumnikon Formation in the Strimon Basin is estimated at 6.3 Ma, which is comparable to the age of the Maeotian-Pontian boundary in the Dacic Basin. In the adjacent Orphanic Gulf area, shallow marine clastics and gypsum beds, followed by a brackish/fresh water fluvio-lacustrine unit, constitute the local equivalents of the Choumnikon Formation. The evaporites are correlated to the Lower Evaporites of the Mediterranean, dated at 5.96-5.59 Ma, whereas a widespread travertine marker bed in the non-marine unit on top is interpreted to reflect the desiccation event of the MSC, between 5.59 and 5.5 Ma. The Miocene-Pliocene boundary, represented in the Strimon Basin by a brief, shallow marine interruption of the fluvio-lacustrine conditions, is marked along the Orphanic Gulf by a transition to open marine conditions in an already relatively deep basin. Calcareous nannofossils are discontinuously present in the upper Miocene strata, mainly associated with the shallow marine intervals. However, their occurrence in the latter area prior to the first appearance of foraminifera at the assumed base of the Pliocene needs clarification and may indicate reworking of older Messinian deposits or sporadic influxes of oceanic water at the end of the MSC.

**Chapter 4**, which also appeared in the thesis of Douwe van Hinsbergen (Van Hinsbergen, 2004: his chapter 6), reports on the Miocene and Pliocene continental and marine sequences (6.0-3.5 Ma) and overlying volcanoclastic sediments on the Southern Aegean islands of Milos and Aegina in Greece. These islands were formed by Plio-Pleistocene volcanism that concurred with late-orogenic extension in the Aegean region. Reconstruction of the early Pliocene paleobathymetry history, using the ratio between planktonic and benthic foraminifera and an age model based on an integrated biostratigraphy, magnetostratigraphy, and cyclostratigraphy, shows that up to 1 km of rapid regional subsidence has occurred, probably associated with large-scale extension in the Southern Aegean and 1-1.5 Myr before the onset of volcanism. This subsidence caused a relative sea level rise from 5.0 Ma onward, thus ~300 kyr after the end of the MSC. The alternating fluvial, brackish, and shallow marine upper Miocene and lowermost Pliocene sediments on Milos and Aegina possibly represent the paleoenvironments of a threshold region between the Mediterranean proper and the bordering part of the Aegean, which may have been too shallow to record the successive desiccation and flooding events of the MSC. Although extension of the Aegean lithosphere did not directly cause melting of the underlying mantle, it probably did control the timing of the volcanism and facilitated magma rise through the formation of extensional faults. The depth of the subducted slab below the Aegean probably controlled the generation of melts and determined the location of the volcanic centres.

Research by Van Assen et al. (2006) in the Melilla Basin, at the western end of the Mediterranean, documented the stepwise restriction of the Rifian Corridor, which heralded the MSC. Together with the Betic Passage, this entrance constituted the western gateway to the Atlantic before the final opening of the modern Strait of Gibraltar at the Miocene-Pliocene boundary. For correlation of the actual MSC interval with the open ocean record, the upper Miocene reference sections of the Bou Regreg composite at Oued Akrech and Ain el Beida,

located on the Atlantic side of the Rifian Corridor, needed upward extension across the Miocene-Pliocene boundary interval. **Chapter 5**, also included in the thesis of Erwin van der Laan (Van der Laan, 2010: his chapter 4), presents the two promising Loulja sections that were selected for an integrated, high-resolution stratigraphy study in this area. The combination of precession-controlled cyclicity of section Loulja-A (5.59-5.12 Ma), which enables unambiguous orbital tuning, and an excellent benthic isotope record permits detailed comparison of the glacial history to paleoenvironmental events in the Mediterranean. Consequently, the section could serve as an alternative for the Miocene-Pliocene boundary stratotype section at Eraclea Minoa on Sicily. It appears that this boundary concurs with a minor precession-related shift to lighter values in  $\delta^{18}\text{O}$  between isotope stages TG7 and TG5. The flooding of the Mediterranean at the end of the MSC is therefore not related to a major glacio-eustatic sea level rise, but more likely to tectonics or headward fluvial erosion. An older, major deglaciation phase between stages TG12 and TG11 corresponds to the onset of the Upper Evaporites following the desiccation event of the MSC.

Finally, the synthetic **chapter 6** covers the Mediterranean Lower Evaporite and Upper Evaporite (Lago Mare) sequences in the Sorbas and Nijar basins (Spain), the Vena del Gesso and Caltanissetta basins (Italy), and on Crete and the Ionian Islands (Greece). Precession-controlled regional climate fluctuations dominated evaporite cyclicity. Analyses of calcareous nannofossils and organic-walled dinoflagellate cysts from cyclostratigraphically constrained samples from these and other land sections along the Orphanic Gulf and in the Strimon and Dacic basins reveal that continuous or repeated inflow of Atlantic water into (at least) the Mediterranean persisted during deposition of the Lower Evaporites (5.96-5.59 Ma). In contrast, and consistent with the interpretation of magnetic susceptibility results from the Bou Regreg area (Atlantic coast, Morocco), the Mediterranean and tributary Eastern Paratethys remained isolated basins throughout the intra-Messinian desiccation event and the subsequent Upper Evaporite interval (5.59-5.33 Ma). These findings are in accordance with conclusions from strontium isotope studies and other marine microfossil evidence found in the literature. To summarize the causes of the successive MSC events: its onset (at 5.96 Ma) had no direct glacio-eustatic origin, but resulted from the climatic effect of the eccentricity cycle superimposed on the regional tectonic trend of gateway restriction at the western entrance to the Mediterranean; the prominent glacial stages TG14 and TG12 strongly controlled the isolation and desiccation phase (5.59-5.55 Ma), after which partial refill ensued during deglaciation associated with stage TG11, and the terminal flooding event, which defines the end of the MSC and led to the return of open marine conditions in the Mediterranean from the basal Pliocene (5.33 Ma) onward, is likely related to geodynamic and/or erosional processes rather than glacio-eustasy.

## References

- Benson, R.H., Rakic-El Bied, K., 1991. Biodynamics, saline giants and late Miocene catastrophism. *Carbonates and Evaporites* 6 (2), 127-168.
- CIESM, 2008. The Messinian Salinity Crisis from mega-deposits to microbiology – A consensus report. In: Briand, F. (Ed.), *CIESM Workshop Monographs* 33, Monaco, pp. 1-168.
- Decima, A., Wezel, F.C., 1971. Osservazioni sulle evaporiti messiniane della Sicilia centro-meridionale. *Rivista Mineralogica Siciliana* anno 22 (nn. 130-132), 172-187.
- Hsü, K.J., Ryan, W.B.F., Cita, M.B., 1973. Late Miocene desiccation of the Mediterranean. *Nature* 242, 240-244. doi:10.1038/242240a0.

- Krijgsman, W., Hilgen, F.J., Raffi, I., Sierro, F.J., Wilson, D.S., 1999. Chronology, causes and progression of the Messinian salinity crisis. *Nature* 400, 652-655. doi:10.1038/23231.
- Krijgsman, W., 2002. The Mediterranean: Mare Nostrum of Earth sciences. *Earth and Planetary Science Letters* 205, 1-12. doi:10.1016/S0012-821X(02)01008-7.
- Laskarev, V., 1924. Sur les équivalents du Sarmatien supérieur en Serbie. In: *Recueil de travaux offert à M. Jovan Cvijić par ses amis et collaborateurs*, pp. 73-85.
- Lourens, L.J., Hilgen, F.J., Laskar, J., Shackleton, N.J., Wilson, D., 2004. The Neogene Period. In: Gradstein, F.M., Ogg, J.G., Smith, A.G. (Eds.), *A geologic time scale 2004*. Cambridge University Press, Cambridge, pp. 409-440.
- Meulenkamp, J.E., Sissingh, W., 2003. Tertiary palaeogeography and tectonostratigraphic evolution of the Northern and Southern Peri-Tethys platforms and the intermediate domains of the African-Eurasian convergent plate boundary zone. *Palaeogeography, Palaeoclimatology, Palaeoecology* 196, 209-228. doi:10.1016/S0031-0182(03)00319-5.
- Popov, S.V., Rögl, F., Rozanov, A.Y., Steininger, F.F., Shcherba, I.G., Kovac, M., 2004. Lithological-paleogeographic maps of Paratethys: 10 maps Late Eocene to Pliocene. *Courier Forschungsinstitut Senckenberg* 250, 1-46.
- Ruggieri, G., 1967. The Miocene and later evolution of the Mediterranean sea. In: Adams, C.G., Ager, D.V. (Eds.), *Aspects of Tethyan biogeography*. Systematics Association Publication 7, Oxford, U.K., pp. 283-290.
- Ryan, W.B.F., 2009. Decoding the Messinian salinity crisis. *Sedimentology* 56 (1), 95-136. doi:10.1111/j.1365-3091.2008.01031.x.
- Selli, R., 1960. Il Messiniano Mayer-Eymar 1867. Proposta di un neostatotipo. *Giornale di Geologia* 28, 1-33.
- Selli, R., 1973. An outline of the Italian Messinian. In: Drooger, C.W. (Ed.), *Messinian events in the Mediterranean*, *Verhandelingen van de Koninklijke Nederlandse Akademie van Wetenschappen*, pp. 150-171.
- Van Assen, E., Kuiper, K.F., Barhoun, N., Krijgsman, W., Sierro, F.J., 2006. Messinian astrochronology of the Melilla Basin: Stepwise restriction of the Mediterranean-Atlantic connection through Morocco. *Palaeogeography, Palaeoclimatology, Palaeoecology* 238, 15-31. doi:10.1016/j.palaeo.2006.03.014.
- Van der Laan, E., 2010. Integrated stratigraphy, astronomical dating and proxy records of the Ain el Beida and Loulja sections (NW Morocco). Implications for the Messinian Salinity Crisis, glacial history and regional climate change (PhD Thesis Utrecht University). *Geologica Ultraiectina* xxx, xxx pp.
- Van Hinsbergen, D.J.J., 2004. The evolving anatomy of a collapsing orogen (PhD Thesis Utrecht University). *Geologica Ultraiectina* 243, 280 pp.
- Van Vugt, N., 2000. Orbital forcing in late Neogene lacustrine basins from the Mediterranean. A magnetostratigraphic and cyclostratigraphic study. *Geologica Ultraiectina* 189, 168 pp.
- Vasiliev, I., 2006. A new chronology for the Dacian Basin (Romania). Consequences for the kinematic and paleoenvironmental evolution of the Paratethys region (PhD Thesis Utrecht University). *Geologica Ultraiectina* 267, 200 pp.
- Wortel, M.J.R., Meulenkamp, J.E., Langereis, C.G., Slingerland, R., 1998. Mediterranean Neogene depositional environments: modelling, validation and perspectives. Proposal for a research programme, Utrecht University and Pennsylvania State University, pp. 1-29.



# Late Miocene to Early Pliocene chronostratigraphic framework for the Dacic Basin, Romania

---

This chapter is published as: Snel, E., Mărunțeanu, M., Macaleț, R., Meulenkamp, J.E., Van Vugt, N., 2006. Late Miocene to Early Pliocene chronostratigraphic framework for the Dacic Basin, Romania. *Palaeogeography, Palaeoclimatology, Palaeoecology* 238, 107-124. doi:10.1016/j.palaeo.2006.03.021.

## Abstract

New magnetostratigraphic results and calcareous nannofossil data of seven sections in the Dacic Basin of southern Romania, covering the latest Maeotian to early Romanian time span (6.4-4.0 Ma), allow a correlation with the current Astronomical Polarity Time Scale. This establishes a chronological framework for the Pontian and Dacian stages of the Paratethys and facilitates to correlate the Paratethys stages with those of the Mediterranean.

The Maeotian-Pontian boundary is estimated at  $6.15 \pm 0.11$  Ma, within subchron C3An.1n, while the age of the Pontian-Dacian boundary is  $5.30 \pm 0.1$  Ma, within subchron C3r. The Odessian-Portaferrian and Portaferrian-Bosphorian substage boundaries can be placed at about 6.0 Ma and 5.6 Ma, at the base and near the end of chron C3r, respectively. Consequently, the Pontian stage has a duration of approximately 0.85 Myr and is coeval with the upper half of the Messinian stage.

The base of the Dacian stage corresponds to the onset of the Pliocene and is coeval with the Pontian-Kimmerian boundary of the Euxinic (Black Sea) Basin. The Dacian-Romanian boundary is recorded either at  $4.58 \pm 0.05$  Ma, in subchron C3n.2n (Nunivak), or at  $4.25 \pm 0.05$  Ma in subchron C3n.1n (Cochiti). The length of the Dacian stage is therefore about 0.7 Myr or approximately 1 Ma. The transition of the Getian into the Parscovian substage can be dated at  $\sim 4.83$  Ma within subchron C3n.3n (Sidufjall), or at  $\sim 4.55$  Ma within subchron C3n.2n (Nunivak).

The occurrence of calcareous nannofossil assemblages in the lower Portaferrian and near the Portaferrian-Bosphorian transition, belonging to the upper part of the *Discoaster quinqueramus*-NN11 Zone, and in the middle Bosphorian, belonging to the *Amaurolithus tricorniculatus*-NN12 Zone, indicates the presence of ephemeral marine connections between the Paratethys Basin and the Mediterranean during the late Messinian. Another marine influx, inferred from nannofossil species characteristic of the NN12 Zone and found in lower Dacian sediments near the top of subchron C3n.4n (Thvera), post-dates the basal-Pliocene transgression of the Mediterranean Basin.

## 2.1 Introduction

Over the past decades progress in various disciplines dealing with late Neogene stratigraphy of the Paratethys has been considerable (for example: Andreescu, 1981; Alexeeva et al., 1983; Nagymarosy and Müller, 1988; Stevanović et al., 1990; Marinescu and Papaianopol, 1995; Jones and Simmons, 1996; Steininger et al., 1996; MăruŃeanu et al., 1998; Papaianopol et al., 1999; MăruŃeanu et al., 2000). However, the exact timing of regional stages in this sedimentary realm caused much controversy (Semenenko, 1989; Marinescu, 1990; Rögl et al., 1991; Clauzon et al., 2005). Without an accurate chronostratigraphic framework, correlation of the Paratethys (Fig. 2.1) with the Mediterranean realm will therefore remain ambiguous. The further development (after pioneering work by Martini, 1971; Bukry, 1973) of a global Neogene calcareous nannofossil zonation (Rio et al., 1990; Raffi et al., 1995; Backman and Raffi, 1997) has accompanied the establishment of a Geomagnetic Polarity Time Scale (GPTS: Cande and Kent, 1995) and, more recently, the refining of the Astronomical Polarity Time Scale (APTS: Hilgen et al., 1995; Lourens et al., 1996; Krijgsman et al., 1999). This last framework comprises the completion of a detailed biomagneto- and cyclostratigraphy of the Miocene and Pliocene in the Mediterranean area. It constitutes a firm reference base for comparison with biostratigraphic and paleomagnetic events in the Paratethys. Previous work (MăruŃeanu and Papaianopol, 1998; Rădan and Rădan, 1998; Popescu, 2001; Van Vugt et al., 2001) has shown that the Dacic Basin in Romania, being a part of the Paratethys, is a promising subject for such an interdisciplinary approach of a Paratethys-Mediterranean correlation.

The aim of this study is to develop a time-stratigraphic framework for the Late Miocene and Early Pliocene in the Dacic Basin. To achieve this goal seven sections near the northern border of the Dacic Basin are selected (Fig. 2.1), in which the boundaries of the Late Miocene and Early Pliocene regional stages (the Pontian and Dacian) have been recognized previously. A paleomagnetic polarity record is established in all sections and the nannofossil content of the samples is verified qualitatively. In this way, the sections are linked to the APTS, and the ages and duration of the Pontian and Dacian stages can be estimated. Subsequently, these regional stages will be correlated with the Pontian and Kimmerian stages of the Euxinic part of the Eastern Paratethys, and with the Messinian and Zanclean stages of the Mediterranean. Finally, the consequences of the obtained correlation will be discussed concerning the timing of possible connections of the Paratethys with the Mediterranean Basin.

## 2.2 Definitions and geological setting

Laskarev (1924) introduced the term Paratethys to indicate the isolated sedimentary realm of the northern part of the Tethys Ocean. The gradual emerging of the Alpine orogenic belt and, consequently, the successive isolation of the Paratethyan basins from the Tethys are reflected in the periodical endemism of the Paratethyan aquatic biota. Three periods of endemic faunal development were observed: during the Early Oligocene (Báldi, 1984, 1989; Rusu, 1985), between the late Ottnangian and the late Karpatian (Early-Middle Miocene, Nagymarosy and Müller, 1988), and between the late Badenian (Middle Miocene) and the end of the Neogene (Popescu and Gheta, 1984). The resulting unique palaeobiological character necessitated the use of regional stages to subdivide the Neogene of the Paratethys.

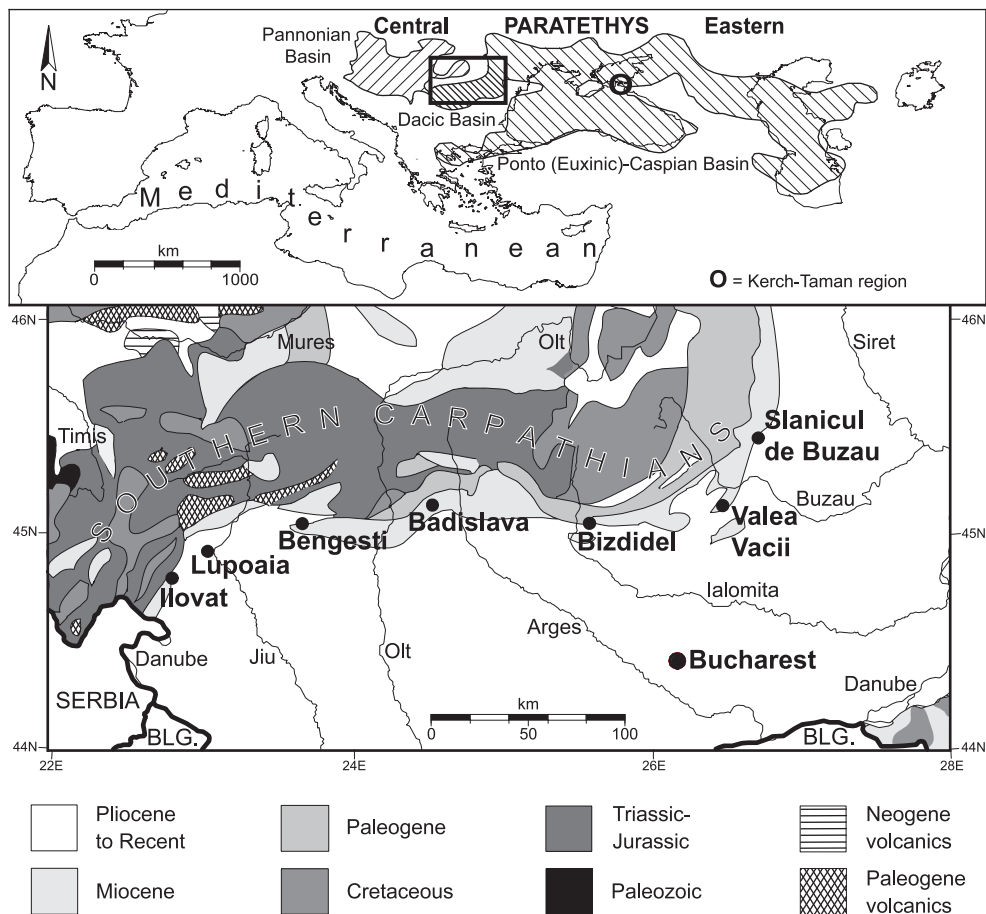


Figure 2.1. Simplified geological map of southern Romania, showing the locations of the sections of Illovăț (IL), Lupoia (LU), Bengesti (BE), Bădăslava (BA), Bizdidel (BI), Valea Vacii (VA), and Slănicul de Buzău (SL). Modified from Berza (1994). Inset map of the palaeogeography of the Paratethys region during the Late Miocene superimposed on modern geography, with location of the Dacic Basin and of the Kerch-Taman peninsulas. After Steininger and Papp (1979).

### 2.2.1 Stage nomenclature

This study covers the stratigraphic units near the Miocene–Pliocene boundary: the Pontian and Dacian stages. Barbot de Marny (1869) introduced the Pontian stage, previously referred to as the Pontian Tertiary formation by Le Play (1842), to classify the upper Miocene limestones of the Black Sea coast. In 1897, Andrusov (in Bertels, 1963, pp. 26–31) redefined the Pontian stage to include older brackish water deposits of the Danube depression, as well as the overlying deposits of Pliocene age (Stevanović et al., 1990). Andrusov’s introduction of the Maeotian stage in 1905 (Bertels, 1963) and the subsequent recognition of the Dacian stage (Teisseyre, 1907; Andreescu (1972) limited the, respectively, lower and upper extent of the Pontian (Marinescu and Papaianopol, 1995). For the upper part of the Pliocene series, above the last brackish sediments of the Dacian stage, Krejci-Graf (1932) proposed the name Romanian. This stage represents the final

Pliocene phase of the Paratethys and thus, in the at that time fresh-water Dacic Basin, the end of its Neogene aquatic evolution (Papaianopol et al., 1999).

The definitions of the (sub) stage boundaries, recognized in the studied sections, were based on the appearance and development of mollusc taxa in the Dacic Basin. Upper Maeotian (Moldavian) beds mainly contain species of *Unio* and *Viviparus*, and rarely *Congeria*. The Maeotian-Pontian stage boundary is defined by the first occurrence of *Congeria rumana* and the appearances of the genera *Paradacna*, *Pontalmyra*, and *Prosodacnomya*. The lower Pontian (Odessian) contains in addition *Didacna* and *Limnocardium* species, while the index species of the middle Pontian (Portaferrian) substage is *Congeria rhomboidea*. The upper Pontian (Bosphorian), characterized by the first occurrences of *Lunadacna lunae* and *Pontalmyra constantinae*, contains also *Phyllocardium planum planum* (Stevanović et al., 1990; MăruŃeanu et al., 1998, 2000). The Pontian-Dacian boundary corresponds to the first appearances of *Parapachydacna* species and *Zamphiridacna orientalis*. The lower Dacian (Getian) is characterized by the presence of the genera *Dacicardium*, *Euxinocardium*, *Pachydacna*, *Parapachydacna*, *Pontalmyra*, *Prosodacna*, *Pseudocatillus*, *Psilodon*, *Psilunio*, *Viviparus*, and *Zamphiridacna*. The lower-upper Dacian (Getian-Parscovian) boundary is contemporaneous with the first occurrences of *Psilodon haueri* and *Zamphiridacna zamphiri*, whereas the upper Dacian (Parscovian) contains other species of *Psilodon*, *Zamphiridacna*, in addition to *Congeria*, *Dreissena*, *Euxinocardium*, *Gyraulus*, *Horiiodacna*, *Limnodacna*, *Lithoglyphus*, *Melanoides*, *Pachydacna*, *Plagiodacna*, *Pontalmyra*, *Pseudocatillus*, and *Viviparus* (Marinescu and Papaianopol, 1995; MăruŃeanu et al., 1998, 2000). While the Dacian-Romanian boundary is defined by the first occurrences of *Jaskoa sturdze* and *Viviparus bifarcinatus*, the subsequent early Romanian (Siensian) substage is characterized by species of the genera *Unio*, *Viviparus*, and *Melanopsis* (Andreescu, 1983; MăruŃeanu et al., 1998; Papaianopol et al., 1999; MăruŃeanu et al., 2000).

### 2.2.2 Geological setting of the Dacic Basin

The Paratethys was divided into a western/central part, between the Alpine and the Carpathian foredeep, and an eastern part comprising the Black Sea-Lake Aral region (Fig. 2.1). As a transition zone between these two bioprovinces, the Dacic Basin occupies the area between the Southern Carpathians in the northwest, the Balkans in the south, and the Dobrogea in the east. In the Neogene, until the middle Sarmatian (near the Middle-Late Miocene transition), the Dacic Basin belonged to the eastern part of the Central Paratethys. However, during the middle Sarmatian to Pliocene interval, the Dacic basin became part of the western part of the Eastern Paratethys bioprovince. Fossil (mollusc) assemblages from the clays and sands of the Dacic Basin are similar during this second period to assemblages from the Euxinic and Caspian basins (Eastern Paratethys), but very different from the fossil communities of the Transylvanian Depression, the eastern part of the Central Paratethys (Nagymaryosi and Müller, 1988; Papaianopol and MăruŃeanu, 1993; Marinescu and MăruŃeanu, 1994). The strong uplift of the Carpathian belt, starting in the middle Sarmatian, determined the isolation of the Central Paratethys and the occurrence of endemic fauna and floral communities in this part of the Paratethys realm.

The palaeogeographic connections between the Dacic Basin and the Transylvanian Depression were restored in the early Pontian. This Odessian transgression reconnected the brackish Caspian, Euxinic, and Dacic basins and caused a greater faunal uniformity (Stevanović et al., 1990). The transgression had its maximum extension across the western part of the Dacic Basin towards the Pannonian Basin in the Portaferrian, when lacustrine facies had already returned in the central part of the Dacic Basin. Flooding of the southern part of the Dacic Basin was most widespread



in the Bosphorian, when connections with and within the Eastern Paratethys had narrowed and the Pannonian Basin was completely isolated again (Stevanović et al., 1990; Papaianopol and Marinescu, 1995; Papaianopol et al., 1995a). Further restriction dominated the Dacian stage. The desalinisation led to the extension of vast coal swamps over the central and western parts of the Dacic Basin in the Getian. Predominantly fresh waters covered the Dacic Basin, being deepest in the Carpathian foredeep during the Getian and in the south at Parscovian times. The partial absence of Parscovian beds in the north of the Carpathian foredeep reflects the southward shift of the centre of deposition (Andreescu, 1983; Marinescu and Papaianopol, 1995; Papaianopol et al., 1995b). In the early Romanian only a large fresh-water lake remained, supplied with molasse-type sediments by the Southern Carpathians (Papaianopol et al., 1999). Continued uplift of this range affected the northernmost units of the Carpathian Foredeep, causing tilting and weak folding of the strata of the studied sections in this area (Motăș et al., 1976; Rabăgia and Mațenco, 1999).

## 2.3 Sections and sampling

### 2.3.1 Bizdidel

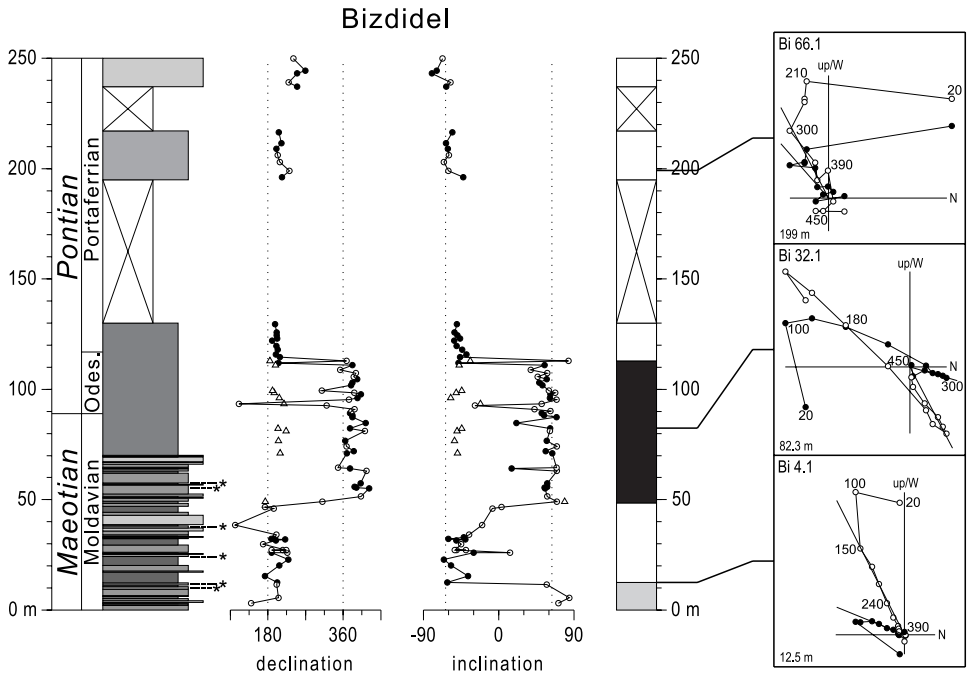
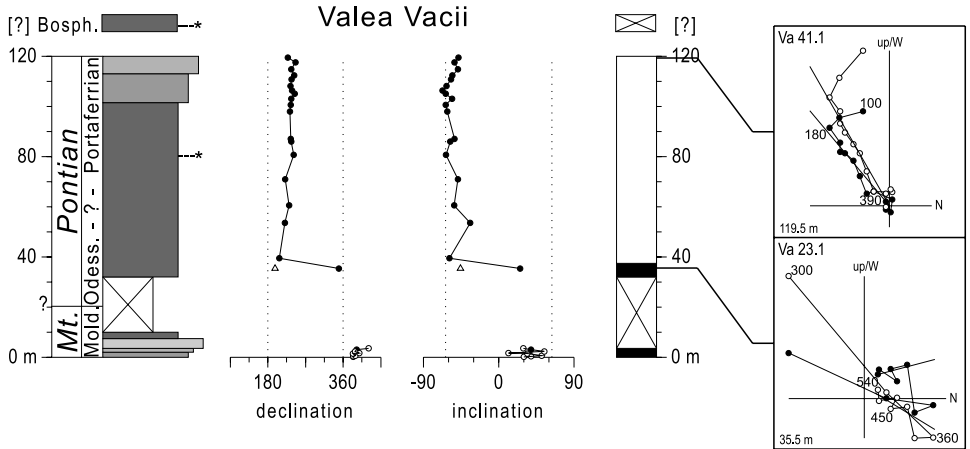
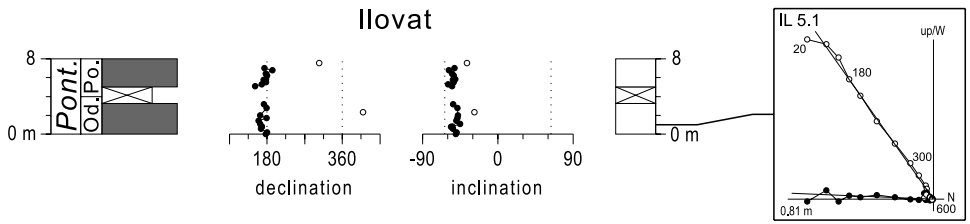
The transition from the Maeotian into the Pontian is well recorded in the valley of Bizdidel (Fig. 2.1) along a tributary of the river Ialomița, about 20 km upstream from the town of Tîrgoviște, and east of the village of Pucioasa. The section (Fig. 2.2a) consists of 70 m of alternating, fluvio-lacustrine clays, siltstones, and sand beds, dipping 40°S in outcrops on the western bank of the river, and separated at a bridge from 60 m of younger bluish-grey clays exposed on the eastern bank. In this latter unit, the Maeotian-Pontian boundary was recognized at 89 m, and the Odessian-Portaferrian substage boundary was found at 117 m (pers. comm. I. Papaianopol, 1996). Additionally, partially exposed Portaferrian silts and sands were recorded further downstream. Samples for paleomagnetic and biostratigraphic analysis were taken at every 2-3 m, mainly from the clay beds.

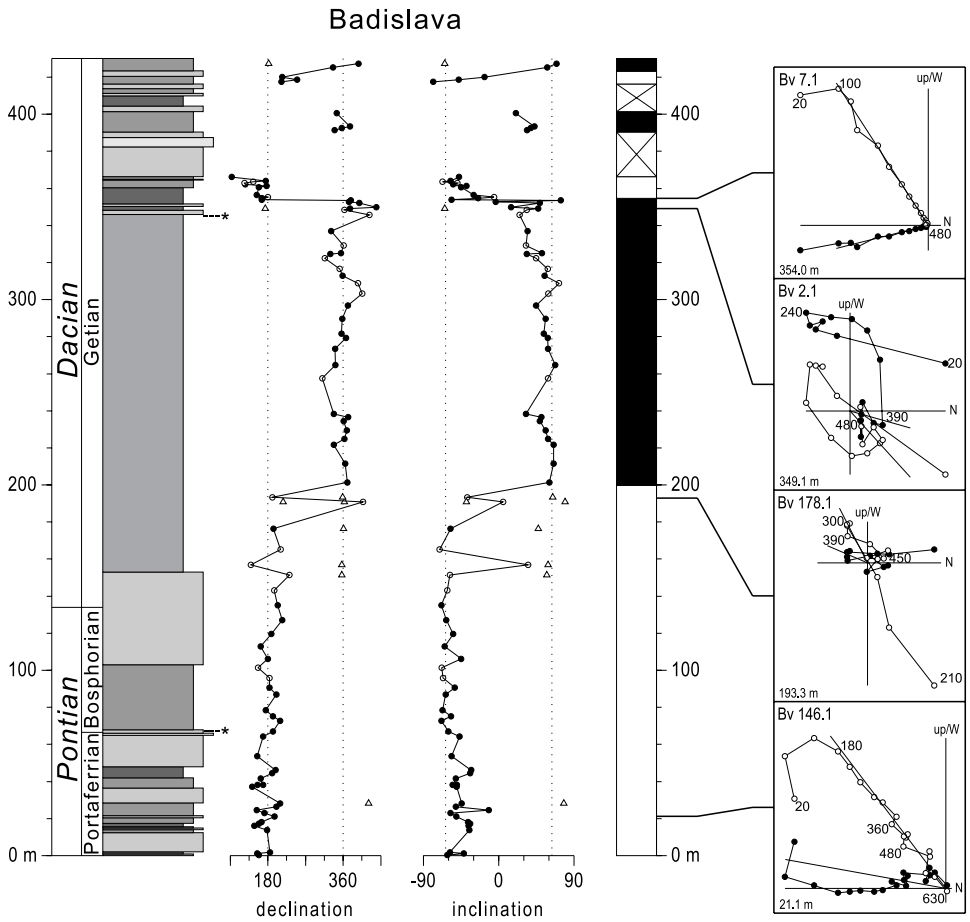
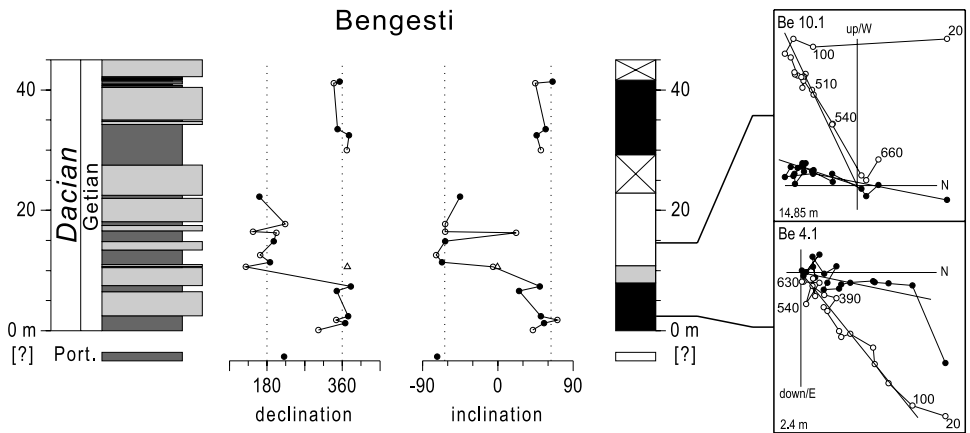
### 2.3.2 Valea Vacii

A succession of approximately the same age was visited in Valea Vacii (Fig. 2.1). It consists of separated outcrops along a left tributary of the Pîriul Sărat, about 30 km northwest of Ploiești, and just east of Săngeru (Marinescu and Papaianopol in Stevanović et al., 1990, pp. 407-410). The 120 m long section (Fig. 2.2a) on the western side of the valley consists of clays and sands of latest Maeotian (Moldavian) age, followed on the eastern side by poorly exposed Odessian blue-grey clays. The upper part of the section, of Portaferrian age, consists of sandy clays with reddish iron oxide layers. Further north only sparse patches of upper Portaferrian and Bosphorian clays are present. In the 60°N-dipping Moldavian clays and sands samples were taken at every 0.5 m, in the 35°-45°N-dipping Pontian part of the section at every 2-10 m. Two additional hand samples of the Bosphorian clays were collected for biostratigraphic analysis.

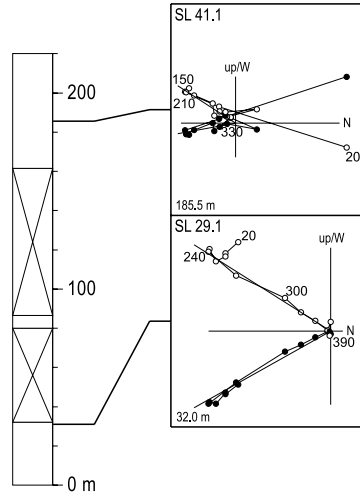
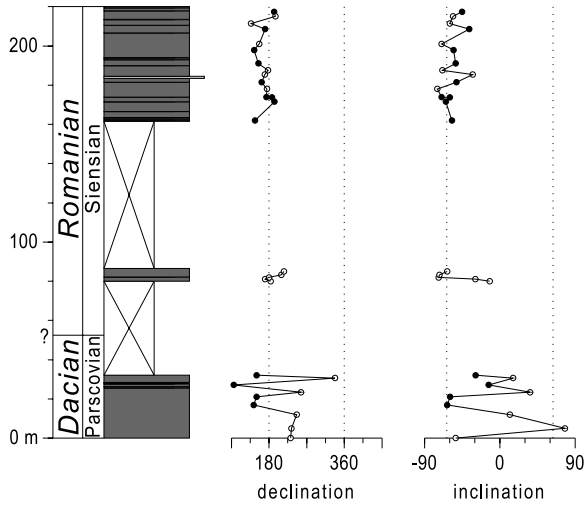
### 2.3.3 Ilovăț

Near the village of Ilovăț (Fig. 2.1), a short section was recorded on the banks of the river Coșuștea, 15 km west of Motru (Papaianopol et al., 1995b). It consists of two stretches of 10°E-dipping, greyish clays of 3 m each, separated by a short stratigraphic gap (Fig. 2.2a). The lower part exposes Odessian beds, whereas the top part is of Portaferrian age. Samples were taken at approximately every 0.3 m.

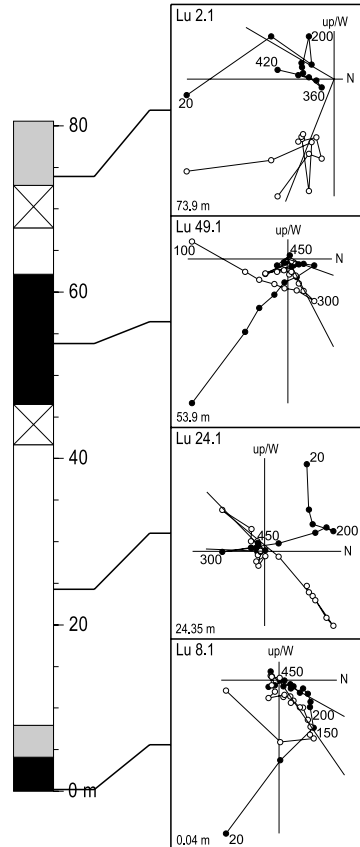
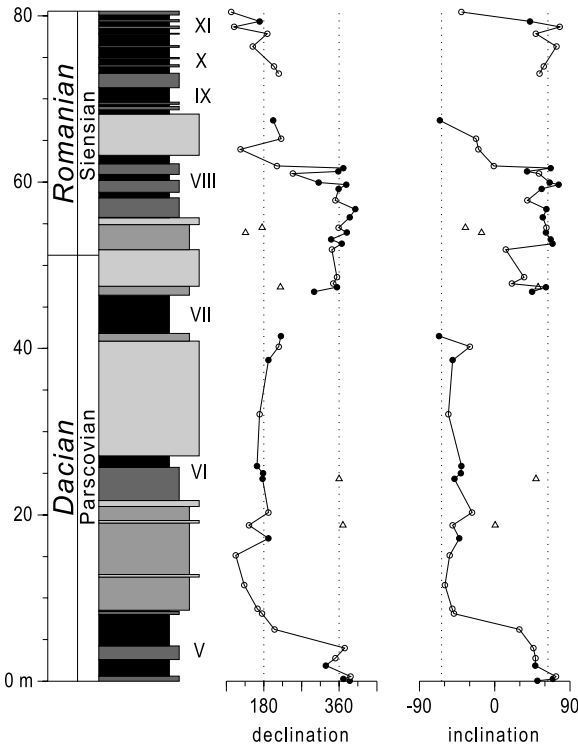




### Slanicul de Buzau



### Lupoaia



*Figure 2.2.* Sections in the Dacic Basin. Lithology plus regional (sub) stages, paleomagnetic results, interpreted polarity zones, and thermal demagnetization diagrams of selected samples. In the lithology column dark (light) shaded indenting (protruding) intervals represent clayey/silty (sandy) beds; black intervals represent coal beds. An asterisk (\*) indicates levels with calcareous nannofossils. Note variation in the meter-scale of the sections. Solid (open) circles denote (less) reliable ChRM directions; for low-temperature components, triangles are used. In the polarity column, black (white) denotes normal (reversed) polarity, grey indicates undetermined polarity, and for intervals without samples, white with a cross is used. Demagnetization diagrams denote orthogonal projections of NRM vector end-points, after tectonic correction, with open (Solid) symbols on the vertical (horizontal) plane; values represent temperature increments in °C; best-fit lines indicate interpreted polarity directions. Stratigraphic levels and sample numbers are in the lower and upper left corners, respectively. a) Sections of Bizdidel, Valea Vacii, and Ilovăț. b) Sections of Bădislava and Bengești. c) Sections of Lupoia and Slănicul de Buzău. Roman numerals indicate principle lignite units according to regional nomenclature (Rădan and Rădan, 1998).

### 2.3.4 Bădislava

The valley of Bădislava is located 14 km west of Curtea de Argeș, near Tigveni, where it merges with the valley of the river Topolog (Fig. 2.1). The section (Fig. 2.2b) begins 3.6 km upstream from the bridge west of Tigveni, above gravel and sand beds of presumably Maeotian age. Exposed on either side of the stream, the Portaferrian (the Odessian substage is not represented here; pers. comm. I. Papaianopol, 1998) starts with 150 m of sands with mollusc lags and intercalated blue-grey silty clays. At 64 m, the Portaferrian-Bosphorian substage boundary is recognized; the Pontian-Dacian boundary was observed in the sands at 135 m. Downstream, the succession continues with another 200 m of grey silty clays of Getian age. The upper 50 m of partly exposed yellow sands and grey sandy clays of the Dacian, near the church of Bălilești (1.6 km from the bridge), were described in more detail by Papaianopol et al. (1995b). Samples were taken at every 4-5 m in the 10°-20°SSE-dipping strata.

### 2.3.5 Bengești

Other lower Dacian outcrops are found east of Bengești (Fig. 2.1) in Valea Mare, 25 km east of Tirgu Jiu (Papaianopol in Marinescu and Papaianopol, 1995, pp. 106-109; Papaianopol et al., 1995b). On the eastern slope above the valley floor, a continuous section of 45 m was recorded containing nine rhythmites of 2.5-7.5 m each (Fig. 2.2b). The sedimentary cycles consist of bluish-grey clays and silts followed by ochre sands that are often cemented at the top. In the uppermost cycle, lignitic sediments partly replace the clays and silts. The clay-silt beds of these 7.4°SE-dipping Getian deposits were sampled at every 2 m on average. An additional sample was taken in clays of Portaferrian age from a site in the lower part of the valley, closer to the village.

### 2.3.6 Lupoia

Parscovian and Siensian deposits are very well exposed in the lignite quarry of Lupoia (Fig. 2.1), located on the northwest side of Motru (Papaianopol et al., 1995b, 1999). The sampled section of 80 m (Fig. 2.2c), consisting of five lignite and clay units separated by silts and sands, starts just above the Getian-Parscovian boundary and contains the Dacian-Romanian boundary at 52 m above the base (Rădan and Rădan, 1998; Popescu, 2001). A relatively thick lignite-clay complex (X-XI) forms the uppermost coal seam. Samples in the sub-horizontal deposits were taken at nearly every 1.5 m.

### 2.3.7 Slănicul de Buzău

This section (Fig. 2.1) was recorded 25 km north of Buzău in outcrops along the riverbanks of the Slănicul de Buzău valley, a left tributary of the Buzăul valley (Papaianopol in Marinescu and Papaianopol, 1995, pp. 103-106; Papaianopol et al., 1999). Clays and silts constitute the dominant sediments and are intercalated by numerous thin, lignitic levels and occasionally by thin sand beds (Fig. 2.2c). The lower 30 m of the succession, of Parscovian age, are exposed on the western bank of the stream and are separated by a stratigraphic gap from silty clays of Siensian age (Andreescu, 1983; pers. comm. I. Papaianopol, 1996). Further upstream along the eastern side of the flow another 60 m of lower Romanian deposits could be recorded. Samples were taken at every 1-5 m in the 40°NW-dipping beds.

## 2.4 Magnetostratigraphy

### 2.4.1 Method

At most sample levels two oriented cores were taken with a water-cooled, generator-powered electric drill. The samples from the fresh-cut sediment surface were directly wrapped in aluminium paper for better preservation during transport, and were sawn into ~10.5 cm<sup>3</sup> specimens at the laboratory.

The natural remanent magnetization (NRM) of the specimens was thermally demagnetized to obtain a magnetic polarity record for the seven sections. For measurements, a 2G Enterprises horizontal DC SQUID and a vertical RF SQUID magnetometer were used. At least one specimen per sample level was progressively heated in a magnetically shielded, laboratory-built furnace with temperature steps of 30°C, up to a maximum of 700°C.

### 2.4.2 Results

Thermal demagnetization diagrams (Zijderveld, 1967) give in general straightforward results. In a number of specimens low-temperature components, often parallel to the direction of the present-day field before bedding plane correction, were removed at 100°-240°C (for instance samples Bi 4.1, Bi 66.1, Bv 2.1, Be 10.1, SL 41.1; Figs. 2.2a-c). These were considered secondary signals, either laboratory-induced or recent overprints caused by weathering. Both normal and reversed magnetic field components, interpreted as primary, characteristic remanent magnetization (ChRM) directions, were gradually removed at higher temperatures varying from 360°C to over 600°C (Figs. 2.2a-c). Occasionally, an intermediate-temperature component with a polarity opposite to the ChRM direction was revealed between 200°C and 360°C (samples Bi 32.1, Va 23.1, Bv 178.1, Bv 2.1, Lu 24.1; Figs. 2.2a-c). Few specimens gave ambiguous results (sample Lu 2.1, e.g.; Fig. 2.2c). Best-fit lines through the NRM vector end-points, for a representative temperature interval, determined declination and inclination components of the ChRM.

The obtained magnetostratigraphic records of the sections of Bizdidel, Valea Vacii, and Ilovăț (Fig. 2.2a) are all in good agreement and show the occurrence of the Maetian-Pontian boundary in a normal polarity zone and of the Odessian-Portaferrian boundary in a reversed polarity zone. In the section of Bădislava (Fig. 2.2b) six polarity intervals were recorded altogether; the two reversals below and above the 400 m level have no exact stratigraphic position. The Portaferrian-Bosphorian and Pontian-Dacian boundaries can be found in the lowermost reversed interval. In the Getian succession of Bengești two normal intervals could be recognized and the separate site in the Portaferrian clays yielded reversed polarity (Fig. 2.2b). Paleomagnetic results from Lupoaia

and Slănicul de Buzău are of variable quality (Fig. 2.2c). Interpretation of the demagnetization diagrams of relatively high-intensity specimens nevertheless reveals a coherent record of predominantly reversed directions. The Dacian-Romanian boundary was only recorded in the section of Lupoia, in the upper of two normal polarity zones.

## 2.5 Calcareous nannofossils

### 2.5.1 Method

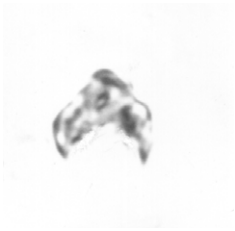
In order to obtain biostratigraphic age constraints of the deposits, the microfossil content of the sampled horizons was studied. Foraminifera were absent, but due to the presence of diagnostic calcareous nannofossils, a number of levels in the sections of Bizdidel, Valea Vacii, and Bădislava proved to be suitable for this purpose. Standard preparation techniques of Bramlette and Sullivan (1961) were followed, supplemented by filtering the samples with a 36µm sieve. Smear slides were examined with a light microscope using transmitted and cross-polarized light at 1250× magnification.

### 2.5.2 Results

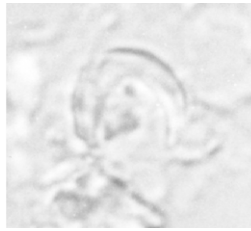
In the section of Bizdidel nannofossils were found at six levels in the Maeotian (lower) part of the section (Fig. 2.2a). The studied nannofossil assemblage consists of: *Calcidiscus leptoporus*, *C. macintyreii*, *Coccolithus pelagicus*, *Discoaster challengerii*, *D. variabilis*, *Helicosphaera kamptneri*, *Reticulofenestra dornicoides*, *R. minuta*, *R. minutula*, *R. pseudoumbilicus*, and *Sphenolithus abies*. Samples from the two lowermost levels, at 11-12 m, contain in addition *Amaurolithus primus* and *D. quinquaramus*, which are characteristic for the NN11b Zone sensu Martini (1971). At 26 m a few specimens of *A. primus* and *A. bizzarus* were recorded.

In the section of Valea Vacii two horizons were found to contain nannofossils (Fig. 2.2a), one in the Portaferrian at 81 m and the other in the separate outcrop of Bosphorian clays further down the valley. The assemblage of the first sample (Plate 2.I, 1-4) indicates Zone NN11b (Martini, 1971). It contains: *Amaurolithus* cf. *A. amplificus*, *A. delicatus*, *A. primus*, *Braarudosphaera bigelowii*, *Calcidiscus leptoporus*, *C. macintyreii*, *Coccolithus pelagicus*, *Discoaster berggrenii*, *D. icarus*, *D. cf. D. loeblichii*, *D. misconceptus*, *D. quinquaramus*, *D. variabilis*, *D. variabilis-D. pansus* intergrade, *Geminolithella rotula*, *Helicosphaera carteri*, *H. paleocarteri*, *H. wallichii*, *Reticulofenestra minuta*, *R. minutula*, *R. pseudoumbilicus*, *Scyphosphaera* sp., *Triquetrorhabdulus rugosus*, and *Umbilicosphaera* sp. The younger sample (Plate 2.I, 5-8) yields a nannofossil assemblage belonging to Zone NN12 (Martini, 1971), consisting of small and rare specimens of: *A. delicatus*, *A. tricorniculatus*, *B. bigelowii*, *C. macintyreii*, *Ceratolithus acutus*, *C. pelagicus*, *D. brouweri*, *D. misconceptus*, *D. pansus*, *R. pseudoumbilicus*, and *T. rugosus*.

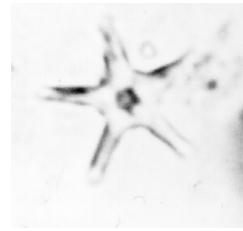
Similar results were obtained in the section of Bădislava, where nannofossils were found near the Portaferrian-Bosphorian transition at 64 m and in the Dacian at 345 m (Fig. 2.2b). The nannofossil content in the lower sample (Plate 2.I, 9) includes: *Calcidiscus leptoporus*, *Coccolithus pelagicus*, *Discoaster icarus*, *D. cf. D. quinquaramus*, *D. variabilis*, *Helicosphaera carteri*, and *Scapholithus fossilis*, together with rare specimens of *Amaurolithus delicatus*, *A. primus*, and *Triquetrorhabdulus rugosus*, suggesting Zone NN11b (Martini, 1971). In the Dacian sample (Plate 2.I, 10-12) an assemblage belonging to Zone NN12 (Martini, 1971) was identified containing small specimens of: *A. bizzarus*, *A. delicatus*, and *A. tricorniculatus*, together with *Braarudosphaera*



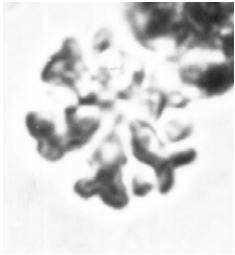
1



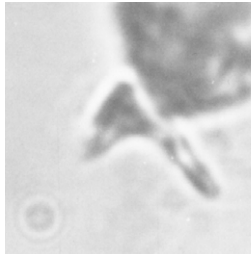
2



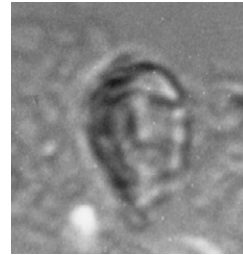
3



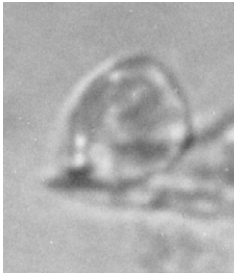
4



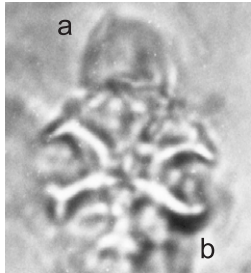
5



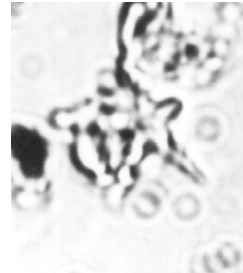
6



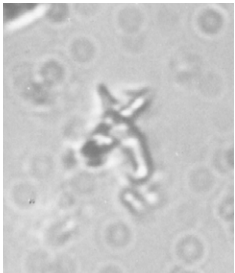
7



8



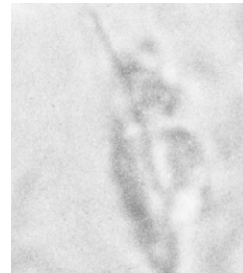
9



10



11



12



Plate 2.I. Calcareous nannofossils from the sections of Valea Vacii (VA) and Bădislava (BV). All specimens: parallel light.

- 1) *Amaurolithus primus* (Bukry and Percival),  $\times 3000$ ; sample VA 28.
- 2) *Amaurolithus delicatus* Gartner and Bukry,  $\times 2500$ ; sample VA 28.
- 3) *Discoaster berggrenii* Bukry,  $\times 3500$ ; sample VA 28.
- 4) *Discoaster icarus* Stradner,  $\times 3500$ ; sample VA 28.
- 5) *Ceratolithus acutus* Gartner and Bukry,  $\times 2500$ ; sample VA 43.
- 6) *Amaurolithus delicatus* Gartner and Bukry,  $\times 2500$ ; sample VA 43.
- 7) *Amaurolithus delicatus* Gartner and Bukry,  $\times 2500$ ; sample VA 43.
- 8a) *Amaurolithus delicatus* Gartner and Bukry,  $\times 2000$ ; b) *Discoaster pansus* (Bukry and Percival),  $\times 2000$ ; sample VA 43.
- 9) *Discoaster* cf. *D. quinqueringus* Gartner,  $\times 3500$ ; sample BV 158.
- 10) *Ceratolithus* cf. *C. atlanticus* Perch-Nielsen,  $\times 3000$ ; sample BV 200.
- 11) *Triquetrorhabdulus rugosus* Bramlette and Wilcoxon,  $\times 3000$ ; sample BV 200.
- 12) *Triquetrorhabdulus rugosus* Bramlette and Wilcoxon,  $\times 3000$ ; sample BV 200.

*bigelowii*, *Ceratolithus* cf. *C. atlanticus*, *Coccolithus pelagicus*, *Discoaster brouweri*, *D. misconceptus*, *D. pansus*, *D. variabilis*, *Lithostromation perdurum*, and *Triquetrorhabdulus rugosus*.

## 2.6 Age model for the Dacic Basin

The reversal pattern of the polarity records of the studied sections (Figs. 2.2a-c) is combined with age constraints provided by the nannofossil results, to correlate the observed magnetic polarity zones with the APTS of Hilgen et al. (1995), modified by Lourens et al. (1996) and Krijgsman et al. (1999). Interpolation between the thus derived absolute ages of the stratigraphic levels representing polarity reversals gives the approximate ages of the observed (sub) stage boundaries (Fig. 2.3).

### 2.6.1 Pontian stage

In the sections of Bizdidel and Valea Vacii (Fig. 2.2a), the stratigraphic interval surrounding the Maeotian-Pontian boundary corresponds to a zone of normal polarity and is followed by a vast lower and middle Pontian interval representing a period of entirely reversed magnetic polarity. This reversed interval includes the Odessian-Portaferrian substage boundary, recorded in Bizdidel and Ilovăț (Fig. 2.2a), directly preceded by the reversal above the base of the Pontian. Other middle and upper Pontian sediments, both exposed in Bădislava (Fig. 2.2b), correspond to an interval of reversed polarity as well. Alexeeva et al. (1983), and Rădan (2002), evaluated the position of the Pontian-Dacian boundary using paleomagnetic results from sections in the north-eastern part of the Dacic Basin. They documented the exclusively reversed polarity of the Pontian deposits and suggested a correspondence with the lower part of the Gilbert epoch (C3r). Recent work in the western part of the Dacic Basin by Clauzon et al. (2005) provides additional evidence for this correlation.

Nannofossil assemblages with *Amaurolithus primus* are found in the upper Maeotian strata of Bizdidel underlying the normal polarity interval, indicating a maximum age for these beds of  $7.430 \pm 0.002$  Ma (Negri and Villa, 2000), or  $7.392 \pm 0.004$  Ma (Backman and Raffi, 1997). Moreover, the middle Pontian strata of Valea Vacii above the normal zone contain besides *A. delicatus* and *A.*

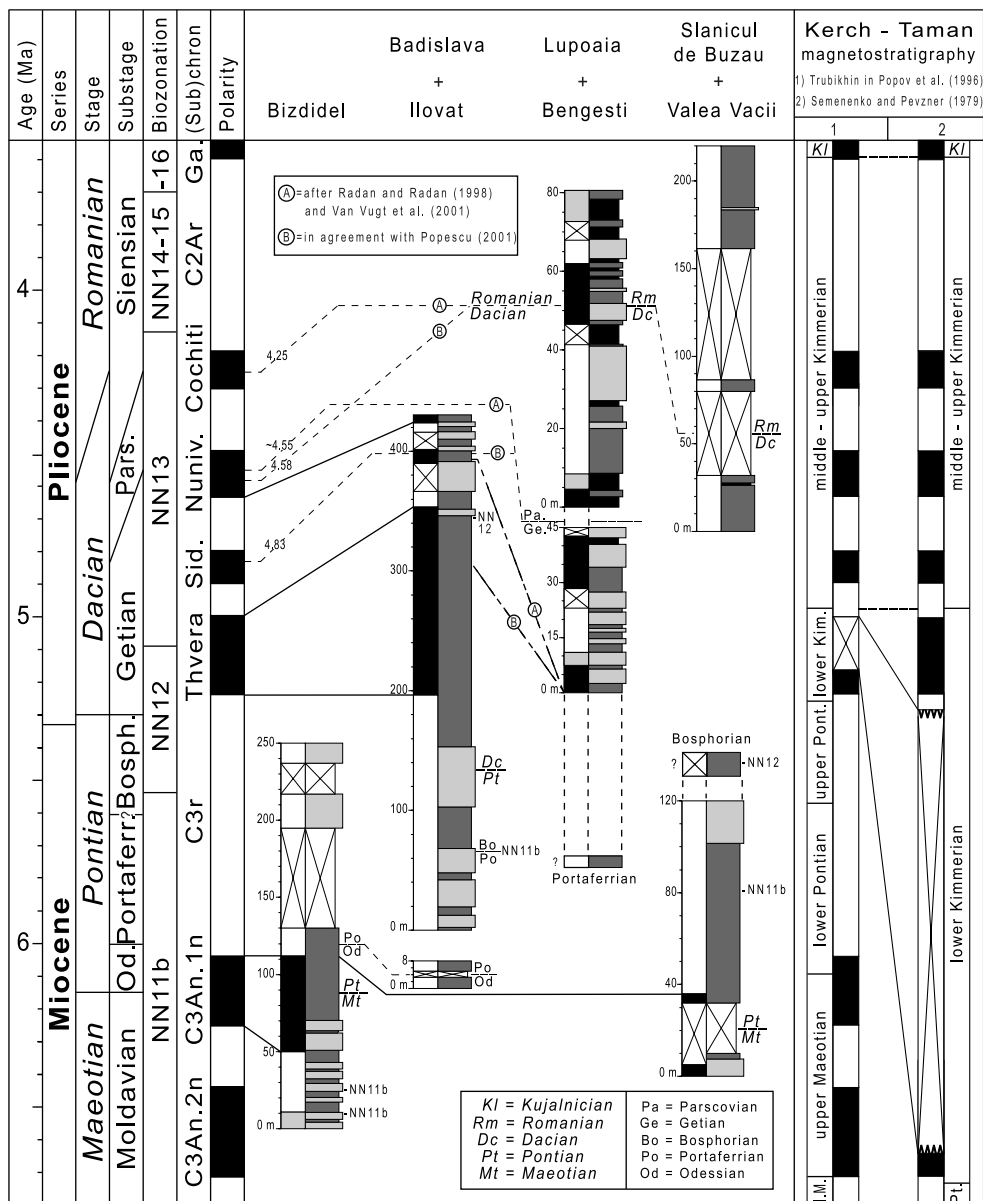


Figure 2.3. Magneto- and biostratigraphic correlation of the Dacic Basin sections with the Astronomical Polarity Time Scale (APTS) and comparison with two interpretations of the magnetostratigraphy of the Kerch-Taman composite section. Columns display (from left): global series, Dacic stages and substages, NN-biozonation of calcareous nannofossils (sensu Martini, 1971, with modifications according to Backman and Raffi, 1997), and magnetic polarity zones of the APTS (of Hilgen et al., 1995, and Lourens et al., 1996, with modifications according to Krijgsman et al., 1999). Solid lines connect corresponding reversals; dashed lines are used for (sub) stage boundary correlations. Levels with nannofossil marker species are indicated by the code of the concerning biozone. Note variation in the meter-scale of the sections. The Kerch-Taman composite is scaled to age.

*primus* also *A. cf. A. amplificus*, a species that appeared in the Mediterranean at  $7.388 \pm 0.002$  Ma (Negri and Villa, 2000) and in the Atlantic Ocean at  $6.840 \pm 0.003$  Ma (Backman and Raffi, 1997). In other geological profiles in the Dacic Basin, Papaianopol and Mărunțeanu (1993), Mărunțeanu (1998), and Mărunțeanu and Papaianopol (1998) found nannofossil assemblages with *A. primus* and *A. delicatus* (with Atlantic and Mediterranean first occurrences at, respectively, 7.323 Ma and 7.250 Ma: Raffi et al., 1998; Negri and Villa, 2000) as low as in the top of the lower Maeotian. The nannofossil assemblage in the Portaferrian/Bosphorian horizon of Bădislava is characterized by the presence of *A. delicatus*, *A. primus*, *Discoaster quinqueramus*, and *Triquetrorhabdulus rugosus*, still indicating Zone NN11b of Martini (1971). In Valea Vacii the Bosphorian sample has a nannofossil assemblage of Zone NN12, containing *A. tricorniculatus* and *Ceratolithus acutus* (with a first occurrence at  $5.372 \pm 0.003$  Ma: Backman and Raffi, 1997). Mărunțeanu (in Marinescu and Papaianopol, 1995, pp. 504-505), Mărunțeanu and Papaianopol (1995), and Papaianopol et al. (1995b) reported the findings of calcareous nannofossils in Bosphorian strata belonging to the *Discoaster quinqueramus*-NN11 Zone. In fact, according to Mărunțeanu and Papaianopol (1998) and supported by our data, the NN11-NN12 transition occurs in the Bosphorian. Finally, the Dacian level in the upper part of the normal zone in Bădislava contains *A. bizzarus*, *A. tricorniculatus*, and *Ceratolithus cf. C. atlanticus*, which had first occurrences in the Atlantic Ocean at  $\sim 5.25$  Ma,  $\sim 5.32$  Ma (Raffi et al., 1998), and  $5.398 \pm 0.003$  Ma (Backman and Raffi, 1997), respectively. Previous observations of these and other NN12 Zone index species in the lower Dacian by Mărunțeanu and Papaianopol (1995, 1998), and Mărunțeanu et al. (1998), are consistent with our results.

Because of the presence of NN12 markers within and NN11b markers below the lower Dacian normal polarity interval, only one correlation option for this zone remains: the Thvera subchron (C3n.4n, dated by Lourens et al. (1996) at 5.236-4.998 Ma), thus confirming the conclusions of Alexeeva et al. (1983), Rădan (2002), and Clauzon et al. (2005). Since no other normal zone was recorded below the Thvera than the one containing the Maeotian-Pontian boundary, the majority of the Pontian stage can be correlated with the lower part of the Gilbert chron (C3r). The Maeotian-Pontian boundary then occurs within subchron C3n.1n and as a result has an age of  $6.15 \pm 0.11$  Ma (Fig. 2.3). As recorded in the section of Bizdidel, the Odessian substage ends after the normal to reversed polarity reversal, at the beginning of chron C3Rr. Consequently, the Portaferrian will have started little later than 6 Ma, passing into the Bosphorian before the NN11-NN12 transition, at 5.537 Ma. The Pontian-Dacian boundary, below the base of the Thvera subchron and in Zone NN12, is estimated at  $5.3 \pm 0.1$  Ma, near the Miocene-Pliocene boundary. The resulting length of the Pontian stage in the Dacic Basin thus becomes  $0.85 \pm 0.21$  Myr.

### 2.6.2 Dacian and Romanian stages

The well-developed, cyclic, Getian deposits of Bengești are succeeded by the Parscovian and Siensian lignite succession of Lupoia. The coal bed in the top of the Bengești section (Fig. 2.2b) is believed to be the equivalent of the first lignite bed below the base of the Lupoia section (pers. comm. I. Papaianopol, 1996), thus correlating with lignite IV of the regional nomenclature (Rădan and Rădan, 1998; Popescu, 2001). The Getian-Parscovian substage boundary is not recorded in the presented sections, but probably occurs above the top of the Bengești section and just below the base of the lowest coal bed (lignite V) in Lupoia. In both sections two normal polarity intervals are recorded, of which the uppermost zone in Lupoia corresponds to the interval containing the Dacian-Romanian stage boundary (Fig. 2.2c). Rădan and Rădan (1998) and Rădan (2000) have documented the Romanian Pliocene magnetostratigraphy in Lupoia and in other sections.

They correlated the Getian-Parscovian boundary with the middle of the Nunivak subchron at 4.55 Ma and demonstrated the occurrence of the Dacian-Romanian boundary within the Cochiti subchron at 4.25 Ma (option A; Fig. 2.3). Their main argument was that the overlying 60 m of Romanian deposits with another four lignite beds (XII-XV, not shown here) yielded only reversed polarity and therefore represented the long, reversed upper part of the Gilbert chron (C2Ar). These conclusions credit the earlier estimates of Andreescu (1981, 1983) and Alexeeva et al. (1983). Furthermore, Van Vugt et al. (2001) discussed a cyclostratigraphic tuning of the lignite beds of Lupoiaia to maxima in the 100 kyr eccentricity curve of Laskar (1990), supporting the correlation of option A. They showed the possibility to correlate the reversed polarity interval between lignite units V and VII with subchron C3n.1r (with a duration of 193 kyr) between Nunivak and Cochiti.

However, the positions of the reversals at the lower (4–8 m) and upper limit (42–47 m) of this interval are not estimated precisely. Hence, the time span of the reversed interval in Lupoiaia (equivalent to about two eccentricity periods, i.e.  $200 \pm 50$  kyr) does not exclude a correlation with subchron C3n.2r between Sidufjall and Nunivak (having a duration of 167 kyr: Lourens et al., 1996). Indeed, Popescu (2001) provided climatostratigraphic arguments for this alternative option (B; Fig. 2.3). Although she conveniently ignored the reported reversed polarity (Rădan and Rădan, 1998) directly above lignite complex X-XI (X-XIII in her Figure 2.2), correlation of her Lupoiaia pollen record with the older Sidufjall-Nunivak segment of the eccentricity and  $\delta^{18}\text{O}$  curves results in a better pattern correspondence. In this correlation, the lignite beds are linked with eccentricity minima. Option B implies that the Dacian-Romanian boundary should be placed in the Nunivak subchron, at  $4.58 \pm 0.05$  Ma. The underlying Getian-Parscovian substage boundary would then occur inevitably within the Sidufjall subchron, around 4.83 Ma, and the Getian Bengești section would correspond to the Thvera-Sidufjall interval (option B; Fig. 2.3). A speculative cyclostratigraphic approach of the Bengești succession, assuming that the rhythmic bedding represents precession cyclicity (with a period of  $\sim 21$  kyr: Laskar, 1990), could support option B. Then, namely, the 4–5 sedimentary cycles in the reversed polarity interval (Fig. 2.2b) would correspond approximately to the duration of 102 kyr (Lourens et al., 1996) of subchron C3n.3r between Thvera and Sidufjall. This would exclude a correlation of the reversed interval in Bengești with the 167 kyr duration of subchron C3n.2r between Sidufjall and Nunivak, as in option A (Fig. 2.3). The hypothesis of a hiatus between lignites VII and VIII in Lupoiaia, separating the lower Dacian from the lower Romanian and assuming the absence of the upper Dacian, (dwelled upon in Papaianopol et al., 1995b) would further complicate the chronology problem. It both supports the position of the Dacian-Romanian boundary (and, automatically, of the Getian-Parscovian boundary) as in option A, and the correlation of the lower half of the Lupoiaia section with subchron C3n.2r (option B).

The considerable length and an assumed average constant sedimentation rate of the succession of Slănicul de Buzău are considered when attempting to estimate its age (Fig. 2.3). Depending on the correlation of the Lupoiaia section, the lower unexposed interval between the Dacian and the Romanian part of the Slănicul de Buzău section will either correspond to the Cochiti subchron (option A) or to the Nunivak subchron (option B). The first 30 m, of Dacian age, will thus represent a part of subchron C3n.1r (below the Cochiti) or C3n.2r (below the Nunivak), whereas the Romanian part of the section will either correspond to a part of subchron C2Ar (option A) or to the interval from subchron C3n.1r up to C2Ar. A solution (theoretically possible in the case of option B) in which the Romanian part would correspond entirely to subchron C3n.1r, between Nunivak and Cochiti, is less likely, given the thickness of 150 m. Alternatively, correlations of the upper part of the section with younger reversed polarity zones are unrealistic, since Andreescu

(1981, 1983), Alexeeva et al. (1983), and Rădan and Rădan (1998) reported that the lower-middle Romanian transition occurred around 3.5 Ma, near the beginning of the Gauss chron (3.596 Ma: Lourens et al., 1996) and the Zanclean-Piacenzian boundary (3.60 Ma: Castradori et al., 1998). Furthermore, MăruŃeanu and Papaianopol (1995, 1998) mentioned the findings of nannofossil elements indicating Zones NN15-16 in the middle Romanian of the Carpathian Foredeep.

The duration of the Dacian stage depends on the preferred position of the Dacian-Romanian boundary, either within the Cochiti subchron as proposed by Rădan and Rădan (1998) and Van Vugt et al. (2001), or within the Nunivak subchron, in accordance with Popescu (2001) and adopted by Clauzon et al. (2005). In option A, the Dacian stage just exceeds 1 Myr, from approximately 5.3 Ma to 4.25 Ma, with the Getian-Parscovian boundary in the upper part of the Sidufjall subchron at 4.83 Ma. In option B, the duration of the Dacian is approximately 700 kyr, until  $4.58 \pm 0.05$  Ma, and the Getian-Parscovian boundary corresponds to the Nunivak subchron at 4.55 Ma. The Siensian substage covers nearly 750 kyr or 1 Myr, respectively.

## 2.7 Time-equivalents of the Pontian-Dacian and palaeogeographic implications

### 2.7.1 Euxinic Basin

As a test of the potential for regional correlations of the framework presented here a comparison is made with the chronostratigraphy in the adjacent Euxinic (Black Sea) Basin. In the major part of the Pontian strata of the Black Sea area (the Kerch-Taman region; Fig. 2.1) Semenenko and Pevzner (1979) observed reversed polarities as well. Nevertheless, the discovery of nannofossils of NN10 in the upper Maeotian beds together with nannofossils characteristic of Zone NN11 and NN12 in the lower Kimmerian deposits and the absence of any zonal marker-species in the intermediate Pontian led Semenenko (1989) to correlate the reversed Pontian stage with the older chron C3Ar instead. Consequently, he assumed the presence of a large hiatus in the lower Kimmerian (Azovian) from the base of subchron C3An.2n up to C3n.4n, the Thvera subchron (Fig. 2.3).

Trubikhin (in Stevanović et al., 1990, pp. 76-79; in Popov et al., 1996) used the lithological similarities of upper Pontian and transitional Azovian sediments, plus the uninterrupted development of early Kimmerian molluscs in particular, as arguments for correlating the majority of the Pontian stage with chron C3r (Fig. 2.3). This second option would be in agreement with our results, implying that the Thvera was (partially) recorded as the normal polarity interval in the overlying Azovian beds. The middle and upper Kimmerian (Kamyshburunian and Panticapean beds) correspond to the upper part of the Gilbert chron (Popov et al., 1996) and therefore to the upper Dacian-lower Romanian interval in the Dacic Basin.

### 2.7.2 Mediterranean Basin

As mentioned before, the Pontian-Dacian stage boundary (Fig. 2.3) probably is roughly the equivalent of the Miocene-Pliocene (or Messinian-Zanclean) boundary, which was defined at 5.33 Ma by Van Couvering et al. (2000). Our age-estimate of the Maeotian-Pontian boundary is  $6.15 \pm 0.11$  Ma (Fig. 2.3), approximately 200 kyr before the onset of the Messinian Salinity Crisis at 5.96 Ma (Krijgsman et al., 1999). This correlation reduces the duration of the Pontian stage to that of the late Messinian, which is different from most previous models summarized by Jones and Simmons (1996), Steininger et al. (1996), and Rögl and Daxner-Höck (1996). The last authors

used additional fossil micro-mammal data from the Pannonian Basin to correlate the Pontian (as in Rögl et al., 1991) with the lower and middle parts of the Messinian, both stages then beginning at 7.1 Ma.

In our opinion, the Dacian stage and the early Romanian substage correspond to the Zanclean. Indifferent which option (A or B; Fig. 2.3) proves to be correct, the age of the Dacian-Romanian boundary, at  $4.58 \pm 0.05$  Ma or at 4.25 Ma, is younger than the 4.8 Ma mentioned by Steininger et al. (1996). Jones and Simmons (1996) on the contrary considered the Dacian stage as an equivalent of the Kimmerian stage. They arrived, consequently, at a position of the Dacian-Romanian boundary near the base of the Gauss chron, corresponding to the upper Kimmerian limit.

### 2.7.3 Paratethys-Tethys connections

The proposed timing of previously and newly discovered levels with calcareous nannofossil assemblages, presented above, raises the question of how the Dacic Basin exchanged water with the open ocean. The intermittent and short standing presence of the typical marine nannofossils in the brackish to fresh-water deposits can be explained only by short marine incursions in the Dacic Basin. These calcareous nannofossils arrived in water with lower salinity and either died immediately or tried to adapt to the new conditions through reduced sizes or changes of morpho-structure.

The arguments of Krijgsman et al. (1999) for postponing total isolation of the Mediterranean Basin from the Atlantic Ocean to approximately 5.59 Ma are supported by our findings of Portaferrian nannofossil assemblages in the Dacic Basin. The presence of these NN11b Zone species may reflect the influence of one or more marine incursions into the Paratethys during the late Messinian. And vice versa, migrations of Paratethyan mollusc and ostracode faunas into the Mediterranean have been documented by many authors, especially in Pontian-type Lago-Mare beds from the eastern part of the basin. Latest Bosphorian and Getian marine influxes, responsible for the NN12 assemblages in the Dacic sections, possibly illustrate re-established connections with the Mediterranean/Atlantic in the course of the Early Pliocene. Thus far, the existence and location of an open corridor between the Paratethys and the Mediterranean Basin during the Late Miocene and Early Pliocene has not been demonstrated irrefutably. Rögl et al. (1991) reported nannofossil species of Zone NN12 in the upper Pontian of the Aegean area, indicating possible connections through this basin.

## 2.8 Conclusions

Paleomagnetic results from sections along the northern margin of the Dacic Basin can be combined to develop a complete magnetostratigraphy for the latest Maeotian into the early Romanian. Age constraints provided by calcareous nannofossils enable a good correlation of these Dacic Basin sediments with the Late Miocene and the Early Pliocene part of the present APTS.

The Maeotian-Pontian stage boundary is found in a normal polarity interval corresponding to subchron C3An.1n and has an age of  $6.15 \pm 0.11$  Ma, whereas the Odessian-Portaferrian limit (6.0 Ma) is slightly younger than the top of this normal zone. While the Portaferrian-Bosphorian substage boundary is estimated at 5.6 Ma, the Pontian-Dacian boundary predates the base of the Thvera (C3n.4n) and has an age of approximately 5.3 Ma. This implies that the Pontian of the Dacic Basin has the same magnetostratigraphic signature as its counterpart in the Euxinic Basin and that it is coeval with the upper Messinian of the Mediterranean region. The

debut of the Dacian stage is coeval with the base of the Pliocene, whereas the Getian-Parscovian substage boundary corresponds either to the upper part of the Sidufjall subchron (C3n.3n), at approximately 4.83 Ma or to the Nunivak subchron (C3n.2n), at approximately 4.55 Ma. In the Nunivak subchron (at  $4.58 \pm 0.05$  Ma), or in the Cochiti subchron (at 4.25 Ma) the Dacian-Romanian transition is recorded. The Siensian substage corresponds to the last part of the Gilbert epoch, up to and including subchron C2Ar.

Calcareous nannofossil assemblages belonging to Zone NN11b are found in distinct levels of upper Maeotian and middle Pontian sediments. Upper Pontian and lower Dacian deposits yielded levels with assemblages of Zone NN12. As a result, possibly brief marine connections of the Paratethys with the Mediterranean during the late Messinian and earliest Pliocene are likely.

## Acknowledgements

Dan Jipa, Marloes Kloosterboer-van Hoeve, Wout Krijgsman, Cor Langereis, Radu Olteanu, Ioan Papaianopol, Speranța-Maria Popescu, Maria and Sorin Rădan, Joris Steenbrink, Nicolae Țicleanu, and the technicians/drivers of the Geological Institute of Romania (Bucharest) are gratefully thanked for discussions and their assistance in the field. We acknowledge the Romanian mining company and its friendly employees for their permission and cooperation. Geert Ittmann and Gerrit van 't Veld skilfully provided washed/sieved samples and nanno-smear slides. We particularly thank the reviewers O. Oms and F. Steininger for their valuable comments on an earlier version of the manuscript, and also W. Krijgsman and C. Langereis who improved the original text with helpful suggestions.

This work was conducted under the programme of the Netherlands Research School of Sedimentary Geology (NSG) and the Vening Meinesz Research School of Geodynamics (VMSG). The Netherlands Research Centre for Integrated Solid Earth Science (ISES) provided funds for visiting research fellowships for the second author (M.M.). This is NSG publication 20020804.

## References

- Alexeeva, L.I., Andreescu, I., Bandrabur, T., Cepaliga, A.L., Ghenea, C., Miăhilă, N., Trubikhin, V.M., 1983. Correlations of the Pliocene and Lower Pleistocene deposits in the Dacic and Euxinic Basins. *Annuaire de l'Institut de Géologie et de Géophysique* 59, 143-152.
- Andreescu, I., 1972. Contribuții la stratigrafia Dacianului și Romanianului din zona de curbură a Carpaților Orientali. *Dari de Seama ale Sedintelor-Institutul Geologie si Geofizica (Stratigrafie)* 58 (4), 131-156.
- Andreescu, I., 1981. Middle to Upper Neogene and Early Quaternary chronostratigraphy from the Dacic Basin and correlations with neighbouring areas. *Annales Géologiques des Pays Helléniques*, tome hors série 4, 129-138.
- Andreescu, I., 1983. Biochronology and chronostratigraphy of the Upper Pliocene-Lower Pleistocene in the Dacic Basin. *Annuaire de l'Institut de Géologie et de Géophysique* 59, 153-160.

- Backman, J., Raffi, I., 1997. Calibration of Miocene nannofossil events to orbitally tuned cyclostratigraphies from Ceara Rise. *Proceedings of the Ocean Drilling Program, Scientific Results* 154, 83-100. doi:10.2973/odp.proc.sr.154.101.1997.
- Báldi, T., 1984. The terminal Eocene and early Oligocene events in Hungary and separation of an anoxic, cold Paratethys. *Eclogae Geologicae Helvetiae* 77, 1-27.
- Báldi, T., 1989. Tethys and Paratethys through Oligocene times. Remarks to a comment. *Geologický Zborník-Geologica Carpathica* 40 (1), 85-99.
- Barbot de Marny, N., 1869. Geological essay of the Khersonian District. Demakova, B., St. Petersburg.
- Bertels, E.È., 1963. Jizbrannyye trudy 2 (Nizani i Fuzúli), *Izvestiya Akademii Nauk SSSR, Moscow*. (in Russian)
- Berza, T., 1994. ALCAPA II field guidebook. *Romanian Journal of Tectonics and Regional Geology* 75 (2), 149 pp.
- Bramlette, M.N., Sullivan, F.R., 1961. Coccolithophorids and related nannoplankton of the early Tertiary in California. *Micropaleontology* 7 (2), 129-188.
- Bukry, D., 1973. Low-latitude coccolith biostratigraphic zonation. *Initial Reports of the Deep Sea Drilling Project* 15, 685-703. doi:10.2973/dsdp.proc.15.116.1973.
- Cande, S.C., Kent, D.V., 1995. Revised calibration of the Geomagnetic Polarity Time Scale for the Late Cretaceous and Cenozoic. *Journal of Geophysical Research* 100 (B4), 6093-6095. doi:10.1029/94JB03098.
- Castradori, D., Rio, D., Hilgen, F.J., Lourens, L.J., 1998. The Global Standard Stratotype-section and Point (GSSP) of the Piacenzian Stage (Middle Pliocene). *Episodes* 21 (2), 88-93.
- Clauzon, G., Suc, J.-P., Popescu, S.-M., Mărunțeanu, M., Rubino, J.-L., Marinescu, F., Melinte, M.C., (2005). Influence of Mediterranean sea-level changes on the Dacic Basin (Eastern Paratethys) during the late Neogene: the Mediterranean Lago Mare facies deciphered. *Basin Research* 17, 437-462. doi:10.1111/j.1365-2117.2005.00269.x.
- Hilgen, F.J., Krijgsman, W., Langereis, C.G., Lourens, L.J., Santarelli, A., Zachariasse, W.J., 1995. Extending the astronomical (polarity) time scale into the Miocene. *Earth and Planetary Science Letters* 136, 495-510. doi:10.1016/0012-821X(95)00207-S.
- Jones, R.W., Simmons, M.D., 1996. A review of the stratigraphy of Eastern Paratethys (Oligocene-Holocene). *Bulletin of the Natural History Museum, London (Geology Series)* 52 (1), 25-49.
- Krejci-Graf, K., 1932. Parallellisierung des südosteuropäischen Pliozäns. *Sonderausgabe der Geologischen Rundschau* 23 (6), 300-339.
- Krijgsman, W., Hilgen, F.J., Raffi, I., Sierro, F.J., Wilson, D.S., 1999. Chronology, causes and progression of the Messinian salinity crisis. *Nature* 400, 652-655. doi:10.1038/23231.
- Laskar, J., 1990. The chaotic motion of the solar system: a numerical estimate of the size of the chaotic zones. *Icarus* 88, 266-291. doi:10.1016/0019-1035(90)90084-M.
- Laskarev, V., 1924. Sur les équivalents du Sarmatien supérieur en Serbie. In: *Recueil de travaux offert à M. Jovan Cvijić par ses amis et collaborateurs*, pp. 73-85.
- Le Play, F., 1842. Formation tertiaire de la steppe pontique. In: *Demidof (Ed.), Voyage dans la Russie méridionale et la Crimée*, St. Petersburg 4, pp. 150-168.
- Lourens, L.J., Antonarakou, A., Hilgen, F.J., Van Hoof, A.A.M., Vergnaud-Grazzini, C., Zachariasse, W.J., 1996. Evaluation of the Plio-Pleistocene astronomical timescale. *Paleoceanography* 11 (4), 391-413. doi:10.1029/96PA01125.



- Marinescu, F., 1990. Le Pannonien, toujours un problème d'actualité? *Geologica Carpathica* 41 (1), 39-48.
- Marinescu, F., MăruŃeanu, M., 1994. Le problème de l'endémisme par rapport à la paléogéographie du Bassin Pannonique. *Annales Universitatis "Babes-Bolyai" Cluj-Napoca*, Sp. no. "The Miocene from the Transylvanian Basin", 355-359.
- Marinescu, F., Papaianopol, I., 1995. Pliozän Pl<sub>1</sub> Dazien. Serie Chronostratigraphie und Neostatotypen, Neogen der Zentrale Paratethys 9. Editura Academiei Române, Bucharest.
- Martini, E., 1971. Standard Tertiary and Quaternary calcareous nannoplankton zonation. In: Farinacci, A. (Ed.), *Proceedings of the 2<sup>nd</sup> International Conference on Planktonic Microfossils*, Roma 1970, 2, Edizioni Tecnoscienza, Rome, pp. 739-785.
- MăruŃeanu, M., 1998. The Meotian nannoplankton study. *Anuarul Institutului Geologic al României* 70, 87-90.
- MăruŃeanu, M., Papaianopol, I., 1995. The connection between the Dacic and Mediterranean Basins based on calcareous nannoplankton assemblages (abstracts of the X<sup>th</sup> RCMNS Congress, Bucharest). *Romanian Journal of Stratigraphy* 76 (Suppl. 7, vol. 1), 169-170.
- MăruŃeanu, M., Papaianopol, I., 1998. Mediterranean calcareous nannoplankton in the Dacic Basin. *Romanian Journal of Stratigraphy* 78, 115-121.
- MăruŃeanu, M., Papaianopol, I., Popescu, G., Olteanu, R., Pestrea, S., MacaleŃ, R., 1998. Studies for Neogene biostratigraphic scale-Muntenian Subcarpathians. *Anuarul Institutului Geologic al României* 70, 108-112.
- MăruŃeanu, M., Papaianopol, I., Popescu, G., Olteanu, R., MacaleŃ, R., Pestrea, S., Petcu, I., 2000. Biostratigraphic studies for the standard scale of the Neogene-Moesian and Moldavian platforms. *Anuarul Institutului Geologic al României* 71, 63-68.
- Motăş, I.C., Marinescu, F., Popescu, G., 1976. Essai sur la Néogène de Roumanie. *Annuaire de l'Institut de Géologie et de Géophysique* 50, 127-147.
- Nagymarosy, A., Müller, P., 1988. Some aspects of Neogene biostratigraphy in the Pannonian Basin. *AAPG Memoir* 45, 69-77.
- Negri, A., Villa, G., 2000. Calcareous nannofossil biostratigraphy, biochronology and paleoecology at the Tortonian/Messinian boundary of the Faneromeni section (Crete). *Palaeogeography, Palaeoclimatology, Palaeoecology* 156, 195-209. doi:10.1016/S0031-0182(99)00140-6.
- Papaianopol, I., Marinescu, F., 1995. Lithostratigraphy and age of Neogene deposits on the Moesian Platform, between Olt and Danube rivers. *Romanian Journal of Stratigraphy* 76, 67-70.
- Papaianopol, I., MăruŃeanu, M., 1993. Biostratigraphy (molluscs and calcareous nannoplankton) of the Sarmatian and Maeotian in eastern Muntenia (Dacic Basin-Romania). *Zemní plyn a nafta* 38 (1), 9-15.
- Papaianopol, I., Dumitrică, P., Olteanu, R., MacaleŃ, R., 1995a. Neogene in the eastern part of the Moesian Platform (Dacic Basin, Romania). *Romanian Journal of Stratigraphy* 76, 71-78.
- Papaianopol, I., Jipa, D., Marinescu, F., Ţicleanu, N., MacaleŃ, R., 1995b. Upper Neogene from the Dacic Basin (guide to excursion B2, X<sup>th</sup> RCMNS Congress, Bucharest). *Romanian Journal of Stratigraphy* 76 (Suppl. 1), 1-45.
- Papaianopol, I., Marinescu, F., MăruŃeanu, M., Krstic, N., MacaleŃ, R., 1999. Pliozän Pl<sub>2</sub> Romanien. Serie Chronostratigraphie und Neostatotypen, Neogen der Zentrale Paratethys 10. Editura Academiei Române, Bucharest.

- Popescu, G., Gheta, N., 1984. Comparative evolution of the marine Middle Miocene calcareous nannofossils from Middle Miocene Carpathian and Pannonian areas. *Dari de Seama ale Sedintelor-Institutul Geologie si Geofizica* 80, 125-133.
- Popescu, S.-M., (2002). Repetitive changes in Early Pliocene vegetation revealed by high-resolution pollen analysis: revised cyclostratigraphy of southwestern Romania. *Review of Palaeobotany and Palynology* 120, 181-202. doi:10.1016/S0034-6667(01)00142-7.
- Popov, S.V., Goncharova, I.A., Kozyrenko, T.F., Radionova, E.P., Pevzner, M.A., Sychevskaya, E.K., Trubikhin, V.M., Zhegallo, V.I., 1996. Neogene stratigraphy and palaeontology of the Taman and Kerch peninsulas (excursion guidebook). Palaeontological Institute RAS, Moscow, 32 pp.
- Rabăgia, T., Mațenco, L., 1999. Tertiary tectonic and sedimentological evolution of the South Carpathians foredeep: tectonic vs eustatic control. *Marine and Petroleum Geology* 16, 719-740. doi:10.1016/S0264-8172(99)00045-8.
- Rădan, S.C., 2000. Magnetostratigraphic constraints on the coal bed codification; errors found. *Proceedings of the Romanian Academy, Series B*, vol. 2 (3), pp. 239-243.
- Rădan, S.C., 2002. The Earth's magnetic palaeofield in Tertiary, in magnetostratigraphic context; a brief review of two geomagnetic polarity records recovered from Neogene sedimentary sequences. *Proceedings of the Romanian Academy, Series B*, vol. 4 (1), pp. 33-39.
- Rădan, S.C., Rădan, M., 1998. Study of the geomagnetic field structure in the Tertiary in the context of magnetostratigraphic scale elaboration. I-The Pliocene. *Anuarul Institutului Geologic al României* 70, 215-231.
- Raffi, I., Rio, D., d'Atri, A., Fornaciari, E., Rochetti, S., 1995. Quantitative distribution patterns and biomagnetostratigraphy of middle and late Miocene calcareous nannofossils from equatorial Indian and Pacific Oceans (Legs 115, 130 and 138). *Proceedings of the Ocean Drilling Program, Scientific Results* 138, 479-502. doi:10.2973/odp.proc.sr.138.125.1995.
- Raffi, I., Backman, J., Rio, D., 1998. Evolutionary trends of tropical calcareous nannofossils in the late Neogene. *Marine Micropaleontology* 35, 17-41. doi:10.1016/S0377-8398(98)00014-0.
- Rio, D., Fornaciari, E., Raffi, I., 1990. Late Oligocene through early Pleistocene calcareous nannofossils from western equatorial Indian Ocean (Leg 115). *Proceedings of the Ocean Drilling Program, Scientific Results* 115, 175-235. doi:10.2973/odp.proc.sr.115.152.1990.
- Rögl, F., Daxner-Höck, G., 1996. Late Miocene Paratethys correlations. In: Bernor, R.L., Fahlbusch, V., Mittmann, H.-W. (Eds.), *The evolution of Western Eurasian Neogene mammal faunas*, Columbia University Press, New York, pp. 47-55.
- Rögl, F., Bernor, R.L., Dermitzakis, M.D., Müller, C., Stancheva, M., 1991. On the Pontian correlation in the Aegean (Aegina Island). *Newsletters in Stratigraphy* 24, 137-158.
- Rusu, A., 1985. Oligocene events in Transylvania (Roumania) and the first separation of Paratethys. *Dari de Seama ale Sedintelor-Institutul Geologie si Geofizica (Tectonica si Geologie Regionala)* 72-73 (5), 207-233.
- Semenenko, V.N., 1989. Problems of the Pliocene correlation of East Paratethys and Tethys. *Geologica Carpathica* 40 (1), 75-79.
- Semenenko, V.N., Pevzner, M.A., 1979. Upper Miocene-Pliocene correlation of the Ponto-Caspian on biostratigraphic and paleomagnetic data. *Izvestiya Akademii Nauk SSSR, Seriya Geologicheskaya* 9, Moscow, 5-15.
- Steininger, F.F., Papp, A., 1979. Current biostratigraphic and radiometric correlations of Late Miocene Central Paratethys stages (Sarmatian s.str., Pannonian s.str., and Pontian) and

- Mediterranean stages (Tortonian and Messinian) and the Messinian Event in the Paratethys. *Newsletters on Stratigraphy* 8 (2), 100-110.
- Steininger, F.F., Berggren, W.A., Kent, D.V., Bernor, R.L., Sen, S., Agustí, J., 1996. Circum-Mediterranean Neogene (Miocene and Pliocene) marine-continental chronologic correlations of European mammal units. In: Bernor, R.L., Fahlbusch, V., Mittmann, H.-W. (Eds.), *The evolution of Western Eurasian Neogene mammal faunas*, Columbia University Press, New York, pp. 7-46.
- Stevanović, P.M., Neveškaja, L.A., Marinescu, F., Sokac, A., Jámbor, A., 1990. Pontien-Pl<sub>1</sub> (sensu F. Le Play, N.P. Barbot de Marny, N.I. Andrusov). *Serie Chronostratigraphie und Neostatotypen, Neogen der Westlichen ("Zentrale") Paratethys* 8. JAZU and SANU, Zagreb-Belgrade.
- Teisseyre, W., 1907. *Stratigraphie des régions pétrolifères de la Roumanie et les contrées avoisinantes*. *Congres International du Pétrol, III-me session, Bucharest*, pp. 18-44.
- Van Couvering, J.A., Castradori, D., Cita, M.B., Hilgen, F.J., Rio, D., 2000. The base of the Zanclean Stage and of the Pliocene Series. *Episodes* 23 (3), 179-187.
- Van Vugt, N., Langereis, C.G., Hilgen, F.J., 2001. Orbital forcing in Pliocene-Pleistocene Mediterranean lacustrine deposits: dominant expression of eccentricity versus precession. *Palaeogeography, Palaeoclimatology, Palaeoecology* 172 (3-4), 193-205. doi:10.1016/S0031-0182(01)00270-X.
- Zijderveld, J.D.A., 1967. A.c. demagnetization of rocks: analysis of results. In: Collinson, D.W., Creer, K.M., Runcorn, S.K. (Eds.), *Methods in palaeomagnetism*. Elsevier, Amsterdam, pp. 254-286.



# **Calcareous nannofossil biostratigraphy and magnetostratigraphy of the upper Miocene and lower Pliocene of the Northern Aegean (Orphanic Gulf-Strimon Basin areas), Greece**

---

This chapter is published as: Snel, E., MăruŃteanu, M., Meulenkamp, J.E., 2006. Calcareous nannofossil biostratigraphy and magnetostratigraphy of the Upper Miocene and Lower Pliocene of the Northern Aegean (Orphanic Gulf-Strimon Basin areas), Greece. *Palaeogeography, Palaeoclimatology, Palaeoecology* 238, 125-150. doi:10.1016/j.palaeo.2006.03.022.

## **Abstract**

The transitional position of the Northern Aegean makes it an important area for studying the relation between the Mediterranean and the Eastern Paratethys. A chronostratigraphic framework has been obtained for the late Neogene deposits along the Orphanic Gulf and in the Strimon Basin of northern Greece by analysing calcareous nannofossil data and paleomagnetic results from eight sections. The local formations and major lithological units have been correlated with the Late Miocene and Early Pliocene stages. Furthermore, the obtained framework has facilitated a more detailed reconstruction of the effects of the Messinian salinity crisis on the sedimentary record.

Magnetostratigraphic data from the Strimon Basin result in an age estimate of 6.3 Ma for the Dafni-Choumnikon Formation transition, between normal polarity subchrons C3An.2n and C3An.1n. Since this Late Miocene age estimate corresponds closely to estimates of the Maeotian-Pontian boundary in the Eastern Paratethys (Dacic Basin), we believe this transition from marine to brackish conditions corresponds to this latter boundary. The gypsiferous unit in the basal part of the Choumnikon-equivalent beds along the Orphanic Gulf can then be correlated with the evaporites in the Northern Aegean and the Lower Evaporites of the Mediterranean Basin. Consequently, we assume that these Northern Aegean evaporites have been deposited between 5.96 and 5.59 Ma.

Freshwater deposits above the evaporites are easily traceable across the Orphanic Gulf area, as a gravel or sandstone unit topped by a travertine marker bed, and have a wide lateral continuation. Since their position is intermediate between the shallow marine gypsum/anhydrite and the more open marine clastics of the Pliocene, we argue that these beds correlate with the desiccation phase of the Mediterranean and Black Sea basins. This intra-Messinian event probably occurred between 5.59 and 5.50 Ma, thus predating the Upper Evaporites or Lago Mare of the Mediterranean.

A clear recognition of the Miocene-Pliocene boundary remains problematic in the Orphanic Gulf area. Nannofossil assemblages in the sections suggest a higher position of the local base of the Pliocene than indicated by the level with the first appearance of planktonic and benthic foraminifera. Discontinuous occurrences of levels containing nannofossil assemblages of Zone MNN11b-c are found between the travertine unit and the lowermost Pliocene beds, representing

brief marine ingressions. The latter show that in the latest Messinian, (presumably) temporary connections of Atlantic/Mediterranean waters with the Northern Aegean Basin existed. These marine ingressions likely extended further into the Eastern Paratethys, as demonstrated by the presence of nannofossil assemblages in the middle and upper Pontian of the Dacic and Euxinic basins. The events around the Miocene-Pliocene transition resulted in an abrupt change from brackish to open marine conditions in a relative deep basin that was subject to increased rates of subsidence from the onset of evaporite deposition in the late Messinian onward.

### 3.1 Introduction

During the late Neogene, the connection between the Atlantic Ocean and the Paratethys via the Mediterranean Sea was restricted and periodically interrupted. This prevents straightforward bio- and chronostratigraphic correlations between the Mediterranean and the Paratethys realms. Marine and brackish faunas in the Miocene and Pliocene successions of the Northern Aegean (the Orphanic Gulf area and the Strimon Basin in northern Greece; Fig. 3.1) show the influence of both the Mediterranean and the Paratethys realm on the palaeoenvironment of this sedimentary domain (Gramann and Kockel, 1969; Papp and Steininger, 1979; Steffens et al., 1979; Stevanović et al., 1990, pp. 340-352; Syrides, 1998; Popov and Nevesskaya, 2000). Apparently, this part of the Northern Aegean served as an intermediate basin linking both water masses. Therefore, the Orphanic Gulf-Strimon Basin area is a key area for studies of aquatic connections and faunal exchanges between the Mediterranean and the Paratethys.

The relation of observed evaporites, i.e. the gypsum of the Orphanic Gulf area (Meulenkamp, 1979) and anhydrite with halite found in offshore drillings near the island of Thasos (Pollak, 1979; Proedrou, 1979), with the Messinian salinity crisis is not clearly demonstrated (Rögl et al., 1991), because of inaccurate dating of these deposits. Furthermore, the effect and timing of the desiccation event in the Mediterranean and Black Sea basins is still subject of debate (Clauzon et al., 1996; Krijgsman et al., 1999; Roveri et al., 2001; Clauzon et al., 2005).

This study aims to provide an age model for the various sections and outcrops within the Orphanic Gulf-Strimon Basin area by correlating these with the sequence of Mediterranean and Paratethys stages. For this purpose, several sections in the coastal area of the Orphanic Gulf and on both sides of the river Strimon have been sampled. The calcareous nannofossil content of all sections has been analysed qualitatively; from two sections, a magnetic polarity record was obtained. The resulting chronostratigraphic framework will be used to link bio- and lithostratigraphic observations from the Orphanic Gulf area and the Strimon Basin with events in the Mediterranean and the Eastern Paratethys.

### 3.2 Geological setting and stratigraphy

The contours of the present-day Orphanic Gulf-Strimon Basin area (Fig. 3.1) were formed during the Late Pliocene in response to strike-slip movements in the North Aegean trough, along a splay of the North Anatolian Fault (Dinter and Royden, 1993; Dinter, 1998). This relatively recent extensional deformation resulted in a series of North Aegean basins with Late Pliocene and younger infill and was superimposed on the effects of extension along a shear zone at the northern margin of the Aegean Sea during the Middle Miocene to Early Pliocene. This earlier deformation,

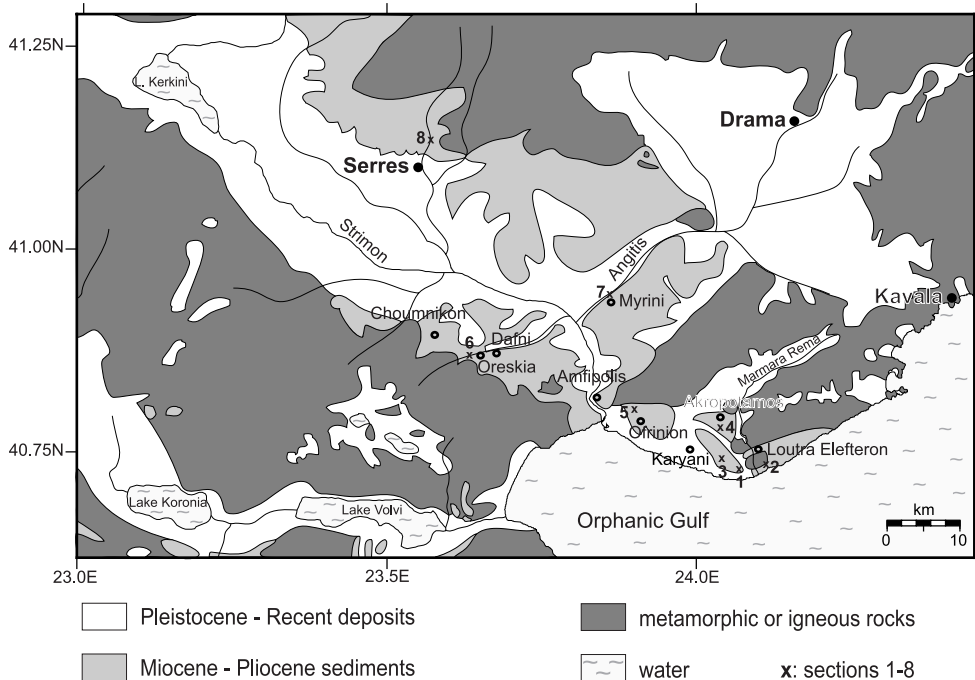
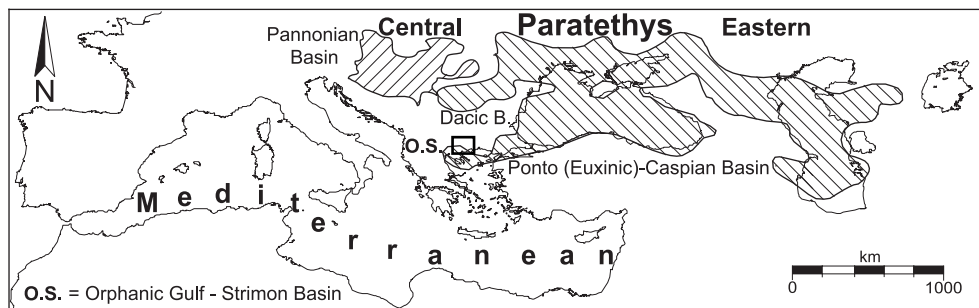
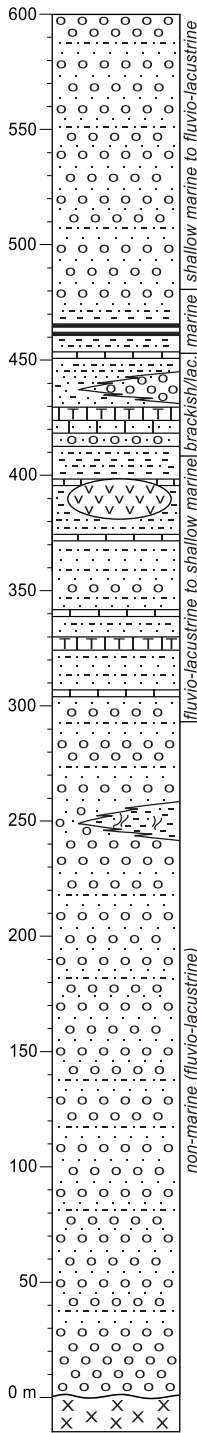


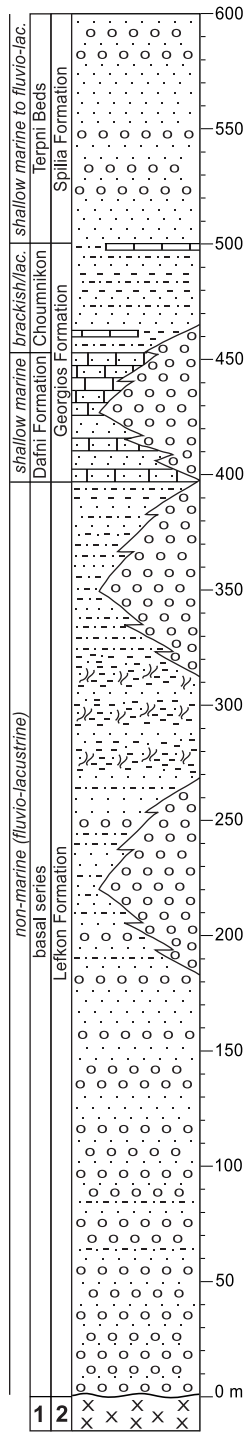
Figure 3.1. Simplified geological map of the Orphanic Gulf and Strimon Basin areas (after Bornovas and Rondogianni-Tsiambaou, 1983) showing the locations of sections Kavala Road West (1), Kavala Road East (2), “Rema Marmara” (3), Akropotamos (4), Ofrinion (5), Eziovis Rema (6), Myrini (7), and Labyrinthos (8). Inset map shows the palaeogeography of the Paratethys region during the Late Miocene, superimposed on present-day geography, with location of the Orphanic Gulf-Strimon Basin. Modified after Steininger and Papp (1979).

on a larger scale related to extension in the back-arc of the Hellenic subduction zone, created the accommodation space for the older Neogene sediments. For reasons of convenience, the terms Orphanic Gulf and Strimon Basin are used, rather than the various (local) names for the presently peripheral basins in these areas, such as the Akropotamos, Pieria, and Strymonikos basins, or the Angitis and Serres basins, respectively (Psilovikos and Syrides, 1983; Karistineos and Georgiades-Dikeoulia, 1986; Dermitzakis et al., 1986).




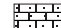

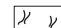
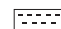
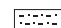
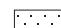
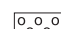
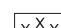
# Orphanic Gulf



# Strimon Basin



### legend:

-  evaporite
-  sapropels
-  limestone
-  sandstone
-  travertine
-  lignite, or palaeo-sol
-  clay
-  silt
-  sand
-  breccia, or gravel
-  basement

1: Gramann and Kockel (1969)

2: Armour-Brown et al. (1979)



*Figure 3.2.* Composite stratigraphic columns and interpretation in terms of general depositional environments for the Neogene of the Orphanic Gulf and Strimon Basin areas. Modified after Gramann and Kockel (1969), Armour-Brown et al. (1979), Steffens et al. (1979), Psilovikos and Syrides (1983), and Popov and Neveeskaya (2000).

Miocene and Pliocene deposits are exposed on both sides of the river Strimon and east of its mouth along the Orphanic Gulf coast (Fig. 3.1). In the latter area approximately 300 m of fluvio-lacustrine conglomerates, sands, and occasionally clays with lignite intercalations constitute the lower part of the Neogene sequence (Fig. 3.2). They are followed by alternating clastics and carbonates, reflecting lacustrine, brackish water, or shallow marine conditions. In the relatively open marine sandy or silty clays above (370–410 m), locally lenticular gypsum bodies occur that underlie lacustrine and brackish beds containing Pontian age ostracodes (Meulenkamp, 1979; Steffens et al., 1979). These well-bedded strata are covered by a conglomerate or sandstone unit, with on top freshwater limestones and travertines, followed by brackish water clastics. The overlying open marine clastics and sapropel-marl alternations (from 450 m upwards) were reported to be of earliest Pliocene age (Steffens et al., 1979). Finally, uplifted shallow marine sands and gravels of the last, Late Pliocene-Pleistocene, marine series in the Orphanic Gulf area unconformably cover the tilted and disrupted sediments of the previous, Late Miocene-Early Pliocene marine cycle (Psilovikos and Syrides, 1983; Dinter and Royden, 1993).

The sequences of coarse clastics exposed along the river Strimon and near the city of Serres, resemble those of the Orphanic Gulf area. They pass upwards into sands and clayey lignites, locally interrupted by conglomerates and breccias of basement rocks, and are collectively referred to as basal series or Lefkon Formation (Fig. 3.2; Gramann and Kockel, 1969; Armour-Brown et al., 1979). The oldest marine beds above this fluvio-lacustrine basal part constitute the Dafni Formation. This marine unit, containing sands, sandstones, and (coral) limestones, has been regarded by these authors to be the equivalent of sediments of the Eastern Paratethys assignable to the Maeotian. The overlying Choumnikon beds are mainly brackish water sand, silt, and clay deposits, which contain mollusc and ostracod associations of (early) Pontian age. In the northern part of the basin, near Serres, these marine and brackish successions (Georgios Formation of Armour-Brown et al., 1979) contain granite breccia interbeds. There, these (partly) tilted and folded upper Miocene beds are unconformably covered by lower Pliocene fluvio-lacustrine, locally shallow marine (Popov and Neveeskaya, 2000), sand and gravel successions of the Spilia Formation. The Terpni beds comprise the equivalent of this formation along the river Strimon.

### 3.3 Sections and sampling

A selection of the sections described by Gramann and Kockel (1969) and Armour-Brown et al. (1979), in the Strimon Basin, and of those described by Steffens et al. (1979), Psilovikos and Syrides (1983) and Syrides (1998), in the Orphanic Gulf area, was sampled for this study. Many localities, especially the sites documented by Gramann and Kockel (1969), were severely weathered or overgrown with vegetation. The eight sections that yielded (age-diagnostic) calcareous nannofossils, or conclusive paleomagnetic results, will be presented here.

### 3.3.1 Kavala Road West

Steffens et al. (1979) recorded a section along the north side of the coastal Thessaloniki-Kavala highway (E90), under construction at that time, between the mouth of the river Strimon and the town of Kavala. The exact location is 5 km east of the Karyani village traffic lights, 3 km east of section “Rema Marmara”, 4 km west of the Marmara Rema-bridge (at the turn-off to Loutra Elefteron), and 5.5 km west of section Kavala Road East (section 1; Fig. 3.1). Outcrops along the road are presently limited to 50 m of the lower 100 m of the original section. On the hill slopes within 100 m off the road, more and fresher outcrops are exposed. Overlying a series of sands and conglomerates, they constitute a continuous section of approximately 177 m (Fig. 3.3a). The lower 90 m consist of conglomerates and red, sandy palaeo-sols at the base, followed by fluvio-lacustrine sands, clays, limestones, and travertinous limestones (samples ST 60-65), containing many levels with freshwater molluscs and ostracodes. One bed with oysters (at 65 m) indicates that occasionally brackish to shallow marine conditions occurred. Marine influence is supported by the presence of *Scaphopoda* and *Ditrupa* in a thick calcareous bed at 97 m (sample ST 66). The overlying finely bedded silts and sands also contain fragments of these invertebrates (samples ST 67-69). The limestone forms an east facing dip-slope, extending towards the top of the still existing outcrops along the road. Samples 70-72 were taken from an 18 m thick succession of laminated silts and clays that are, in the lower part of the succession, alternating with platy limestones, and contain brackish water molluscs. In the upper part, the silts and clays are folded because of slumping. On top, forming a second dip-slope, lies a massive conglomerate, sandstone, and travertine bed that is also exposed in the base of the next hill to the east. This non-marine bed is covered by 6 m of partially calcified sands, followed by 36 m of marine clayey marls that alternate with a few sandy limestone beds and a regular series of sapropels. Of samples ST 73-75, recovered from the lower part of these marls, ST 74 and especially ST 75 contain abundant benthic and planktonic foraminifera (without index species, however). The marls, grading upward into sands, end with a gravel deposit. These uppermost 45 m of the present-day section, constituting the lower part of a previously excellently exposed sequence, were sampled by Steffens et al. (1979; samples Gr 395-430) during road construction and interpreted as lower Pliocene.

### 3.3.2 Kavala Road East

At km 124 along the same road to Kavala, 5.5 km east of section Kavala Road West, a 72 m thick, predominantly sandy section with gypsum/anhydrite was recorded on the northern side (section 2; Figs. 3.1 and 3.3a). The upper half of the succession is also partly exposed in less weathered outcrops along the track towards the beach below the road. Intercalated between 9 m and 21 m in the well-bedded sands, limestones, and conglomerates are four sandy palaeo-sols, indicative of non-marine conditions. Sample ST 59 was taken from laminated clays and sands below the first gypsum bed in an outcrop below the south side of the road. Eastward, along the beach, the sequence ends with conglomerate beds and travertine deposits on top.

### 3.3.3 “Rema Marmara”

This is a misleading name (Steffens et al., 1979; De Bruijn, 1989) for the discontinuous section exposed along a gravel road on the bed of a small, unnamed stream, south of the village of Akropotamos and 7 km west of the bridge over the real Marmara Rema (section 3; Fig. 3.1). Neogene deposits of several hundreds of metres, including a basal conglomerate series overlying the granite basement, are at present only partly exposed. A composite section, showing three exposed intervals (subsections I, II, and III; Fig. 3.3a), was recorded above the conglomerates.

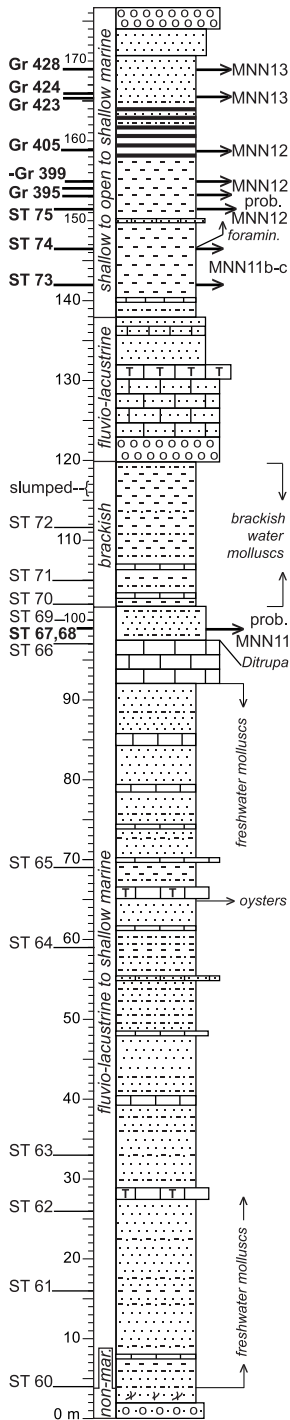
The lower subsection (I), 1 km north from the main road to Kavala, consists of 15 m of lacustrine clays and sands with mollusc lags. In these beds, De Bruijn (1989) found a small rodent fauna suggesting a middle Turolian age (MN 12), which is approximately time-equivalent with the late Tortonian (about 8 to 7 Ma; Steininger et al., 1996). After an unexposed interval of 18 m, the succession continues with 6 m of sands and marls, containing *Unio* fragments and a 3 m thick *Ditrupa*-bearing shallow marine sand and carbonate bed at the top (samples ST 54-58). These beds are strongly sheared due to extensional block rotations (Dinter, 1998). Beyond a water basin, 250 m upstream, subsection II is exposed. The variable orientation of the bedding and the many faults hamper a reliable estimation of the thickness of the unexposed beds between subsections I and II. Outcrops in the lower part of subsection II consist of 15 m of sandstone and travertine with sand intercalations and a lag-deposit with *Planorbis* at the base. In scattered outcrops of the overlying laminated sandy clays, samples ST 35-39 were collected along a right tributary of the dry stream. Samples ST 40-42 were taken from a 20 m thick sand and conglomerate unit in the uppermost outcrops in this side valley. The well-bedded sands, alternating with sandstones and silts, contain a few levels with brackish water molluscs and oysters.

Sampling was continued in subsection III along the main stream. Approximately 150 m upstream of the calcareous base of subsection II, a 10 m thick sand and gravel series covering the first silty clay bed (sample ST 43), is encountered on the western side of the valley. Directly above this coarse clastic unit, further up the slope, a thin limestone bed underlies 8 m of silts and clays with rich and diversified benthic and planktonic foraminiferal associations (samples ST 44-46). Samples ST 47-53 were collected from a 20 m thick series of thin-bedded silts and clays, alternating with sapropels, limestones, sands, and sandstones exposed 100 m upstream on the bottom of the valley. Steffens et al. (1979) described the strata from the same interval (samples Gr 1583-1585), presented here as subsection III, and interpreted them as a series of brackish beds containing ostracodes indicative of the Pontian, immediately followed by open marine clays with Early Pliocene foraminifera. Succession III ends with a coarsening upward sand and gravel unit, showing metre-scale slumps near the top. The position of the top of subsection II with respect to the base of subsection III is unclear, but the lithological differences between the two units exclude the probability of an overlap of more than ten metres.

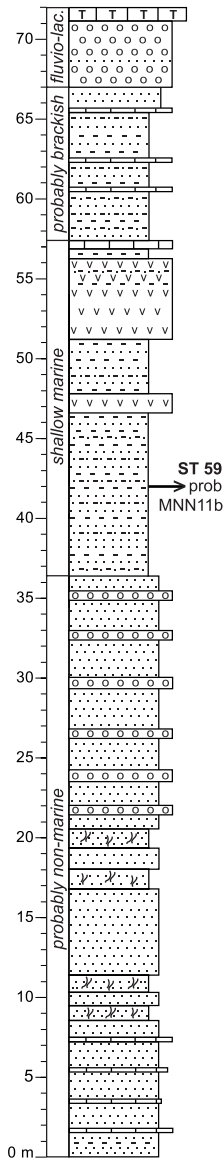
### 3.3.4 Akropotamos

South of this village, several outcrops of Neogene sediments can be observed (section 4; Fig. 3.1). These sediments unconformably overlie the faulted limestone basement. The strata are often severely disturbed by normal faulting (Dinter, 1998), thereby preventing the recording of a long continuous section. Steffens et al. (1979) described hundreds of metres of fluvial to shallow marine fine-grained clastics and conglomerates in the basal part of the Neogene. Thin-bedded clays and sands also contain leaf and fish fossils, while in the uppermost part oysters, *Pecten* and calcareous nannofossils belonging to Zone NN11 or higher occur (Steffens et al., 1979). In a small outcrop above this marine level (sample Gr 440), the top of the basal subsection (I) is presently represented by 5 m of conglomerate, silt, and limestone (Fig. 3.3b). These beds are overlain by a second, 40 m thick subsection (II), which is exposed in an adjacent, new quarry 1.5 km south of the village. It consists of gypsum, with on top a calcareous bed containing *Ditrupa*, limestone beds, and silty clays with sandstones and travertine deposits in the uppermost part. Samples ST 1-19 have been taken from a laterally identical succession, in an old quarry 500 m to the northeast. Dermitzakis et al. (1986) studied marine bivalves and lagoonal fish remains from the beds above the evaporites and correlated subsection II of section Akropotamos with the Messinian. Above

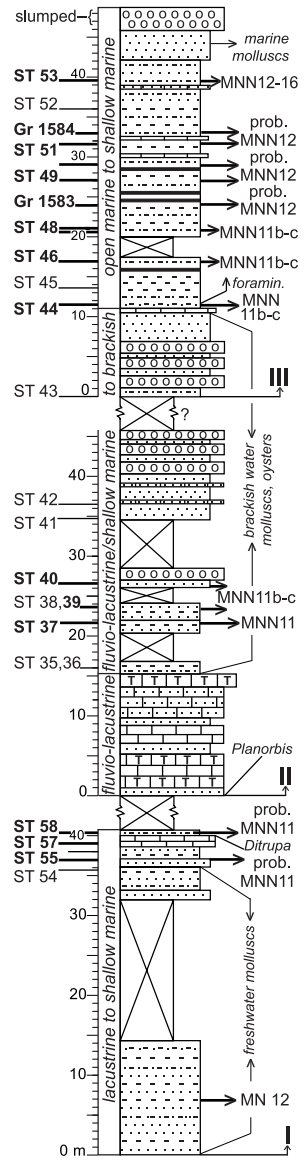
### Kavala Road West (1)



### Kavala Road East (2)



### "Rema Marmara" (3)



legend:

	limestone		clay		massflow
	diatomite		sandstone		silt
	evaporite		travertine		sand
	sapropels		palaeo-sol		basement
			gravel		not exposed
					nannofossil or micromammal-level

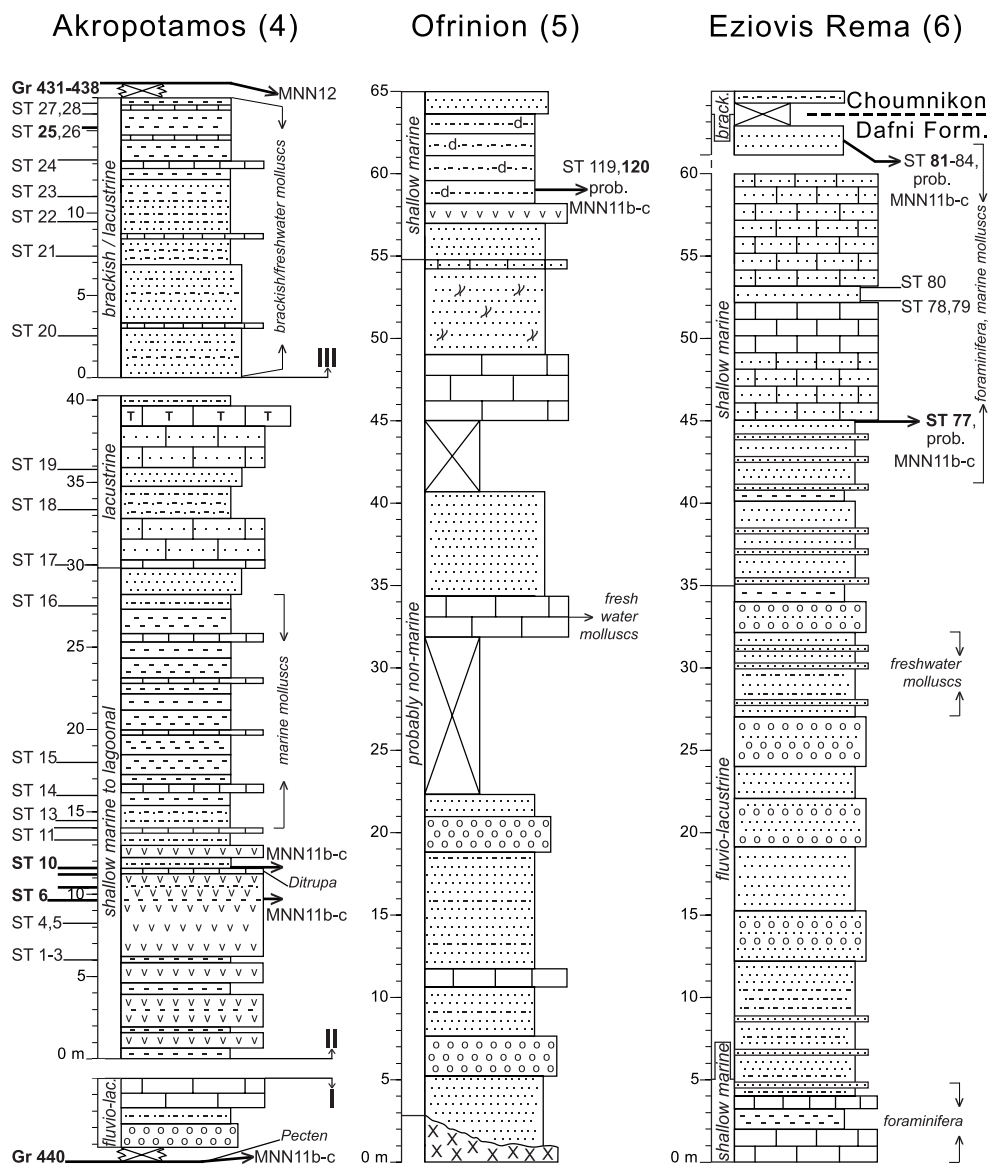


Figure 3.3. Lithology, depositional environment, position of samples, fossil content, and calcareous nannofossil zonal assignments of the (composite) sections of (a): Kavala Road West (1), Kavala Road East (2), and “Rema Marmara” (3), and (b): Akropotamos (4), Ofrinion (5), and Eziovis Rema (6). Sections (1) and (3) are based on Steffens et al. (1979) and on our own observations; Section (4): modified after Dermitzakis et al. (1986) and based on Steffens et al. (1979) and on our own observations; Section (6): based on Gramann and Kockel (1969) and on our own observations. Bold sample codes and arrows with interpreted MNN-zone indicate levels with calcareous nannofossils.

*Figure 3.4.* Magnetostratigraphy of sections Myrini (7) and Labyrinthos (8), Strimon Basin. Lithology, mollusc content, depositional environment, paleomagnetic results, interpreted polarity zones, and thermal demagnetization diagrams of selected samples. For legend, see Figure 3.3; stratigraphy and mollusc content of the schematic section Labyrinthos are based on Gramann and Kockel (1969), on Popov and Neveeskaya (2000), and on our own observations. Paleomagnetic results (from samples LA 1-55 and MY 1-20) are interpreted as virtual geomagnetic polar (VGP) latitude. (Open) solid circles denote (less) reliable ChRM directions; plusses are used for inconclusive results. In the polarity column black (white) denotes normal (reversed) polarity, grey indicates undetermined polarity; crossed intervals are used for those parts of the section where no samples were taken.

*Demagnetization diagrams* denote orthogonal projections of NRM vector end-points, after tectonic correction, with open (solid) symbols on the vertical (horizontal) plane; values represent temperature increments in °C; best-fit lines indicate interpreted polarity directions. Stratigraphic levels and sample numbers are in the lower and upper left corners, respectively. Bold sample codes and arrows with interpreted MNN-zone indicate levels with calcareous nannofossils.

the sandstone and travertine beds, samples ST 20-28 from a third, 61 m thick subsection (III, of which only the well-exposed lower 17 m are shown in Figure 3.3b) of alternating laminated fluvio-lacustrine clays, silts, sands, and limestones contain brackish and freshwater ostracodes and molluscs. Calcareous nannofossils, belonging to Zone NN12 and indicating an Early Pliocene age, were reported by Steffens et al. (1979) from still younger, marine clastic units closer to the village (samples Gr 431-438). These beds are at present poorly exposed.

### 3.3.5 Ofrinion

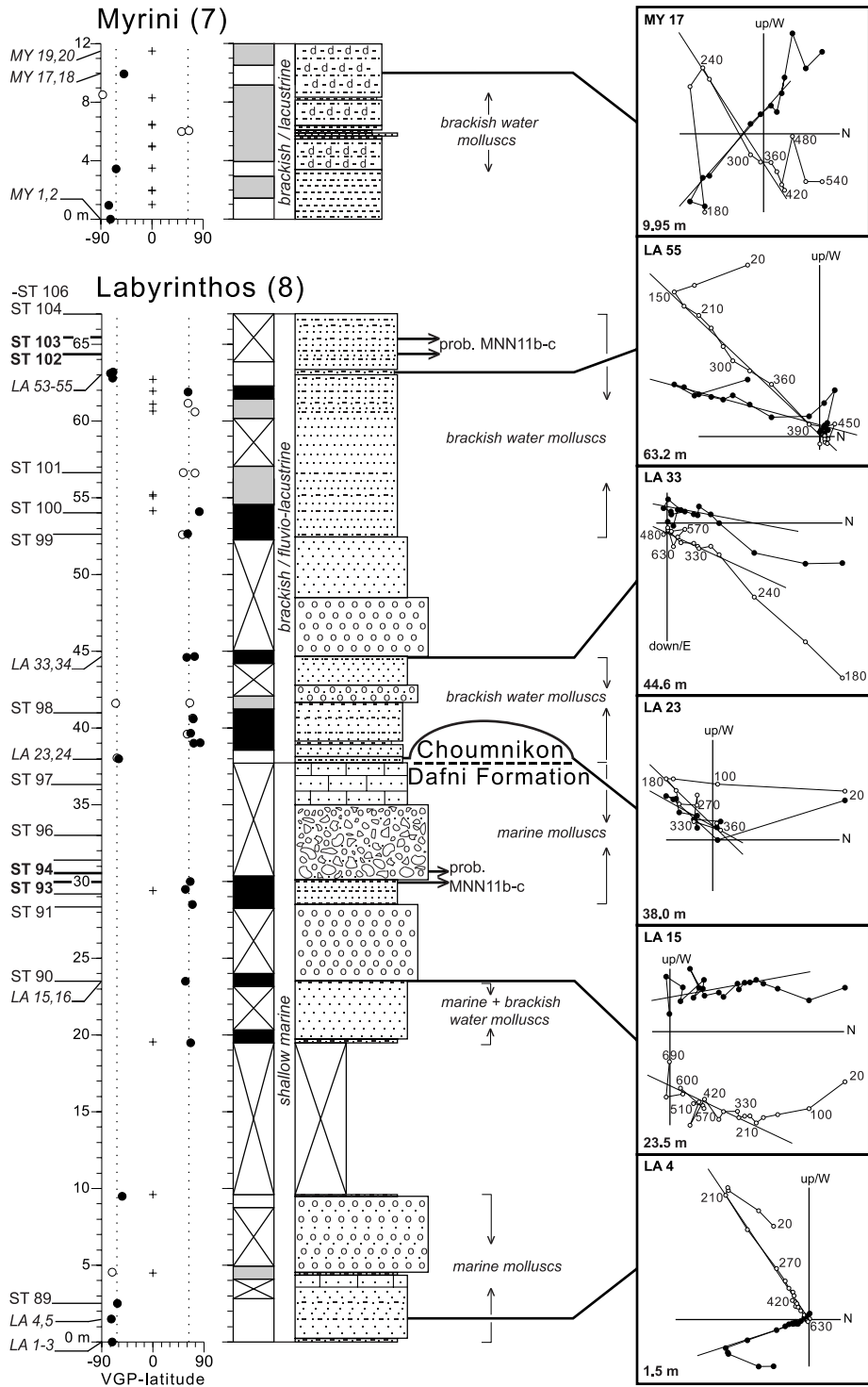
Other scattered outcrops of gypsum are found north of the village of Ofrinion (or Ophrynio; Psilovikos and Syrides, 1983), near the margin of the basin (section 5; Fig. 3.1). There, the lower part of the poorly exposed Neogene succession is separated from the crystalline basement by normal faults. The succession, presented as an idealized section of at least 65 m (Fig. 3.3b), consists of a probably non-marine part with conglomerate, sand, (travertinous) limestone beds, and sandy palaeo-sols, followed upwards by a shallow marine part with gypsum/anhydrite and laminated, diatomaceous limestones, alternating with thin clay and sand beds (samples ST 119 and 120), and overlain by sands.

### 3.3.6 Eziovis Rema

West of Oreskia, Gramann and Kockel (1969; their profile 4) recorded a section in the Dafni beds on the northern bank of this stream (section 6; Figs. 3.1 and 3.3b). They described a succession of 60 m of marine sands and sandy limestones (samples ST 77-80), with a non-marine clastic intercalation between 5 and 35 m. On top of the southern bank of the stream, near the village entrance, two metres of sands with *Pecten* and oysters are exposed (samples ST 81-84). These beds represent the uppermost part of the Dafni Formation, and are followed by brackish marls and sands of the Chournikon beds.

### 3.3.7 Myrini

A new quarry, 1 km north of this village, is situated at the location of profile 62 of Gramann and Kockel (1969) on the south side of the bridge of the Serres-Amfipolis road across the river Angitis (section 7; Fig. 3.1). In the quarry at the foot of a hill, a section of 12 m with diatomaceous clays and silts was recorded (Fig. 3.4). These sediments form a part of the Chournikon Formation (Gramann and Kockel, 1969) and are rich in brackish water molluscs, ostracodes, diatoms, and



fish remains. On top of the hill, 20 m above the rear wall of the quarry, shallow marine gravels and sands with *Pecten* and oysters, still attached to the limestone cobbles, unconformably overlie the laminated brackish water deposits (pers. comm. G. Syrides, 2000). The beds of the Choumnikon Formation, dipping 15°SE, are intersected by listric normal faults. Samples MY 1-20, for magnetostratigraphy, were taken every 1-2 m.

### 3.3.8 Labyrinthos

A section in this valley northeast of Serres (section 8; Fig. 3.1) was recorded by Gramann and Kockel (1969; profile 31) and revisited by Karistineos and Georgiades-Dikeoulia (1986), by Syrides (1998: Perdikari locality), and by Popov and Neveeskaya (2000). The record originally documented by Gramann and Kockel measured 170 m, including an unexposed interval between 70 and 140 m. Their section covered marine sands, sandy limestones, and gravels of the Dafni beds, followed by brackish clays, sands, and (in the lower part) gravel beds of the Choumnikon Formation, which contain ostracodes and molluscs characteristic of the Pontian. Popov and Neveeskaya (2000) included the overlying Pliocene Spilia Formation in their study of the Neogene. This unit starts with marine clays including oysters, followed by fluvio-lacustrine sands and conglomerates. Unlike Popov and Neveeskaya (2000), who adopted the older subdivision of Dafni and Choumnikon Formation, Karistineos and Georgiades-Dikeoulia (1986) correlated the generically equivalent Georgios Formation with the sediments supposed to reflect the Early Pliocene transgression. This interpretation was based on the presence of *Pecten benedictus* in the middle part of the Georgios Formation (or the top of the Dafni beds) in section Labyrinthos.

The 30°-36°NE-dipping beds of section Labyrinthos were sampled for bio- and magnetostratigraphy (samples ST 89-106 and LA 1-55; Fig. 3.4). The basal and middle parts of the Dafni Formation, as well as the interval straddling the Choumnikon-Spilia transition (not shown), are poorly exposed at present and were not sampled. In addition, the interval containing the Dafni-Choumnikon transition is poorly visible, making the field determination of its exact position uncertain. The position of this last formation boundary was therefore adopted from Gramann and Kockel (1969).

## 3.4 Magnetostratigraphy

### 3.4.1 Method

Two oriented cores per sample level were taken with a water-cooled, generator-powered electric drill and oriented with respect to the present-day north with a magnetic compass. The samples from the fresh-cut sediment surface were sawn into ~10.5 cm<sup>3</sup> specimens at the laboratory.

The natural remanent magnetization (NRM) of the specimens was thermally demagnetized by progressive heating in a magnetically shielded, laboratory-built furnace with temperature steps of 30°-50°C, up to a maximum of 700°C. At least one specimen per sample level was measured on a 2G Enterprises horizontal DC SQUID magnetometer to obtain a magnetic polarity record.

### 3.4.2 Results

The samples from section Kavala Road West, taken from levels between 135 m and 165 m, and those recovered from subsection III of section “Rema Marmara” appeared to be strongly weathered and proved useless for magnetostratigraphic interpretations. In sections Myrini and Labyrinthos thermal demagnetization diagrams (Zijderveld, 1967) yielded in general straightforward results



(Fig. 3.4). In a number of specimens, low-temperature components, often parallel to the direction of the present-day field before bedding plane correction, were removed at 100°–240°C (e.g., samples LA 4, 23, and 55; Fig. 3.4). These were considered secondary signals, either laboratory-induced or recent overprints caused by weathering. Both normal and reversed magnetic field components, interpreted as primary, characteristic remanent magnetization (ChRM) directions, were gradually removed at higher temperatures, varying from 360°C to over 600°C. Specimens from section Myrini and from the upper 10 m of section Labyrinthos gave occasionally inconclusive results. The ChRM was determined by best-fit lines through the NRM vector end-points for a representative temperature interval.

The results are presented in two polarity columns (Fig. 3.4). Despite the fresh outcrops of clays and silts in the quarry of Myrini, only four levels yielded useful magnetic results. Counter-clockwise rotation, probably associated with listric faulting, affected the reversed polarity signal considerably (sample MY 17). A slightly better record with four polarity reversals was obtained from thin clay and silt beds between the coarse sands and gravels of section Labyrinthos. Two discontinuous intervals of normal polarity are interpreted: from 19 m to 30 m and from 39 m to 62 m, respectively, separated by an interval without samples and a level with reversed polarity at 38 m. The Dafni–Choumnikon transition, at 37.7 m after Gramann and Kockel (1969), corresponds to the end of an interval without samples, just below this reversed polarity level.

## 3.5 Calcareous nannofossils

### 3.5.1 Method

Samples were cut and rinsed to remove the weathered surface and to prevent contamination. Standard preparation techniques of Bramlette and Sullivan (1961) have been followed, supplemented by filtering the samples with a 36- $\mu\text{m}$  sieve. Smear slides were examined with a light microscope using transmitted and cross-polarized light at 1250 $\times$  magnification.

### 3.5.2 Results

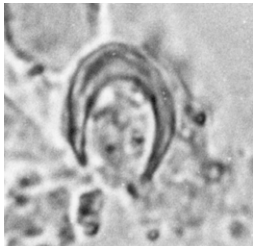
In most sections, with the positive exception of the relatively rich, upper parts of sections Kavala Road East and “Rema Marmara”, occurrences of calcareous nannofossil assemblages are confined to thin intervals, separated by barren beds (Fig. 3.3). The results obtained from those samples that yielded assemblages with stratigraphic value are summarised below; a detailed compilation of our data is included in a distribution chart (Fig. 3.5). The indicated first and last occurrences should be interpreted with caution with respect to their biochronological meaning, given the generally irregular distribution of nannofossils and the partly low-resolution sampling in the sections of the Orphanic Gulf and Strimon Basin area. Zonal assignments are based on the Mediterranean MNN zonal scheme (after Raffi and Rio, 1979), a regionally valid modification of the NN-zonation of Martini (1971), and benefit from biostratigraphic observations and updates by Theodoridis (1984), Rio et al. (1990), Raffi et al. (2003), and Lourens et al. (2004).

#### *Kavala Road West*

The lowermost nannofossil assemblage, with *Helicosphaera stalis*, has been recovered from samples ST 67 and 68 (Figs. 3.3a and 3.5a). The co-occurrence of *Amaurolithus delicatus*, *A. primus*, *Discoaster misconceptus*, *D. quinquerramus*, *Reticulofenestra rotaria*, and *Triquetrorhabdulus rugosus* in samples ST 73 and 74 (Plate 3.I, 1–5) is considered, in accordance with Theodoridis (1984), to



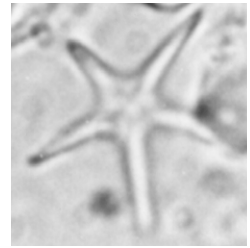
Section	Sample	Species																														MNN Zone																																																																																																																																																																																																																																																																																																																																																																																																																																																																																																																																																																																																																																																																																																																																																																																																																																																																																																																																																																																																																																																																																																																																																																																																																																																									
		<i>Amaurolithus bizarrus</i>	<i>Amaurolithus delicatus</i>	<i>Amaurolithus praevalidus</i>	<i>Amaurolithus sp.</i>	<i>Amaurolithus acutus</i>	<i>Ceratolithus larymayeri</i>	<i>Ceratolithus rugosus</i>	<i>Calcidiscus leptoporus</i>	<i>Calcidiscus macintyrei</i>	<i>Calcidiscus pataecus</i>	<i>Coccolithus pelagicus</i>	<i>Discobolus</i>	<i>Discobolus tenuis</i>	<i>Geomphitella</i>	<i>Umbilicosphaera sibogae foliosa</i>	<i>Umbilicosphaera lafari</i>	<i>Umbilicosphaera mirabilis</i>	<i>Discoaster brouweri</i>	<i>Discoaster berggrenii</i>	<i>Discoaster misconceptus</i>	<i>Discoaster pansus</i>	<i>Discoaster quinqueramus</i>	<i>Discoaster variabilis</i>	<i>Discoaster giganteus</i>	<i>Discoaster micropansus</i>	<i>Discoaster pansus</i>	<i>Discoaster pentadactylus</i>	<i>Discoaster surculus</i>	<i>Helicosphaera carteri</i>	<i>Helicosphaera paleocarteri</i>		<i>Helicosphaera sellii</i>	<i>Helicosphaera stalis</i>	<i>Helicosphaera walliichi</i>	<i>Helicosphaera intermedia</i>	<i>Helicosphaera orientalis</i>	<i>Linosstromation parvum</i>	<i>Parasphaera discipora</i>	<i>Parasphaera multiplex</i>	<i>Parasphaera sp.</i>	<i>Scyathosphaera sp.</i>	<i>Retikulofenestra doronicoides</i>	<i>Retikulofenestra minuta</i>	<i>Retikulofenestra minutula</i>	<i>Retikulofenestra pseudocumbilicis</i>	<i>Retikulofenestra rotaria</i>	<i>Rhabdosphaera claviger</i>	<i>Rhabdosphaera pannonica</i>	<i>Rhabdosphaera protera</i>	<i>Sphenolithus albus</i>	<i>Sphenolithus cf. S. grandis</i>	<i>Sphenolithus cf. S. subquadratus</i>	<i>Traquetorhabdulus rugosus</i>	<i>Traquetorhabdulus martinii</i>	<i>Braarudosphaera bigelowii</i>	<i>Circulifusus ionesi</i>	<i>Florisphaera sp.</i>	<i>Scapholithus fossilis</i>																																																																																																																																																																																																																																																																																																																																																																																																																																																																																																																																																																																																																																																																																																																																																																																																																																																																																																																																																																																																																																																																																																																																																																																																																														
Akropotamos	Gr 438	1	2	3	4	5	6	7	8	9	10	11	12	13	14	15	16	17	18	19	20	21	22	23	24	25	26	27	28	29	30	31	32	33	34	35	36	37	38	39	40	41	42	43	44	45	46	47	48	49	50	51	52	53	54	55	56	57	58	59	60	61	62	63	64	65	66	67	68	69	70	71	72	73	74	75	76	77	78	79	80	81	82	83	84	85	86	87	88	89	90	91	92	93	94	95	96	97	98	99	100	101	102	103	104	105	106	107	108	109	110	111	112	113	114	115	116	117	118	119	120	121	122	123	124	125	126	127	128	129	130	131	132	133	134	135	136	137	138	139	140	141	142	143	144	145	146	147	148	149	150	151	152	153	154	155	156	157	158	159	160	161	162	163	164	165	166	167	168	169	170	171	172	173	174	175	176	177	178	179	180	181	182	183	184	185	186	187	188	189	190	191	192	193	194	195	196	197	198	199	200	201	202	203	204	205	206	207	208	209	210	211	212	213	214	215	216	217	218	219	220	221	222	223	224	225	226	227	228	229	230	231	232	233	234	235	236	237	238	239	240	241	242	243	244	245	246	247	248	249	250	251	252	253	254	255	256	257	258	259	260	261	262	263	264	265	266	267	268	269	270	271	272	273	274	275	276	277	278	279	280	281	282	283	284	285	286	287	288	289	290	291	292	293	294	295	296	297	298	299	300	301	302	303	304	305	306	307	308	309	310	311	312	313	314	315	316	317	318	319	320	321	322	323	324	325	326	327	328	329	330	331	332	333	334	335	336	337	338	339	340	341	342	343	344	345	346	347	348	349	350	351	352	353	354	355	356	357	358	359	360	361	362	363	364	365	366	367	368	369	370	371	372	373	374	375	376	377	378	379	380	381	382	383	384	385	386	387	388	389	390	391	392	393	394	395	396	397	398	399	400	401	402	403	404	405	406	407	408	409	410	411	412	413	414	415	416	417	418	419	420	421	422	423	424	425	426	427	428	429	430	431	432	433	434	435	436	437	438	439	440	441	442	443	444	445	446	447	448	449	450	451	452	453	454	455	456	457	458	459	460	461	462	463	464	465	466	467	468	469	470	471	472	473	474	475	476	477	478	479	480	481	482	483	484	485	486	487	488	489	490	491	492	493	494	495	496	497	498	499	500	501	502	503	504	505	506	507	508	509	510	511	512	513	514	515	516	517	518	519	520	521	522	523	524	525	526	527	528	529	530	531	532	533	534	535	536	537	538	539	540	541	542	543	544	545	546	547	548	549	550	551	552	553	554	555	556	557	558	559	560	561	562	563	564	565	566	567	568	569	570	571	572	573	574	575	576	577	578	579	580	581	582	583	584	585	586	587	588	589	590	591	592	593	594	595	596	597	598	599	600	601	602	603	604	605	606	607	608	609	610	611	612	613	614	615	616	617	618	619	620	621	622	623	624	625	626	627	628	629	630	631	632	633	634	635	636	637	638	639	640	641	642	643	644	645	646	647	648	649	650	651	652	653	654	655	656	657	658	659	660	661	662	663	664	665	666	667	668	669	670	671	672	673	674	675	676	677	678	679	680	681	682	683	684	685	686	687	688	689	690	691	692	693	694	695	696	697	698	699	700	701	702	703	704	705	706	707	708	709	710	711	712	713	714	715	716	717	718	719	720	721	722	723	724	725	726	727	728	729	730	731	732	733	734	735	736	737	738	739	740	741	742	743	744	745	746	747	748	749	750	751	752	753	754	755	756	757	758	759	760	761	762	763	764	765	766	767	768	769	770	771	772	773	774	775	776	777	778	779	780	781	782	783	784	785	786	787	788	789	790	791	792	793	794	795	796	797	798	799	800	801	802	803	804	805	806	807	808	809	810	811	812	813	814	815	816	817	818	819	820	821	822	823	824	825	826	827	828	829	830	831	832	833	834	835	836	837	838	839	840	841	842	843	844	845	846	847	848	849	850	851	852	853	854	855	856	857	858	859	860	861	862	863	864	865	866	867	868	869	870	871	872	873	874	875	876	877	878	879	880	881	882	883	884	885	886	887	888	889	890	891	892	893	894	895	896	897	898	899	900	901	902	903	904	905	906	907	908	909	910	911	912	913	914	915	916	917	918	919	920	921	922	923	924	925	926	927	928	929	930	931	932	933	934	935	936	937	938	939	940	941	942	943	944	945	946	947	948	949	950	951	952	953	954	955	956	957	958	959	960	961	962	963	964	965	966	967	968	969	970	971	972	973	974	975	976	977	978	979	980	981	982	983	984	985	986	987	988	989	990	991	992	993	994	995	996	997	998	999	1000	1001	1002	1003	1004	1005	1006	1007	1008	1009	1010	1011	1012	1013	1014	1015	1016	1017	1018	1019	1020	1021	1022	1023	1024	1025	1026	1027	1028	1029	1030	1031	1032	1033	1034	1035	1036	1037	1038	1039	1040	1041	1042	1043	1044	1045	1046	1047	1048	1049	1050	1051	1052	1053	1054	1055	1056	1057	1058	1059	1060	1061	1062	1063	1064	1065	1066	1067	1068	1069	1070	1071	1072	1073	1074	1075	1076	1077	1078	1079	1080	1081	1082	1083	1084	1085	1086	1087	1088	1089	1090	1091	1092	1093	1094	1095	1096	1097	1098	1099	1100	1101	1102	1103	1104	1105	1106	1107	1108	1109	1110	1111	1112	1113	1114	1115	1116	1117	1118	1119	1120	1121	1122	1123	1124	1125	1126	1127	1128	1129	1130	1131	1132	1133	1134	1135	1136	1137	1138	1139	1140	1141	1142	1143	1144	1145	1146	1147	1148	1149	1150	1151	1152	1153	1154	1155	1156	1157	1158	1159	1160	1161	1162	1163	1164	1165	1166	1167	1168	1169	1170	1171	1172	1173	1174	1175	1176	1177	1178	1179	1180	1181	1182	1183	1184	1185	1186	1187	1188	1189	1190	1191	1192	1193	1194	1195	1196	1197	1198	1199	1200	1201	1202	1203	1204	1205	1206	1207	1208	1209	1210	1211	1212	1213	1214	1215	1216	1217	1218	1219	1220	1221	1222	1223	1224	1225	1226	1227	1228	1229	1230	1231	1232	1233	1234	1235	1236	1237	1238	1239	1240



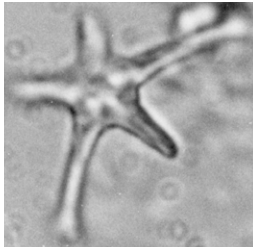
1



2



3



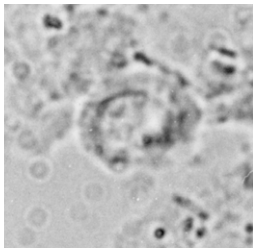
4



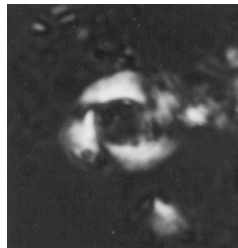
5



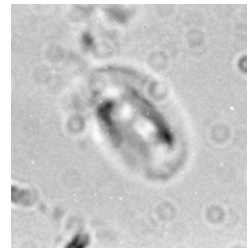
6



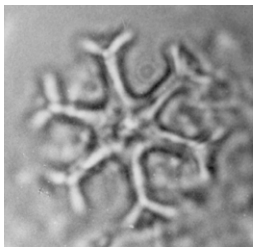
7



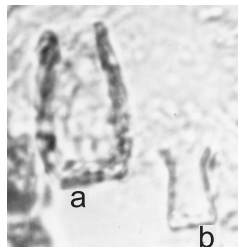
8



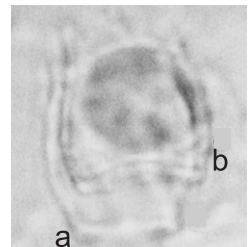
9



10



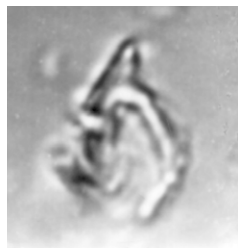
11



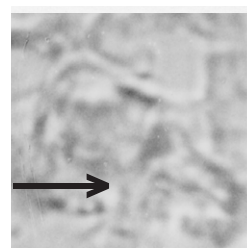
12



13



14



15

Plate 3.I. Calcareous nannofossils from section Kavala Road West, Orphanic Gulf area.

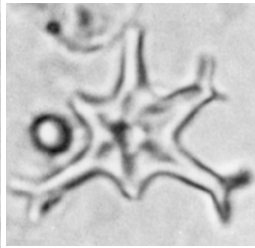
- 1) *Amaurolithus delicatus* Gartner and Bukry,  $\times 1600$ ; sample ST 73. Parallel light.
- 2) *Discoaster quinqueramus* Gartner,  $\times 2000$ ; sample ST 74. Parallel light.
- 3) *Discoaster quinqueramus* Gartner,  $\times 3100$ ; sample ST 74. Parallel light.
- 4-5) *Discoaster misconceptus* Theodoridis,  $\times 2900$ ; sample ST 74. (4) Parallel light; (5) crossed nicols.
- 6) *Amaurolithus delicatus* Gartner and Bukry,  $\times 1700$ ; sample ST 75. Parallel light.
- 7-8) *Reticulofenestra rotaria* Theodoridis,  $\times 2000$ ; sample ST 75. (7) Parallel light; (8) crossed nicols.
- 9) *Helicosphaera sellii* Bukry and Bramlette,  $\times 2000$ ; sample ST 75. Parallel light.
- 10) *Discoaster pansus* (Bukry and Percival),  $\times 1600$ ; sample Gr 397. Parallel light.
- 11a) *Scyphosphaera apsteinii* Lohmann, b) *Scyphosphaera cantharellus* Kamptner,  $\times 1600$ ; sample Gr 398. Parallel light.
- 12a) *Scyphosphaera queenslandensis* Rade, b) *Scyphosphaera pacifica* Rade,  $\times 1600$ ; sample Gr 405. Parallel light.
- 13) *Amaurolithus delicatus* Gartner and Bukry,  $\times 2400$ ; sample Gr 405. Parallel light.
- 14) *Ceratolithus acutus* Gartner and Bukry,  $\times 2000$ ; sample Gr 405. Parallel light.
- 15) *Ceratolithus acutus* Gartner and Bukry,  $\times 2400$ ; sample Gr 405. Parallel light.

*Discoaster pansus*, *Helicosphaera sellii*, and *Scyphosphaera* spp. *D. quinqueramus* was not identified. The co-occurrence in samples Gr 396, 398, and 405 (Plate 3.I, 12-15) of – very rare – individuals of *A. tricorniculatus*, *Ceratolithus acutus*, *C. larrymayeri*, and *Triquetrorhabdulus rugosus* characterizes the beginning of the Pliocene (sensu Theodoridis, 1984; Castradori, 1998; Van Couvering et al., 2000; Cavalezzi et al., 2002) and marks Zone MNN12. In the open ocean, the last occurrence of *D. quinqueramus* defines the end of Zone NN11. Using its disappearance between samples ST 74 and ST 75 to identify here the debut of the *Amaurolithus tricorniculatus*-NN12, or MNN12 Zone is debatable, given the generally rare occurrence (or absence) of *D. quinqueramus* in the Mediterranean towards the end of its range. The nannofossil assemblage of sample ST 75 is nevertheless interpreted to belong to Zone MNN12, because of its intermediate character when compared with the assemblages of the directly underlying (MNN11) and overlying Early Pliocene (i.e. MNN12, upper part) samples. The last occurrences of *H. stalis* and *Reticulofenestra rotaria*, which species are not reported from levels higher than Zone MNN11b or -c (Negri and Villa, 2000; Raffi et al., 2003), may therefore be explained by reworking. The presence of *H. (cf. H.) sellii*, first appearing in the Mediterranean in Zone MNN11 and absent in MNN12 until its re-entry in MNN13 (Rio et al., 1990), poses a similar problem. Possibly, the specimens found here and in the following sections are Miocene forms. *T. rugosus*, present up to sample Gr 397, disappears shortly after the first occurrences of *A. tricorniculatus* and *C. acutus*, exactly as in the Atlantic Ocean (Castradori, 1998; Raffi et al., 1998).

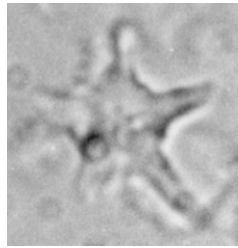
Samples Gr 400-422 contain a less diversified nannofossil assemblage, equally assignable to Zone MNN12. The assemblage of samples Gr 423, 424, and 428 consists, among others, of *Amaurolithus delicatus* and *Ceratolithus rugosus*. The presence of *C. rugosus*, the nominate species of the *Ceratolithus rugosus*-NN13, or MNN13 Zone, indicates a Zanclean age. No nannofossils were found in the top part of the section (samples Gr 413-419, 425-427, 429, and 430).

#### Kavala Road East

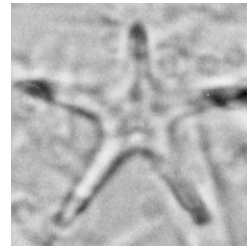
Sample ST 59 (Figs. 3.3a and 3.5a; Plate 3.III, 1) yielded a very poor nannofossil assemblage, containing *Amaurolithus* sp., *Helicosphaera stalis*, and *Triquetrorhabdulus rugosus*. The presence of *Amaurolithus* together with *H. stalis* suggests that this assemblage belongs to Zone MNN11b, in accordance with Negri and Villa (2000).



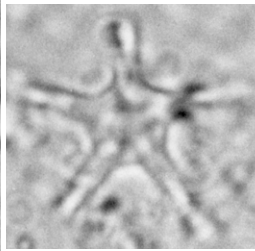
1



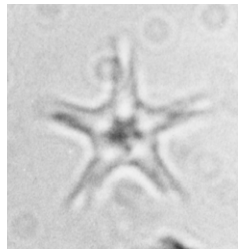
2



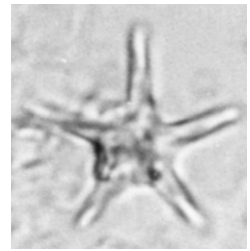
3



4



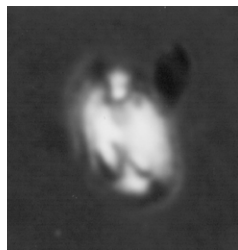
5



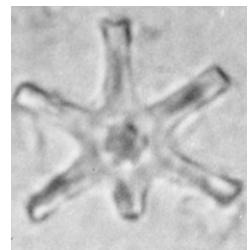
6



7



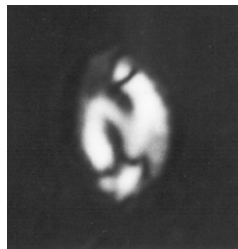
8



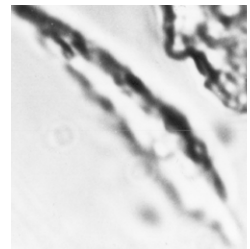
9



10



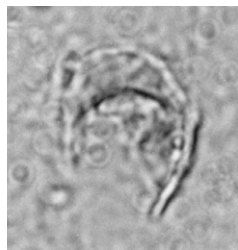
11



12



13



14



15

Plate 3.II. Calcareous nannofossils from section “Rema Marmara”, Orphanic Gulf area.

- 1) *Discoaster pansus* (Bukry and Percival), ×3600; sample ST 37. Parallel light.
- 2) *Discoaster berggrenii* Bukry, ×4100; sample ST 40. Parallel light.
- 3) *Discoaster quinqueramus* Gartner, ×2900; sample ST 39. Parallel light.
- 4) *Discoaster quinqueramus* Gartner, ×3300; sample ST 44. Parallel light.
- 5) *Discoaster berggrenii* Bukry, ×4200; sample ST 47. Parallel light.
- 6) *Discoaster berggrenii* Bukry, ×4200; sample ST 47. Parallel light.
- 7-8) *Helicosphaera sellii* Bukry and Bramlette, ×2300; sample ST 50. (7) Parallel light; (8) crossed nicols.
- 9) *Discoaster giganteus* Theodoridis, ×1900; sample ST 51. Parallel light.
- 10-11) *Helicosphaera stalis* Theodoridis, ×3300; sample ST 50. (10) Parallel light; (11) crossed nicols.
- 12) *Triquetrorhabdulus rugosus* Bramlette and Wilcoxon, ×2400; sample Gr 1583. Parallel light.
- 13) *Amaurolithus delicatus* Gartner and Bukry, ×1800; sample ST 49. Parallel light.
- 14) *Amaurolithus primus* (Bukry and Percival), ×2200; sample ST 51. Parallel light.
- 15) *Triquetrorhabdulus rugosus* Bramlette and Wilcoxon, ×1700; sample ST 51. Parallel light.

#### “Rema Marmara”

The assemblage identified in the top part of subsection I (sample ST 55; Figs. 3.3a and 3.5a) shows a low diversity, while samples ST 57 and 58 contain a more diversified assemblage with *Helicosphaera stalis*. Calcareous nannofossils were recovered from a few sampling levels in the middle part of subsection II only. Sample ST 37 (Plate 3.II, 1) contains numerous *Discoaster* species, such as *Discoaster pansus* and *D. quinqueramus*, and can thus be assigned to Zone MNN11. The nannofossil content of the next-higher samples (ST 39 and 40; Plate 3.II, 2 and 3) is dominated by *D. misconceptus*. Besides this species, *D. berggrenii*, *Reticulofenestra rotaria*, and *Triquetrorhabdulus rugosus* are present, together with rare specimens of *D. quinqueramus*. The assemblage of samples ST 55-58 is non-diagnostic, because it is composed of long ranging species that occur since the Middle Miocene. However, the micromammal fauna of the underlying beds was estimated to have a middle Turolian age (De Bruijn, 1989), which implies that this level is correlative to the upper Tortonian (Steininger et al., 1996). Consequently, the nannofossil assemblage of samples ST 55-58 may belong to Zone MNN11, also because in the overlying samples (ST 39-40) the co-occurrence of *D. quinqueramus* and *R. rotaria* indicates Zone MNN11b-c.

Sample ST 44, in subsection III, contains a relatively rich nannofossil assemblage with *Discoaster quinqueramus* (Plate 3.II, 4) and *Helicosphaera stalis*. In the uppermost part of subsection III (samples ST 46-48; Plate 3.II, 5 and 6), an assemblage with a large species variety is present, consisting, among others, of *D. berggrenii*, *H.* (cf. *H.*) *sellii*, and *Reticulofenestra rotaria*. These species co-occur with those identified in sample ST 44. The presence of *D. quinqueramus*, *H. stalis*, and *R. rotaria* suggests that the assemblages from this part of subsection III belong also to Zone MNN11b-c.

The nannofossil assemblage identified in samples ST 49-51, Gr 1583, and Gr 1584 from the upper part of subsection III shows high species abundances and diversities (Plate 3.II, 7-15). Among the observed species are *Amaurolithus delicatus*, *A. primus*, *Discoaster pansus*, *Helicosphaera sellii*, *H. stalis*, *Reticulofenestra rotaria*, *Scyphosphaera* spp., and *Triquetrorhabdulus rugosus*. The composition of this nannofossil assemblage is very similar to that in sample ST 75 of section Kavala Road West, which suggests that this assemblage belongs to Zone MNN12. This assignment is supported by the abundance (“acme”) of *Scyphosphaera* found in these samples (see also Castradori, 1998; Siesser, 1998).

Plate 3.III. Calcareous nannofossils from the Orphanic Gulf and Strimon Basin areas.

- 1) *Amaurolithus* sp., ×1900; sample ST 59, section Kavala Road East. Parallel light.
- 2) *Amaurolithus delicatus* Gartner and Bukry, ×2800; sample Gr 440, section Akropotamos. Parallel light.
- 3) *Amaurolithus primus* (Bukry and Percival), ×2400; sample Gr 440, section Akropotamos. Parallel light.
- 4-5) *Helicosphaera sellii* Bukry and Bramlette, ×2800; sample ST 10, section Akropotamos. (4) Parallel light; (5) crossed nicols.
- 6) *Discoaster berggrenii* Bukry, ×2800; sample Gr 440, section Akropotamos. Parallel light.
- 7-8) *Scyphosphaera pacifica* Rade, ×1500; sample ST 8, section Akropotamos. (7) Parallel light; (8) crossed nicols.
- 9) *Amaurolithus* sp., ×3200; sample ST 120, section Ofirinon. Parallel light.
- 10) *Amaurolithus* cf. *A. primus* (Bukry and Percival), ×2100; sample ST 77, section Eziovis Rema. Parallel light.
- 11) *Amaurolithus primus* (Bukry and Percival), ×1800; sample ST 81, section Eziovis Rema. Parallel light.
- 12) *Braarudosphaera bigelowii* (Gran and Braarud), ×1200; sample ST 94, section Labyrinthos. Parallel light.
- 13) *Triquetrorhabdulus rugosus* Bramlette and Wilcoxon, ×1800; sample ST 93, section Labyrinthos. Parallel light.
- 14) *Amaurolithus primus* (Bukry and Percival), ×1800; sample ST 103, section Labyrinthos. Parallel light.
- 15) *Amaurolithus* sp., ×2000; sample ST 103, section Labyrinthos. Parallel light.

*Reticulofenestra daronicoides* is present in samples ST 55-58 and 46-51 in upwards increasingly high numbers, which is also occurring in Kavala Road West in samples ST 67-75. Similar observations were made in the upper Miocene (Pontian) deposits from the western Black Sea margin (M. Mărunțeanu, unpublished data).

Sample ST 53, finally, contains a poor assemblage with *Sphenolithus abies*, which can be assigned to Zones MNN12-MNN16 and thus probably being of Zanclean age.

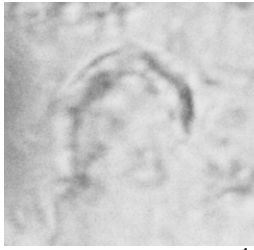
#### *Akropotamos*

Re-examination of sample Gr 440 from subsection I (Figs. 3.3b and 3.5b; Plate 3.III, 2, 3, and 6) revealed that its nannofossil content, characterized by the co-occurrence of *Amaurolithus delicatus*, *A. primus*, *Discoaster berggrenii*, *D. misconceptus*, *Triquetrorhabdulus martini*, and *T. rugosus*, belongs to Zone MNN11b-c, thus confirming the earlier assignment by Steffens et al. (1979).

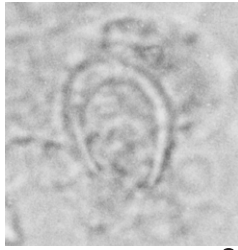
In subsection II, only samples ST 6-10 from the upper part of the evaporite unit contain a rich nannofossil assemblage. It contains *Amaurolithus delicatus*, *A. primus*, *Discoaster berggrenii*, *D. misconceptus*, *Helicosphaera* (cf. *H.*) *sellii*, *H. stalis*, *Triquetrorhabdulus rugosus*, and various species belonging to the genus *Scyphosphaera* (Plate 3.III, 4, 5, 7, and 8). This assemblage is almost similar to those identified higher in the Kavala Road West and “Rema Marmara” profiles. They differ by the presence of *D. quinqueramus* and *Reticulofenestra rotaria* and by the absence of *Lithostromation perdurum* and *Scyphosphaera* in the MNN11-assemblages of the latter sections. Although *D. quinqueramus* is absent in samples ST 6-10, the presence of *Amaurolithus* and *D. berggrenii* indicates that the nannofossil assemblage belongs to Zone MNN11b-c.

A far less diverse assemblage was observed in sample ST 25 of subsection III. The nannofossil assemblage recovered from the beds overlying this subsection, i.e. from the samples taken by Steffens et al. (1979): Gr 431-433, contains *Helicosphaera* cf. *H. sellii* (small and distorted specimens), together with very rare individuals of *Amaurolithus delicatus* and *A. primus*. Samples Gr 434-438 contain a more diverse flora with, among others, common *Scyphosphaera* specimens, as well as rare specimens of *A. delicatus*, *A. primus*, and (in sample Gr 436) *Ceratolithus acutus*. The presence of the latter taxon indicates that the nannofossil assemblage is of Zanclean age and belongs to Zone MNN12.

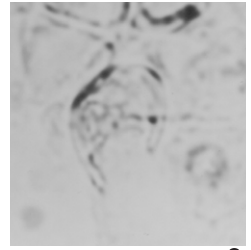




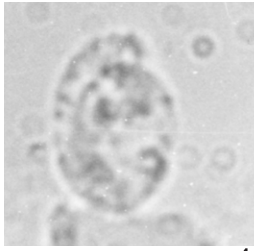
1



2



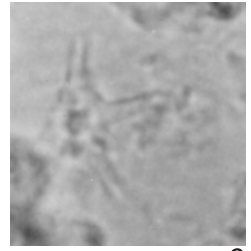
3



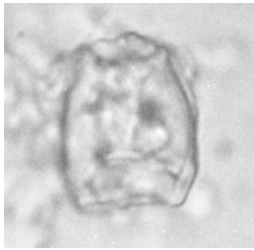
4



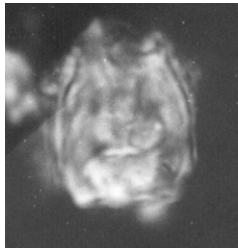
5



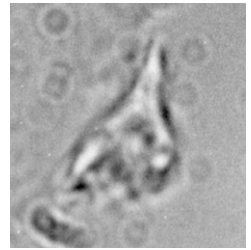
6



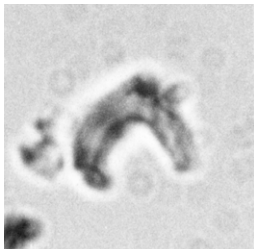
7



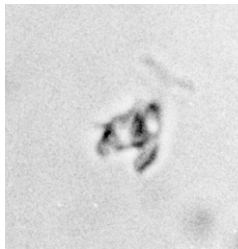
8



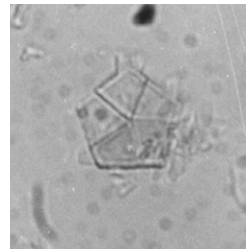
9



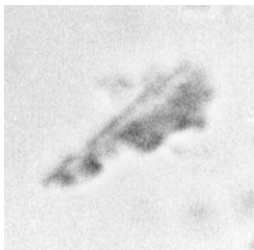
10



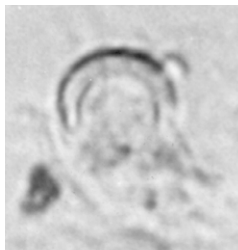
11



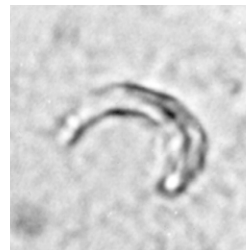
12



13



14



15

### *Ofrinion*

The laminated beds above the gypsum/anhydrite level (sample ST 120; Figs. 3.3b and 3.5b; Plate 3.III, 9) contain a poor nannofossil assemblage with very rare specimens of *Amaurolithus bizzarus*, *Amaurolithus* sp., and *Triquetrorhabdulus rugosus*. The occurrence of *Amaurolithus* suggests that this assemblage belongs to Zone MNN11b-c.

### *Eziovis Rema*

The silts at the base of the calcareous beds contain a poor and badly preserved nannofossil assemblage (sample ST 77; Figs. 3.3b and 3.5b; Plate 3.III, 10), with rare specimens of *Amaurolithus* cf. *A. primus*, *Amaurolithus* sp., and *Triquetrorhabdulus rugosus*. A similar assemblage, with rare *A. primus*, was observed in sample ST 81 (Plate 3.III, 11), taken from the separate outcrop on the southern side of the valley. Both assemblages with *Amaurolithus* belong, probably, to Zone MNN11b-c. It should be mentioned that the observed specimens of *Amaurolithus* are very small in size, in which respect they are fairly similar to those described by Mărunțeanu and Papaianopol (1998) and Snel et al. (2006-chapter 2) from Miocene-Pliocene transitional strata in Romania.

### *Labyrinthos*

In the uppermost part of the Dafni Formation (samples ST 93 and 94; Figs. 3.4 and 3.5b; Plate 3.III, 12 and 13), a nannofossil assemblage dominated by the presence of *Braarudosphaera bigelowii* was identified. Together with this species, small-sized and “regular-sized” *Amaurolithus delicatus* and few individuals of *Triquetrorhabdulus rugosus* were encountered. The presence of these species suggests that the assemblage belongs to Zone MNN11b-c or MNN12. Sample ST 94 has been taken from a clay cobble within the mass-flow bed, probably representing a reworked older level of the Dafni Formation.

The nannofossil assemblage of the Choumnikon Formation (samples ST 102 and 103; Plate 3.III, 14 and 15) is, among others, composed of *Amaurolithus* cf. *A. primus*, *Amaurolithus* sp., *Scyphosphaera* sp., and *Triquetrorhabdulus rugosus*. This assemblage may belong to Zone MNN11 b-c or MNN12 too. Other assemblages where *Amaurolithus* and low numbers of *Scyphosphaera* co-occur are found in samples ST 6-10 (Akropotamos), which are assigned to Zone MNN11b-c. In the profiles of Kavala Road West and “Rema Marmara”, however, *Amaurolithus* and “peak” abundances of *Scyphosphaera* are confined to assemblages indicating Zone MNN12 (Fig. 3.5). We therefore suggest that the nannofossil levels from section Labyrinthos should be interpreted to belong to Zone MNN11b or -c.

## 3.6 Palaeobathymetry

An estimate of the depositional depth was made for the upper parts of sections Kavala Road West (samples ST 75 and Gr 395-428), “Rema Marmara” (ST 44-53 and Gr 1583-1585), and Akropotamos (Gr 431-438). This estimate is based on the general relation between depth and the fraction of planktonic planktonic foraminifera with respect to the total foraminiferal population of Van der Zwaan et al. (1990), following procedures of Van Hinsbergen et al. (2005). Additionally, an independent check of the calculated depth was carried out, using the depth chart of selected species of benthic foraminifera of Van Hinsbergen et al. (2005).

section	n	depth		
		calculated		taxonomic estimate
		depth	SD	
Kavala Road West	16	368	194	500-900
"Rema Marmara"	3	398	258	300-600
Akropotamos	4	518	236	500-900

Figure 3.6. Palaeobathymetry estimates for the sections of Kavala Road West, "Rema Marmara", and Akropotamos. 'N' is the number of analysed samples. An independent check of the depositional depth for a selection of the samples, using the depth chart of selected species of benthic foraminifera (Van Hinsbergen et al., 2005), is given in the right hand column.

The results are listed in Figure 3.6. Most samples contain high amounts of quartz and rock fragments that are indicative of down-slope (mass) transport. Therefore, the calculated depth should be considered as minimum depth values. Moreover, since the foraminifera-bearing intervals of the three sections contain alternating homogeneous silts and sapropelitic layers, clear evidence exists for fluctuating oxygen levels of the bottom waters during sediment deposition. Since the oxygen level has a profound effect on the intensity of benthic life, the calculated depth values should be regarded as rough estimates. The independent check using the benthic foraminiferal depth markers forms a more reliable depth measure. As a rule, the deepest markers indicate the depositional depth.

The benthic foraminiferal content of samples ST 75, Gr 412, and Gr 428 (of the Kavala Road West section), of sample Gr 1585 ("Rema Marmara"), and of sample Gr 431 (Akropotamos) was analysed. The samples of section Kavala Road West contain a diverse and rich deep-marine fauna, including *Karreriella bradyi*, *Cibicides robertsonianus*, *C. bradyi*, *C. kullenbergi*, *Oridorsalis* spp., *Planulina ariminensis*, and *Siphonina reticulata*, indicating a depositional depth of at least 500 m. The absence of *C. italicus* and *C. wuellerstorfi* indicates a maximum depth of approximately 900-1000 m. Sample Gr 1585 of section "Rema Marmara" contains *Oridorsalis* spp., *P. ariminensis*, *Uvigerina* spp., *C. pachydermus*, and *C. pseudoungerianus*, indicative of a depth of 300-600 m. Sample Gr 431 of section Akropotamos contains *K. bradyi*, *C. kullenbergi*, *S. reticulata*, and *P. ariminensis*, which indicate a bathymetry comparable to the one obtained for the Kavala Road West section: 500-900 m (Fig. 3.6).

A large discrepancy exists between the calculated depth and the depth estimate obtained by the analysis of depth markers. Although evidence for down-slope transport is given by the high amounts of quartz and rock fragments, shallow water markers such as *Ammonia beccarii*, *Cibicides lobatulus*, *Elphidium* spp., and *Discorbis* spp. are generally absent or present in low quantities. Possibly, relative enrichment of benthic foraminifera occurred because of winnowing, removing the lighter plankton fraction. If this was the case, the water column directly overlying the sediment-water interface must have been in motion throughout the deposition of the Pliocene of the Strimon basin, possibly in a submarine canyon system.

### 3.7 Stratigraphic framework and regional correlations

In this section, we attempt to establish an integrated stratigraphic framework for the Orphanic Gulf area and the Strimon Basin. At first, this will be done separately for the two areas through the combination of nannofossil biostratigraphy, (lithostratigraphic) correlation of marker beds and the incorporation of paleomagnetic data. The two frameworks will then be correlated with the Mediterranean and (Eastern) Paratethys stages, respectively. This, in turn, will facilitate exploring the interaction between the Mediterranean and the Paratethys in Late Miocene to Early Pliocene time.

#### 3.7.1 Orphanic Gulf area

Our nannofossil results show that the marine and brackish successions of the five sections exposed along the Orphanic Gulf (Fig. 3.1) cover the greater part of Zones MNN11, MNN12, and MNN13 (Figs. 3.3 and 3.5). Consequently, these sections jointly comprise (part of) the upper Miocene and the lower Pliocene. A number of key beds can be used to refine the correlation between the Orphanic Gulf sections (Fig. 3.7).

The first and most prominent correlation level is the travertine marker bed overlying sandstone or gravel units in sections Kavala Road West, Kavala Road East, “Rema Marmara”, and Akropotamos (line ‘T’; Fig. 3.7). This relatively thick limestone bed represents a clear geomorphological feature. Below it, 10–20 m of fine-grained, often laminated brackish water sediments can be observed (not exposed in “Rema Marmara”) that, in turn, covers a gypsiferous interval of approximately 10 m in sections Kavala Road East and Akropotamos. A comparable succession of evaporites and overlying laminites is also exposed in the top of the Ofrinion profile (Fig. 3.3b). The nannofossil assemblages of samples ST 6–10 (Akropotamos: at 10 m in subsection II; Fig. 3.3b) and ST 120 (Ofrinion: at 59 m; Fig. 3.3b), although being quite different in species (Fig. 3.5b) and numbers of specimens, both were recovered from levels within the evaporite unit and both probably belong to Zone MNN11b or -c. Therefore, these evaporites and nannofossil assemblages are tentatively related to the same marine phase. The gypsum beds in section Akropotamos were proposed to correspond to the Messinian evaporites found elsewhere in the Mediterranean (Meulenkamp, 1979; Dermitzakis et al., 1986). These and the other gypsiferous beds of the Orphanic Gulf area may form the, presently onshore, equivalent of the evaporites of the Nestos-Prinos-Kavala Basin near the island of Thasos, where they are up to 800 m thick and include halite cycles (Pollak, 1979; Proedrou, 1979). Indeed, the presence of nannofossil assemblages containing *Amaurolithus* spp. (with a first occurrence at 7.42 Ma: Raffi et al., 2003) below and above the Orphanic Gulf area evaporites gives a possible Messinian age range for these evaporites, which is consistent with that of the Lower or Upper Evaporites in the Mediterranean (5.96–5.59 Ma, or 5.50–5.33 Ma: Krijgsman et al., 1999). The base of the gypsum/anhydrite beds of sections Akropotamos, Kavala Road East, and Ofrinion (line ‘E’; Fig. 3.7) is tentatively correlated with the base of the Lower Evaporites.

Evaporites are absent in sections Kavala Road West and “Rema Marmara” (Fig. 3.3a). There, shallow marine calcareous and sandy beds with *Ditrupea* (in Kavala Road West between 95 m and 100 m; in “Rema Marmara” at 40 m in subsection I) constitute an alternative correlation level. Nannofossil assemblages of samples ST 55–58 (“Rema Marmara”) and samples ST 67 and 68 (Kavala Road West), found close to the *Ditrupea* levels, are correlated with sample ST 59 below the evaporites of Kavala Road East (at 42 m; Fig. 3.3a). The base of the interval of laminated clays, silts, and platy limestones above the calcareous *Ditrupea* beds and below the travertine unit, i.e. at 102 m in Kavala Road West, is suggested to be correlative to the base of the evaporites (Fig.

3.7). This suggestion is supported by the lithological resemblance of the thin-bedded shallow marine beds directly above the gypsum, in sections Akropotamos (between 13 m and 28 m in subsection II) and Ofrinion (from 58 m onward; Fig. 3.3b), and the similarly laminated, brackish beds between 102 m and 120 m in Kavala Road West. In “Rema Marmara”, the interval between the *Ditrupe* and travertine levels of subsections I (top) and II (base), respectively, is unexposed.

The very similar post-travertine beds of sections Kavala Road West and “Rema Marmara” allow a good general litho- and biostratigraphic correlation. Their nannofossil assemblages show diversification in Zones MNN11b-c to MNN12, associated with a rapid change from brackish clays and silts to open marine marls and sapropels (Fig. 3.3a). Sands and conglomerates are found at the top of both sections. In detail, however, some differences are evident. The main lithological distinction between the sediments exposed between the travertine marker bed and the Pliocene sapropelitic beds in Kavala Road West and “Rema Marmara” is the presence of an intercalation of coarse clastics in the latter section (Figs. 3.3a and 3.7). This difference is attributed to the more proximal position of “Rema Marmara” relative to the basin margin.

According to the nannofossil record (Fig. 3.5a), the short interval at 153 m in section Kavala Road West, between samples Gr 395 and 396 (where an assemblage with *Ceratolithus acutus* appears: correlation line labelled ‘3’; Fig. 3.7), should correspond to the Miocene-Pliocene transition. A still younger assemblage, belonging to Zone NN13, is present below the conglomerates at the top of this section. Conversely, in the open marine part of subsection III in “Rema Marmara” Pliocene marker species of the family Ceratolithaceae were not found. Hence, the nannofossils cannot be used to identify the Miocene-Pliocene boundary here.

An alternative indication for this boundary, and more consistent with the facies change both in sections Kavala Road West and “Rema Marmara”, is the appearance of rich and diversified benthic and planktonic foraminiferal associations. In Kavala Road West and “Rema Marmara” these foraminiferal faunas, which might reflect the local impact of the earliest Pliocene flooding, are found upwards from sampling levels ST 74 and ST 44, respectively (Figs. 3.3a and 3.7; correlation line ‘F’). Unfortunately, the foraminiferal associations lack any Pliocene index taxa. This prevents drawing sound conclusions on the discrepancy between calcareous nannofossils and foraminifera with respect to the position of the Miocene-Pliocene transition in this area. Likely, this discrepancy is caused by environmental control on the appearance level of the Pliocene nannofossil markers. The *Amaurolithus* and *Ceratolithus* species are relatively rare and easy to miss, particularly in the sediments from the studied area. The presence of MNN11 – *Discoaster* – marker species in the open marine marl interval, found even above the first sapropel up to 21 m in subsection III in “Rema Marmara” (Fig. 3.3a), can be explained by reworking.

The fossil soils and red beds of the basal part of the sections along Kavala Road, and possibly the palaeo-sol below the gypsiferous bed of section Ofrinion, are the youngest continental deposits and might be correlative to the upper Tortonian level with Zone MN12 micromammal fossils at the base of section “Rema Marmara” (labelled ‘M’; Fig. 3.7).

### 3.7.2 Strimon Basin

As we suggested before, the nannofossil assemblages recovered from the Dafni and Choumnikon beds of sections Eziovis Rema and Labyrinthos (Figs. 3.3b and 3.4) may belong to Zone MNN11b-c. The correlation of the Dafni and Choumnikon Formations with the (Paratethys) Maeotian and Pontian stages, respectively (Gramann and Kockel, 1969; Popov and Nevesskaya, 2000), and the recently established magnetostratigraphy of the Maeotian and Pontian sediments in Romania (Snel et al., 2006-chapter 2) are in agreement with this presumption (Fig. 3.7). The

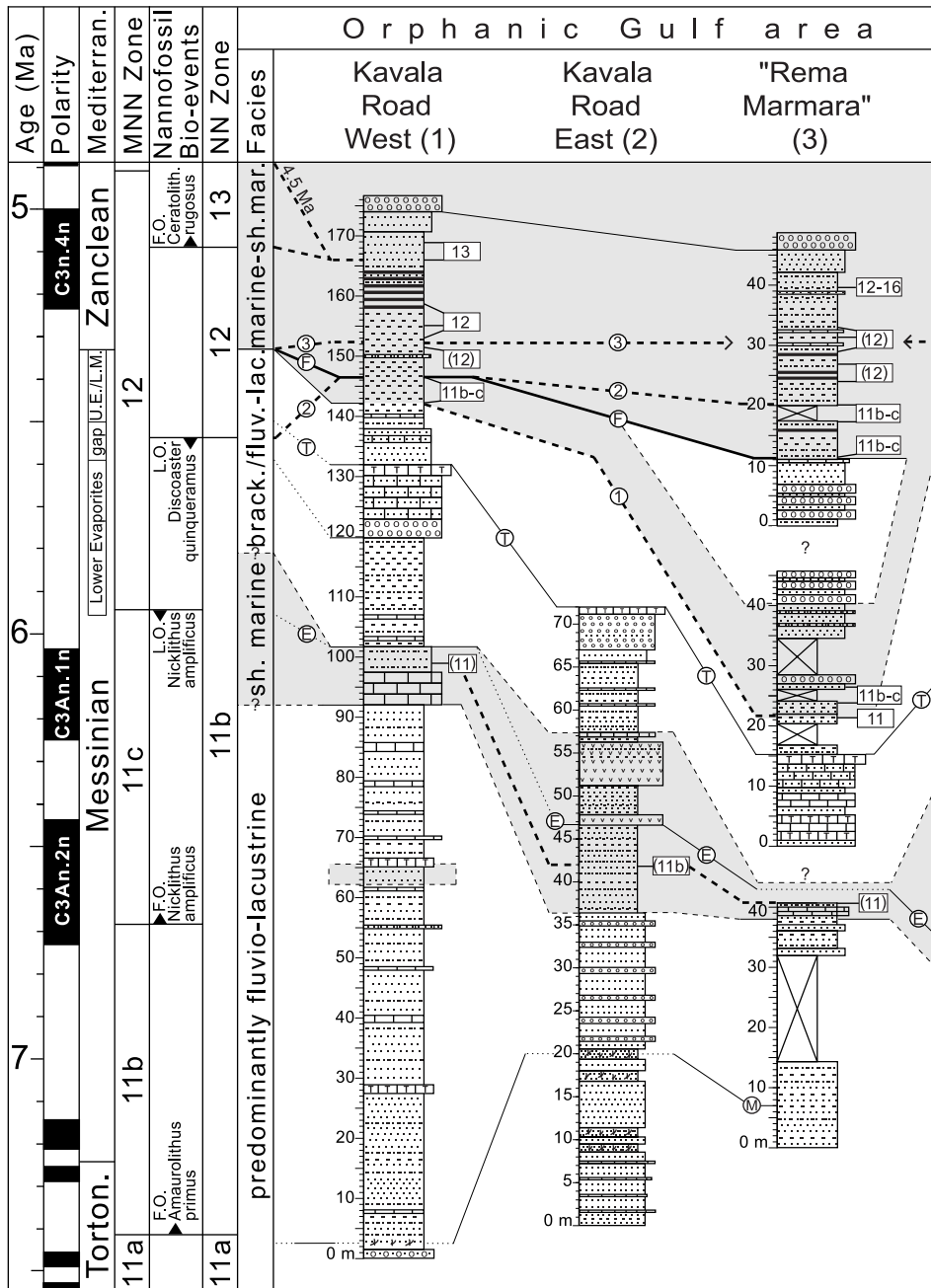
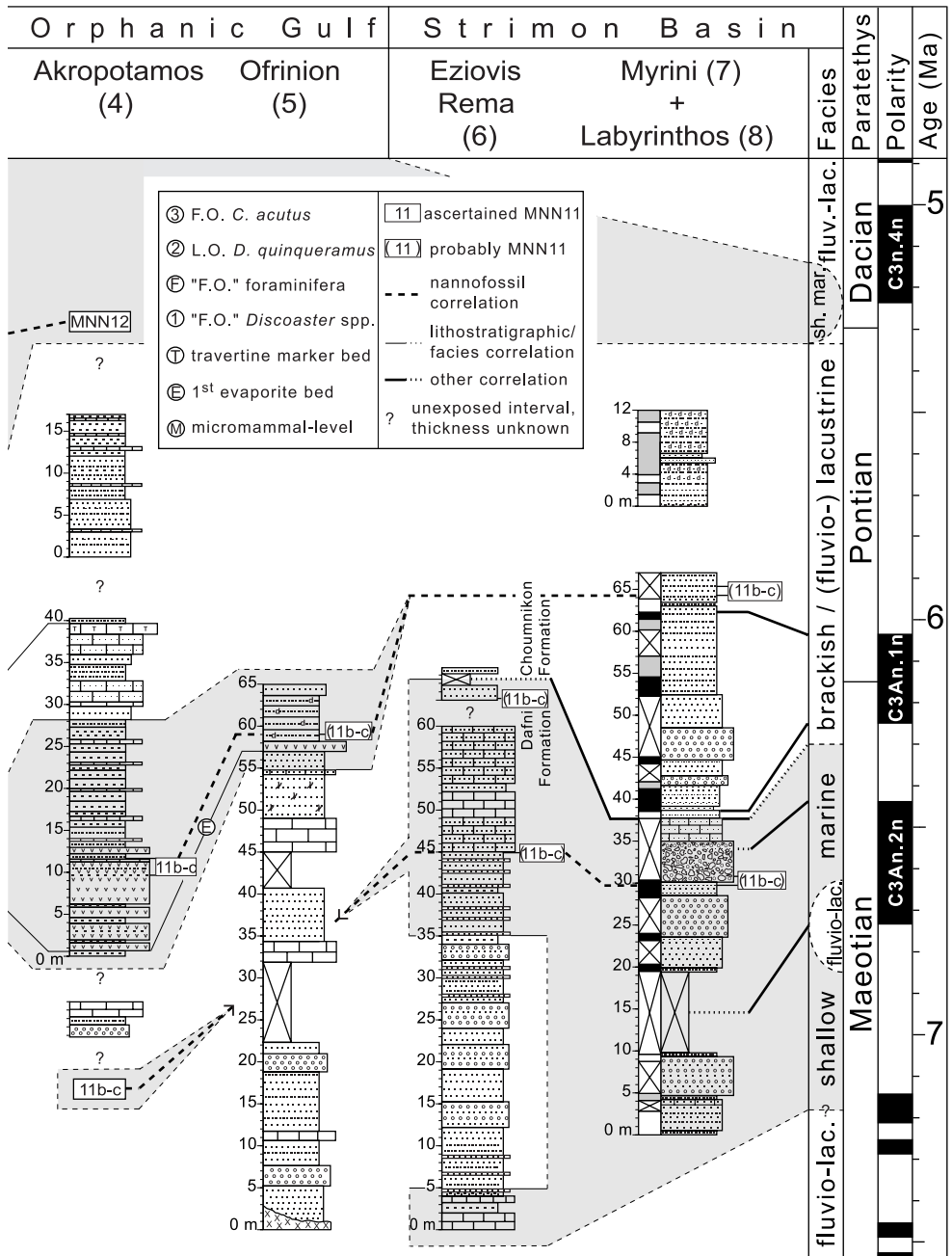


Figure 3.7. Correlation of upper Miocene to lower Pliocene sections of the Orphanic Gulf and Strimon Basin areas (numbered as in Figure 3.1) with calcareous nannofossil zones and bio-events (after Martini, 1971; Raffi and Rio, 1979; Raffi et al., 2003), with the Astronomical Tuned Neogene Time Scale (after Lourens et al., 2004), and with the Eastern Paratethys (Dacic Basin) age calibration (after Snel et al., 2006-chapter 2). The correlation lines



labelled '1', 'F', '2', and '3' refer to local observations of first and last occurrences of calcareous nanofossil species and of benthic and planktonic foraminiferal taxa in sections Kavala Road West and "Rema Marmara". Intervals with a presumed marine depositional environment are shaded. Facies of the Messinian salinity crisis are after Krijgsman et al. (1999); U.E./L.M. denotes Upper Evaporites/Lago Mare.

position of samples ST 102 and 103 in Labyrinthos (at 65 m; Fig. 3.4) in an interval with reversed magnetic polarity, above a normal polarity interval of the (Pontian) Choumnikon beds, suggests an age estimate for these levels with nannofossil assemblages younger than 6.04 Ma: the age of the end of subchron C3An.1n (Krijgsman et al., 1999). The age of sample ST 93, located at 30 m in the lower normal polarity interval of the upper part of the (Maeotian) Dafni beds, which we assume to represent subchron C3An.2n, can be estimated at approximately 6.5 Ma. A similar age can be assigned to sample ST 77 of section Eziovis Rema (45 m; Fig. 3.3b), taking into account its position relative to the position of the Dafni-Choumnikon transition.

Considering the above, the reversed-to-normal polarity reversal between 38 m and 39 m in section Labyrinthos is interpreted to represent the base of normal subchron C3An.1n, dated at 6.26 Ma by Krijgsman et al. (1999). The age of the Dafni-Choumnikon boundary is thus estimated at approximately 6.3 Ma, which is slightly older than the age estimate of the Maeotian-Pontian transition in the Dacic and Euxinic basins (6.15 Ma: Snel et al., 2006–chapter 2). Popov and Nevevskaya (2000) noted, however, that the lowermost part of the Choumnikon Formation in Labyrinthos contains mollusc species deviating from the typical Pontian assemblages. True Pontian-type molluscs are found from approximately 50 m onward, a level corresponding to the middle of C3An.1n, which is more closely resembling the Eastern Paratethys' position of the base of the Pontian.

The Choumnikon beds in the section of Myrini, with exclusively reversed polarity, are likely younger than the highest beds we recorded at the section of Labyrinthos (Fig. 3.4). The oyster beds found directly above the Myrini quarry probably correspond to the same shallow marine phase as the Pliocene oyster-bearing clays sampled at Labyrinthos by Popov and Nevevskaya (2000).

### 3.7.3 Correlation of the Orphanic Gulf and Strimon Basin sequences

Our biostratigraphic and chronostratigraphic data demonstrate that the fluvio-lacustrine and shallow marine to brackish Messinian sequences of the Orphanic Gulf area are correlative with the shallow marine and brackish beds of the Dafni and Choumnikon Formations of the Strimon Basin (Fig. 3.7). This correlation depends on the estimated age of the Maeotian-Pontian boundary (Snel et al., 2006–chapter 2), which has been suggested to be coeval with the Dafni-Choumnikon boundary (Gramann and Kockel, 1969; Popov and Nevevskaya, 2000), and on the assumption that the Orphanic Gulf evaporites are coeval with the evaporites of the Messinian salinity crisis (Meulenkamp, 1979; Dermitzakis et al., 1986).

In view of the above, it would be reasonable to correlate the nannofossil assemblages obtained from or close to the evaporites (samples ST 6-10 of section Akropotamos, at 10 m in subsection II, and sample ST 120 of section Ofrinion, at 59 m; Fig. 3.3b) with those of samples ST 102 and 103 of the Choumnikon beds of section Labyrinthos (at 65 m; Fig. 3.4), since these latter samples probably have a comparable – late Messinian – age. The observation that their nannofossil assemblages are in fact similar, although less diverse (Fig. 3.5b) to those of samples ST 6-10 does not contradict this correlation. The lowest level with nannofossils in the Akropotamos section is tentatively correlated with the oldest assemblages in the Dafni beds of the Strimon area, which would give this level an approximate age of 6.5 Ma (Fig. 3.7). The first shallow marine sediments in the Kavala Road West section (the oyster bed at 65 m; Fig. 3.3a) could have a comparable age. Subsequently, above the evaporites, the lacustrine travertinous interval of the Orphanic Gulf area may correspond to the lacustrine diatomaceous clays and silts exposed in the Myrini quarry. The overlying shallow marine deposits, found on top of both this last section and Labyrinthos, are straightforwardly linked with the Pliocene marine strata exposed along the Orphanic Gulf.



Although the comparisons between the nannofossil assemblages of the Orphanic Gulf and Strimon basin areas should not be regarded as detailed, bed-to-bed correlations, alternative solutions are, in our opinion, less probable. The assumption of synchronism of the marine evaporite and *Ditrupea* beds (lower grey-shaded belt in Figure 3.7) of the Orphanic Gulf area sections with the marine Dafni beds of the Strimon Basin, implicates that either these evaporites are older than the Messinian evaporites in the rest of the Mediterranean, or that the Dafni and Choumnikon Formations would have a much younger age. Besides, this last option would exclude the direct correlation of these formations with the Maeotian and Pontian and be in conflict with our interpretation of the paleomagnetic results of section Labyrinthos.

### 3.8 Discussion and conclusions

The Neogene deposits allow to explore the general palaeogeography of the Orphanic Gulf-Strimon Basin area and to reconstruct the exchange of water masses between the Mediterranean and the Paratethys before, during, and after the Messinian salinity crisis.

Upper Vallesian (MN11, in the Lefkon Formation) and middle Turolian (MN12, in subsection I of “Rema Marmara”) mammal faunas record the debut and the end of continental deposition in the Strimon Basin and Orphanic Gulf areas, respectively (De Bruijn, 1989). Subsequently, in the course of the latest Tortonian/early Messinian, we find the onset of a shallow marine phase in the Strimon Basin, witnessed by the marine beds of the Dafni Formation (Figs. 3.2 and 3.7). The Orphanic Gulf area was at first flooded only locally, as can be observed in Kavala Road West and Akropotamos. More widespread, but still shallow marine conditions existed in this area in the beginning of the late Messinian, during deposition of the Choumnikon Formation in the Strimon Basin. After the marine interval, a phase of brackish to freshwater conditions occurred in the Orphanic Gulf area too, lasting until the end of the Messinian. In the Early Pliocene, both areas connected to the open sea again. In the Strimon Basin, this ingressions was very brief and only shallow marine sedimentation took place, whereas deep marine successions accumulated in the coastal area along the Orphanic Gulf. Finally, in the Plio-Pleistocene, basin infill by renewed massive supply of predominantly coarse clastics led to fluvio-deltaic conditions in the Orphanic Gulf and Strimon Basin areas as before in the Tortonian.

The mixed mollusc faunas from the Dafni and Choumnikon beds show that the Strimon Basin formed (part of) a transitional area between the Mediterranean and the Eastern Paratethys in Messinian/Maeotian-Pontian time (Gramann and Kockel, 1969; Popov and Neveeskaya, 2000). Atlantic-Mediterranean influence in the pre-Pontian Aegean successions during the Maeotian (first half of the Messinian) is illustrated by the presence of marine beds, frequently reefal limestones, including the Dafni beds of the Strimon Basin, and the Trakones limestones near Athens (Gramann and Kockel, 1969; Stevanović et al., 1990, pp. 340-352). Furthermore, marine mollusc faunas and nannofossils were recovered from Maeotian deposits in the Ponto-Caspian Basin (Gramann and Kockel, 1969; Semenenko and Pevzner, 1979; Mărunțeanu and Papaianopol, 1998; Neveeskaya et al., 2003), suggesting ingressions from the Atlantic-Mediterranean realm. Also during the Pontian time, we conclude that intermittent palaeogeographical connections with the Paratethys existed (supposedly via the Aegean area). This is indicated by the discontinuous distribution of levels with nannofossils intercalated in successions of Pontian/late Messinian age in the Orphanic Gulf-Strimon Basin area and in the Dacic and Euxinic basins (Mărunțeanu and Papaianopol, 1998; Snel et al., 2006-chapter 2). Our conclusion on the ephemeral spilling

of Atlantic Ocean waters into the Mediterranean Basin during the Pontian/late Messinian is corroborated by the observations of Castradori (1998). He reported nannofossil assemblages (although anomalous, indicating unfavourable conditions) from the stratigraphic equivalent of the Lago Mare Formation in ODP Site 967 in the Eastern Mediterranean and in Sites 975 and 978 in the Western Mediterranean.

Aside from these brief marine incursions from the Mediterranean, the opposite, i.e. invasion of brackish (Eastern) Paratethys waters in the Aegean domain, prevailed during the Pontian/late Messinian. Brackish water faunas, typical for the early Pontian, are present in the Orphanic Gulf-Strimon Basin area from 6.3 Ma (the age of the base of the Choumnikon Formation) onward. These faunas are also found further to the east in the Xanthi-Komotini Basin, as well as near Athens in the Trakones area and on the island of Aegina (Papp and Steininger, 1979; Rögl et al., 1991; Syrides 1998). In the Orphanic Gulf area, Paratethyan faunas were observed only after the interval of evaporite deposition (Steffens et al., 1979), as in the Lago Mare Formation throughout many parts of the Mediterranean.

The Messinian salinity crisis is characterized by a widely recognised erosional surface across the Mediterranean, including canyons in the margins (Chumakov, 1973; Clauzon, 1973; Hsü et al., 1973; Cita and Ryan, 1978). The responsible regional sea-level drop is also recorded in sequences of the Black Sea Basin, in the uppermost part of the Miocene, and has been discussed by Hsü (1978), Hsü and Giovanoli (1979), Kojumdgieva (1983), and, more recently, by Clauzon et al. (2005) and Popescu (2006). The erosional surface on the Black Sea margin (Hsü and Giovanoli, 1979) and a pre-Pliocene unconformity at the entrance of the Danube in the western part of the Dacic Basin (Clauzon et al., 2005) were interpreted to express the effects of the climax of the Messinian salinity crisis on the Eastern Paratethys. The corresponding desiccation event must equally have affected the Orphanic Gulf-Strimon Basin area. Indeed, we suggest that the late Messinian stage of isolation of the Mediterranean from the Atlantic Ocean resulted in deposition of the non-marine unit of gravel/sandstone and topping travertine marker bed (indicated by line 'T'; Fig. 3.7). The basin-wide effect of the desiccation event can explain that this laterally uniform, sedimentary unit covers a relatively large part of the Orphanic Gulf area.

However, we did not find evidence for a prolonged phase of erosion persisting until the Early Pliocene, as proposed by Clauzon et al. (1996) for the marginal basins of the Mediterranean Sea. Instead, the consistent sequence of evaporite-brackish water-travertine-brackish water beds in the sections of Kavala Road, "Rema Marmara" (even with nannofossil levels between the travertines and the Pliocene marls; Fig. 3.3a), and Akropotamos, which predates the open marine Pliocene beds (Fig. 3.7), suggests that after the (brief) erosional phase aquatic conditions were restored. The inferred marine ingressions in the deep Mediterranean basins (Castradori, 1998), in the marginal basins of our Northern Aegean study area, as well as in the Dacic Basin (Snel et al., 2006-chapter 2), before the beginning of the Pliocene, question a deep basin-shallow water scenario for the entire late Messinian. If the foraminifera beds in the Orphanic Gulf area belong to the very base of the Zanclean, the period of desiccation thus occurred before the end of the Messinian (and Pontian) stage. I.e., probably between the intervals of the Lower Evaporites and the Lago Mare of the Mediterranean Basin: in line with the 'gap' at 5.59-5.50 Ma of Krijgsman et al. (1999).

The Dafni-Choumnikon transition in the Strimon Basin, where the strata of both formations cover roughly the same area, appears to be characterized by a rapid environmental change from marine to brackish water conditions, without a changing basin configuration (Gramann and Kockel, 1969). Similarly, the Miocene-Pliocene boundary of the Orphanic Gulf area seems to comprise the transition from brackish environments to open marine conditions, possibly through

improved connections of the Atlantic and Mediterranean areas. The sudden appearance of benthic and planktonic foraminifera suggests a rapid relative rise of sea level. Our palaeobathymetry data show that the Orphanic Gulf area was already a relatively deep basin in the Early Pliocene (500-900 m; Fig. 3.6). In this area, subsidence kept pace with sedimentation during the late Tortonian/early Messinian, until the deposition of shallow water evaporites. We suggest that between this moment and the Early Pliocene increased subsidence occurred. However, we find no indications for a tectonically induced transgression, caused by ongoing subsidence, at the beginning of the Pliocene. The presence of brackish water faunas and intercalated nannofossil assemblages in the highest part of the Messinian illustrates that, before the Early Pliocene, the basin was not completely desiccated. It might even be possible that in this part of the Northern Aegean no Pliocene flooding proper occurred. Perhaps, the Miocene-Pliocene transition was merely marked here by a change of salinity, caused by the increasing influence of Atlantic-Mediterranean over Paratethyan waters.

## Acknowledgements

Hans de Bruijn (Utrecht) and George Syrides (Thessaloniki) are gratefully thanked for their invaluable guidance, sampling efforts, and discussions in the field. The efforts of Constantin Doukas (Athens), to arrange the necessary permits and to solve logistical problems, are highly appreciated. Stefan Garstman is thanked for his skilful assistance in paleomagnetic sampling. We also thank Geert Ittmann and Gerrit van 't Veld for providing washed/sieved samples and nanno-smear slides, and Douwe van Hinsbergen for carrying out palaeo-bathymetry analyses. We particularly thank the reviewers Isabella Raffi and Silvia Iaccarino for critically reviewing an earlier version of the manuscript, and also Davide Castradori, Frits Hilgen, and Cor Langereis for their valuable comments.

This work was conducted under the programme of the Netherlands Research School of Sedimentary Geology (NSG). The Netherlands Research Centre for Integrated Solid Earth Science (ISES) provided funds for visiting research fellowships for the second author (M.M.) and for sampling campaigns. This is NSG publication 20021204.

## References

- Armour-Brown, A., Bruijn, H. de, Maniati, C., Siatos, G., Niesen, P., 1979. The geology of the Neogene sediments north of Serrai and the use of Rodent faunas for biostratigraphic control. Proceedings of the 6<sup>st</sup> Colloquium on the Geology of the Aegean Region, Athens 1977, 2, 615-622.
- Bornovas, J., Rondogianni-Tsiambaou, Th., 1983. Geological map of Greece. 2<sup>nd</sup> edition, Institute of Geology and Mineral Exploration, Athens.
- Bramlette, M.N., Sullivan, F.R., 1961. Coccolithophorids and related nannoplankton of the early Tertiary in California. *Micropaleontology* 7 (2), 129-188.
- Castradori, D., 1998. Calcareous nannofossils in the basal Zanclean of the Eastern Mediterranean Sea: remarks on paleoceanography and sapropel formation. Proceedings of the Ocean Drilling Program, Scientific Results 160, 113-124. doi:10.2973/odp.proc.sr.160.005.1998.

- Cavalezzi, B., Raffi, I., Biondi, R., 2002. Ceratoliths in the lowermost Pliocene of the Eastern Mediterranean: correlation to the equatorial Atlantic (poster). *Journal of Nannoplankton Research* 24 (2), 81.
- Chumakov, I.S., 1973. Pliocene and Pleistocene deposits of the Nile valley in Nubia and upper Egypt. Initial reports of the Deep Sea Drilling Project 13, 1242-1243. doi:10.2973/dsdp.proc.13.144-3.1973.
- Cita, M.B., Ryan, W.B.F., (Eds.) 1978. Messinian erosional surfaces in the Mediterranean. *Marine Geology* 27, 193-366. doi:10.1016/0025-3227(78)90031-2.
- Clauzon, G., 1973. The eustatic hypothesis and the pre-Pliocene cutting of the Rhone valley. Initial reports of the Deep Sea Drilling Project 13, 1251-1256. doi:10.2973/dsdp.proc.13.144-5.1973.
- Clauzon, G., Suc, J.-P., Gautier, F., Berger, A., Loutre, M.-F., 1996. Alternate interpretation of the Messinian salinity crisis: Controversy resolved? *Geology* 24 (4), 363-366. doi:10.1130/0091-7613(1996)024<0363: AIOTMS>2.3.CO;2.
- Clauzon, G., Suc, J.-P., Popescu, S.-M., Mărușeanu, M., Rubino, J.-L., Marinescu, F., Melinte, M.C., (2005). Influence of Mediterranean sea-level changes on the Dacic Basin (Eastern Paratethys) during the late Neogene: the Mediterranean Lago Mare facies deciphered. *Basin Research* 17, 437-462. doi:10.1111/j.1365-2117.2005.00269.x.
- De Bruijn, H., 1989. Smaller mammals from the Upper Miocene and Lower Pliocene of the Strimon basin, Greece. Part 1. Rodentia and Lagomorpha. *Bollettino della Società Paleontologica Italiana* 28 (2-3), 189-195.
- Dermitzakis, M.D., Georgiades-Dikeoulia, E., Velitzelos, E., 1986. Ecostratigraphic observations on the Messinian deposits of Akropotamos area (Kavala, N. Greece). *Annales Géologiques des Pays Helléniques* 33, 367-376.
- Dinter, D.A., 1998. Late Cenozoic extension of the Alpine collisional orogen, northeastern Greece: Origin of the north Aegean basin. *Geological Society of America Bulletin* 110 (9), 1208-1230. doi:10.1130/0016-7606(1998)110 <1208:LCEOTA>2.3.CO;2.
- Dinter, D.A., Royden, L., 1993. Late Cenozoic extension in northeastern Greece: Strymon Valley detachment system and Rhodope metamorphic core complex. *Geology* 21, 45-48. doi:10.1130/0091-7613(1993)021<0045:LCEING> 2.3.CO;2.
- Gramann, F., Kockel, F., 1969. Das Neogen im Strimonbecken (Griechisch-Ostmazedonien). Teil 1: Lithologie, Stratigraphie und Paläogeographie. *Geologisches Jahrbuch* 87, 445-484.
- Hsü, K.J., 1978. Stratigraphy of the lacustrine sedimentation in the Black Sea. Initial Reports of the Deep Sea Drilling Project 42B, 509-524. doi:10.2973/dsdp.proc.42-2.115.1978.
- Hsü, K.J., Giovanoli, F., 1979. Messinian event in the Black Sea. *Palaeogeography, Palaeoclimatology, Palaeoecology* 29, 75-93. doi:10.1016/0031-0182(79)90075-0.
- Hsü, K.J., Cita, M.B., Ryan, W.B.F., 1973. The origin of the Mediterranean evaporites. Initial Reports of the Deep Sea Drilling Project 42, 1203-1231. doi:10.2973/dsdp.proc.13.143.1973.
- Karistineos, N.K., Georgiades-Dikeoulia, E., 1986. The marine transgression in the Serres basin. *Annales Géologiques des Pays Helléniques* 33, 221-232.
- Kojumdgieva, E., 1983. Palaeogeographic environment during the desiccation of the Black Sea. *Palaeogeography, Palaeoclimatology, Palaeoecology* 43, 195-204. doi:10.1016/0031-0182(83)90011-1.
- Krijgsman, W., Hilgen, F.J., Raffi, I., Sierro, F.J., Wilson, D.S., 1999. Chronology, causes and progression of the Messinian salinity crisis. *Nature* 400, 652-655. doi:10.1038/23231.

- Lourens, L.J., Hilgen, F.J., Laskar, J., Shackleton, N.J., Wilson, D., 2004. The Neogene Period. In: Gradstein, F.M., Ogg, J.G., Smith, A.G. (Eds.), *A geologic time scale 2004*, Cambridge University Press, Cambridge.
- Martini, E., 1971. Standard Tertiary and Quaternary calcareous nannoplankton zonation. In: Farinacci, A. (Ed.), *Proceedings of the 2<sup>nd</sup> International Conference on Planktonic Microfossils*, Roma 1970, 2, Edizioni Tecnoscienza, Rome, pp. 739-785.
- Mărunțeanu, M., Papaianopol, I., 1998. Mediterranean calcareous nannoplankton in the Dacic Basin. *Romanian Journal of Stratigraphy* 78, 115-121.
- Meulenkamp, J.E., 1979. The Aegean and the Messinian salinity crisis. *Proceedings of the 6<sup>st</sup> Colloquium on the Geology of the Aegean Region*, Athens 1977, 3, 1253-1263.
- Negri, A., Villa, G., 2000. Calcareous nannofossil biostratigraphy, biochronology and paleoecology at the Tortonian/Messinian boundary of the Faneromeni section (Crete). *Palaeogeography, Palaeoclimatology, Palaeoecology* 156, 195-209. doi:10.1016/S0031-0182(99)00140-6.
- Neveeskaya, L.A., Goncharova, I.A., Il'ina, L.B., Paramonova, N.P., Khondkarian, S.O., 2003. The Neogene stratigraphic scale of the Eastern Paratethys. *Stratigraphy and Geological Correlation* 11 (2), 105-127.
- Papp, A., Steininger, F.F., 1979. Paleogeographic implications of Late Miocene deposits in the Aegean region. *Annales Géologiques des Pays Helléniques*, Tome hors série 2, 955-959.
- Pollak, W.H., 1979. Structural and lithological development of the Prinos-Kavala Basin, Sea of Thrace, Greece. *Annales Géologiques des Pays Helléniques*, Tome hors série 2, 1002-1011.
- Popescu, S.-M., 2006. Late Miocene and early Pliocene environments in the southwestern Black Sea region from high-resolution palynology of DSDP Site 380A (Leg 42B). *Palaeogeography, Palaeoclimatology, Palaeoecology* 238, 64-77. doi:10.1016/j.palaeo.2006.03.018.
- Popov, S.V., Neveeskaya, L.A., 2000. Late Miocene brackish water mollusks and the history of the Aegean basin. *Stratigraphy and Geological Correlation* 8 (2), 195-205.
- Proedrou, P., 1979. The evaporites formation in the Nestos-Prinos Graben in the Northern Aegean Sea. *Annales Géologiques des Pays Helléniques*, Tome hors série 2, 1013-1020.
- Psilovikos, A., Syrides, G.E., 1983. Stratigraphy, sedimentation, and palaeogeography of the Strymon Basin, eastern Macedonia/northern Aegean Sea, Greece. *Clausthaler Geologische Abhandlungen* 44, 55-87.
- Raffi, I., Rio, D., 1979. Calcareous nannofossil biostratigraphy of DSDP Site 132, Leg 13 (Tyrrhenian Sea, Western Mediterranean). *Rivista Italiana di Paleontologia e Stratigrafia* 85, 127-172.
- Raffi, I., Backman, J., Rio, D., 1998. Evolutionary trends of tropical calcareous nannofossils in the late Neogene. *Marine Micropaleontology* 35, 17-41. doi:10.1016/S0377-8398(98)00014-0.
- Raffi, I., Mozzato, C., Fornaciari, E., Hilgen, F.J., Rio, D., 2003. Late Miocene calcareous nannofossil biostratigraphy and astrobiochronology for the Mediterranean region. *Micropaleontology* 49 (1), 1-26. doi:10.2113/49.1.1.
- Rio, D., Raffi, I., Villa, G., 1990. Pliocene-Pleistocene calcareous nannofossil distribution patterns in the Western Mediterranean. *Proceedings of the Ocean Drilling Program, Scientific Results* 107, 513-533. doi:10.2973/odp.proc.sr.107.164.1990.
- Rögl, F., Bernor, R.L., Dermitzakis, M.D., Müller, C., Stancheva, M., 1991. On the Pontian Correlation in the Aegean (Aegina Island). *Newsletters in Stratigraphy* 24, 137-158.

- Roveri, M., Bassetti, M.A., Ricci Lucchi, F., 2001. The Mediterranean Messinian salinity crisis: an Apennine foredeep perspective. *Sedimentary Geology* 140, 201-214. doi:10.1016/S0037-0738(00)00183-4.
- Semenenko, V.N., Pevzner, M.A., 1979. Upper Miocene-Pliocene correlation of the Ponto-Caspian on biostratigraphic and paleomagnetic data. *Izvestiya Akademii Nauk SSSR, Seriya Geologicheskaya* 9, Moscow, 5-15.
- Siesser, W. G., 1998. Calcareous nannofossil Genus *Scyphosphaera*: structure, taxonomy, biostratigraphy, and phylogeny. *Micropaleontology* 44 (4), 351-384.
- Snel, E., Mărunțeanu, M., Macaleț, R., Meulenkamp, J.E., Van Vugt, N., 2006. Late Miocene to Early Pliocene chronostratigraphic framework for the Dacic Basin, Romania. *Palaeogeography, Palaeoclimatology, Palaeoecology* 238, 107-124. doi:10.1016/j.palaeo.2006.03.021.
- Steffens, P., Bruijn, H. de, Meulenkamp, J.E., Benda, L., 1979. Field guide to the Neogene of Northern Greece (Thessaloniki area and Strimon basin). Publications of the Department of Geology and Paleontology of the University of Athens, Series A, 35, 1-14.
- Steininger, F.F., Papp, A., 1979. Current biostratigraphic and radiometric correlations of Late Miocene Central Paratethys stages (Sarmatian s.str., Pannonian s.str., and Pontian) and Mediterranean stages (Tortonian and Messinian) and the Messinian Event in the Paratethys. *Newsletters on Stratigraphy* 8 (2), 100-110.
- Steininger, F.F., Berggren, W.A., Kent, D.V., Bernor, R.L., Sen, S., Agustí, J., 1996. Circum-Mediterranean Neogene (Miocene and Pliocene) marine-continental chronologic correlations of European mammal units. In: Bernor, R.L., Fahlbusch, V., Mittmann, H.-W. (Eds.), *The evolution of Western Eurasian Neogene mammal faunas*, Columbia University Press, New York, pp. 7-46.
- Stevanović, P.M., Neveškaja, L.A., Marinescu, F., Sokac, A., Jámbor, A., 1990. Pontien-Pl<sub>1</sub> (sensu F. Le Play, N.P. Barbot de Marny, N.I. Andrusov). Serie Chronostratigraphie und Neostatotypen, Neogen der Westlichen ("Zentrale") Paratethys 8. JAZU and SANU, Zagreb-Belgrade.
- Syrides, G.E., 1998. Paratethyan mollusc faunas from the Neogene of Macedonia and Thrace, Northern Greece. *Romanian Journal of Stratigraphy* 78, 171-180.
- Theodoridis, S., 1984. Calcareous nannofossil biozonation of the Miocene and revision of the Helicoliths and Discoasters. *Utrecht Micropaleontological Bulletins* 32, 1-272.
- Van Couvering, J.A., Castradori, D., Cita, M.B., Hilgen, F.J., Rio, D., 2000. The base of the Zanclean Stage and of the Pliocene Series. *Episodes* 23 (3), 179-187.
- Van der Zwaan, G.J., Jorissen, F.J. and De Stigter, H.C., 1990. The depth dependency of planktonic/benthonic foraminiferal ratios: Constraints and applications. *Marine Geology*, 95: 1-16. doi:10.1016/0025-3227(90)90016-D.
- Van Hinsbergen, D.J.J., Kouwenhoven, T.J., Van der Zwaan, G.J., 2005. Paleobathymetry in the backstripping procedure: correction for oxygenation effects on depth estimates. *Palaeogeography, Palaeoclimatology, Palaeoecology* 221 (3-4), 245-265. doi:10.1016/j.palaeo.2005.02.013.
- Zijderveld, J.D.A., 1967. A.c. demagnetization of rocks: analysis of results. In: Collinson, D.W., Creer, K.M., Runcorn, S.K. (Eds.), *Methods in palaeomagnetism*. Elsevier, Amsterdam, pp. 254-286.

# **Vertical motions in the Aegean volcanic arc: evidence for rapid subsidence preceding volcanic activity on Milos and Aegina**

---

This chapter is published as: Van Hinsbergen, D.J.J., Snel, E., Garstman, S.A., MăruŃeanu, M., Langereis, C.G., Wortel, M.J.R., Meulenkamp, J.E., 2004. Vertical motions in the Aegean volcanic arc: evidence for rapid subsidence preceding volcanic activity on Milos and Aegina. *Marine Geology* 209, 329-345. doi:10.1016/j.margeo.2004.06.006.

## **Abstract**

Late-orogenic extension in the Aegean region has been ongoing since the Late Eocene or Early Oligocene. Contemporaneously, numerous volcanic centres developed. In the south-central Aegean region, Plio-Pleistocene volcanism formed a number of islands. On two of these, Milos and Aegina, a sequence of Late Miocene and Pliocene marine sediments underlies the oldest volcanoclastics. To determine whether extension of the Aegean lithosphere played a role in the formation and location of the Early Pliocene volcanoes of the Aegean, we aimed to reconstruct the vertical motion history as it occurred prior to the onset of volcanism. To this end, we reconstructed the paleobathymetry evolution using foraminifera recovered from sedimentary sections in the lower Pliocene of Milos and Aegina. Age dating on the Milos sections was based on bio-, magneto-, and cyclostratigraphy; from Aegina, only bio- and magnetostratigraphy were available. The results show that prior to the onset of volcanism on both islands many hundreds of metres of Early Pliocene subsidence occurred, on Milos even 900 m between 5.0 and 4.4 Ma. It is unlikely that extension of the Aegean lithosphere led to melting of the underlying mantle. However, the extension probably did play a significant role in the timing of the onset of Pliocene volcanic activity in the Aegean. The position of the volcanic centres is probably the result of the depth of the subducted slab below the Aegean and the formation of a network of extensional faults in the overriding Aegean lithosphere.

## **4.1 Introduction and Geological Setting**

After the main phase of late Mesozoic and Tertiary collision between the African and Eurasian plates, lithospheric extension started to fragment the Aegean area in the course of the Early Miocene (see Gautier et al., 1999, for a review). During the lithospheric extension, subduction has been ongoing, continuing a compressional regime in the external part of the Aegean domain. Behind and crosscutting the external outer Aegean, extensional basins formed, as well as volcanic centres (McKenzie, 1978a; Le Pichon and Angelier, 1979; Fytikas et al., 1984). Since the Late Miocene, volcanic centres have developed in the southern part of the Aegean (Fig. 4.1), notably

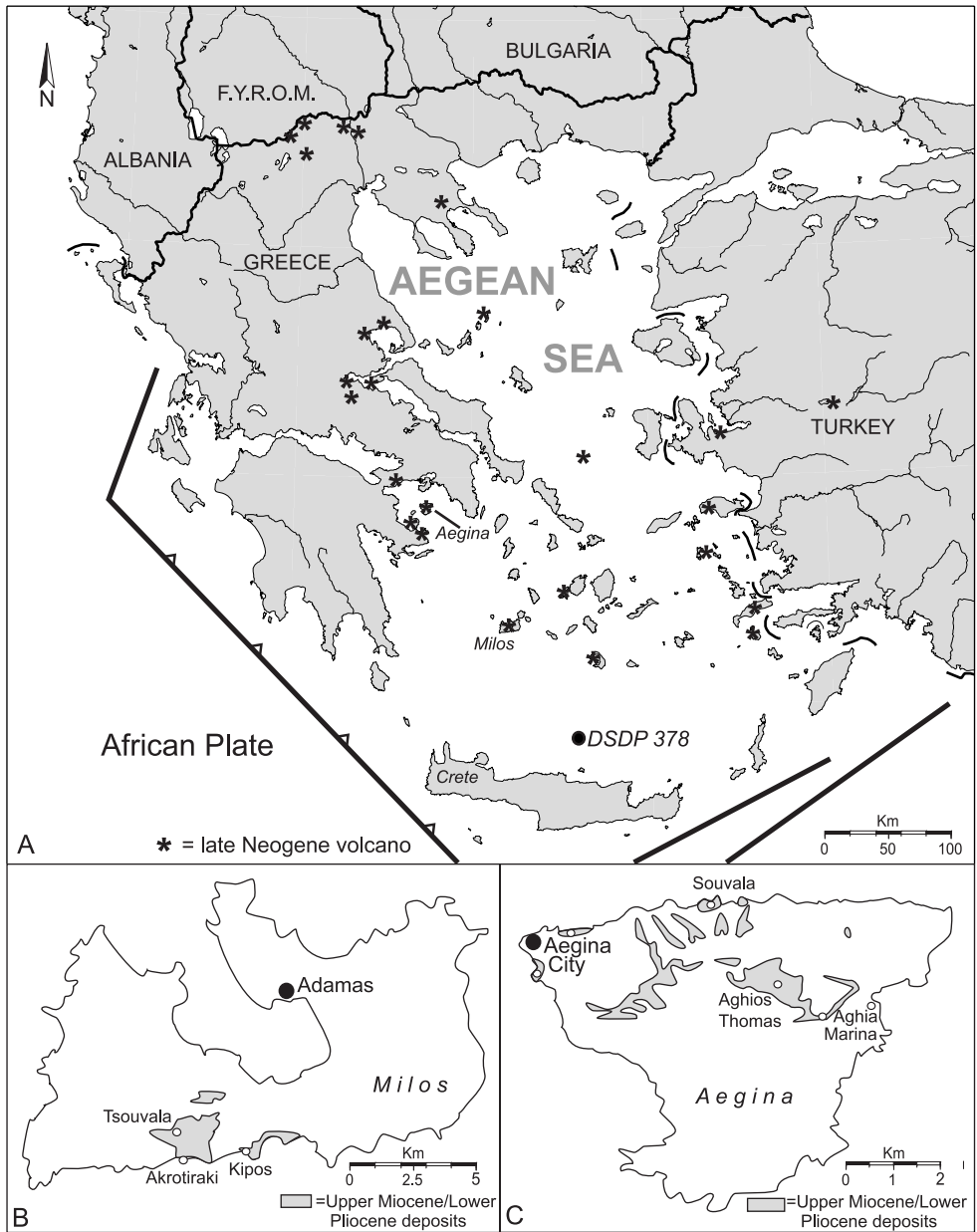


Figure 4.1. a) Map of Aegean area. Locations of Neogene volcanoes taken from Pe-Piper and Piper (2002); b, c) maps with the selected sections on the islands of Milos and Aegina, respectively.



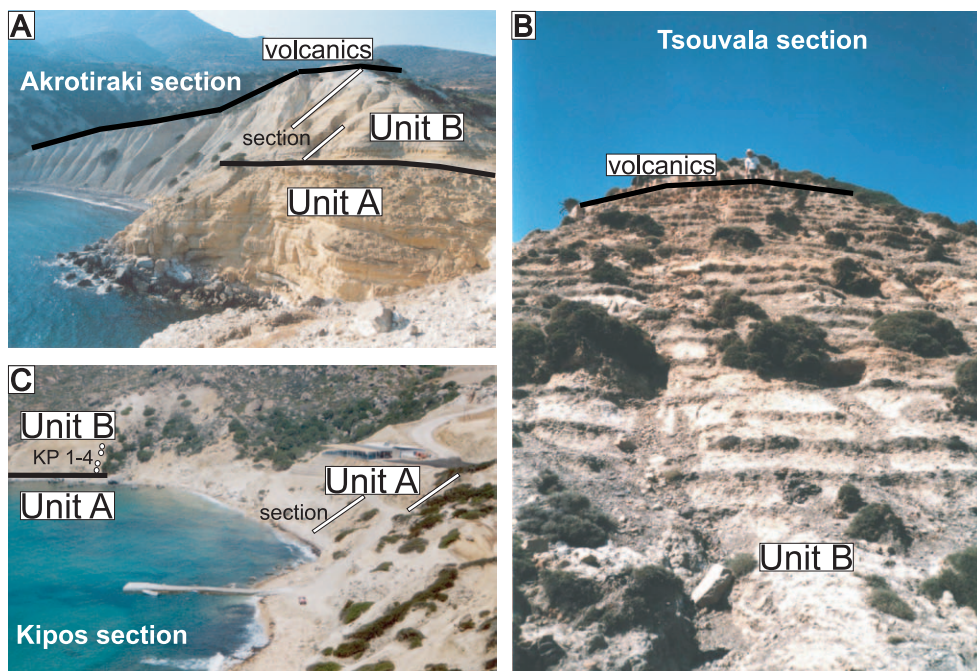


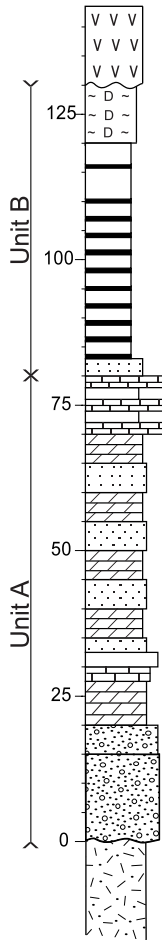
Figure 4.2. Photograph of the sections on Milos. a) Akrotiraki; b) Tsouvala; c) Kipos and position of samples KP 1-4.

during the Early Pliocene (4-2.5 Ma) and the middle Pleistocene to Holocene (1 Ma-recent; e.g., Fytikas et al., 1984).

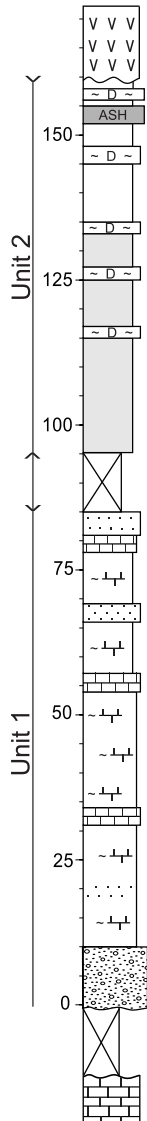
In tectonically active settings, volcanism can generally be associated with melting due to subduction of hydrated lithosphere or extension of the lithosphere leading to partial melting because of extension-induced (adiabatic) decompression. In the Aegean example, where both subduction and extension occur simultaneously, Pe and Piper (1972) and Briquieu et al. (1986) consider Aegean volcanism to be the result of melting associated with subduction of African lithosphere. Subduction has been ongoing since the late Mesozoic (Van Hinsbergen et al., 2005b). Thus, the question arises why volcanism was initiated in the southern Aegean in the Early Pliocene, instead of being active throughout the entire subduction history. Pe-Piper and Hatzipanagiotou (1997) suggested that volcanism was triggered by a combination of extension of the overriding lithosphere and subduction and Perissoratis (1995) suggested that an early Pleistocene change in fault patterns led to the formation of the Santorini volcanic centre.

If rapid crustal extension played a significant role in the origin of Aegean volcanism, one would expect rapid pre-volcanic subsidence on the site of the present-day volcanoes. To test this, we aimed to carry out a vertical motion study based on paleobathymetry fluctuations (following Steckler and Watts, 1978; Watts et al., 1982; Van Hinsbergen et al., 2005a) and a detailed integrated stratigraphic study to derive high-resolution timing of vertical motions preceding the onset of volcanism. Promising successions were reported by Benda et al. (1979), Meulenkamp (1979), and Fytikas et al. (1986) from the upper Miocene to lower Pliocene of Milos and Aegina islands (Fig. 4.1), where volcanism developed in the course of the Early Pliocene (Müller et al., 1979; Fytikas et al., 1986).

**a Milos**



**b Aegina**



**legend:**

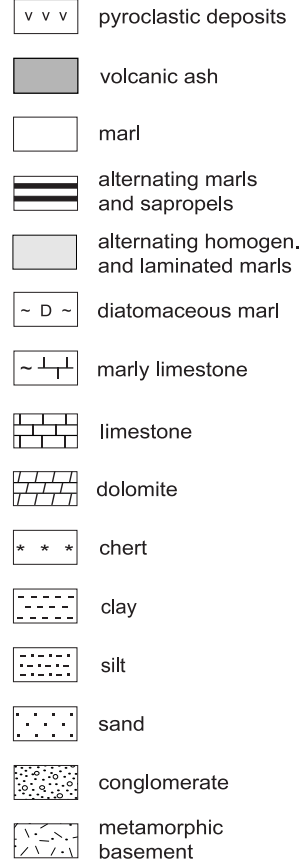


Figure 4.3. Composite lithostratigraphic columns of the Neogene sediments on (a) Milos and (b) Aegina.

**4.1.1 Milos**

The oldest Neogene sediments unconformably overlie metamorphosed basement along the southern coast of Milos (Fig. 4.1; Fytikas, 1977; Meulenkamp, 1979). These Neogene sediments can be subdivided into Unit A, Unit B, and a series of volcanoclastic sediments that unconformably overlie Unit B (Figs. 4.2 and 4.3a).

Unit A contains 80 m of fluvio-lacustrine, brackish, and shallow marine conglomerates, sandstones, dolomites, and occasional reefal (coral) limestone. The top 20 m of Unit A contains

a well-recognisable *Limnocardium* mould-bearing lacustrine limestone bed amidst intercalations of shallow marine hardgrounds, slumped marls, and sand- and limestones (see also Meulenkamp, 1979).

The overlying Unit B (Figs. 4.2 and 4.3a) was deposited in a marine environment. It locally starts with a 2 m thick sandy base, containing pycnodonts and shark teeth, followed by a rhythmic alternation of marine marls and sapropels. The top of the unit consists of diatomaceous (sandy) marls. The thickness of Unit B varies between 25 and 60 m because of the irregular character of an unconformity that separates this unit from the overlying volcanoclastic series having ages of  $3.5 \pm 0.14$  Ma and younger (Fig. 4.2; Fytikas et al., 1986).

A selection of three sections was made to construct a composite record covering a maximum time-interval. The section of Akrotiraki (Figs. 4.1, 4.2a, and 4.4a) comprises the upper 18 m of Unit A (samples AT V-IX), the lower 30 m of Unit B (samples Gr 10.431-536) and 2 m of the overlying volcanics. The Tsouvala section (Figs. 4.1, 4.2b, and 4.4b) contains 28 m of the marl-sapropel alternations of Unit B (samples Gr 10.151-245) and 2 m of the lowermost part of the overlying volcanics. Scarce outcrops of limestones of Unit A are present, but the transition to Unit B is not exposed. Both the upper part of Unit A and Unit B display mm-sized biotite-bearing volcanic ash intercalations (ashes 1-5; Fig. 4.4). The third section (Kipos; Figs. 4.1, 4.2c, and 4.4c) is 21 m thick and consists of alternating shallow marine sands, marls, and limestones (upper part of Unit A; samples Gr 10.541-586). A hundred metres further to the west, marly siltstones and sandstones of Unit B were sampled (KP 1-4; Fig. 4.2c), which directly overlie the uppermost hardground of Unit A. Severe fracturing made it impossible to correlate samples KP 1-4 to section Kipos, but the presence of the transition from Unit A to Unit B enabled correlation to section Akrotiraki (KP 2; Fig. 4.4a). Section Kipos can be correlated with section Akrotiraki through the beds with *Limnocardium*-moulds exposed at the base of both sections. From the three sections on Milos, 99, 95, and 32 levels were sampled for paleomagnetic purposes from the Akrotiraki, Tsouvala, and Kipos sections, respectively (Fig. 4.4).

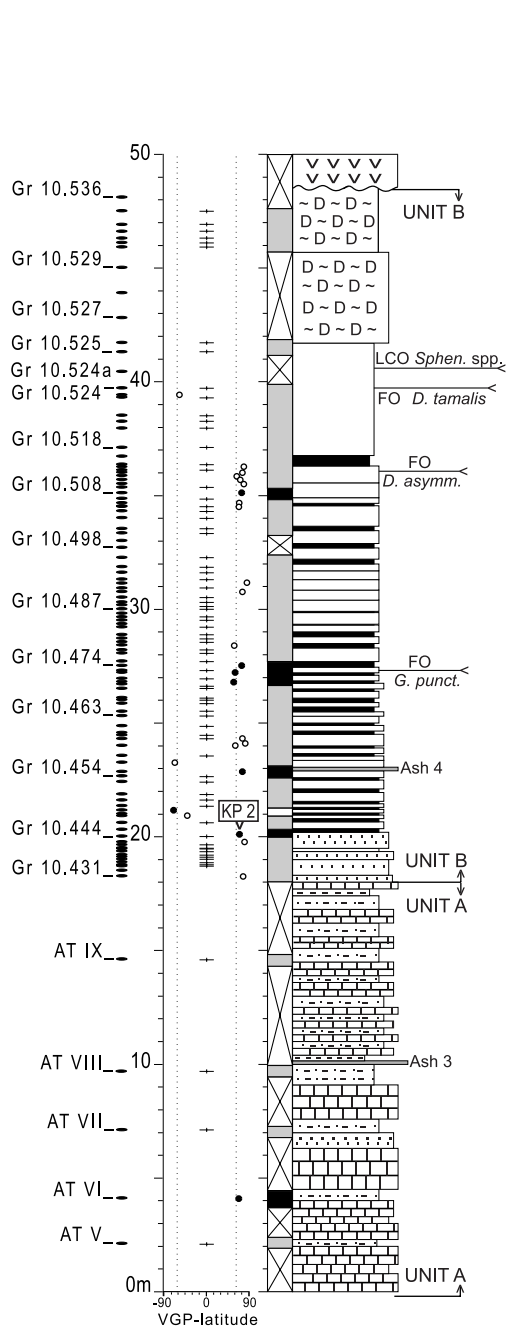
#### 4.1.2 Aegina

The Neogene sedimentary sequence of Aegina (Fig. 4.3b) unconformably overlies folded, unmetamorphosed Mesozoic carbonates, radiolarites, and siliciclastics. The Neogene deposits crop out in the northern part of the island (Fig. 4.1). Late Pliocene and Pleistocene volcanoclastics cover the central and southern parts of Aegina (Müller et al., 1979; Pe-Piper et al., 1983; Morris, 2000). The oldest reported Neogene sediments (Unit 1) are continental conglomerates, grading upwards into (at least) 75 m of marls, sands and marly limestones of lacustrine and brackish facies, containing brackish-water molluscs and ostracods (Rögl et al., 1991). A sequence (Unit 2) of at least 70 m of alternating laminated and homogeneous marls overlies Unit 1 (Benda et al., 1979). The contact between the two units is not exposed. Unit 2 contains a volcanic ash layer, and is unconformably overlain by an andesitic volcanoclastic series (Figs. 4.3 and 4.5; Pe, 1973; Müller et al., 1979; Pe-Piper et al., 1983).

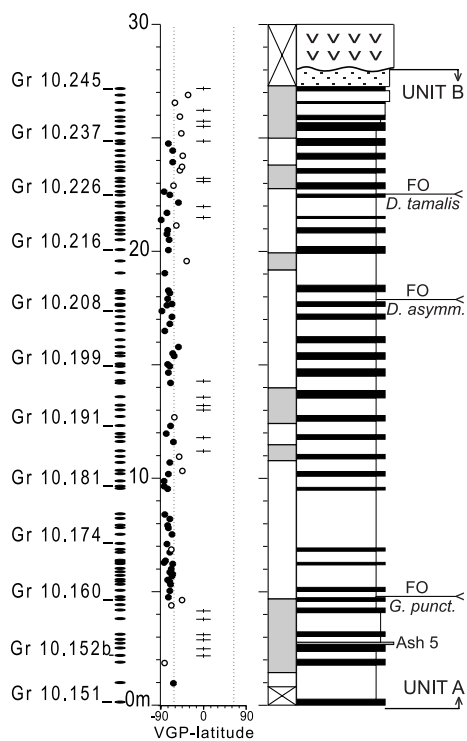
Approximately 25 m of Unit 1 were studied by Rögl et al. (1991) in the Souvala section along the northern coast (Figs. 4.1 and 4.5a), while Unit 2 was described and sampled in the Aghios Thomas section (Benda et al., 1979) a few kilometers inland (Figs. 4.1 and 4.5b).

We resampled the Souvala section (Aeg 1-19 for paleomagnetic purposes and So 1-61 for biostratigraphic analysis) and logged an additional 50 m compared to Rögl et al. (1991; Fig. 4.5a). Samples Gr 1401-1444, collected by Benda et al. (1979), and two additional samples at the base of the Aghios Thomas section (Ag 1-2; Fig. 4.5b) were analysed. Additionally, five outcrops of

**a** Akrotiraki



**b** Tsouvala



**c** Kipos

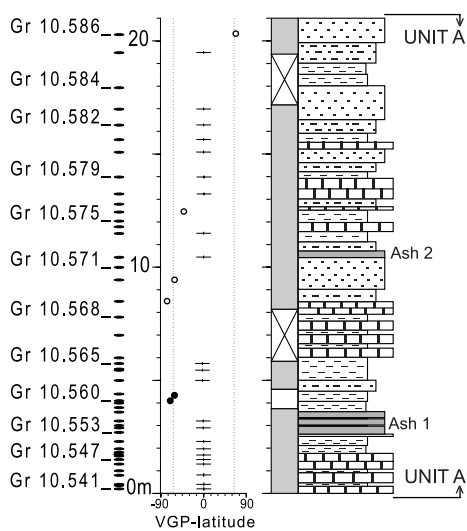


Figure 4.4. Lithostratigraphic columns of the analysed sections on Milos, including the recorded bio-events. Gr (and other) numbers correspond to samples collected and held by the Faculty of Earth Sciences, Utrecht University. a) Akrotiraki section. Sample KP 2 was taken from a laterally equivalent outcrop (Fig. 4.2c); b) Tsouvala section; c) Kipos section. Lithology, samples and paleomagnetic results, represented as virtual geomagnetic polar (VGP) latitude, with polarity zone interpretation. (Open) solid circles denote projections of (less) reliable ChRM directions; '+' denotes inconclusive results (Fig. 4.6a). In the polarity column, black (white) denotes normal (reversed) polarity; grey indicates less reliable and inconclusive polarity; for intervals without data, white and cross is used. Sphen. spp. = *Sphenolithus* spp.; *D. tamalis* = *Discoaster tamalis*; *D. asymm.* = *Discoaster asymmetricus*, *G. punct.* = *Globorotalia punctulata*. For lithology key, see Figure 4.3.

marine marls near Aegina city (AC 1-5) and scattered outcrops of marine marls and limestones in the northeast of the island near Aghia Marina (Fig. 4.1) were sampled (Gr 10.961-10.998) and analysed.

## 4.2 Biostratigraphy

Planktonic foraminiferal and calcareous nannoplankton biostratigraphies are based on the stratigraphical distribution of the Early Pliocene marker species in the Mediterranean (Lourens et al., 2004, and references therein).

The samples collected for analysis of the foraminiferal content were washed and sieved with a 125- $\mu\text{m}$  sieve; nannofossil samples were prepared according to standard preparation techniques (Bramlette and Sullivan, 1961).

### 4.2.1 Milos

Unit A contains only few fossil-bearing beds, without age-diagnostic biomarkers. Except for the sandy base, Unit B in sections Akrotiraki and Tsouvala contains moderately to well-preserved foraminiferal and calcareous nannofossil assemblages.

The first occurrence (FO) of the planktonic foraminifer *Globorotalia punctulata* is found both in the Akrotiraki-section (between Gr 10.473 and Gr 10.474) and in the Tsouvala-section (between Gr 10.160 and Gr 10.161; Fig. 4.4).

Three nannofossil bio-events are recorded: the FO of *Discoaster asymmetricus* between Gr 10.512 and Gr 10.513 in the Akrotiraki-section and between Gr 10.211 and Gr 10.212 in the Tsouvala-section; the FO of *D. tamalis* between Gr 10.523 and Gr 10.524 in the Akrotiraki section and between Gr 10.226 and Gr 10.227 in the Tsouvala-section (Fig. 4.4; Plate 4.I). The last common occurrence (LCO) of *Sphenolithus* spp. is recorded between Gr 10.524 and Gr 10.524a of the Akrotiraki section.

### 4.2.2 Aegina

Samples So 1-61 from the Souvala section (Unit 1 in Figs. 4.3b and 4.5a) did not contain any age-diagnostic nannofossils or foraminifera. In contrast, Rögl et al. (1991) reported the occurrence of *Ceratolithus acutus* from a single level in the section, a taxon belonging to the NN12 Zone sensu Martini (1971).

The two samples Ag 1-2 collected at the base of section Aghios Thomas (Unit 2 in Figs. 4.3b and 4.5b) are assigned to the upper part of the NN12 Zone, based on the absence of *Triquetrorhabdulus rugosus* and *C. rugosus* in combination with the co-occurrence of *Amaurolithus*

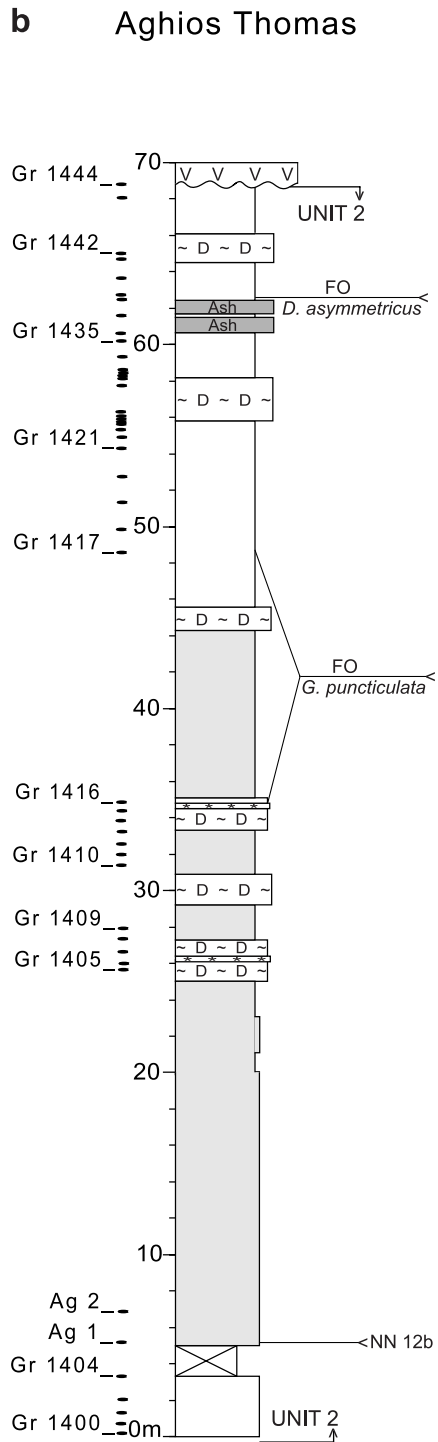
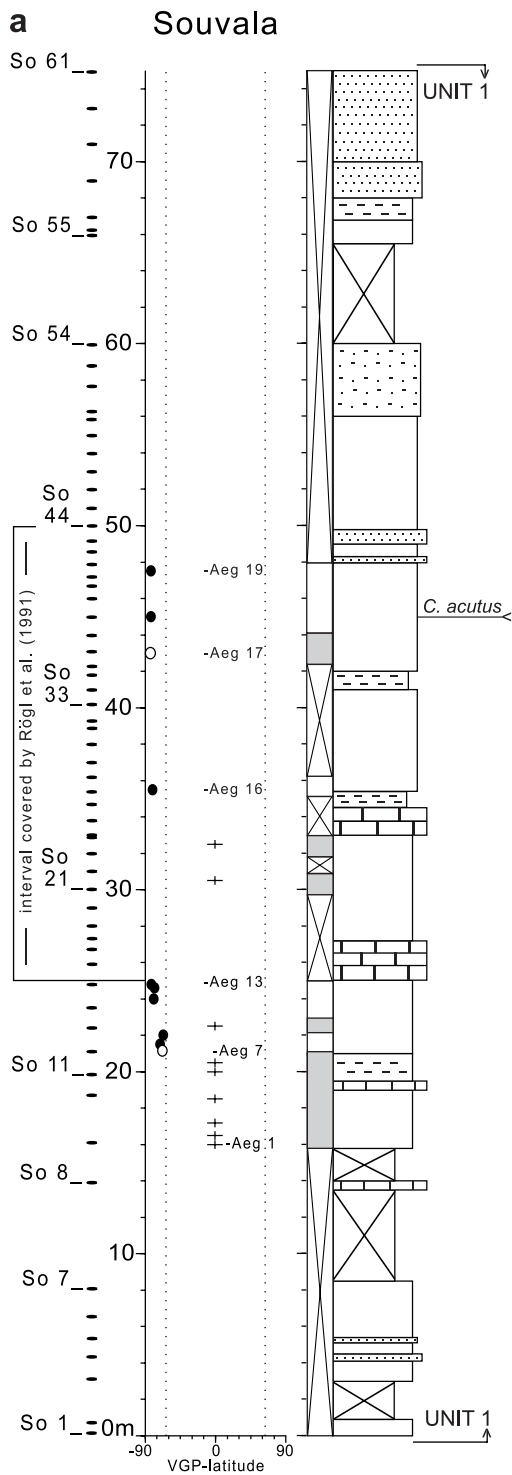


Figure 4.5. Lithostratigraphic columns of the analysed sections on Aegina, including the recorded bio-events. Gr- and other numbers refer to samples collected and held by the Faculty of Earth Sciences, Utrecht University. a) Souvala section, in part modified from Rögl et al. (1991); b) Aghios Thomas section, modified from Benda et al. (1979). Lithology, samples and paleomagnetic results, represented as virtual geomagnetic polar (VGP) latitude, with polarity zone interpretation. (Open) solid circles denote projections of (less) reliable ChRM directions. In the polarity column, white denotes reversed polarity; grey indicates less reliable and inconclusive polarity; for intervals without data, white and cross is used. For lithology key, see Figure 4.3.

*delicatus* and *Helicosphaera sellii*. Benda et al. (1979) reported the FO of *Globorotalia puncticulata* between Gr 1416 and Gr 1417 and the FO of *Discoaster asymmetricus* between Gr 1438 and Gr 1439 (Fig. 4.5b). Two of the additionally collected samples from the northeast of Aegina (Gr 10.961-10.998) contained age-diagnostic nannofossil assemblages: both Gr 10.983 and Gr 10.997 (near Aghia Marina; Fig. 4.1) were assigned to NN13-14, based on the absence of *Pseudoemiliana lacunosa* and the abundance of *H. sellii*. Samples AC 4 and 5 belong to the NN14-15 Zone, based on the presence of *D. asymmetricus* and the absence of *D. tamalis*.

In summary, the biostratigraphy of the marine marls of Milos (Unit B) and Aegina (Unit 2) indicates that both units were deposited during the Early Pliocene.

### 4.3 Magnetostratigraphy

The paleomagnetic samples were taken with a water-cooled, generator-powered electric drill and oriented with a magnetic compass. At least one specimen per sampling level was thermally demagnetised with small temperature increments of 20-50°C up to a maximum temperature of 690°C in a magnetically shielded, laboratory-built furnace. The natural remanent magnetisation (NRM) of the specimens was measured on a 2G Enterprises horizontal DC SQUID cryogenic magnetometer.

Almost all samples from sections Souvala, Akrotiraki, and Kipos have very low intensities. In most cases, a normal polarity component is removed at temperatures between 100 and 210°C. This relatively low-temperature component typically has a present-day field direction before bedding plane correction and can thus be regarded as a secondary, recent overprint, likely caused by weathering. After removal of the low-temperature component, the remaining intensity of most samples of Akrotiraki and Kipos is too low to reliably interpret a characteristic remanent magnetisation (ChRM) direction from the demagnetisation diagrams (Fig. 4.6a; Zijdeveld, 1967), although occasionally a clear indication of the polarity of the ChRM can be interpreted (Fig. 4.6b). Some samples of the Souvala (Aegina), Akrotiraki, and Kipos sections and most samples of the Tsouvala section show that a relatively high temperature component is gradually removed between temperatures of 210°C and 390-450°C or 580°C (Figs. 4.6c and 4.6d). This component is taken as the ChRM.

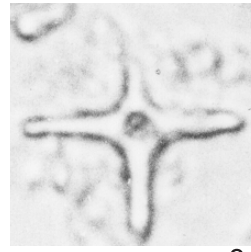
Maximum unblocking temperatures in the range of 290-410°C indicate that the NRM is (in part) carried by iron sulphides. In addition, magnetite is indicated as carrier of the magnetic signal considering the maximum unblocking temperature of ~580°C. In some cases, a (normal polarity) high-temperature (up to 650°C) haematite component is present in the Tsouvala-section, which is interpreted as a recent magnetisation (Fig. 4.6e). In some cases, these magnetite and haematite components have a largely overlapping unblocking temperature spectrum, resulting in a 'cluster' between 230°C and 590°C (Fig. 4.6f). In such cases, no ChRM can be derived; grey intervals in



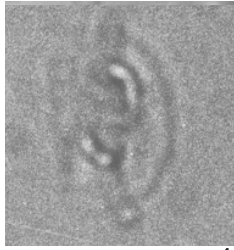
1



2



3



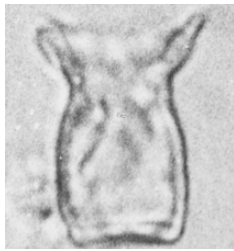
4



5



6



7



8



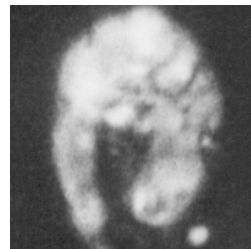
9



10



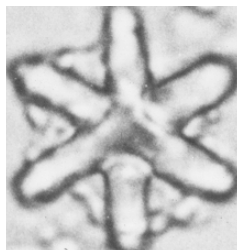
11



12



13



14



15



Plate 4.I. Calcareous nannofossils from the Akrotiraki section on Milos.

- 1) *Discoaster asymmetricus* Gartner,  $\times 1800$ ; sample Gr 10.517. Parallel light.
- 2) *Discoaster asymmetricus* Gartner,  $\times 2300$ ; Gr 10.517. Parallel light.
- 3) *Discoaster tamalis* Kamptner,  $\times 2800$ ; Gr 10.532. Parallel light.
- 4-5) *Helicosphaera sellii* Bukry and Bramlette,  $\times 2000$ ; Gr 10.447. (4) Parallel light; (5) crossed nicols.
- 6) *Coccolithus pelagicus* (Wallich), coccosphere,  $\times 2100$ ; Gr 10.445. Crossed nicols.
- 7-8) *Scyphosphaera halldallii* Deflandre,  $\times 2200$ ; Gr 10.453. (7) Parallel light; (8) crossed nicols.
- 9) *Amaurolithus tricorniculatus* (Gartner),  $\times 2100$ ; Gr 10.446. Parallel light.
- 10) *Amaurolithus delicatus* Gartner and Bukry,  $\times 2500$ ; Gr 10.445. Parallel light.
- 11-12) *Ceratolithus rugosus* Bukry and Bramlette,  $\times 2900$ ; Gr 10.454. (11) Parallel light; (12) crossed nicols.
- 13) *Ceratolithus rugosus* Bukry and Bramlette,  $\times 3000$ ; Gr 10.455. Parallel light.
- 14) *Discoaster jobani* n. sp.,  $\times 2200$ ; Gr 10.501. Parallel light.
- 15) *Discoaster jobani* n. sp.,  $\times 2300$ ; Gr 10.518. Parallel light.

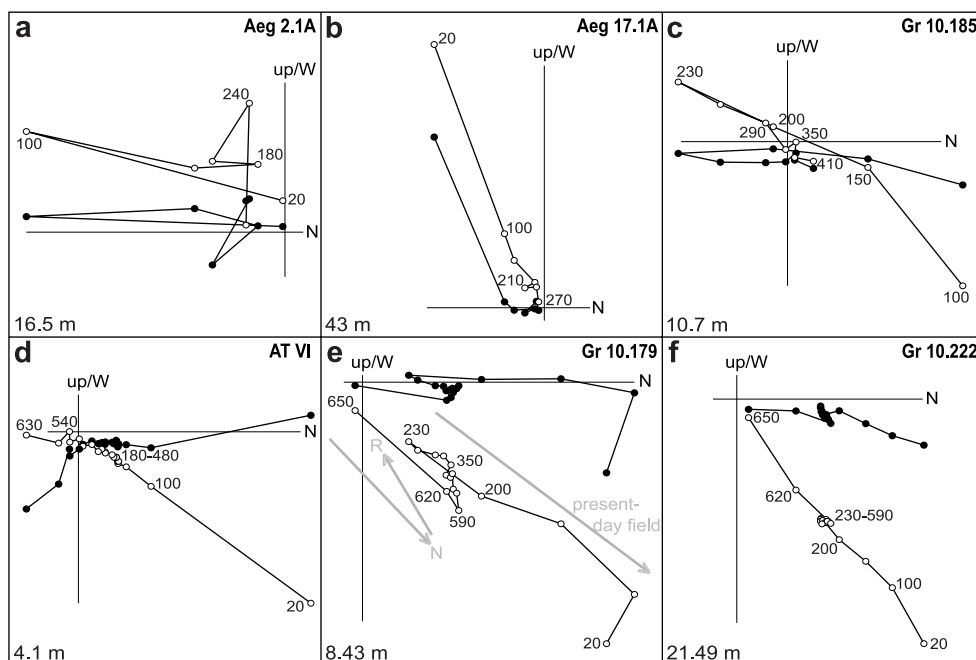


Figure 4.6. Thermal demagnetisation diagrams of selected samples of the paleomagnetically analysed sections. Orthogonal projections with open (solid) symbols denote ChRM vector end-points (corrected for bedding tilt) on the vertical (horizontal) plane; values represent temperature increments in °C. Stratigraphic levels are in the lower left corners. a) Inconclusive; b) unreliable reversed; c) reliable reversed (iron sulphide); d) reliable normal (magnetite); e) reliable reversed (magnetite) with normal maghaemite or haematite overprint and (f) inconclusive (either normal polarity with haematite as the carrier of the signal or reversed with magnetite as the carrier with a haematite overprint) ChRM directions.

Figure 4.7. Correlation of the sections of southern Milos to the 65°N summer insolation curve of Laskar et al. (1993) and the cyclo- and magnetostratigraphy of the Rossello composite section (Lourens et al., 1996). Bio-events taken from Lourens et al. (2004). Thick solid tie lines indicate bio-events: A) FO *Globorotalia puncticulata* (4.52 Ma); B) FO *Discoaster asymmetricus* (4.12 Ma); C) FO *Discoaster tamalis* (3.97 Ma); D) LCO *Sphenolithus* spp. (3.70 Ma). Dotted tie lines indicate magnetic reversals and thin solid lines represent the tuning of marl-sapropel alternations to the Laskar-curve. For lithology key, see Figure 4.3.

Figures 4.4 and 4.5 represent these samples. Directions were calculated for each reliable ChRM component, after correction for bedding tilt.

In summary, the ChRM do not allow the construction of an unambiguous polarity zonation in section Akrotiraki (Fig. 4.4a). All samples of sections Kipos, Tsouvala, and Souvala that can be reliably interpreted reveal a reversed polarity (Figs. 4.4 and 4.5a).

## 4.4 Age model

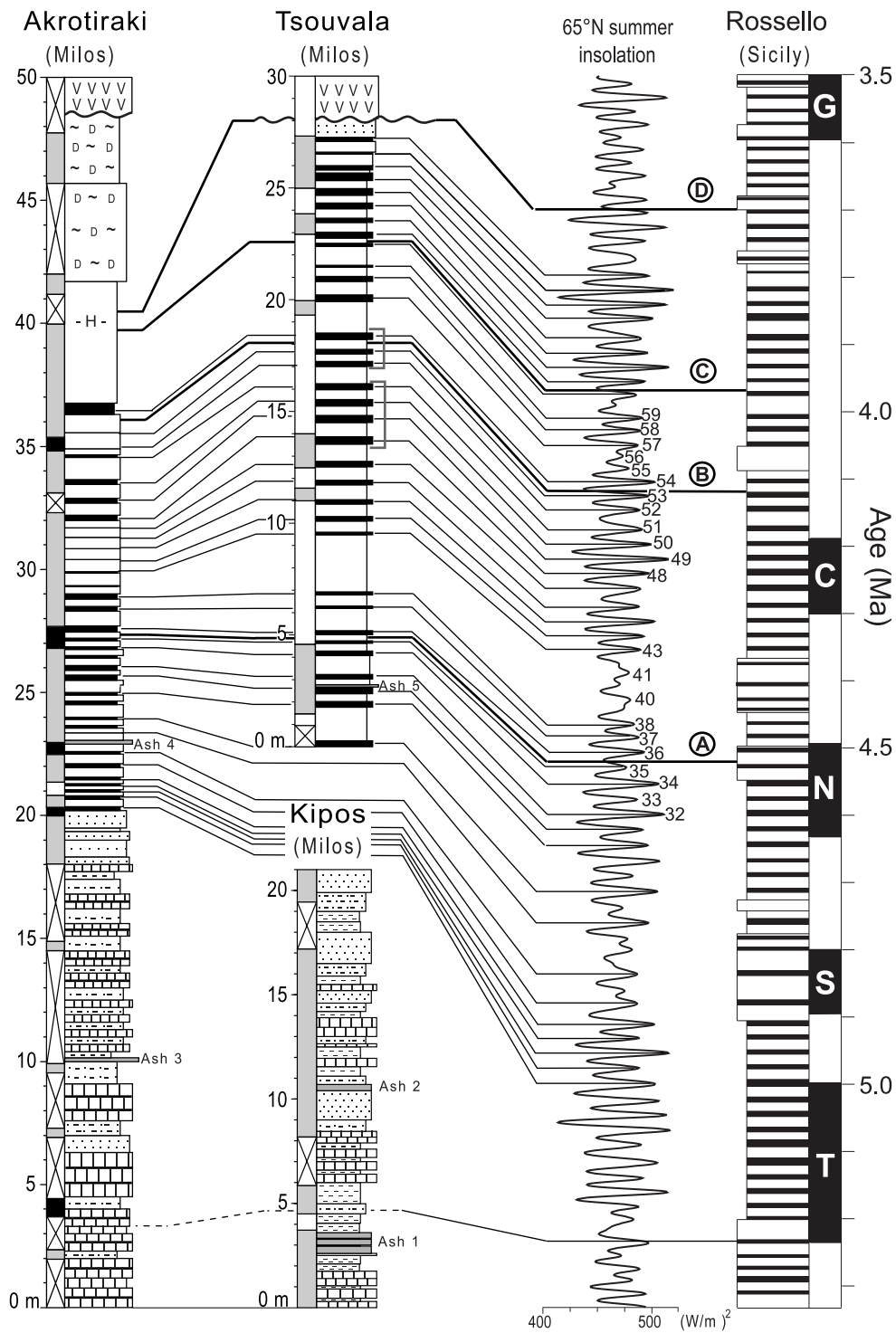
### 4.4.1 Age model for the Neogene deposits predating volcanism on Milos

Astronomical calibration of cyclic lithology alternations in Late Miocene and Pliocene sections in the Mediterranean (e.g., Hilgen, 1991; Steenbrink et al., 1999; Lourens et al., 2004) has shown that these alternations can be tuned to the target curve of summer insolation of Laskar et al. (1993). This tuning has enabled the construction of astronomical polarity time scales (APTS).

The marine succession of Unit B on Milos reveals a cyclic pattern of marls and sapropels (Figs. 4.4a and 4.4b). Since the biostratigraphy indicates Early Pliocene ages, a correlation to the Rossello composite section on Sicily (Langereis and Hilgen, 1991) can be attempted.

This correlation must mainly rely on the biostratigraphic events, since the magnetostratigraphy of our sections is insufficiently precise. The following bio-events recorded in the Tsouvala and Akrotiraki sections are correlated with those in the Rossello composite section (Lourens et al., 2004): (event A) the FO of *Globorotalia puncticulata* at 4.52 Ma, (event B) the FO of *Discoaster asymmetricus* at 4.12 Ma, (event C) the FO of *D. tamalis* at 3.97 Ma, and (event D) the LCO of *Sphenolithus* spp. at 3.70 Ma (Fig. 4.7).

The framework provided by biostratigraphy can now be used for further astronomical tuning of the individual marl-sapropel cycles to the target-curve of Laskar et al. (1993; Fig. 4.7). This tuning is based on pattern correspondence between the marl-sapropel alternations and the cyclic variations in the intensity of summer insolation at 65°N caused by the interference of three Milankovitch cycles: the eccentricity (with a period of 400 and 100 kyr), obliquity (41 kyr) and precession (21 kyr). 400 kyr eccentricity minima result in 'missing sapropels', such as seen in cycles 40 and 41 (Fig. 4.7). In the 400 kyr eccentricity maxima, the interference between the 100 kyr eccentricity and precession cyclicity led to development of triplets (52-54) or quadruplets (48-51) of sapropels (Fig. 4.7). Finally, interference between obliquity and precession can be inferred from alternating clearly developed (32, 34) and poorly (35) or non-developed (33) sapropels (Fig. 4.7). Tuning of Tsouvala is rather straightforward, since the above-described patterns are clearly developed. Between 27 and 32 m in Akrotiraki, the patterns are less well developed and an apparent decrease in sedimentation rate occurred. The quadruplet of 48-51, however, is clear, as is the duplet 37-38. It follows that the age of the lowest sapropel in the Akrotiraki section (at 20.3 m; Fig. 4.7) is estimated at 5.0 Ma.



In the top 15 m of Unit B, sapropel-marl alternations are lacking, which impedes cyclostratigraphical correlation with the APTS. Moreover, the short stratigraphical distance (less than 1 m) between bio-events C and D in the upper part of the Akrotiraki section suggests the presence of a hiatus (-H-; Fig. 4.7). The age of the unconformably overlying volcanic series ( $3.5 \pm 0.14$  Ma and younger; Fytikas et al., 1986), however, provides the minimum age for the top of Unit B.

A reversed polarity is found for all reliable samples from the Tsouvala section. The correlation of the bio-events with the Rossello composite section indicates, however, that during the deposition of the Tsouvala-section at least three magnetic reversals must have occurred. This suggests that the reversed ChRM directions are caused by a post-depositional overprint during a reversed interval.

Although the magnetostratigraphic data obtained from the Akrotiraki section are of poor quality (Fig. 4.4a), the available results do not contradict the bio- and cyclostratigraphic correlations. This implies that the normal polarity of samples AT VI (4m) and KP 2 (20m) in the Akrotiraki section must be interpreted to belong to the Thvera subchron (C3n.4n: 5.236-4.998 Ma; Lourens et al., 2004). The correlation of Unit A to the APTS is impossible, since no clear cycles can be distinguished.

From the 28 samples recovered from section Kipos, only samples Gr 10.560 and Gr 10.561 (~4m) give a conclusive ChRM direction, indicating a reversed polarity. These levels are interpreted to correspond to the uppermost part of subchron C3r just below the Thvera subchron.

In summary, Unit A was deposited prior to ~5.0 Ma, the marine marls and sapropels of Unit B have an age range of  $\sim 5.0$ - $3.5 \pm 0.14$  Ma, after which volcanism commenced.

#### 4.4.2 Age model for the Neogene deposits predating volcanism on Aegina

The age of the basal conglomerates is estimated at 8-6 Ma by Rögl et al. (1991), based on the recovery of two teeth of an advanced species of *Hipparion* s.s. The nannofossil *Ceratolithus acutus* at 45 m in the overlying Souvala section (Fig. 4.5a) has an age range of 5.372-5.046 Ma (Backman and Raffi, 1997). We thus interpret the reversed polarity between 21 and 48 m in the Souvala-section to belong to subchron C3r (6.04-5.236 Ma; Hilgen et al., 1995; Krijgsman et al., 1999). This is in good agreement with the ostracod and mollusc associations found between 25 and 50 m in the Souvala section (Fig. 4.5a), which have been assigned by Rögl et al. (1991) to the Pontian (6.15-5.3 Ma; Snel et al., 2006-chapter 2).

The oldest open marine clays of the section of Aghios Thomas have a calcareous nannofossil assemblage that is characteristic for the upper part of the NN12 Zone, which ranges from 5.23 to 5.09 Ma (Backman and Raffi, 1997). The first occurrences of *Globorotalia puncticulata* and *Discoaster asymmetricus* higher in the section (Fig. 4.5b; Benda et al., 1979) are calibrated to an age of 4.52 and 4.12 Ma, respectively (Lourens et al., 2004).

The marine marls in the northeast of the island near Aghia Marina (NN13-NN14: 5.09-4.0 Ma; Berggren et al., 1995a, 1995b; Backman and Raffi, 1997) and the marls in the northwest near Aegina City (NN14-NN15: 4.12-3.97; Lourens et al., 2004) serve to illustrate that marine sedimentation covered at least the entire northern part of Aegina during the Early Pliocene (Fig. 4.1).

In summary, deposition of Unit 1 commenced before or at 8-6 Ma and lasted into at least the late Messinian. Unit 2 has Early Pliocene ages, but the very base of the Pliocene has not been found. The age of the oldest lavas overlying Unit 2 is  $3.87 \pm 0.05$  Ma (Müller et al., 1979; Pe-Piper et al., 1983), slightly older than those on Milos.

#### 4.4.3 Age estimate of the oldest volcanic ash deposits on Milos

The oldest volcanic deposits that have been reported from Milos are the late Early Pliocene lavas overlying Unit B (Fytikas, 1977; Fytikas et al., 1986). However, we found older volcanic ash layers within Unit B that require some further discussion.

The biotite crystals in the volcanic ash layers in the Milos sections were too weathered to obtain reliable radiometric ages (pers. comm. K. Kuiper, 2001). Therefore, we estimate the ages of the ash layers by using the age model presented in paragraph 4.4.1 (Fig. 4.7).

The age estimate of Ash 1 (Fig. 4.7) is only based on the age of the overlying strata, which have a reversed polarity interpreted as subchron C3r (6.04–5.236 Ma; Hilgen, 1991; Krijgsman et al., 1999). The possible age range of ashes 2 and 3 (Fig. 4.7) is determined by the normal polarity of the strata on top of and below Ash 3 in section Akrotiraki, interpreted as the Thvera subchron (C3n.4n: 5.236–4.998 Ma; Lourens et al., 2004). The age estimates of Ash 4 in Akrotiraki and of Ash 5 in Tsouvala (Fig. 4.4) are based on the correlation of the marl-sapropel cycles to the APTS: 4.82 Ma and 4.62 Ma, respectively (Fig. 4.7). These volcanic ash layers and the one on Aegina with an age of  $4.4 \pm 0.2$  Ma (Müller et al., 1979) may originate from the older volcanic centres of, e.g., Antiparos or Patmos-Chiliomodi (Fig. 4.1), from which islands Fytikas et al. (1984) reported lavas with comparable ages. Thus, from the presented integrated stratigraphy it can be concluded that a sequence of lower Pliocene marine sediments was deposited just prior to the onset of volcanism on Aegina and Milos indeed.

#### 4.5 Paleobathymetry and vertical motions

Paleobathymetry analyses of the marine marls of Unit B on Milos and Unit 2 on Aegina were carried out to explore any changes in bathymetry that occurred prior to the oldest volcanic activity. The paleobathymetry reconstructions are based on the general relation between the plankton fraction (%P) of the total foraminiferal population and depth (Van der Zwaan et al., 1990), following procedures for the reconstruction of vertical motions described by Van Hinsbergen et al. (2005a).

The %P graphs versus time for both the Milos and Aegina sections are shown in Figure 4.8a. The graphs of Milos include a moving average curve with the standard deviation calculated per moving interval; it was chosen in such a way that approximately 100 kyr is averaged at every sample level. The obtained curves give a similar trend, but the %P values derived for the Tsouvala section are slightly lower than those of comparable ages obtained from the Akrotiraki-section.

The %P increase between ~5 and 4.4 Ma obtained from the Milos appears to take place in two distinct episodes. From the %S curves (percentage stress markers of the total number of benthic foraminifera) that are included in Figure 4.8a, however, a strong cyclic oxygen level variation can be concluded with a periodicity of 400kyr. Generally, an oxygen level-driven %S increase results in a relative drop in %P, which, superimposed on a deepening trend, can explain the episode of %P-decrease in the curve of Figure 4.8a (see Van Hinsbergen et al., 2005a, for further discussion on the relationship between %P, oxygen level, and depth). The intervals of lowest %S are thus considered to represent actual depth and are connected to construct a depth-induced %P trend (Van Hinsbergen et al., 2005a).

The calculated paleobathymetry versus time graphs of the studied sections are shown in Figure 4.8b. Following the scheme of Van Hinsbergen et al. (2005a), an independent bathymetry check was carried out on selected samples of the Akrotiraki and Aghios Thomas sections, based on

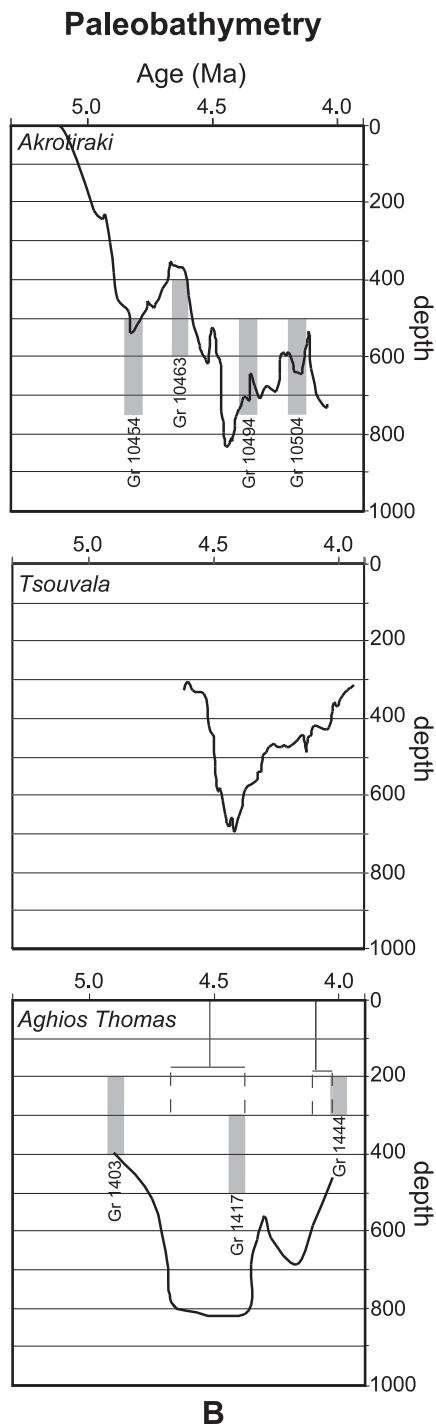
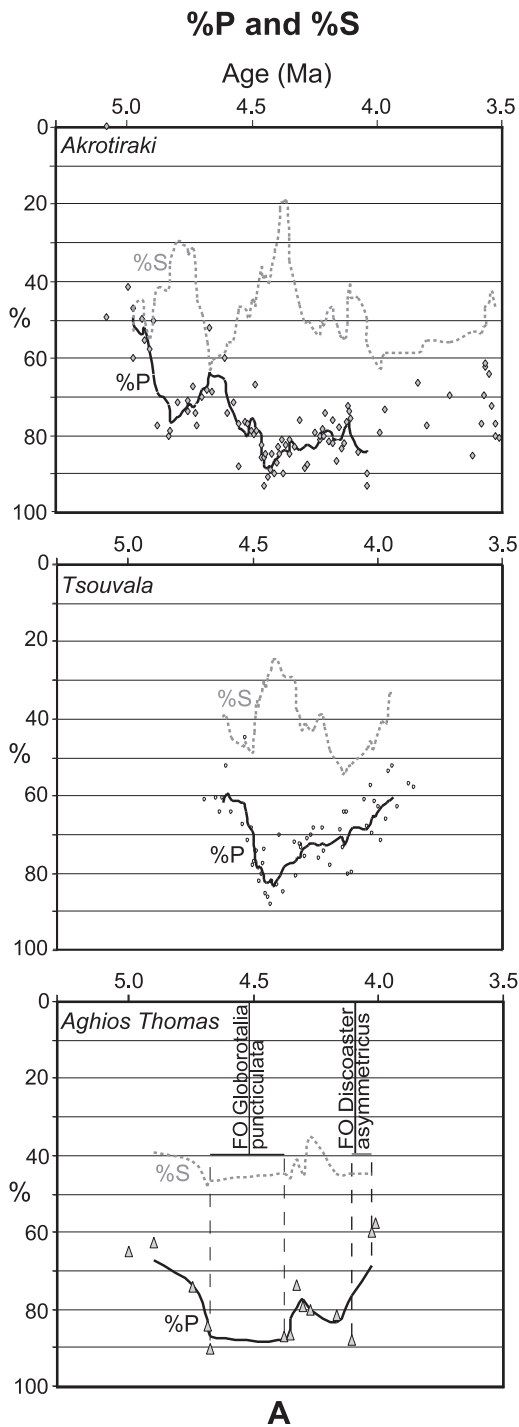


Figure 4.8. a,b) Paleobathymetry curves, determined from the Akrotiraki and Tsouvala sections on Milos and the Aghios Thomas section on Aegina, respectively. The moving averages are chosen to average approximately 100 kyr. The first occurrences (FO) of *Globorotalia puncticulata* and *Discoaster asymmetricus* are included in the graphs for the Aghios Thomas section to indicate the uncertainty in the age determination of the Aghios Thomas samples. For the age determination of the Milos curves, see Figure 4.7. Figure 4.8b includes the bathymetry estimations based on the independent taxonomy check.

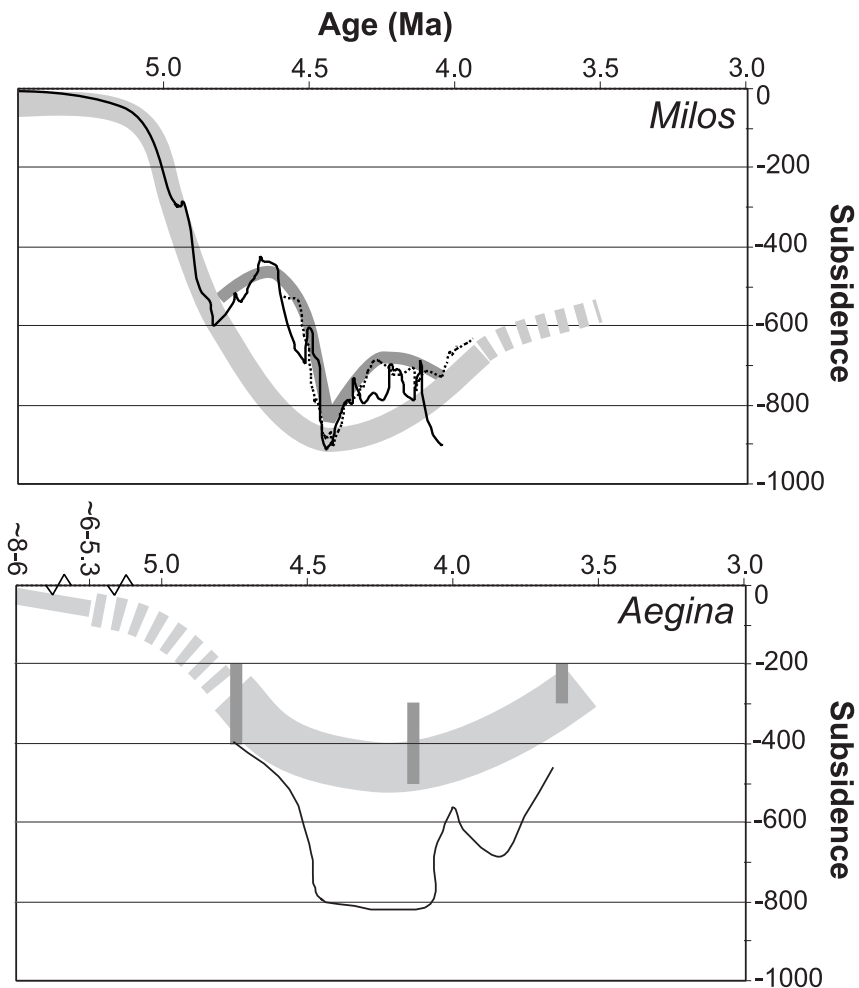


Figure 4.9. Vertical motion curves for Milos and Aegina. The bases of Unit A and Unit 1 were chosen as reference level for Milos and Aegina, respectively. Note that we follow the depth trend obtained from the qualitative depth markers on Aegina, which are considered more accurate than the calculated values, due to the high amount of stress-markers.

selected benthic foraminifera that are considered as depth markers. The results reveal benthic assemblages indicating biotope depth ranges that are in good agreement with the obtained depth values for the Akrotiraki section (Fig. 4.8b). The results for the Aghios Thomas section confirm the deepening trend, but may indicate that the calculated depth of 700-800 m is an over-estimation (Fig. 4.8b).

Now, paleobathymetry variations can be converted to (tectonically induced) vertical motions. For this purpose, three additional corrections were carried out. Firstly, the effects on paleobathymetry of sediment accumulation and compaction were corrected for. Furthermore, our high-resolution time control makes it possible to correct accurately for the sea level changes using the astronomically tuned sea level curve of (Lourens and Hilgen, 1997).

Figure 4.9 shows the thus obtained vertical motion curve constructed for the oldest Neogene of Milos and Aegina. The bases of Unit A and Unit 1 were taken as reference level. As a net result, during the deposition of Unit A and Unit 1, sedimentation kept pace with subsidence and eustatic sea level changes.

The paleobathymetry record and age control, obtained from the Aghios Thomas section on Aegina are of much poorer resolution than those derived from the Milos sections, but they serve to illustrate that the non-marine to brackish-water sedimentation of the Late Miocene was succeeded by the deposition of deep-marine Early Pliocene sediments pre-dating the earliest volcanism. The trends in vertical motion on both islands are thus comparable and occur within the same time span.

## 4.6 Analysis

The debut of Neogene subsidence on Milos and Aegina is reflected by the onset of deposition of Unit A and Unit 1, respectively. On Aegina, the oldest datable deposits have an age range of 8-6 Ma (Rögl et al., 1991). Our suggestion that sedimentation generally kept pace with basin subsidence during the deposition of Unit A and Unit 1 is supported by their respective lithologies, which are interpreted as representing alternating fluvial, brackish and shallow marine environments. Hence, approximately 80 m of subsidence during the deposition of Unit A and Unit 1 is reconstructed (Fig. 4.9).

The ages derived from Unit 1 on Aegina indicate that upper Messinian (Pontian) strata are included in the stratigraphy. Unit A of Milos may also cover (part of) the Messinian, but conclusive evidence is lacking. During the late Messinian, the Messinian Salinity Crisis occurred throughout the Mediterranean region (Krijgsman et al., 1999). However, both on Aegina and on Milos, no geologic evidence was found for the accompanying drastic sea level drop and subsequent rise. A dramatic relative sea level rise (~900m) occurred around 5 Ma on Milos, i.e., approximately 300 kyr after the Pliocene Flooding, which ended the Messinian Salinity Crisis (Krijgsman et al., 1999). This relative sea level rise is interpreted as the consequence of tectonic subsidence. This is in line with the seismic profiles and submarine tectonic maps of the Saronic Gulf of Papanikolaou et al. (1988), which show a complex pattern of E-W, N-S, and WNW-ESE trending normal faults, along which the WNW-ESE trending Saronic Gulf subsided during the Plio-Quaternary.

The comparable trends for Milos and Aegina shown in the curves of Figure 4.9 suggest that the high-resolution subsidence record obtained from Milos represents a regional rather than a local phenomenon. This is supported by a semi-quantitative paleobathymetry reconstruction carried out



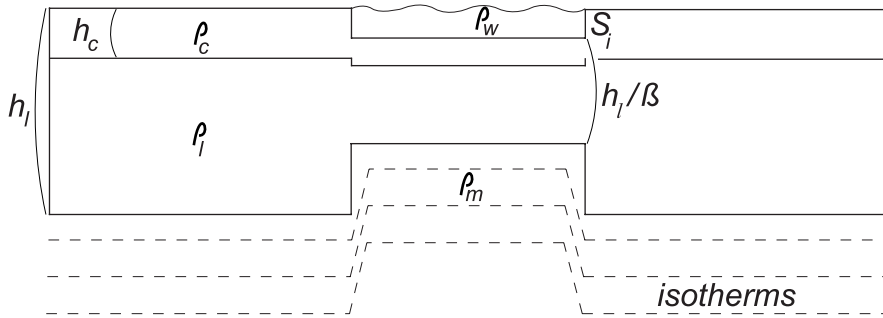


Figure 4.10. Stretching model for the lithosphere simplified after McKenzie (1978b). See text for further explanation.

on DSDP core 378 in the Sea of Crete by Wright (1978; Fig. 4.1), who estimated approximately 1000 m of Early Pliocene deepening in the Cretan basin.

In summary, immediately prior to the onset of volcanism on the islands of Milos and Aegina rapid subsidence occurred, with a maximum of approximately 1 km in the central Aegean. This subsidence is a regional phenomenon and is probably associated with large-scale extension in the southern and central Aegean.

We assume that the stretching model of McKenzie (1978b) can describe the extension. In this model, stretching-induced subsidence can be subdivided in an initial subsidence phase  $S_i$ , which is of tectonic origin, followed by a thermal subsidence (or uplift) phase as a result of cooling of the welled up asthenosphere. Since the Early Pliocene subsidence we determined from Milos and Aegina occurs rapidly, we consider this subsidence to correspond to  $S_i$ . The stretching factor  $\beta$  can be calculated from isostatic equilibrium conditions preceding and following the initial subsidence  $S_i$ . We simplified the model of McKenzie (1978b) by assuming constant densities for the crust ( $\rho_c = 2850 \text{ kg/m}^3$ ), lithospheric mantle ( $\rho_l = 3380 \text{ kg/m}^3$ ), sub-lithospheric mantle or asthenosphere ( $\rho_m = 3300 \text{ kg/m}^3$ ), and seawater ( $\rho_w = 1000 \text{ kg/m}^3$ ; Fig. 4.10):

$$\beta = (h_c \rho_c + (h_l - h_c) \rho_l - h_l \rho_m) / (h_c \rho_c + (h_l - h_c) \rho_l - h_l \rho_m - S_i \rho_w + S_i \rho_m) \quad (1)$$

where  $h_l$  is the initial thickness of the lithosphere including the crust and  $h_c$  is the initial thickness of the crust. Following McKenzie (1978b), we chose the initial thickness of the crust to correspond to the thickness of the present day crust below mainland Greece, i.e., to approximately 40 km (Makris, 1977). We assume that the thickness of the lithosphere prior to extension  $h_l$  equals 100 km. Using equation (1), the rapid, 1 km subsidence we obtained from Milos yields a stretching factor  $\beta$  of  $\sim 1.2$ .

McKenzie and Bickle (1988) determined that stretching of continental lithosphere generates only little melt, unless  $\beta > 2$  and the (dry) mantle potential temperature exceeds  $1380^\circ\text{C}$ . Thus, it seems highly unlikely that the stretching associated with the rapid Early Pliocene subsidence of Milos preceding volcanism led to melting of the underlying mantle.

The magmas that were erupted in the Aegean during the Early Pliocene probably must already have been present prior to the extension phase. The generation of the magmas is likely to have been caused by the addition of water to the mantle because of the subduction of the African plate,

lowering the melting temperature, as was suggested based on geochemical data by Barton et al. (1983) and Briquieu et al. (1986).

Extension not only occurred on the site of the present-day volcanic centres but also, e.g., in the Sea of Crete. The volcanic centres lie approximately at the 130–150 km isodepth line of a seismically defined north-dipping Benioff zone, interpreted to represent the top of the subducting African slab (Makropoulos and Burton, 1984; Hatzfeld, 1994; Giuchi et al., 1996; Papazachos et al., 2000). Hydrous minerals generally start to dehydrate when they are subducted to a depth of approximately 100–150 km (Philpotts, 1990). The depth of the subducted slab thus probably determines the position of the volcanic centres. The fact that during the Early Pliocene rapid subsidence occurred prior to the onset of volcanism leads us to conclude that there is a causal relationship between extension and the timing of the onset of volcanism, probably by the generation of a network of extensional faults facilitating magma rise.

#### 4.7 Summary and conclusions

To determine whether extension of the Aegean overriding lithosphere played a significant role in the formation and location of the Early Pliocene volcanoes of the Aegean we aimed to reconstruct the vertical motion history as it took place prior to the onset of volcanism. To this end, we reconstructed the paleobathymetry evolution of selected sections in the lower Pliocene of Milos and Aegina using the general relationship between the percentage of planktonic foraminifera amongst the total population and depth. Age dating on the Milos sections was based on bio-, magneto-, and cyclostratigraphy; on Aegina only bio- and magnetostratigraphic dating was possible. About 900 m of subsidence occurred on Milos between ~5 Ma and 4.4 Ma. Although less well constrained, a similar history is reconstructed from Aegina. Volcanic eruptions followed 1–1.5 Myr after the onset of rapid subsidence. We used a simplified model, based on McKenzie (1978b), to show that adiabatic decompression is highly unlikely to have led to the generation of the melts that were erupted during the Pliocene on Milos and Aegina. The fact that the onset of volcanism is preceded by a regional phase of rapid subsidence, however, leads us to conclude that the timing of the formation of the volcanoes is probably the result of Early Pliocene extension and the creation of associated faults, providing a way to the surface for pre-existing, subduction-related melts.

#### Acknowledgements

Francisco Sierro and David Piper are thanked for constructive reviews. Frits Hilgen, Charon Duermeijer, Nicole van Vugt and Sandra Langezaal carried out sampling of the Tsouvala section in 1997. Nicole van Vugt carried out the paleomagnetic analysis of these samples. Charon Duermeijer sampled and analysed the Souvala samples from Aegina. Constantin Doukas and Frosso Georgiades-Dikeoulia are thanked for their assistance in the Milos sampling campaign in 2000. Rob Lengkeek, Koenraad Elewaut, Maria Triantaphyllou and Yiannis Dimitriou are thanked for their assistance in sampling on Milos and Aegina in 2001. Frits Hilgen is acknowledged for his assistance in determining planktonic foraminifera. Bert van der Zwaan and Tanja Kouwenhoven are thanked for the fruitful discussions about the paleobathymetry-estimations and the determination of the benthic depth markers. Suzanne Bijl is acknowledged for the advice and discussion concerning the statistic analyses and Jason Herrin is thanked for

discussion on volcanism and melt generation. Gerrit van 't Veld and Geert Ittman are thanked for the preparation of the samples used for foraminiferal analysis.

This research was conducted under the research programmes of the Vening Meinesz Research School of Geodynamics (VMSG) and the Netherlands Research School of Sedimentary Geology (NSG). This is a VMSG and NSG publication (NSG publication number 20030206).

## References

- Backman, J., Raffi, I., 1997. Calibration of Miocene nannofossil events to orbitally tuned cyclostratigraphies from Ceara Rise. *Proceedings of the Ocean Drilling Program, Scientific Results* 154, 83-100. doi:10.2973/odp.proc.sr.154.101.1997.
- Barton, M., Salters, V.J.M., Huijsmans, J.P.P., 1983. Sr isotope and trace element evidence for the role of continental crust in calcalkaline volcanism on Santorini and Milos, Aegean Sea, Greece. *Earth and Planetary Science Letters* 63, 273-291. doi:10.1016/0012-821X(83)90042-0.
- Benda, L., Jonkers, H.A., Meulenkamp, J.E., Steffens, P., 1979. Biostratigraphic correlations in the Eastern Mediterranean Neogene: 4. Marine microfossils, sporomorphs and radiometric data from the lower Pliocene of Aghios Thomas, Aegina, Greece. *Newsletters on Stratigraphy* 8, 61-69.
- Berggren, W.A., Hilgen, F.J., Langereis, C.G., Kent, D.V., Obradovich, J.D., Raffi, I., Raymo, M.E., Shackleton, N.J., 1995a. Late Neogene chronology: new perspectives in high-resolution stratigraphy. *GSA Bulletin* 107 (11), 1272-1287. doi:10.1130/0016-7606(1995)107<1272:LNCNPI>2.3.CO;2.
- Berggren, W.A., Kent, D.V., Swisher III, C.C., Aubry, M.-P., 1995b. A revised Cenozoic geochronology and chronostratigraphy, geochronology time-scales and global stratigraphic correlation. *SEPM Special Publication* 54, 129-212.
- Bramlette, M.N., Sullivan, F.R., 1961. Coccolithophorids and related nannoplankton of the early Tertiary in California. *Micropaleontology* 7 (2), 129-188.
- Briqueu, L., Javoy, M., Lancelot, J.R., Tatsumoto, M., 1986. Isotope geochemistry of recent magmatism in the Aegean arc: Sr, Nd, Hf, and O isotopic ratios in the lavas of Milos and Santorini-geodynamic implications. *Earth and Planetary Science Letters* 80, 41-54. doi:10.1016/0012-821X(86)90018-X.
- Fytikas, M., 1977. *Carte Géologique de Milos*. IGMR, Athens.
- Fytikas, M., Innocenti, F., Manetti, P., Mazzuoli, R., Peccerillo, A., Villari, L., 1984. Tertiary to Quarternary evolution of volcanism in the Aegean region. In: Dixon, J.E. (Ed.), *The Geological Evolution of the Eastern Mediterranean*. Geological Society of London Special Publication 17, pp. 687-699. doi:10.1144/GSL.SP.1984.017.01.55.
- Fytikas, M., Innocenti, F., Kolios, N., Manetti, P., Mazzuoli, R., Poli, G., Rita, F., Villari, L., 1986. Volcanology and petrology of volcanic products of the island of Milos and neighbouring islets. *Journal of Volcanology and Geothermal Research* 28, 297-317. doi:10.1016/0377-0273(86)90028-4.
- Gautier, P., Brun, J.-P., Moriceau, R., Sokoutis, D., Martinod, J., Jolivet, L., 1999. Timing, kinematics and cause of Aegean extension: a scenario based on a comparison with simple analogue experiments. *Tectonophysics* 315, 31-72. doi:10.1016/S0040-1951(99)00281-4.

- Giunchi, C., Kiratzi, A., Sabadini, R., Louvari, E., 1996. A numerical model of the Hellenic subduction zone: active stress field and sea-level changes. *Geophysical Research Letters* 23 (18), 2485-2488. doi:10.1029/96GL02166.
- Hatzfeld, D., 1994. On the shape of the subducting slab beneath the Peloponnese, Greece. *Geophysical Research Letters* 21, 173-176. doi:10.1029/93GL03079.
- Hilgen, F.J., 1991. Extension of the astronomically calibrated (polarity) time scale to the Miocene-Pliocene boundary. *Earth and Planetary Science Letters* 107, 349-368. doi:10.1016/0012-821X(91)90082-S.
- Hilgen, F.J., Krijgsman, W., Langereis, C.G., Lourens, L.J., Santarelli, A., Zachariasse, W.J., 1995. Extending the astronomical (polarity) time scale into the Miocene. *Earth and Planetary Science Letters* 136, 495-510. doi:10.1016/0012-821X(95)00207-S.
- Krijgsman, W., Hilgen, F.J., Raffi, I., Sierro, F.J., Wilson, D.S., 1999b. Chronology, causes and progression of the Messinian salinity crisis. *Nature* 400, 652-655. doi:10.1038/23231.
- Langereis, C.G., Hilgen, F.J., 1991. The Rossello composite: a Mediterranean and global reference section for the early to early late Pliocene. *Earth and Planetary Science Letters* 104, 211-225. doi:10.1016/0012-821X(91)90205-V.
- Laskar, J., Joutel, F., Boudin, F., 1993. Orbital, precessional, and insolation quantities for the Earth from -20 Ma to +10 Ma. *Astronomy and Astrophysics* 270, 522-533.
- Le Pichon, X., Angelier, J., 1979. The Hellenic arc and trench system: a key to the neotectonic evolution of the Eastern Mediterranean area. *Tectonophysics* 60, 1-42. doi:10.1016/0040-1951(79)90131-8.
- Lourens, L.J., Hilgen, F.J., 1997. Long-periodic variations in the earth's obliquity and their relation to third-order eustatic cycles and late Neogene glaciations. *Quaternary International* 40, 43-52. doi:10.1016/S1040-6182(96)00060-2.
- Lourens, L.J., Hilgen, F.J., Laskar, J., Shackleton, N.J., Wilson, D., 2004. The Neogene Period. In: Gradstein, F.M., Ogg, J.G., Smith, A.G. (Eds.), *A geologic time scale 2004*. Cambridge University Press, Cambridge, pp. 409-440.
- Makris, J., 1977. Geophysical investigations of the Hellenides. *Hamburger Geophysikalische Einzelschriften* 34, 1-124.
- Makropoulos, K.C., Burton, P.W., 1984. Greek tectonics and seismicity. *Tectonophysics* 106, 275-304. doi:10.1016/0040-1951(84)90181-1.
- Martini, E., 1971. Standard Tertiary and Quaternary calcareous nannoplankton zonation. In: Farinacci, A. (Ed.), *Proceedings of the 2<sup>nd</sup> International Conference on Planktonic Microfossils*, Roma 1970, 2, Edizioni Tecnoscienza, Rome, pp. 739-785.
- McKenzie, D., 1978a. Active tectonics of the Alpine-Himalayan belt: the Aegean Sea and surrounding regions. *Geophysical Journal of the Royal Astronomical Society* 55, 217-254.
- McKenzie, D., 1978b. Some remarks on the development of sedimentary basins. *Earth and Planetary Science Letters* 40, 25-32. doi:10.1016/0012-821X(78)90071-7.
- McKenzie, D., Bickle, M.J., 1988. The volume and composition of melt generated by extension of the lithosphere. *Journal of Petrology* 29, 625-679. doi:10.1093/petrology/29.3.625.
- Meulenkamp, J.E., 1979. The Aegean and the Messinian salinity crisis. *Proceedings of the 6<sup>st</sup> Colloquium on the Geology of the Aegean Region*, Institute of Geological and Mining Research, Athens 1977, 3, 1253-1263.
- Morris, A., 2000. Magnetic fabric and paleomagnetic analyses of the Plio-Quaternary calc-alkaline series of Aegina Island, South Aegean volcanic arc, Greece. *Earth and Planetary Science Letters* 176, 91-105. doi:10.1016/S0012-821X(99)00318-0.

- Müller, P., Kreuzer, H., Lenz, H., Harre, W., 1979. Radiometric dating of two extrusives from a Lower Pliocene marine section on Aegina Island, Greece. *Newsletters on Stratigraphy* 8, 70-78.
- Papanikolaou, D., Lykousis, V., Chronis, G., Pavlakis, P., 1988. A comparative study of neotectonic basins across the Hellenic Arc: the Messiniakos, Argolikos and Southern Evoikos Gulfs. *Basin Research* 1, 167-176. doi:10.1111/j.1365-2117.1988.tb00013.x.
- Papazachos, B.C., Karakostas, V.G., Papazachos, C.B., Scordilis, E.M., 2000. The geometry of the Wadati-Benioff zone and lithospheric kinematics in the Hellenic arc. *Tectonophysics* 319, 275-300. doi:10.1016/S0040-1951(99)00299-1.
- Pe, G.G., 1973. Petrology and geochemistry of volcanic rocks of Aegina, Greece. *Bulletin of Volcanology* 37, 491-514. doi:10.1007/BF02596888.
- Pe, G.G., Piper, D.J.W., 1972. Volcanism at subduction zones; The Aegean area. *Bulletin of the Geological Society of Greece* 9, 113-144.
- Pe-Piper, G., Hatzipanagiotou, K., 1997. The Pliocene volcanic rocks of Crommyonia, western Greece and their implications for the early evolution of the South Aegean arc. *Geological Magazine* 134, 55-66. doi:10.1017/S0016756897006390.
- Pe-Piper, G., Piper, D.J.W., 2002. The igneous rocks of Greece. The anatomy of an orogen. Gebrüder Borntraeger, Berlin-Stuttgart, 573 pp.
- Pe-Piper, G., Piper, D.J.W., Reynolds, P.H., 1983. Paleomagnetic stratigraphy and radiometric dating of the Pliocene volcanic rocks of Aegina, Greece. *Bulletin of Volcanology* 46, 1-7. doi:10.1007/BF02598241.
- Perissoratis, C., 1995. The Santorini volcanic complex and its relation to the stratigraphy and structure of the Aegean arc, Greece. *Marine Geology* 128, 37-58. doi:10.1016/0025-3227(95)00090-L.
- Philpotts, A.R., 1990. *Principles of Igneous and Metamorphic Petrology*. Prentice Hall, Englewood Cliffs, NJ, 498 pp.
- Rögl, F., Bernor, R.L., Dermitzakis, M.D., Müller, C., Stancheva, M., 1991. On the Pontian Correlation in the Aegean (Aegina Island). *Newsletters on Stratigraphy* 24, 137-158.
- Snel, E., Mărunțeanu, M., Macaleț, R., Meulenkamp, J.E., Van Vugt, N., 2006. Late Miocene to Early Pliocene chronostratigraphic framework for the Dacic Basin, Romania. *Palaeogeography, Palaeoclimatology, Palaeoecology* 238, 107-124. doi:10.1016/j.palaeo.2006.03.021.
- Steckler, M.S., Watts, A.B., 1978. Subsidence of the Atlantic-type continental margin off New York. *Earth and Planetary Science Letters* 41, 1-13. doi:10.1016/0012-821X(78)90036-5.
- Steenbrink, J., Van Vugt, N., Hilgen, F.J., Wijbrans, J.R., Meulenkamp, J.E., 1999. Sedimentary cycles and volcanic ash beds in the lower Pliocene lacustrine successions of Ptolemais (NW Greece): discrepancy between  $^{40}\text{Ar}/^{39}\text{Ar}$  and astronomical ages. *Palaeogeography, Palaeoclimatology, Palaeoecology* 152, 283-303. doi:10.1016/S0031-0182(99)00044-9.
- Van der Zwaan, G.J., Jorissen, F.J., De Stigter, H.C., 1990. The depth dependency of planktonic/benthonic foraminiferal ratios: constraints and applications. *Marine Geology* 95, 1-16. doi:10.1016/0025-3227(90)90016-D.
- Van Hinsbergen, D.J.J., Kouwenhoven, T.J., Van der Zwaan, G.J., 2005a. Paleobathymetry in the backstripping procedure: correction for oxygenation effects on depth estimates. *Palaeogeography, Palaeoclimatology, Palaeoecology* 221 (3-4), 245-265. doi:10.1016/j.palaeo.2005.02.013.

- Van Hinsbergen, D.J.J., Zachariasse, W.J., Wortel, M.J.R., and Meulenkaamp, J.E., 2005b, Underthrusting and exhumation: A comparison between the External Hellenides and the 'hot' Cycladic and 'cold' South Aegean core complexes (Greece), *Tectonics* 24 (2), TC2011, doi:10.1029/2004TC001692.
- Watts, A.B., Karner, K.D., Steckler, M.S., 1982. Lithosphere flexure and the evolution of sedimentary basins. *Philosophical Transaction of the Royal Society of London* 305, 249-281.
- Wright, R., 1978. Neogene paleobathymetry of the Mediterranean based on benthic foraminifers from DSDP leg 42A. In: Hsü, K.J., Montadert, L., et al. (Eds.), *Initial Reports of the Deep Sea Drilling Project XLII*, pp. 837-846. doi:10.2973/dsdp.proc.42-1.141.1978.
- Zijderveld, J.D.A., 1967. A.C. demagnetization of rocks: analysis of results. In: Collinson, D.W., Creer, K.M., Runcorn, S.K. (Eds.), *Methods in palaeomagnetism*. Elsevier, Amsterdam, pp. 254-286.

# No major deglaciation across the Miocene-Pliocene boundary: integrated stratigraphy and astronomical tuning of the Loulja sections (Bou Regreg area, NW Morocco)

---

This chapter is published as: Van der Laan, E., Snel, E., De Kaenel, E., Hilgen, F.J., Krijgsman, W., 2006. No major deglaciation across the Miocene-Pliocene boundary: Integrated stratigraphy and astronomical tuning of the Loulja sections (Bou Regreg area, NW Morocco). *Paleoceanography* 21, PA3011, doi:10.1029/2005PA001193.

## Abstract

An integrated high-resolution stratigraphy and orbital tuning is presented for the Loulja sections located in the Bou Regreg area on the Atlantic side of Morocco. The sections constitute the upward continuation of the upper Messinian Ain el Beida section and contain a well-exposed, continuous record of the interval straddling the Miocene-Pliocene (M-P) boundary. The older Loulja-A section, which covers the interval from ~5.59 to 5.12 Ma, reveals a dominantly precession-controlled colour cyclicity that allows for a straightforward orbital tuning of the boundary interval and for detailed cyclostratigraphic correlations to the Mediterranean; the high-resolution and high-quality benthic isotope record allows us to trace the dominantly obliquity-controlled glacial history. Our results reveal that the M-P boundary coincides with a minor, partly precession-related shift to lighter “interglacial” values in  $\delta^{18}\text{O}$ . This shift and hence the M-P boundary may not correlate with isotope stage TG5, as previously thought, but with an extra (weak) obliquity-controlled cycle between TG7 and TG5. Consequently, the M-P boundary and basal Pliocene flooding of the Mediterranean following the Messinian salinity crisis are not associated with a major deglaciation and glacio-eustatic sea level rise, indicating that other factors, such as tectonics, must have played a fundamental role. On the other hand, the onset of the Upper Evaporites in the Mediterranean marked by hyposaline conditions coincides with the major deglaciation step between marine isotope stage TG12 and TG11, suggesting that the associated sea level rise is at least partly responsible for the apparent onset of intermittently restricted marine conditions following the main desiccation phase. Finally, the Loulja-A section would represent an excellent auxiliary boundary stratotype for the M-P boundary as formally defined at the base of the Trubi marls in the Eraclea Minoa section on Sicily.

## 5.1 Introduction

The Miocene-Pliocene boundary formally defined at the base of the deep marine Trubi marls on Sicily (Van Couvering et al., 2000) marks the basal Pliocene flooding of the Mediterranean and

the end of the Messinian salinity crisis (MSC). Although there are increasing indications that (restricted) marine conditions may have occurred already intermittently during deposition of the Upper Evaporites (e.g., Müller, 1990; Castradori, 1998; Spezzaferri et al., 1998; Iaccarino et al., 1999; Rouchy et al., 2001; Aguirre and Sánchez-Almazo, 2004), the base of the Trubi marls and time-equivalent sediments elsewhere in the Mediterranean represent the sedimentary expression of the re-establishment of full open marine conditions in the Mediterranean (Hsü et al., 1973; Cita, 1975; Hilgen and Langereis, 1993; Iaccarino et al., 1999). To unravel the exact cause of the flooding event, the time-correlative level of the M-P boundary should be precisely pinpointed in a continuous orbitally tuned open marine succession outside the Mediterranean. In addition, an excellent benthic oxygen isotope record should be available to detect any significant reduction in ice volume associated with the flooding event.

Attempts have recently been made to pinpoint the position of the M-P boundary in marine cores from the open ocean. Shackleton et al. (1995a, 1995b), Clauzon et al. (1996), and McKenzie et al. (1999) all link the boundary to the prominent interglacial oxygen isotope stage TG5 defined by Shackleton et al. (1995b) in ODP Site 846, suggesting that the associated glacio-eustatic sea level rise played a primary role in controlling the Pliocene flooding of the Mediterranean. For this purpose, most of these studies compared the tuned age of 5.33 Ma for the base of the Trubi (Lourens et al., 1996) with the age of TG5 according to the initial tuned age model developed for Site 846 (Shackleton et al., 1995a). However, the latter age model has subsequently been revised leaving a younger age of 5.31 Ma for TG5 (Shackleton et al., 1999).

In our opinion, the Bou Regreg area located on the Atlantic side of Morocco remains the location most critical to solve the problem of the exact timing and origin of the Pliocene flooding of the Mediterranean. The open marine succession in the area shows a distinct dominantly precession-controlled colour banding that is related to the sedimentary cyclicity in the Mediterranean, and the Trubi marls in particular. The colour cycles allow the sections to be astronomically tuned and to be correlated cyclostratigraphically to Mediterranean sections (Hilgen et al., 2000). Secondly, high-quality benthic isotope records can be generated due to the good to excellent preservation of the foraminifera shells while the relatively high average sedimentation rate (of 7-8 cm/kyr) guarantees an optimal temporal resolution (Van der Laan et al., 2005).

In fact, Benson and Rakic-El Bied (1996) proposed to define the M-P boundary in a continuous open marine section, Ain el Beida, located outside the Mediterranean because they considered the Messinian to be a regional stage representing the sedimentary expression of the MSC only. For this purpose, they selected a much older level that corresponds with the younger end of Chron C3An. On the other hand, Suc et al. (1997), while recognizing the problem of the possible unconformable nature of the base of the Trubi, preferred to maintain the Mediterranean option. They proposed to define the M-P boundary near Salé, some 5 km northwest of Ain el Beida, at the stratigraphic level that corresponds with the base of oxygen isotope stage TG5. This isotope shift was supposed to reflect the marked deglaciation held responsible for the Pliocene flooding of the Mediterranean. The proposal was considered less favourable because the level was only indicated in the Salé drill core but not in any existing outcrop.

Nevertheless, the M-P boundary level might be present in one of the quarries located in between Ain el Beida, where this level is not reached, and Salé with its exposures of Early Pliocene marine sediments. Because of the clearly visible colour banding we selected the Loulja section with the aim (1) to extend the tuned open marine succession exposed at Ain el Beida across the M-P boundary into the Pliocene and (2) to pinpoint as accurately as possible the position of the M-P boundary in a well-tuned, open marine section with an excellent oxygen isotope stratigraphic



record in the Bou Regreg area. The outcome of this study may provide the final answer to the question whether glacio-eustatic sea level rise was involved in triggering the Pliocene flooding of the Mediterranean.

In addition, special attention will be given to identify the major isotope shift to lighter values between isotope stages TG12 and TG9. According to the tuned age model for Ain el Beida, only the beginning of this shift was reached in the topmost part of the section (Van der Laan et al., 2005). This shift, which marks a more dramatic deglaciation than TG5 as noticed by Shackleton et al. (1995b), Hodell et al. (2001), and Vidal et al. (2002), is particularly interesting because it may be coincident with and thus responsible for the beginning of the Upper Evaporites in the Mediterranean (Shackleton et al., 1995b).

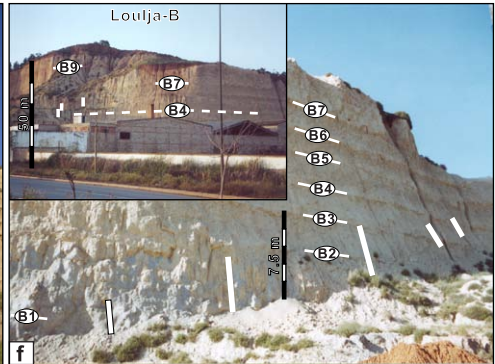
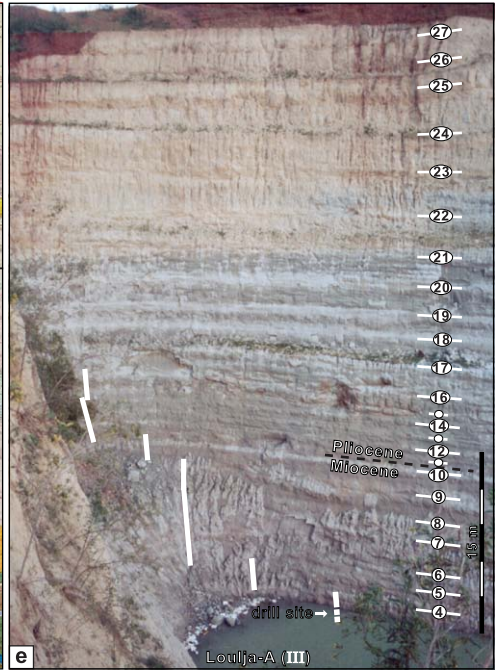
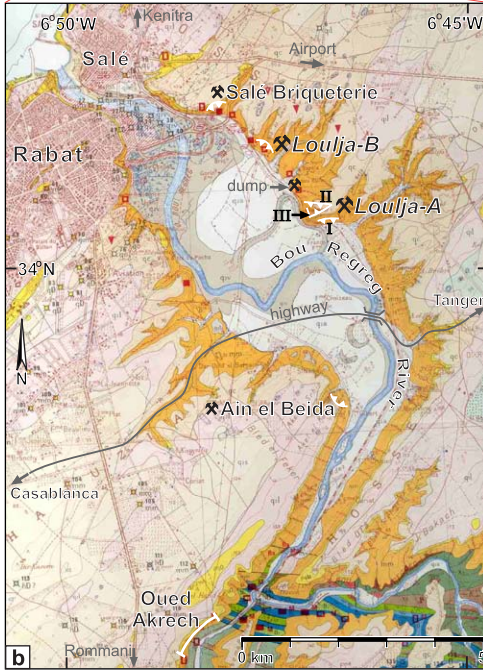
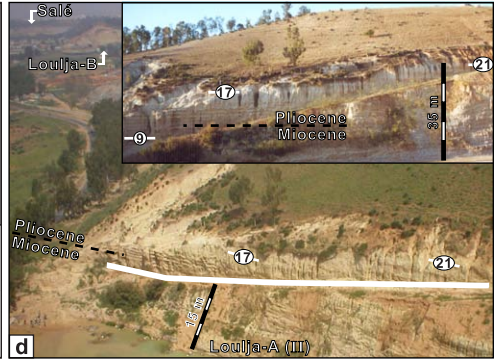
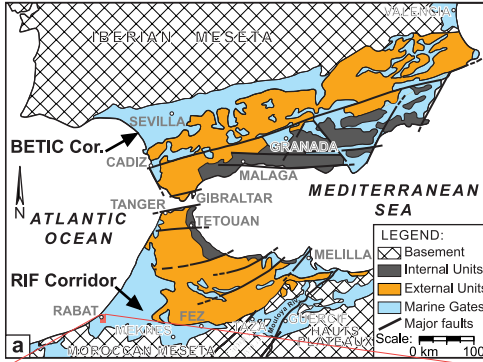
## 5.2 Setting and sections

### 5.2.1 Bou Regreg valley

The classic Blue Marl of Atlantic Morocco has been subject of numerous studies, reflecting the progress made in Neogene stratigraphy. It is best known from the Bou Regreg river valley where it constitutes a continuous open marine record from the late Tortonian into the Pliocene that overlies Devonian limestones with an angular unconformity (Benson and Rakic-El Bied, 1996). The Blue Marl was deposited in the Gharb basin, which formed the westward extension of the Rifian Corridor (Fig. 5.1a). This corridor acted as an extensional foredeep and formed one of the two Atlantic-Mediterranean connections during the Late Miocene before its tectonic closure in the course of the Messinian (Benson et al., 1991; Krijgsman et al., 1999). Deposition of the Blue Marl in the Gharb Basin continued well into the Pliocene and its stratigraphic succession is exposed in a number of quarries and outcrops albeit in an incomplete way. The Oued Akrech section contains the basal part of the Blue Marl, straddling the Tortonian-Messinian boundary and covering the interval from 7.6 to 7.1 Ma (Hilgen et al., 2000). The middle part of the Blue Marl is exposed in the Ain el Beida quarry and covers the interval from 6.5 to 5.5 Ma (Krijgsman et al., 2004), while lower Pliocene marine sediments are exposed at Salé (see Hodell et al., 1994; Benson and Rakic-El Bied, 1996). The succession has been completed by drilling at Ain el Beida and Salé (Hodell et al., 1989; Benson et al., 1991; Hodell et al., 1994; Benson et al., 1995), but up to now, the interval straddling the Miocene-Pliocene boundary has not been documented in detail from any outcrop.

### 5.2.2 The Loulja-A section

The Loulja-A section is located in a brick quarry at the northern side of the Bou Regreg valley along the road to Salé (Figs. 5.1a and 5.1b). Colour banding is clearly visible in the steep south face of an old quarry next to the road, which shows a regular alternation of slightly protruding, light beige coloured silty marls and softer, darker (reddish) coloured, clayey marls (partial section I; Fig. 5.1c). A much larger quarry is located on the opposite northern side of the hill. The weathered south face (partial section II; Fig. 5.1d) of this quarry shows the same colour banding and pattern as observed along the road. The entire sequence is also exposed in the relatively fresh, north face (partial section III; Fig. 5.1e) of the quarry, which is approximately 60 m high. Younger stratigraphic levels showing relatively thick colour cycles are reached in the upper half of this quarry face. The colour cycles are less distinct in such fresh exposures and consist of alternating lighter and darker coloured bluish-grey marls.



*Figure 5.1.* a) Simplified geological map of the Gibraltar area with the location of the Late Miocene Betic and Rifian Corridors (modified after Krijgsman et al., 2004). b) Map of the lower Bou Regreg valley showing locations of the quarries of Loulja-A and Loulja-B, Ain el Beida, and Salé Briqueterie, and the road section of Oued Akrech (modified after Millies-Lacroix, 1974). c) Old quarry of Loulja-A (partial section I) along the road to Salé. d) View in NW direction, towards the Loulja-B and Salé quarries showing the weathered side (section II) of the main Loulja-A quarry. White horizontal bar in inset shows detail of sample trajectory. e) Fresh north-facing side (section III) of the main Loulja-A quarry. White bars indicate sample trajectories. f) Detail of right, southeast-facing wall of the Loulja-B quarry (inset shows the entire quarry). Note the variable meter scales in c-f. Cycle numbers refer to the stratigraphy in Figure 5.2.

Sampling started at the base of the accessible eastern side of section Loulja-A III (lower 20 m.) and was continued along the path that crosses section II (from 9 to 33.5 m.). An additional 5.5 m was drilled below the reference level of the quarry floor with a hand drill at section III (Fig. 5.1e) to ensure a stratigraphic overlap with the top part of the (supposedly older) Ain el Beida section. Usually 8 to 10 samples were taken per cycle, which corresponds to a temporal resolution of 2-3 kyr in case the colour cycles are precession-related. In the drill hole, one sample was taken every 10 cm. Finally, additional samples with a resolution of two samples per cycle were taken from the lower part of section I and from the lower part of section II for a check on the cycle patterns and the correlations between partial sections. Sampling was not extended to include all the thick cycles observed in the top part of Loulja-A due to the intense weathering of section II and the steepness of the upper part of section III.

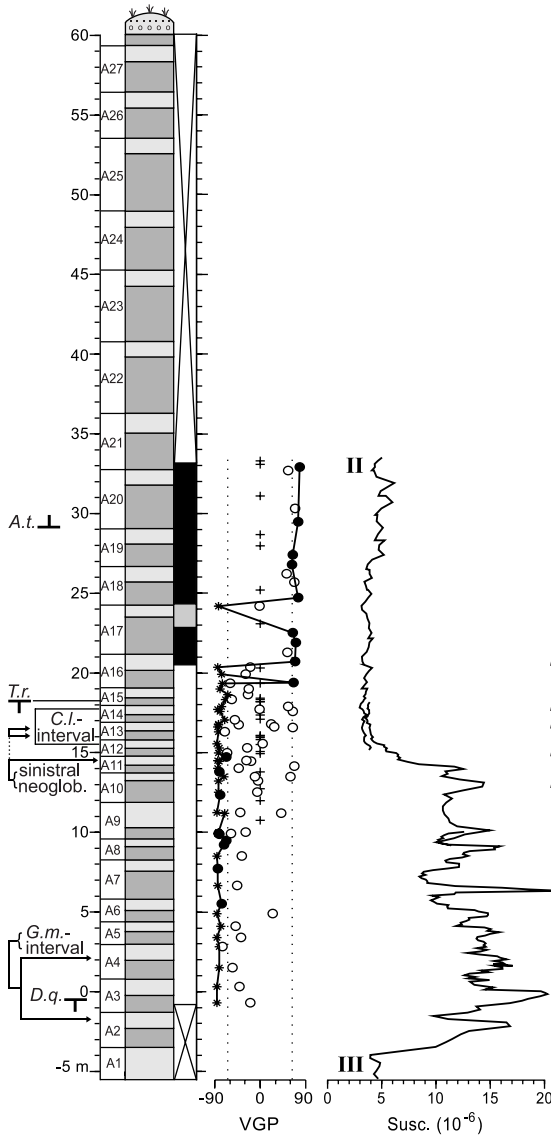
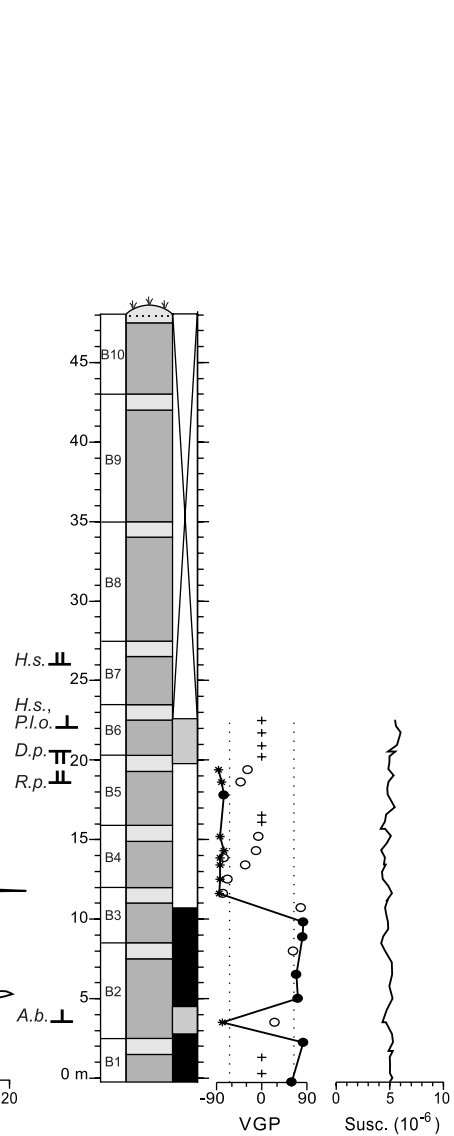
### 5.2.3 The Loulja-B section

The Loulja-A section can be extended upward in another brick quarry along the road to Salé (Figs. 5.1b and 5.1f), located about 1.5 km northwest of Loulja-A. This section, named Loulja-B, displays similar thick and well developed colour cycles as the upper half of the Loulja-A section. Inaccessibility of the vertical southwest face of this quarry limited the detailed sampling to the lower half of the exposed section. Nevertheless, seven additional samples were collected from the upper four cycles for biostratigraphic analysis.

## 5.3 Cyclostratigraphy

In total 27 cycles were recognized at Loulja-A, labelled LA-1 to LA-27 in stratigraphic order (Fig. 5.2a). In weathered outcrop, the cycles consist of an alternation of more indurated, light-beige coloured silty marls and softer, reddish coloured clayey marls. Rather arbitrarily, reddish marl layers are taken as to define the base of a cycle and labelled LA- $X_R$  where X is the number of the cycle in the section and  $_R$  denotes the colour of the marl (red); the overlying beige marl is denoted LA- $X_B$ . The lowermost 3 cycles are found only in the drill hole and are distinguished based on the geochemical data (see paragraph 5.6). Cycles LA-4 to base LA-21 were logged and sampled in detail in partial sections II and III whereas only the (approximate) thickness of cycles LA-21 to LA-27 was measured with a tape from the top of section III downward.

The cycles reveal a very characteristic pattern (Fig. 5.2a). LA-1 to LA-10 reach an average thickness of 2 m with very thick reddish layers in LA-7 and LA-10 and relatively thin reddish layers in LA-5 and LA-6. The thickest whitish layers are found in LA-1 and LA-9. The lower part of the section is followed by a very characteristic interval that consists of six successive thin

**(a) Loulja-A****(b) Loulja-B**

colour cycles (LA-10<sub>B</sub>-15<sub>B</sub>), which are very regular and have an approximate thickness of 1 m. This interval can be recognized both in partial section I as well as in sections II and III, and was used to correlate the different partial sections in detail. Cycle LA-16 has an intermediate thickness and marks the transition to thicker cycles LA-17 to LA-21 (and up to LA-27). The thickness of these cycles ranges from 2.5 to 4 m.

The Loulja-B section contains 10 thick colour cycles labelled LB-1 to LB-10 (Fig. 5.2b). The lowermost 7 cycles have an average thickness of ~4 m with a very thick reddish layer of 5 m in LB-2. Cycles LB-8 and LB-9 are extremely thick and reach a thickness of 7.5-8 m, i.e. almost twice as thick as LB-1 to LB-7.

Figure 5.2. Litho-, bio-, and magnetostratigraphy of the (a) Loulja-A and (b) Loulja-B sections. Sedimentary cycle numbers are based on the colour cycles and, for the lowermost part of Loulja-A, also on the PC-1 data shown in Figure 5.4. Light shading marks the light coloured, relatively carbonate-rich marls, and darker shading marks the relatively clayey, often reddish coloured marls. Last and first (regular) occurrences of nannofossil species are indicated on the left side of the lithological columns: D.q., *Discoaster quinqueramus*; C.l., *Ceratolithus larrymayeri*; T.r., *Triquetrorhabdulus rugosus*; A.t., *Amaurolithus tricorniculatus*; A.b., *Amaurolithus bizzarus*; R.p., *Reticulofenestra pseudumbilicus* (>8  $\mu\text{m}$ ); D.p., *Dictyococcites perplexus*; P.l.o., *Pseudoemiliania lacunosa ovata*; H.s., *Helicosphaera sellii*. Furthermore, G.m.-interval stands for the interval with common *Globorotalia menardii*. In the VGP curves, (open) solid circles denote (less) reliable ChRM directions; asterisks indicate great circle solutions; pluses are used for inconclusive results. In the polarity columns, black (white) denotes normal (reversed) polarity, grey indicates undetermined polarity, and crossed intervals are used for those parts of the sections where no paleomagnetic samples were taken. Magnetic susceptibility of untreated sediment is shown to the right of the VGP-curves; II and III refer to partial sections of Loulja-A (see Figure 5.1). Stratigraphic scales are in meters.

## 5.4 Magnetostratigraphy

### 5.4.1 Sampling

Standard oriented paleomagnetic cores were drilled with the help of a water-cooled, generator-powered electric drill at two to twelve levels per sedimentary cycle (four on average). Samples were taken in partial sections I and II (between -1 and 33 m; Figs. 5.1c, 5.1d, and 5.2a). Care was taken to remove the weathered surface before drilling. In addition to the regular sampling, oriented hand-samples were collected from the middle part (10-20 m) of section III with a resolution of one sample per cycle. Standard cores were drilled from these samples with compressed air at the paleomagnetic laboratory Fort Hoofddijk.

### 5.4.2 Demagnetization

One specimen per sampling level was thermally demagnetized with temperature increments of 15-80°C up to a maximum temperature of 700°C in a magnetically shielded, laboratory-built furnace. The natural remanent magnetization (NRM) of the specimens was measured on a 2G Enterprises horizontal DC SQUID cryogenic magnetometer.

Demagnetization diagrams (Zijderveld, 1967) are of mixed quality (Fig. 5.3). A normal polarity component is generally removed at temperatures between 100 and 250°C (e.g., Fig. 5.3b). This relatively low-temperature component typically has a present-day field direction and is interpreted as a secondary, recent overprint, likely caused by weathering. Therefore, low intensity samples showing clustering from 250°C onward are ignored. A relatively high temperature component is gradually removed between temperatures of 280 and 360°C (as in Figure 5.3d), after which spurious magnetizations prevail, probably due to the formation of pyrite or magnetite. In the last group of samples the high temperature component is removed between 280 and 600°C, up to 700°C (e.g., Fig. 5.3b), indicating magnetite or haematite as the principal carriers of the magnetization. The high-temperature component is taken as the characteristic remanent magnetization (ChRM) direction. In approximately 50% of the samples, the demagnetization diagrams allow straightforward interpretation of reversed (Figs. 5.3a, 5.3b, and 5.3e) or normal (Figs. 5.3c and 5.3d) polarity. In other samples, (linear) decay towards the origin is not shown but, apparently, decay to the reversed side of the diagram occurs (Figs. 5.3f-5.3h). In these cases, great circles are used to approximate the reversed ChRM directions. Best-fitting directions from the

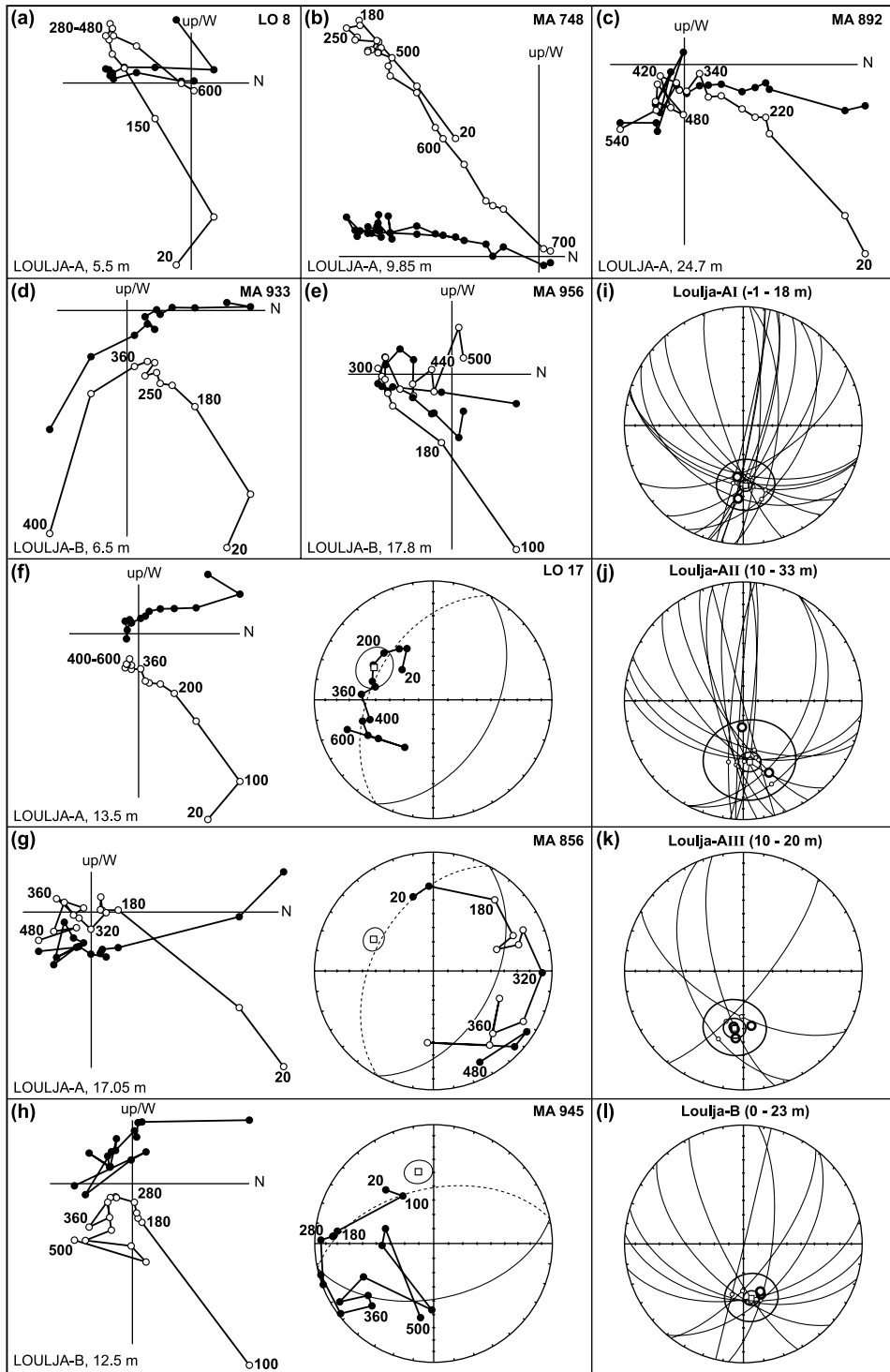


Figure 5.3. Examples of stepwise thermal demagnetization of selected samples. Diagrams denote orthogonal projections of NRM vector end-points, where open (solid) symbols are used for the vertical (horizontal) plane. Values represent temperatures in °C; stratigraphic level is indicated in the lower left corner. Reliable samples show both (a, b, e) reversed and (c, d) normal polarity. f-h) For samples where the ChRM is less well resolved, great circles are used to approximate the (reversed) directions, with squares indicating the normals to the great circle planes and ellipses representing the maximum angular deviations. i-l) Best-fitting directions from the great circles are shown per analyzed interval in the Loulja-A and Loulja-B sections (small circles). Thick circles indicate the used setpoints; small and large ellipses denote the  $\alpha_{95}$  and  $\tau_{95}$  confidence limits (McFadden and McElhinny, 1988).

great circles (indicated by small circles in Figures 5.3i-5.3l) are determined by using the reliable directions as setpoints (thick circles) according to the method of McFadden and McElhinny (1988).

The ChRM directions, represented as virtual geomagnetic polar (VGP) latitudes, reveal two intervals of normal polarity: from  $20.53 \pm 0.18$  m upwards in the Loulja-A section (LA-16<sub>B</sub> to LA-21<sub>R</sub>; Fig. 5.2a), and below  $10.70 \pm 0.90$  m in cycle LB-3 in the Loulja-B section (Fig. 5.2b).

#### 5.4.3 Magnetic susceptibility

The initial bulk magnetic susceptibility ( $\chi_{in}$ ) was measured at room temperature on a KLY-2 Kappabridge (Hrouda, 1994). Magnetic susceptibility (MS) is a measure of the magnetic response of a sample to a small, applied magnetic field and proportional to the concentration and grain size of ferro- and paramagnetic minerals in the sample. It can therefore be used to detect variations in lithology.

Magnetic susceptibility reaches relatively high values of  $10\text{-}20 \cdot 10^{-6}$  SI units in samples from Loulja-A III, and from the hand-drilled samples below (-2 to 14 m), defining a marked peak interval (Fig. 5.2a). The record shows a distinct rhythmic pattern, which can easily be correlated with the sedimentary cycles in the more weathered outcrops (sections I and II). In this interval, peak values clearly correspond to the reddish layers. A very pronounced peak in MS is found between 6 and 7 m, followed by much lower values that are not consistent with the lithological expression of the corresponding colour cycle (LA-7).

By contrast, MS values are much lower in the younger cycles (LA-12 to LA-15, up to 18.15 m in section III) while changes are less pronounced. In addition, the records obtained from the basal part of section III (-5.5 to -2 m), from section II (14 to 33.5 m), and from Loulja-B (0-23 m) show low values of MS not exceeding  $3\text{-}6 \cdot 10^{-6}$  SI units (Figs. 5.2a and 5.2b).

## 5.5 Biostratigraphy

### 5.5.1 Planktonic foraminifera

A semi-quantitative analysis of potential marker species was carried out on the >125 mm fraction of the washed residue of at least every other sample. In addition, the coiling direction of the neogloboquadrinids was determined. *Sphaeroidinellops* spp. and *Globorotalia margaritae* are present throughout the section and do not reveal changes in abundance that allow recognition of the *Sphaeroidinellops* acme and the *Globorotalia margaritae* FCO known from the Mediterranean. Next to *G. margaritae*, another species of left coiling keeled globorotalids, *G. menardii*, is commonly but discontinuously found over a short interval in the lower part of the section (from  $-1.75 \pm 0.20$  m

up to  $2.15 \pm 0.05$  m; Fig. 5.2a). Its distribution corresponds to the reappearance of common *G. miotumida* group in the top part of the underlying Ain el Beida section (Krijgsman et al., 2004).

The determination of the neogloboquadrinid coiling direction is complicated by the presence of two different types, *Neogloboquadrina acostaensis* and *N. humerosa*. The coiling direction of the small- to medium-sized *N. acostaensis* type is dominantly dextral. Approximately equal numbers of sinistral and dextral specimens are found at the 14.65 m level (LA-11<sub>B</sub>), and a short but prominent incursion of left-coiling specimens occurs between 16.15 and 16.75 m (cycle LA-13; see also Figure 5.2a). Specimens of the *N. humerosa* type, which are often large-sized, are frequently encountered in the lower part of the section although they are always less abundant than *N. acostaensis*. Their coiling direction is dominantly sinistral. Dominantly dextral *N. acostaensis* is the only neogloboquadrinid species present from the top of the marked (second) sinistral influx upwards.

An estimate of the paleobathymetry of the Loulja sections using the ratio of planktonic and benthic foraminifera (Van Hinsbergen et al., 2005) yielded values between 300 and 500 m. A check on this ratio for the Ain el Beida section revealed paleobathymetric values between about 600 and 1000 m, which are in good agreement with previous estimates (Benson and Rakic-El Bied, 1996).

### 5.5.2 Calcareous nannofossils

The samples selected for analysis of the calcareous nannofossil content were prepared according to standard preparation techniques (Bramlette and Sullivan, 1961). Two samples per sedimentary cycle were qualitatively examined from both Loulja-A and Loulja-B. Samples from Loulja-A III (-5.5-21 m) provided the best-preserved nannofossil assemblages; all other samples yielded moderately to well-preserved nannofossils.

The Loulja-A section comprises several important nannofossil bioevents (Fig. 5.2; Plate 5.I). Only a single specimen of *Discoaster quinqueramus* was observed at -0.7 m in cycle LA-3, pinpointing the LO of the species between -0.7 m and -0.18 m (Fig. 5.2a). Rare specimens of *Ceratolithus larrymayeri* were found between 15.5 m and 17.9 m (cycles LA-12 to LA-14),

*Plate 5.I.* Calcareous nannofossils from the Loulja-A and Loulja-B sections; (\*) by courtesy of E. De Kaenel.

1-2) *Discoaster quinqueramus* Gartner; sample LO 1, -0.7m, cycle LA-3R. Parallel light.

3-4) *Triquetrorhabdulus rugosus* Bramlette and Wilcoxon; LO 15, 11.2m, LA-9B. (3) Parallel light; (4) crossed nicols.

5) *Ceratolithus larrymayeri* Raffi, Backman and Rio; LO 23, 16.6m, LA-13B. Parallel light.

6-7\*) *Triquetrorhabdulus rugosus* Bramlette and Wilcoxon; LO 26, 18.2m, LA-15R. (6) Parallel light; (7) crossed nicols.

8-10) *Amaurolithus tricorniculatus* (Gartner); MA 910, 30.3m, LA-20R. (8,9) Parallel light; (10) crossed nicols.

11-12,13-14\*) *Amaurolithus tricorniculatus* (Gartner); MA 921, -0.25m, LB-1R. (11,13) Parallel light; (12,14) crossed nicols.

15) *Amaurolithus bizzarus* (Bukry); MA 931, 5.0m, LB-2R. Parallel light.

16\*) *Dictyococcites perplexus* Burns; MA 947, 13.4m, LB-4R. Crossed nicols.

17-18\*) *Amaurolithus bizzarus* (Bukry); MA 968, 22.5m, LB-6B. (17) Parallel light; (18) crossed nicols.

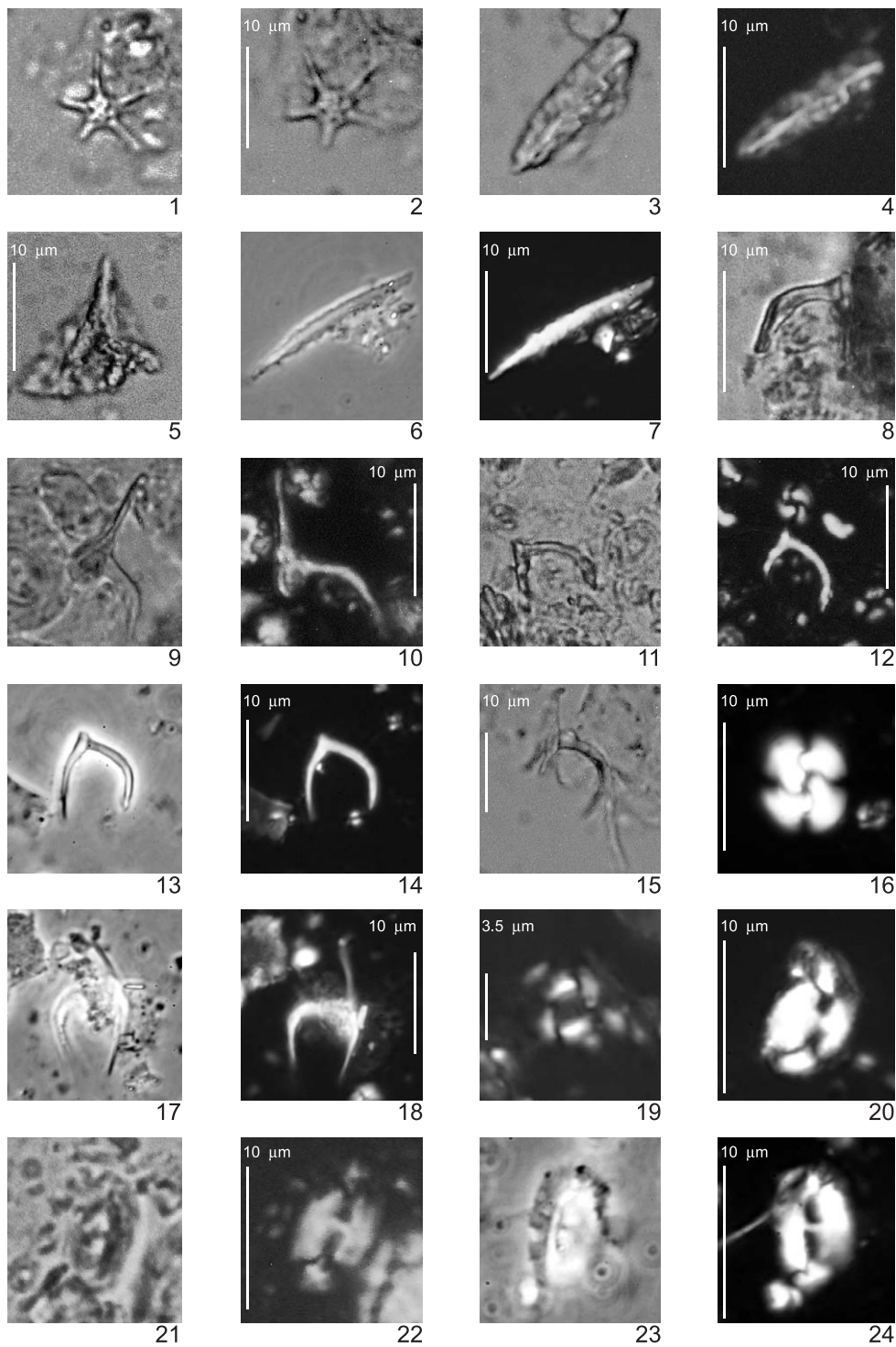
19\*) *Pseudoemiliania lacunosa ovata* (Young); MA 968, 22.5m, LB-6B. Crossed nicols.

20\*) *Helicosphaera sellii* Bukry and Bramlette; MA 968, 22.5m, LB-6B. Crossed nicols.

21-22) *Helicosphaera sellii* Bukry and Bramlette; 27m, cycle LB-7B. (21) Parallel light; (22) crossed nicols.

23-24\*) *Helicosphaera sellii* Bukry and Bramlette; 39m, cycle LB-9R. (23) Parallel light; (24) crossed nicols.





defining the FO and LO of this species. The *Triquetrorhabdulus rugosus* LO was reached between 18.2 and 18.3 m (LA-15), while *Amaurolithus tricorniculatus* was first observed at 30.3 m (LA-20; *A. tricorniculatus* FO between 28.0 and 30.3 m).

In Loulja-B, *Amaurolithus bizzarus* was found at the 5 m level (LB-2; *A. bizzarus* FO between 2.25 and 5.0 m in Figure 5.2b). The subbottom of *Reticulofenestra pseudoumbilicus* (>8  $\mu\text{m}$ ) is recorded between 17.8 m and 19.4 m, in cycle LB-5, while the *Dictyococcites perplexus* subtop is placed between 19.4 m and 21.7 m (LB-5<sub>B</sub> and LB-6<sub>R</sub>) and the *Pseudoemiliania lacunosa ovata* FO (forms with less than 12 rim slits) between 21.7 m and 22.5 m, in cycle LB-6. Finally, *Helicosphaera sellii* first appeared between 21.7 and 22.5 m (LB-6; *H. sellii* FO), and is more frequently present from between 25 and 27 m upwards (LB-7; *H. sellii* FRO).

## 5.6 Chemostratigraphy

### 5.6.1 Geochemistry

Samples were dried, crushed, powdered, and homogenized in an agate mortar prior to further treatment. Approximately 125 mg of each sample was then dissolved in 2.5 ml HF (40%) and 2.5 ml of mixed HNO<sub>3</sub> (16.25%) and HClO<sub>4</sub> (45.5%) and heated at 90°C in closed “Teflon” tubes (bombs) for a minimum of 8 hours. The solutions were subsequently evaporated (in open bombs) at a temperature of 160°C, after which approximately 25 ml HNO<sub>3</sub> (4.5%) was added to each residue. The resulting solutions were analyzed using a Perkin Elmer Optima 3000 ICP-OES apparatus for the elements Al, Ba, Ce, Ca, Co, Cr, Cu, Fe, K, Li, Mg, Mn, Na, Ni, P, S, Sc, Sr, Ti, V, Y, and Zn. The relative errors in duplicate measurements of international standards was lower than 3% for all elements, except for Ce, Co, P, S, Sr, and Y (>5%).

A standardized Principal Component Analysis (PCA) (SPSS software) was applied to extract the primary components responsible for the main variance in the data set. The first (PC-1) and second principal component together describe already 73% of the total variance in the data, of which PC-1 explains about 59% and is statistically significant. The interpretation of the first principal component is based on the loadings of individual elements on this component (Table 5.1). PC-1 reveals very high positive loadings for K, Al, V, Fe, Ti, and Li whereas Ca displays the strongest negative loading. The elements that show high positive loadings are main constituents in clay minerals and often represented in the fine-grained (clayey) terrigenous sediment fraction. On the contrary, Ca is primarily associated with the marine (biological) fraction of the sediment. The PC-1 record shows obvious cyclic variations and follows the sedimentary colour cycles observed in the field, where PC-1 minima and Ca maxima correspond to the more indurated, beige coloured marls. The record comprises 21 cycles, which vary in thickness between about 1 and 4 m with thicker cycles generally showing higher-amplitude changes (Fig. 5.4). Thicker geochemical cycles are found between -4.5 and +2.5 m (which correspond to colour cycles LA-2 to LA-4) and between 5.5 and 8 m (LA-7) in the lower part of the section and between ~21 m and 33.5 m (cycles 17-21) in the upper part. The middle part reveals a series of six thin geochemical cycles with low amplitude changes (Fig. 5.4). This part, which is marked by a decrease in PC-1 values, corresponds to the characteristic interval with thin colour cycles observed in the field (cycles LA-10<sub>B</sub>-15<sub>B</sub>; Figs. 5.1c and 5.2a).

Element	Value
K	0.973
Al	0.962
V	0.939
Fe	0.938
Ti	0.913
Li	0.901
Ba	0.867
Mn	0.779
Cr	0.774
Ni	0.743
Zn	0.608
Na	0.248
Mg	0.046
Sr	-0.138
Ca	-0.764

Table 5.1. Loadings of individual elements on the first principal component (PC-1).

### 5.6.2 Stable isotopes

For isotope analyses, between 15 and 40 specimens (size-dependent) of the benthic foraminifer *Planulina ariminensis* were picked from in total 145 samples. Preservation is generally good to excellent without any indication for recrystallization or pyritization. Where *P. ariminensis* was not abundant enough (<500 µg per sample), the *Cibicides* species *C. dutemplei* and *C. pachyderma* were picked in addition. In order to remove any organic remains, each sample was roasted for 30 minutes at 470°C under vacuum. The samples were analyzed using an ISOCARB, which is directly coupled to the mass spectrometer and has the capacity to measure 44 samples, including 1 international (IAEA-CO-1) and 9 in-house (NAXOS) standards, during a run. Each sample reacted with 103% phosphoric acid (H<sub>3</sub>PO<sub>4</sub>) for 6 to 7 minutes at 90°C. All isotope data are reported as per mil (‰) relative to the PeeDee belemnite (PDB) standard. After correction of the *Cibicides* values by adopting a value equal to the average offset from the *Planulina* values, twelve data points were incorporated in the δ<sup>18</sup>O series. The analytical precision and accuracy were determined by replicate analyses of samples and by comparison with the IAEA-CO-1 standard. The relative standard deviations, analytical precision, and accuracy were better than 0.1‰ both for δ<sup>18</sup>O as well as for δ<sup>13</sup>C.

#### *The δ<sup>18</sup>O record*

The δ<sup>18</sup>O record shows a stepwise shift in mean δ<sup>18</sup>O to lighter values from -5.5 to +8 m. The average δ<sup>18</sup>O value is 1.05‰ for the interval between -5.5 and -0.5 m, 0.9‰ between -0.5 and 6.25 m, and 0.6‰ between 6.25 and 30 m (Fig. 5.4). These intervals (“plateaus”) are separated by two main shifts, which occur between -1.5 and 1 m (from 1.4 to 0.4‰) and between 5.5 and 7 m (from 1.1 to 0.2‰). Less pronounced shifts to lighter values occur between -5 and -3 m and between 26.5 and 29 m. The most prominent shifts (of ~0.6‰) to heavier values are found between -3 and -1.5 m, 1 and 1.7 m, and 7 and 8.2 m (Fig. 5.4).

High-frequency variations in δ<sup>18</sup>O show a distinct relation with lithology with lighter values in the reddish layers (amplitude changes of ~0.5‰; Fig. 5.4). Close inspection of the δ<sup>18</sup>O record reveals additional high-frequency variability with a spacing of about twice that of the lithology-

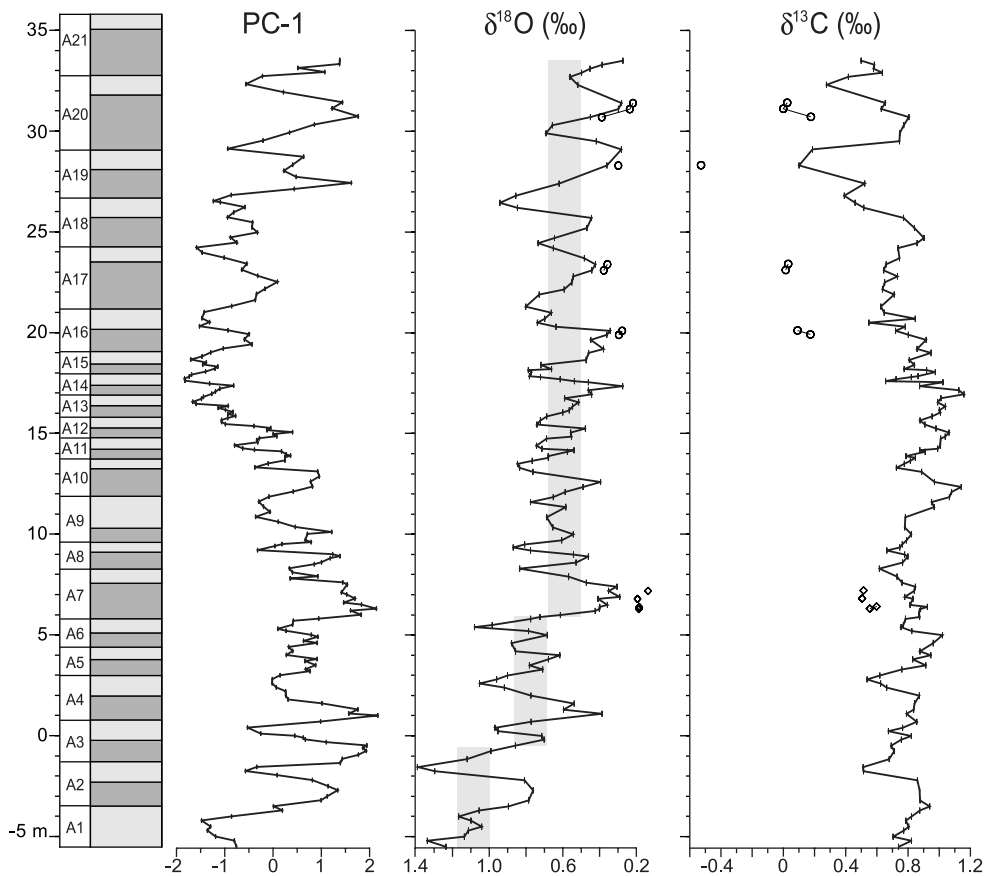


Figure 5.4. Geochemical records (PC-1, benthic  $\delta^{18}\text{O}$ , and benthic  $\delta^{13}\text{C}$ ) of the Loulja-A section. For key, see caption to Figure 5.2. Open squares in the isotope records represent data obtained from *Cibicides dutemplei*; open circles denote the *C. pachyderma* values. Correction of the *Cibicides* values was done using a value equal to the average offset from the *Planulina* values; these values are 0.214 ( $\delta^{18}\text{O}$ ) and 0.324 ( $\delta^{13}\text{C}$ ) for *C. dutemplei* and 0.065 ( $\delta^{18}\text{O}$ ) and 0.627 ( $\delta^{13}\text{C}$ ) for *C. pachyderma*.

bound changes. Most of the prominent shifts described above are part of this high-frequency variability.

#### The $\delta^{13}\text{C}$ record

The  $\delta^{13}\text{C}$  record does not reveal a clear trend but significantly lighter values are reached in the top part of the record (Fig. 5.4). Higher-frequency variations are less prominent than in the  $\delta^{18}\text{O}$  record. Nevertheless, lithology-bound changes are present with lighter values recorded in the beige layers. The expression of a cycle with approximately twice the thickness of a colour cycle is more evident. The signal follows the same frequency changes as in  $\delta^{18}\text{O}$ , with shifts to lighter  $\delta^{13}\text{C}$  values coinciding with shifts to heavier  $\delta^{18}\text{O}$  values (Fig. 5.4). This relation does not hold, however, in the uppermost part of the section, i.e., from ~27 m upwards.

## 5.7 Age model

### 5.7.1 Loulja-A

The Loulja-A section must be slightly younger than the Ain el Beida section of late Messinian age in view of the overall orientation of the bedding plane and its location approximately halfway between Ain el Beida and Salé (lower Pliocene). Moreover, the characteristic interval with six successive thin cycles (LA-10<sub>B</sub>-15<sub>B</sub>) is unknown from Ain el Beida. Paleobathymetric estimates of 300-500 m follow logically from the deeper estimates for the latter section. An age of around the M-P boundary is also suggested by the calcareous nannofossil biostratigraphy. The *Discoaster quinqueramus* LO, *Ceratolithus larrymayeri* FO and LO, and *Triquetrorhabdulus rugosus* FO are recorded in the same order across the boundary at ODP Site 926 in the equatorial Atlantic (Backman and Raffi, 1997). The younger events are found in sediments of Early Pliocene age at DSDP Site 502 in the North Atlantic and in southern Italy, albeit not always in the same order (Driever, 1988; Lourens et al., 1996; Raffi et al., 1998; E. De Kaenel, unpublished data, 2001). The nannofossil events exclude any other correlation than with the Miocene-Pliocene boundary interval.

The initial astronomical tuning of Loulja-A is based on the colour cycles. Because of the close proximity of the sections in the Bou Regreg area and the identical expression of the cycles, it is assumed that the phase relations between the colour cycles and the orbital parameters are the same as for Ain el Beida. Phase relations for the colour cycles in the latter section were based on similarities in proxy signals with sapropels in the Mediterranean for which the phase relations are known (Lourens et al., 1996; Krijgsman et al., 2004). This implies that midpoints of individual, Ca-poor (paragraph 5.6.1), reddish layers correspond to precession minima and summer insolation maxima and that thicker and more prominent reddish layers correspond to high-amplitude precession minima and insolation maxima and, hence, to eccentricity maxima (Krijgsman et al., 2004).

We start the tuning from the characteristic interval of six thin cycles (LA-10<sub>B</sub> up to LA-15<sub>B</sub>). According to the phase relations and initial age constraints, these cycles correspond to the 400-kyr eccentricity minimum around 5.25 Ma (Fig. 5.5). Tuning the individual sedimentary cycles to the precession and/or insolation target curve usually follows such a first-order tuning. Instead, we preferred at this stage to introduce the PC-1 record as an additional tool in the tuning exercise because of its distinct cyclic character. A detailed study of the Ain el Beida section revealed a very good fit between a component with similar element loadings (E. Van der Laan, unpublished data, 2002) and the astronomical target curve. However, this component could better be compared with ETP (a combined record of normalized Eccentricity, Tilt (obliquity), and (negative) Precession (Imbrie et al., 1984)) than with insolation because of an apparent non-linear response to the insolation forcing. According to our phase relations, maxima in PC-1 correspond to maxima in ETP (maxima in obliquity and eccentricity/minima in precession).

The PC-1 record of Loulja-A is in almost excellent agreement with ETP, allowing for a straightforward tuning of the section up to at least cycle LA-16 (Fig. 5.5). The two groups of three distinct maxima in PC-1 in the lower part of Loulja-A (LA-2-4; LA-7-9) correlate with two similar clusters of maxima in ETP between 5.58 and 5.38 Ma, which reflect two successive prominent 100-kyr eccentricity maxima. The two weaker maxima of cycles LA-5 and LA-6 correlate with the two low-amplitude maxima in ETP that correspond to the intervening 100-kyr eccentricity minimum around 5.48 Ma. The amplitude pattern in PC-1 generally mimics that of ETP. The thick reddish layer LA-10<sub>R</sub> is partly explained by the composite character of this cycle in

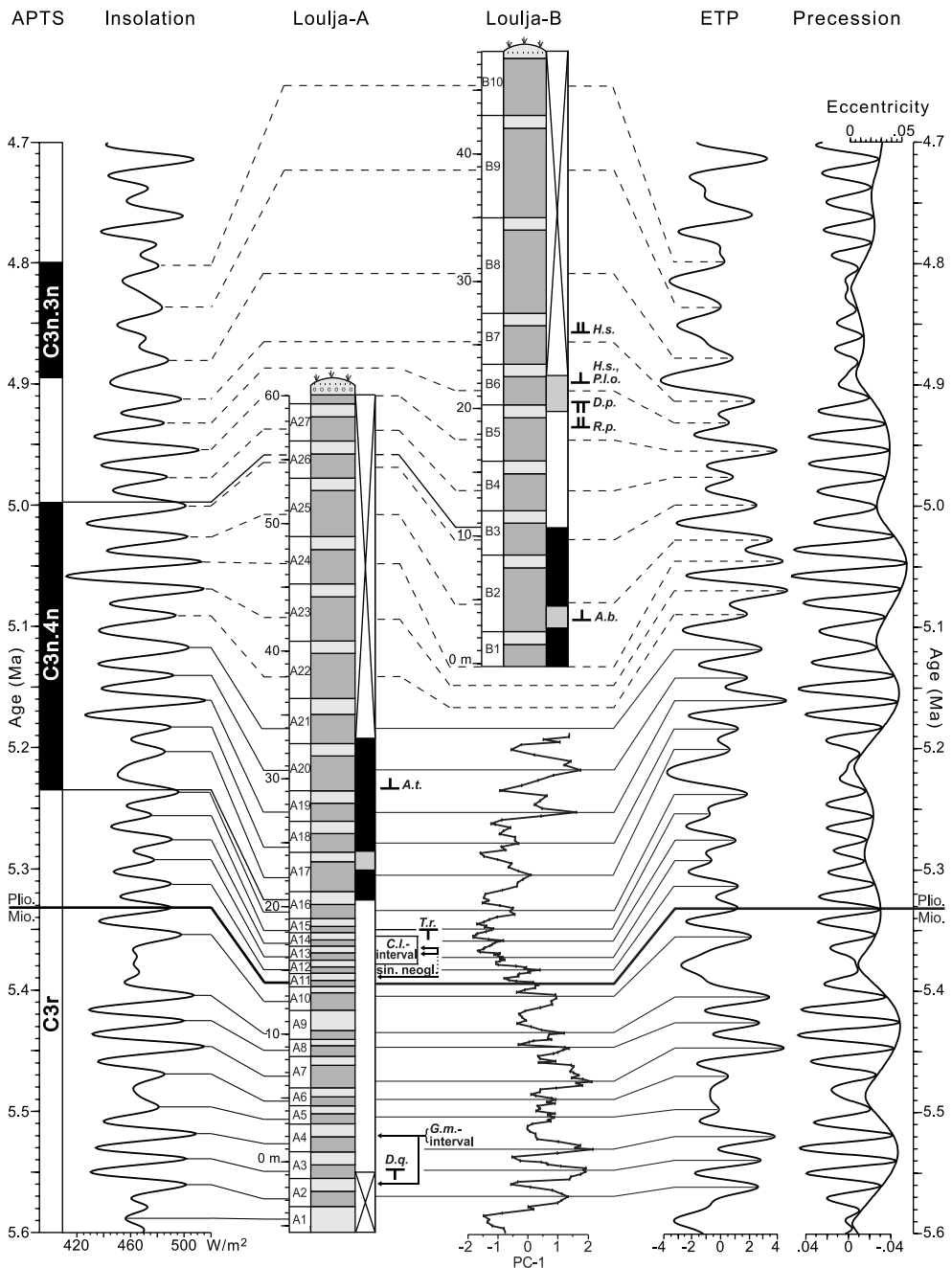


Figure 5.5. Calibration of the magnetostratigraphy of the Loulja-A and Loulja-B sections (for key, see caption to Figure 5.2) to the astronomical polarity timescale (ATNTS2004 of Lourens et al., 2004) and tuning of colour cycles and PC-1 to the 65°N summer insolation and ETP (normalized eccentricity, tilt, and precession) time series of the La2004 solution (Laskar et al., 2004) with present-day values for dynamical ellipticity and tidal dissipation. Also shown are the precession and eccentricity curves of the same solution.

ETP. The correlative ETP maximum shows a “shoulder” at its base corresponding to an additional low-amplitude precession cycle. Similar shoulders (but in opposite direction) may explain the thickness of LA-1<sub>B</sub> and LA-9<sub>B</sub>. Following the tuning of cycles LA-1 to LA-10, the characteristic interval of thin colour cycles (LA-10<sub>B</sub> to LA-15<sub>B</sub>) can be correlated straightforwardly to the interval with reduced amplitude variations in ETP and insolation that corresponds to the 400-kyr eccentricity minimum around 5.25 Ma.

The tuning of cycles LA-17 to LA-21 proved more difficult. The preferred option is presented in Figure 5.5 and implies that all the colour cycles correspond to single precession cycles, even though this does not explain the extra peaks in PC-1 observed in some of the cycles. Following this option, LA-20<sub>R</sub> correlates with the precession minimum/insolation maximum at 5.14/5.15 Ma. The relatively thick reddish layer of cycle LA-17 does not reflect a high-amplitude precession minimum/insolation maximum as expected, but is related to the longer than average duration of the correlative precession-insolation cycle. Sedimentation rates, which are 5 cm/kyr on average in the interval with the six thin cycles LA-10<sub>B</sub>-15<sub>B</sub>, increase to ~13 cm/kyr in cycle LA-17 and to ~16 cm/kyr in cycle LA-20 (Fig. 5.6). Other options imply that the reddish layers of one or all of cycles LA-18 to LA-21 contain an extra cycle that lacks sedimentary expression. Although double cycles are known from Ain el Beida, extra cycles are not developed in reddish layers in that section (Krijgsman et al., 2004).

We favour the first option for several reasons. Firstly, the increase in sedimentation rate resulting from this option is expected because sedimentation rate is positively correlated with eccentricity and hence with precession amplitude both in Ain el Beida (Van der Laan et al., 2005) as well as in the lower half of Loulja-A (see Figure 5.4). Nevertheless, the increased sedimentation rate starts somewhat earlier than expected based on the amplitude changes in ETP and insolation. However, the increase markedly coincides with the top of the 400-kyr carbonate maximum in the deep marine Trubi marls in southern Italy; this maximum corresponds to the 400-kyr eccentricity minimum around 5.25 Ma and consists of the first six precession-related cycles of the Trubi (Hilgen, 1991; Hilgen and Langereis, 1993). Overall, the higher sedimentation rates are in good agreement with sedimentation rates calculated for the lower part of Loulja-A and Loulja-B (see paragraph 5.7.3) where cycles reach similar thicknesses at times of maximum eccentricity. The double cycle option does not result in higher sedimentation rates in the top part of Loulja-A, which is difficult to explain. Moreover, out-of-phase relationships between the 41-kyr component in  $\delta^{18}\text{O}$  and obliquity start to develop if this option is used for tuning (not shown). Finally, the remaining cycles LA-22-27 should also represent double cycles since they reach similar thicknesses as cycles LA-18-21. However, as we demonstrate in paragraph 5.7.3, it is clear from the tuning of Loulja-B that the extremely thick cycles LB-8-9 (which do represent double cycles) should then be reached in the top part of Loulja-A, which is clearly not the case. We therefore prefer the tuning option in which all colour cycles are regarded as single precession cycles. The sampled time interval covered by the Loulja-A section thus ranges from ~5.59 to 5.12 Ma.

### 5.7.2 Spectral analysis

To test the correctness of our preferred age model further, we applied (cross-) spectral analysis and band-pass filtering using the Analyseries software of Paillard et al. (1996) to determine the main periodicities in our proxy records and the phase relationships relative to the astronomical forcing. The PC-1 spectrum reveals peaks at the main precession frequencies, which is not surprising because of the strong link with the colour cycles and the tuning to a precession-dominated target curve (Fig. 5.6). Additional variance near the main obliquity frequency is also apparent although

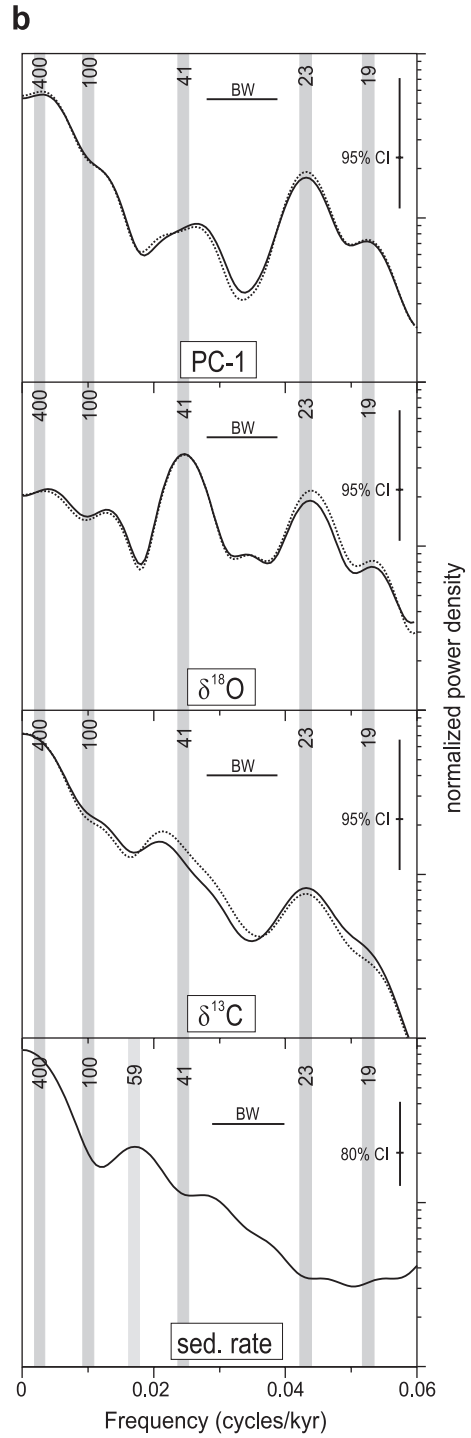
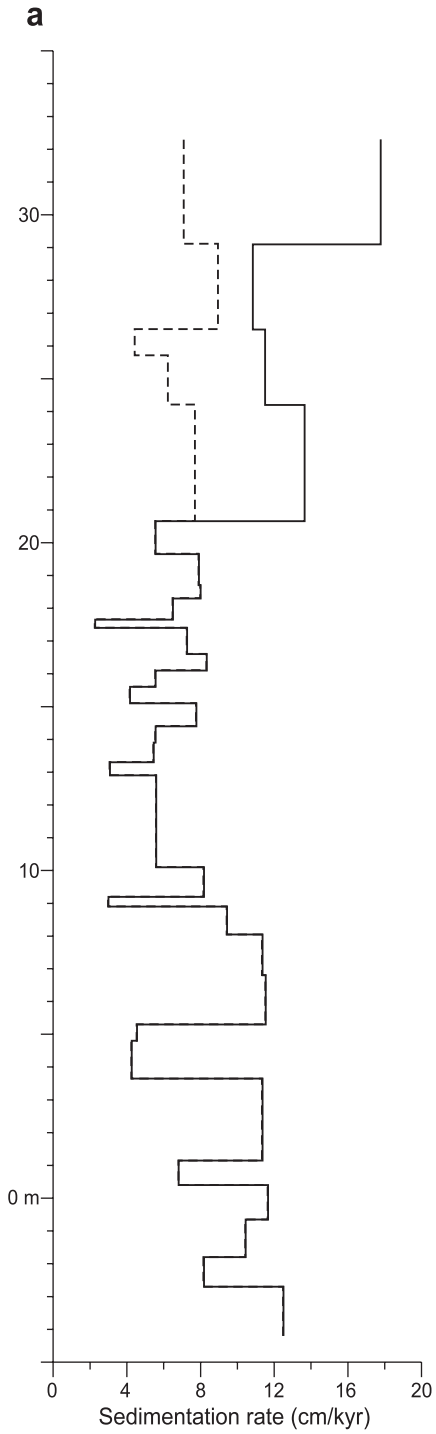




Figure 5.6. a) Sedimentation rate curve versus lithology of Loulja-A according to our preferred age model. Dashed line shows sedimentation rate if cycles LA-17-20 represent double cycles. b) Power spectra of PC-1, benthic  $\delta^{18}\text{O}$ , benthic  $\delta^{13}\text{C}$ , and sedimentation rate, using the preferred age model to generate time series. Solid and dotted lines in each spectral panel represent spectral power after tuning to ETP and insolation, respectively. Horizontal bar denotes the band width (BW) that is 0.011 for PC-1,  $\delta^{18}\text{O}$ , and  $\delta^{13}\text{C}$  and 0.012 for sedimentation rate. Vertical bar denotes the 95% confidence interval (CI); for the sedimentation rate the 80% confidence interval is indicated.

a separate peak is lacking. In addition, power is concentrated around ~400 kyr, which is probably related to the long-term eccentricity cycle. The  $\delta^{18}\text{O}$  spectrum reveals a strong peak at the main obliquity frequency and an additional peak at the 23-kyr precession period. Subsidiary peaks occur at the low-frequency end of the spectrum, at ~260 kyr and ~80 kyr. The  $\delta^{13}\text{C}$  spectrum reveals a concentration of power at the low-frequency end of the spectrum, while a 'shoulder' is recorded at ~90 kyr, presumably related to short-term eccentricity. Additional peaks at the main obliquity and precession frequencies are present although their power is relatively low. Because the  $\delta^{18}\text{O}$  and  $\delta^{13}\text{C}$  time series were constructed by means of tuning PC-1 to ETP, we carried out an independent check on the correctness of our age model by filtering the 41-kyr components in  $\delta^{18}\text{O}$ ,  $\delta^{13}\text{C}$ , and PC-1 and comparing them with obliquity. The 41-kyr components generally show an in-phase relationship with obliquity and similar amplitude variations (Fig. 5.7), although the 41-kyr components in PC-1 and  $\delta^{13}\text{C}$  start to run out of phase with obliquity in the younger part of the record (from 5.22 Ma onwards). For  $\delta^{13}\text{C}$ , the out-of-phase relationship stems from the fact that it does not co-vary inversely with  $\delta^{18}\text{O}$  in this part of the record, as mentioned before (see paragraph 5.6.2). In addition, a clear obliquity-related signal is lacking in the interval between 5.48 and 5.36 Ma, where amplitude variations are low and the ~100-kyr signal is well developed (Fig. 5.7). For PC-1, the (near) out-of-phase relationship with obliquity in the younger (and oldest) part of the record stems from the high-amplitude precession-related variations in PC-1 associated with the eccentricity maxima at ~5.15 and 5.55 Ma; these strong variations prevent the filter from picking up the obliquity-related signal.

Results of cross-spectral analysis reveal that the precession components in PC-1,  $\delta^{13}\text{C}$ , and  $\delta^{18}\text{O}$  vary in phase with ETP (Fig. 5.8). Again this is not surprising in view of the strong link of these components with lithology and the tuning (of PC-1) to a precession-dominated target curve. The results also confirm the in-phase relation for the 41-kyr component in  $\delta^{18}\text{O}$  with respect to obliquity as inferred from the band-pass filtering. Note, however, that the latter in-phase relation changes to a lag of several kyr if the tidal dissipation in the La2004<sub>(1,1,0)</sub> solution is reduced to half its present-day value (not shown). This outcome is comparable with the results from the slightly older Ain el Beida section (Van der Laan et al., 2005) and provides additional supportive evidence for our tuned age model of the Loulja-A section. Our age model provides astronomical ages, not only for the sedimentary cycles and for bioevents, but also for the dominantly obliquity-controlled  $\delta^{18}\text{O}$  stages (Tables 5.2 and 5.3).

### 5.7.3 Loulja-B

The calcareous plankton biostratigraphic data from Loulja-B indicate that this section is slightly younger than Loulja-A (thereby confirming the information from the field) and that the N-R polarity reversal must represent the Upper Thvera. Using the position of the Upper Thvera, dated astronomically at 4.997 Ma (Lourens et al., 2004), as starting point the tuning of Loulja-B is rather straightforward (Fig. 5.5). The two very thick cycles LB-8 and 9 are interpreted as double cycles in which one cycle lacks sedimentary expression and correspond to the 400-kyr eccentricity

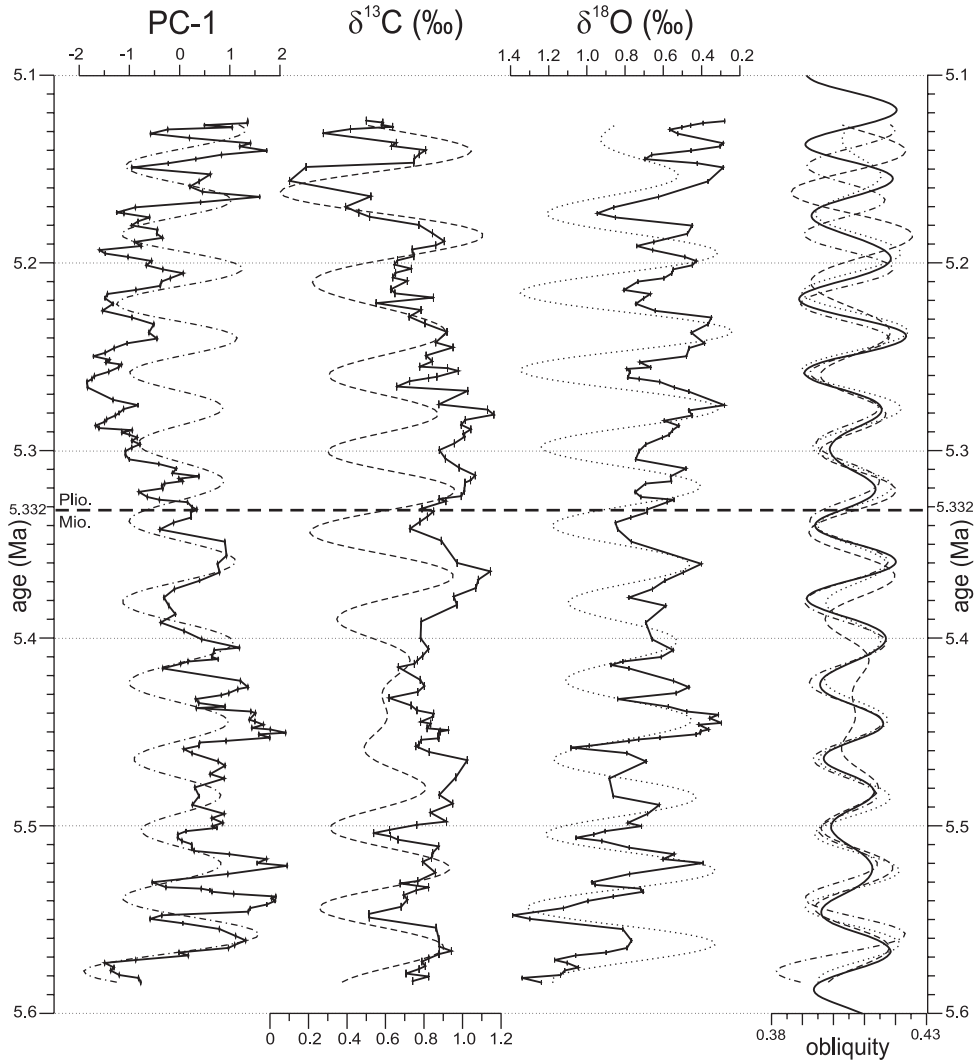


Figure 5.7. PC-1, benthic  $\delta^{13}\text{C}$ , and benthic  $\delta^{18}\text{O}$  time series (solid lines) with 41-kyr filtered components (dotted and dashed lines) and comparison with obliquity. The proxy time series were filtered using Gaussian band-pass filters with central frequencies of 0.0255 (PC-1), 0.023 ( $\delta^{13}\text{C}$ ), and 0.0245 ( $\delta^{18}\text{O}$ ) and a band width of 0.012 cycles/kyr.

minimum around 4.85 Ma; this minimum is characterized by strongly reduced amplitudes in precession and hence insolation. In this case, the very weak summer insolation minima (precession maxima) at 4.87 and 4.83 Ma are not expressed in the sedimentary record as additional thin beige marls. This pattern strongly resembles that observed in the Trubi marl formation where cycles 21 and 22 represent double cycles as well (Hilgen, 1991; Lourens et al., 1996). The very thick reddish layer of cycle LB-2 is the only uncertainty that remains in the tuning of Loulja-B. Similarly, this cycle may represent a double cycle.

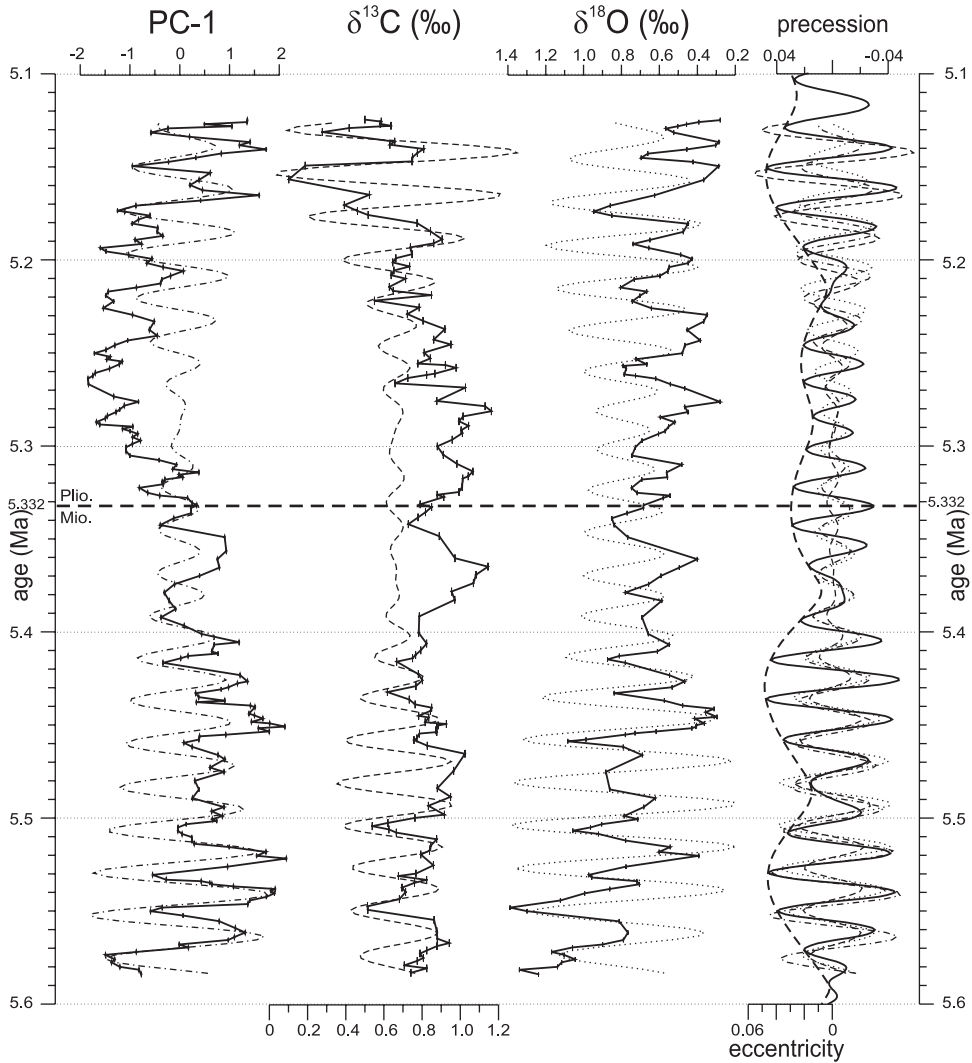


Figure 5.8. PC-1, benthic  $\delta^{13}\text{C}$ , and benthic  $\delta^{18}\text{O}$  time series (solid lines) with 23-kyr filtered components (interrupted lines) and comparison with precession. Thick dashed line shows the eccentricity envelope of the precession curve. The proxy time series were filtered using Gaussian band-pass filters with central frequencies of 0.043 (PC-1), 0.042 ( $\delta^{13}\text{C}$ ), and 0.0435 ( $\delta^{18}\text{O}$ ) and band widths of 0.014 (PC-1), 0.015 ( $\delta^{13}\text{C}$ ), and 0.011 ( $\delta^{18}\text{O}$ ) cycles/kyr.

#### 5.7.4 Calcareous plankton events and magnetic reversals

With the tuning of the Loulja sections, astronomical ages are obtained not only for the sedimentary and geochemical cycles but also for the calcareous plankton events and magnetic polarity reversals (Table 5.3). The *Discoaster quinquerramus* LO at 5.537 Ma and the *Triquetrorhabdulus rugosus* LO at 5.255 Ma are near synchronous with the low-latitude Atlantic (5.54 and 5.24 Ma, respectively; Backman and Raffi, 1997; Raffi et al., 1998). The *Ceratolithus larrymayeri* acme corresponds with the younger part of the short total range of this species at Ceara Rise (Raffi et al., 1998).

Cycle	Stratigraphic position (m)	Age (Ma)	
		ETP	Summer insolation
LA-2R	-2.70	5.561	5.560
LA-2B	-1.80	5.550	5.550
LA-3R	-0.65	5.539	5.539
LA-3B	0.40	5.530	5.530
LA-4R	1.15	5.519	5.518
LA-5R	3.65	5.497	5.496
LA-6R	4.80	5.470	5.469
LA-6B	5.30	5.459	5.459
LA-7R	6.80	5.446	5.446
LA-7B	8.05	5.435	5.436
LA-8R	8.90	5.426	5.425
LA-8B	9.20	5.416	5.416
LA-9R	10.10	5.405	5.404
LA-10R	12.90	5.355	5.354
LA-10B	13.30	5.342	5.343
LA-11R	13.90	5.331	5.332
LA-11B	14.40	5.322	5.322
LA-12R	15.10	5.313	5.312
LA-12B	15.60	5.301	5.302
LA-13R	16.10	5.292	5.292
LA-13B	16.60	5.286	5.285
LA-14R	17.40	5.275	5.275
LA-14B	17.65	5.264	5.265
LA-15R	18.30	5.254	5.255
LA-15B	18.70	5.249	5.248
LA-16R	19.65	5.237	5.236
LA-16B	20.65	5.219	5.222
LA-17B	24.20	5.193	5.193
LA-18B	26.50	5.173	5.173
LA-19B	29.10	5.149	5.151
LA-20B	32.30	5.131	5.130

Table 5.2. Stratigraphic position of midpoints of reddish and beige layers of lithologic cycles in the Loulja-A section and their astronomical ages after tuning to the ETP and summer insolation curves of the La2004(1,1) solution (Laskar et al., 2004).

Consequently, also the *C. larrymayeri* LO is synchronous between Loulja and the low-latitude Atlantic. The *Amaurolithus tricorniculatus* FO, which is not considered a useful event in view of the rare and discontinuous presence of the species (Raffi et al., 1998), clearly postdates the same event in the equatorial Atlantic (5.15 versus 5.31 Ma; see also Table 5.3).

The three cosmopolitan nannofossil events recorded in the lower part of the Loulja-B section, namely the subbottom of *Reticulofenestra pseudoumbilicus* (>8 µm), the *Dictyococcites perplexus* subtop, and the *Pseudoemiliania lacunosa ovata* FO, were also recorded by Driever (1988) in the Mediterranean Singa and Rossello composite sections dated astronomically by Lourens et al. (1996). Our astronomical ages for these events are in good agreement with Driever (1988) and Lourens et al. (1996). The difference of one cycle for the *D. perplexus* subtop is due to a difference in defining the n1-event of Driever (1988), which marks the transition from predominantly *D.*

	This study			Other Age (Ma)
	Cycle	Position (m)	Age (Ma)	
<i>Magnetostratigraphy</i>				
<b>Reversal</b>				
C3n.4n (old)	LA-16B	20.35 - 20.70	5.222 ± 0.003	5.235 (1)
C3n.4n (young)	LB-3	9.8 - 11.6	4.994 ± 0.007	4.997 (1)
<i>Biostratigraphy</i>				
<b>Bioevent</b>				
interval with common <i>Globorotalia menardii</i>	LA-2B	-1.95 to -1.55	5.550 ± 0.002	5.556 ± 0.002 (2)
	LA-4B	2.10 - 2.20	5.511 ± 0.001	5.523 (2)
influx sinistral neogloboquadrinids	LA-11B	14.55 - 14.75	5.319 ± 0.001	5.325 ± 0.005 (3)
influx sinistral neogloboquadrinids	LA-13A	16.15 - 16.25	5.291 ± 0.001	5.305 ± 0.005 (3)
	LA-13B	16.65 - 16.75	5.285 ± 0.001	
<i>L.O. Discoaster quinqueramus</i>	LA-3R	-0.7 to -0.18	5.537 ± 0.002	5.58 / 5.59 (1); 5.537 (4)
<i>F.O.D. Ceratolithus larrymayeri</i>	LA-12B	15.50 - 15.55	5.303 ± 0.001	5.338 (4)
<i>L.O.D. Ceratolithus larrymayeri</i>	LA-14B	17.7 - 17.9	5.262 ± 0.002	5.264 (4)
<i>L.O. Triquetrorhabdulus rugosus</i>	LA-15R	18.2 - 18.3	5.255 ± 0.001	5.231 (4)
<i>F.O. Amaurolithus tricorniculatus</i>	LA-20R	28.0 - 30.3	5.151 ± 0.009	5.31 (5)
<i>F.O. Amaurolithus bizzarus</i>	LB-2R	2.25 - 5.0	5.033 ± 0.004	5.24 (5)
subbottom <i>Reticulofenestra pseudoumbilicus</i> (>8 µm)	LB-5B	17.8 - 19.4	4.950 ± 0.005	4.91 (3)
subtop <i>Dictyococcites perplexus</i>	LB-6B	19.4 - 21.7	4.938 ± 0.007	4.91 (3, 6)
<i>F.O. Pseudoemiliana lacunosa ovata</i>	LB-6B	21.7 - 22.5	4.929 ± 0.003	4.91 (3, 6)
<i>F.O. Helicosphaera sellii</i>	LB-6B	21.7 - 22.5	4.929 ± 0.003	~4.55 (7)
<i>F.R.O. Helicosphaera sellii</i>	LB-7B	25.0 - 27.0	4.906 ± 0.008	-
<i>Isotope stratigraphy</i>				
<b>Marine isotope stages</b>				
TG14		-5.20	5.582	
TG13		-2.70	5.560	
TG12		-1.55	5.548	
TG11		1.10	5.519	
<i>TG10.2</i>		2.60	5.505	
<i>TG10.0</i>		5.40	5.458	
TG9		6.90	5.445	
<i>TG8.2</i>		8.30-9.35	5.433-5.414	
<i>TG8.0</i>		11.60	5.377	
TG7		12.60	5.359	
<i>TG6.2</i>		13.50	5.339	
[x]		14.10-15.25	5.327-5.309	
<i>TG6.0</i>		15.65	5.301	
TG5		17.35	5.276	
<i>TG4.2</i>		18.05	5.259	
<i>TG4.1</i>		18.65-20.10	5.248-5.230	
<i>TG4.0</i>		21.30	5.217	
TG3		23.10-25.70	5.202-5.180	
TG2		26.45	5.173	
TG1		28.30-31.40	5.151-5.136	

Table 5.3. Tuned ages of magnetic reversals, calcareous plankton events, and marine isotope stages in the Loulja sections and comparison with ages from other studies. Numbers in parentheses refer to (1) Lourens et al. (2004); (2) Krijgsman et al. (2004); (3) Lourens et al. (1996); (4) Backman and Raffi (1997); (5) Raffi et al. (1998); (6) Driever (1988); (7) Rio et al. (1997). Marine isotope stages follow Shackleton et al. (1995b); (sub) stages in italics and stage [x] are introduced by us and indicated in Figures 5.10 and 5.11.

*perplexus* to predominantly *R. pseudoumbilicus* (>8 µm), rather than a problem of the astronomical tuning. The very rare occurrence of *P. lacunosa ovata* at the beginning of its range explains the slightly different age obtained for this event in the present study.

The planktonic foraminifera do not show clear-cut primary events, but the neogloboquadrinid coiling direction reveals two sinistral influxes of very short duration. Two similar influxes of sinistral neogloboquadrinids have also been found in the Mediterranean where they occur in the homogeneous marl of basic cycles 1 and 2 in the Trubi Formation (Di Stefano et al., 1996;

Lourens et al., 1996). The independent tuning of the Loulja colour cycles indicates that the first influx corresponds exactly in time with the first influx in the Mediterranean but that the second influx occurs one precession-related cycle later at Loulja.

The astronomical calibration implies that Loulja-A cycles 1-21 cover the time interval from 5.59 to 5.12 Ma. Therefore, the base of the normal polarity chronozone recorded between 20.35 and 20.7 m in cycle LA-16 should correspond to the base of the Thvera subchron (C3n.4n (o)); the astronomical age of  $5.222 \pm 0.005$  Ma for the reversal at Loulja is very close to the astrochronologic age of 5.235 Ma (Lourens et al., 1996, 2004). In addition, the reversal is neatly located five precession cycles (~100 kyr) above the Miocene-Pliocene boundary, dated astronomically at 5.332 Ma (Lourens et al., 1996; Van Couvering et al., 2000), and pinpointed at 13.90 m in the middle of LA-11<sub>R</sub>. The N>R transition below the 11 m level in LB-3<sub>R</sub> corresponds to the Upper Thvera, as previously assumed. Its position is consistent with the Mediterranean, indicating that the very thick cycles LB-8 and 9 are indeed the equivalent of the double cycles 21 and 22 in the Trubi Formation. Note however that the position of this reversal was used during the tuning procedure.

## 5.8 Discussion

### 5.8.1 Isotope stratigraphy and chronology

With the tuned age model for Loulja at hand it becomes timely to discuss the isotope stratigraphy and chronology for the latest Miocene and earliest Pliocene by comparing the Loulja isotope records with previously published records from the Bou Regreg area and with records from the open ocean (e.g., Hodell et al., 1994; Shackleton et al., 1995b, 1999; Hodell et al., 2001; Van der Laan et al., 2005). Note that we will adopt our age model as basis for discussing the isotope stratigraphy and chronology. We will not attempt to match the Loulja isotope record to the isotope records from the open ocean and thus adopt alternative age models based on tuning of dominantly obliquity controlled isotope records. The reason for this is that we consider our age model an improvement because it is based on the tuning of precession dominated colour cycles, which reveal a much more distinctive pattern.

The Loulja-A  $\delta^{18}\text{O}$  record reveals a much stronger obliquity-related signal than PC-1, which mainly tracks the colour cycles observed in the field. Because of the additional influence of precession, it is not always easy to recognize the obliquity-related signal in  $\delta^{18}\text{O}$ . The latter signal was illustrated by extracting the 41-kyr component in  $\delta^{18}\text{O}$  and showing it as an overlay on the  $\delta^{18}\text{O}$  time series; comparison with obliquity reveals an almost perfect in-phase relationship (Fig. 5.7).

Like at Ain el Beida, the strong 41-kyr  $\delta^{18}\text{O}$  cycle at Loulja-A is interpreted as to reflect a dominant obliquity-controlled glacial cyclicity, which has been recognized in open ocean benthic isotope records of latest Miocene to early Pleistocene age (e.g., Ruddiman et al., 1986; Raymo et al., 1989; Tiedemann et al., 1994; Shackleton et al., 1995b). This glacial record reveals a characteristic pattern of distinct and less distinct glacial cycles. The more prominent peaks in  $\delta^{18}\text{O}$  have been labelled to facilitate communication and global correlation of the oxygen isotope stages (Tiedemann et al., 1994; Shackleton et al., 1995b). For the latest Miocene to Early Pliocene, i.e. the time span covered by the Loulja-A section, the codification scheme of Shackleton et al. (1995b) based on ODP Site 846 in the eastern equatorial Pacific is used. This scheme links isotope stages to magnetochrons whereby, similar to other schemes, even numbers indicate cold stages.

Shackleton et al. (1999) revised the initial tuned age model for the isotope record of Site 846 (Shackleton et al., 1995a) later on.

At Loulja-A, the correct identification of isotope stages is crucial if one aims to determine whether the basal Pliocene flooding of the Mediterranean is related to the (peak) deglaciation and associated sea level rise leading to TG5. The straightforward and unambiguous tuning of (the lower part of) Loulja-A reveals a stratigraphic overlap with Ain el Beida, indicating that the two prominent and characteristic maxima in  $\delta^{18}\text{O}$  at -5 and -1.5 m correspond to TG14 and TG12 (Fig. 5.9). The identification of the younger stages depends on the detailed correlation to the  $\delta^{18}\text{O}$  record of Site 846 in which they were originally defined (Shackleton et al., 1995b). The stepwise shift to lighter isotope values between 5.55 Ma (TG12) and 5.45 Ma at Loulja is easily recognized at Site 846, indicating that the prominent  $\delta^{18}\text{O}$  minimum at 5.45 Ma represents peak interglacial TG9. The  $\delta^{18}\text{O}$  pattern in this interval is remarkably similar between both records showing additional precession-related variations that would allow a (further) subdivision of several of the stages (e.g., TG10). The Loulja-A record further confirms the presence of an extra obliquity-related cycle between TG11 and TG9.

The isotope stage identification is difficult from TG9 onward due to the relative low amplitude and therefore less characteristic pattern in  $\delta^{18}\text{O}$  between 5.4 and ~5.2 Ma at ODP Site 846 (Shackleton et al., 1995b, 1999). Comparison of the Loulja-A and ODP Site 846  $\delta^{18}\text{O}$  time series, using the revised tuning of Shackleton et al. (1999), shows that TG9 to TG3 occur in both records at the same time and are in phase with obliquity, but that the filtered 41-kyr component starts to run out of phase with obliquity between TG3 and T7 at Site 846 (Fig. 5.9). This would imply that the  $\delta^{18}\text{O}$  minimum in the Loulja-A record at 5.315 Ma indeed corresponds to TG5 at Site 846.

However, this identification becomes less certain if one compares the carbon and oxygen isotope records of Site 846 in the depth and time domain. In addition, the isotope records from ODP Site 982 in the North Atlantic (Hodell et al., 2001) and from Salé Briqueterie (Hodell et al., 1994) located near Loulja were included in the comparison because ages for  $\delta^{18}\text{O}$  stages at Site 982 and for those in the redated Salé record (Hodell et al., 2001) deviate significantly from our tuned ages. The comparison for  $\delta^{18}\text{O}$  and  $\delta^{13}\text{C}$  in the depth and time domain is shown in Figure 5.10 ( $\delta^{18}\text{O}$ : Figs. 5.10a and 5.10b;  $\delta^{13}\text{C}$ : Figs. 5.10c and 5.10d). For Site 846, the depth-time conversion results in an increase in sedimentation rate between TG7 and TG5 if the (manual) revision of the initial tuned age model by Shackleton et al. (1999) is adopted (Fig. 5.9). The TG7-5 interval is significantly thicker as that observed between regular obliquity-controlled cycles while these stages have been tuned to successive obliquity maxima. In fact, the Site 846  $\delta^{13}\text{C}$  record suggests that an additional obliquity-controlled cycle (labelled [x] in Figure 5.10c) is present between TG7 and TG5. This characteristic interval reveals the highest  $\delta^{13}\text{C}$  values throughout the critical interval across the M-P boundary and is preceded by a long-term increase leading to TG7. It can relatively easily be recognized in the other  $\delta^{13}\text{C}$  records, showing a very similar character at Loulja and ODP Site 982 with three distinct  $\delta^{13}\text{C}$  maxima. The first and last of these maxima correspond to stages TG7 and TG5 if we follow the  $\delta^{18}\text{O}$  stage numbering of Shackleton et al. (1995b) and the expression of these stages in the Site 846  $\delta^{13}\text{C}$  record. Consequently, the extra (obliquity-controlled) stage is also recognized in the Site 982 and Loulja  $\delta^{13}\text{C}$  depth records. The extra cycle would have the immediate consequence that the M-P boundary does not coincide with TG5 but with the unnamed extra cycle between TG5 and TG7, if we assume that the identification and tuning of TG7 is correct.

Using characteristic patterns in especially  $\delta^{13}\text{C}$ , the correlation between Loulja-A, Salé, and ODP Sites 846 and 982 can be extended up to TG2 (Figs. 5.10 and 5.11; Table 5.3). These

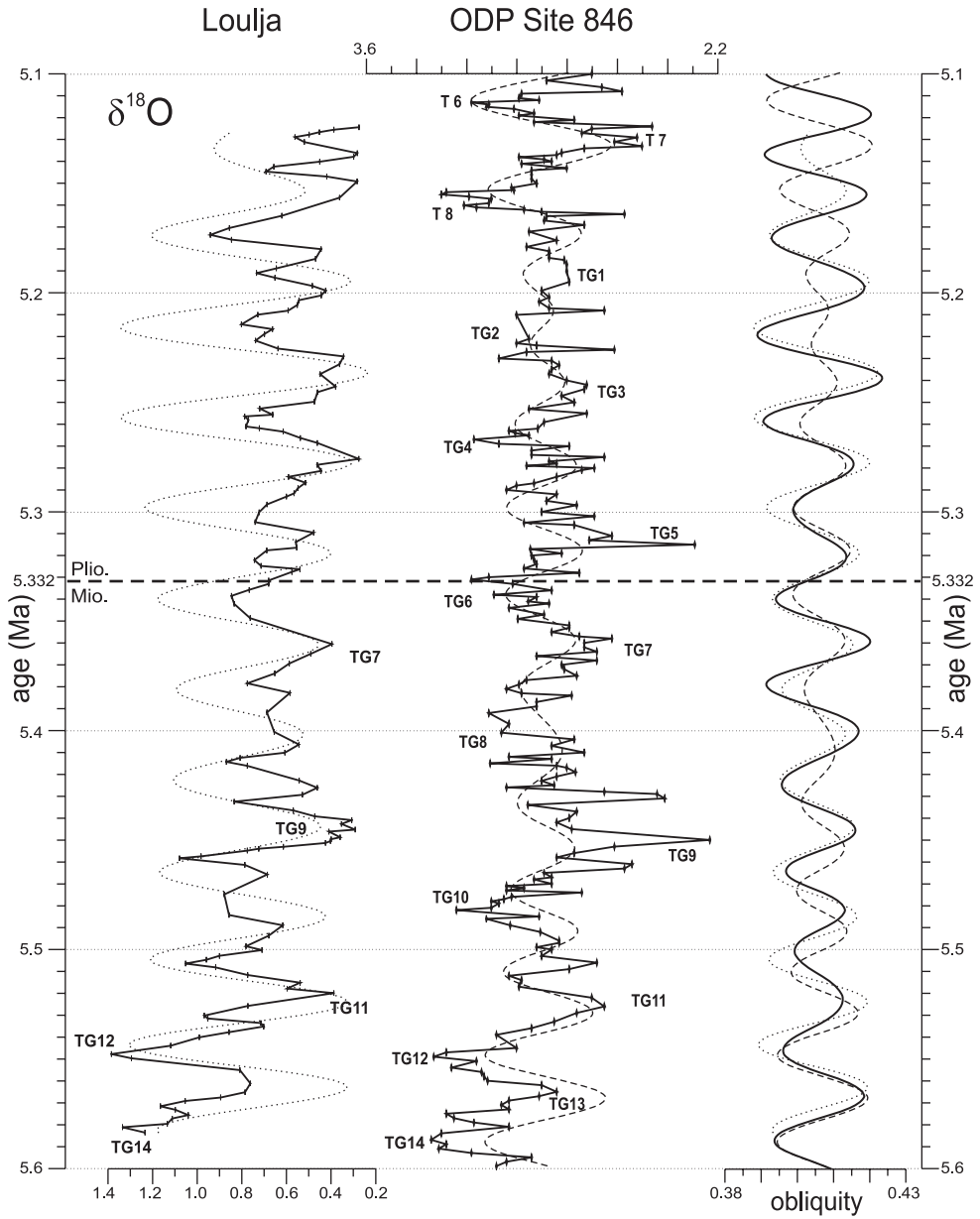


Figure 5.9. Comparison between the Loulja-A and ODP Site 846  $\delta^{18}\text{O}$  records in the time domain. For Site 846 the manually revised age model of Shackleton et al. (1999) was used to construct the proxy time series. The 41-kyr components are shown as overlays and were extracted using Gaussian band-pass filters with central frequencies of 0.0245 and a band width of 0.012 cycles/kyr. Indicated TG-stages for Site 846 are from Shackleton et al. (1995b).



patterns include the marked shift to lighter values between TG3 and TG2 and the “glacial”  $\delta^{13}\text{C}$  signature of TG4 and TG6. Ideally, one would prefer to check the implications of the revised tuning up to the prominent glacial stages Si4 and Si6. However, this exercise is less straightforward and falls outside the scope of the present study, which aimed to unravel the influence of glacio-eustatic sea level change on the Pliocene flooding of the Mediterranean and the beginning of the Upper Evaporites.

Finally, the correlations between Loulja-A and Salé based on the stable isotope patterns are in agreement with the occurrence of a peak interval in magnetic susceptibility observed at both localities (Fig. 5.12). However, the relatively low sample resolution at Salé hampers a more detailed correlation of both susceptibility records.

### 5.8.2 Absolute isotope values

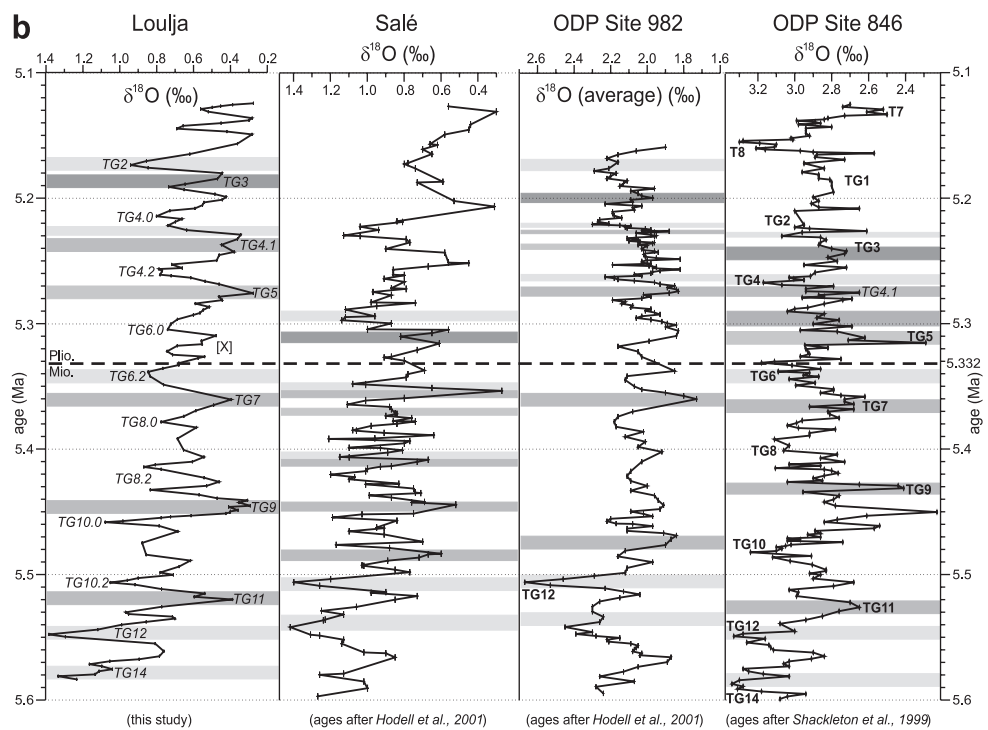
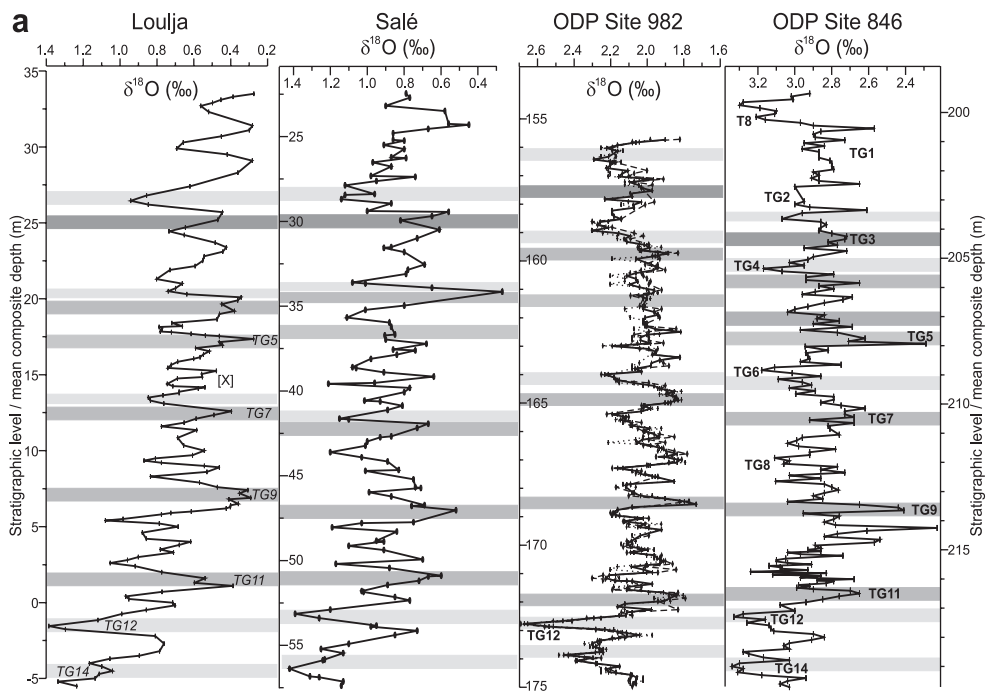
Although the isotope records discussed above correlate in considerable detail, they differ in absolute values. The absolute values of the oxygen isotopes are very similar for the Loulja and Salé sections, but are different for Sites 982 and 846. A shallower depth and higher bottom water temperatures at the Moroccan sites can explain this. Nevertheless, the overprint of the dominantly obliquity-controlled global ice volume signal is clearly reflected in all records and was used to correlate them in detail. The precession-related variations at Loulja most likely reflect a combination of a local temperature and/or salinity signal associated with the sedimentary colour cycles and a global ice volume signal. Indications for the presence of a precession-related component in global ice volume change during the latest Miocene previously came from comparing the slightly older record from Ain el Beida with records from the open ocean (Van der Laan et al., 2005).

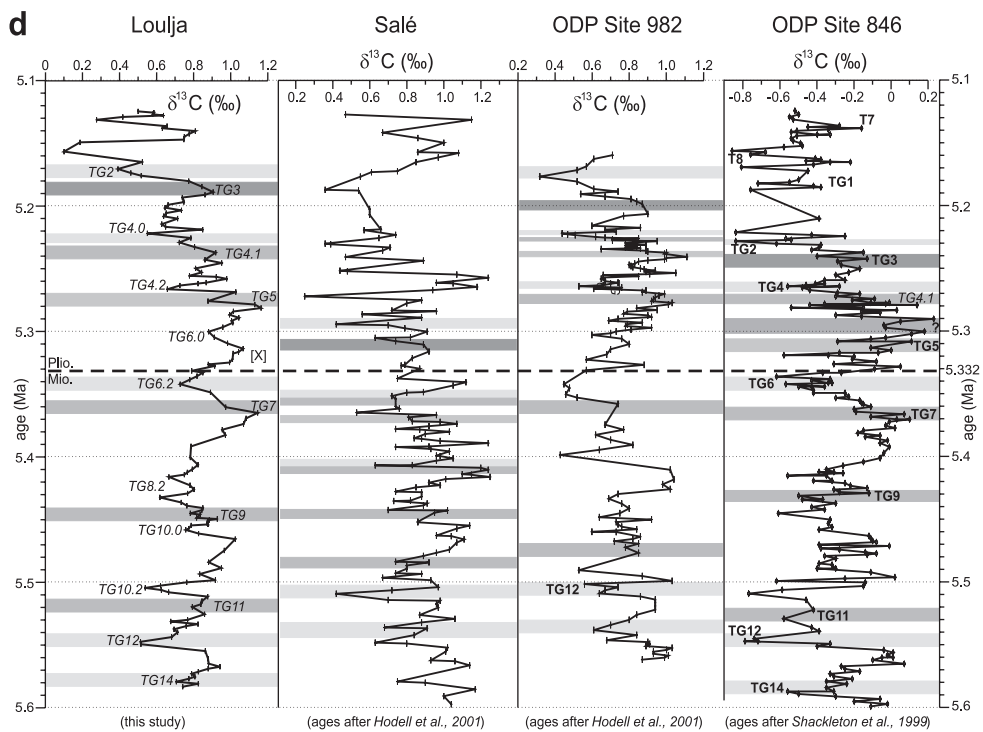
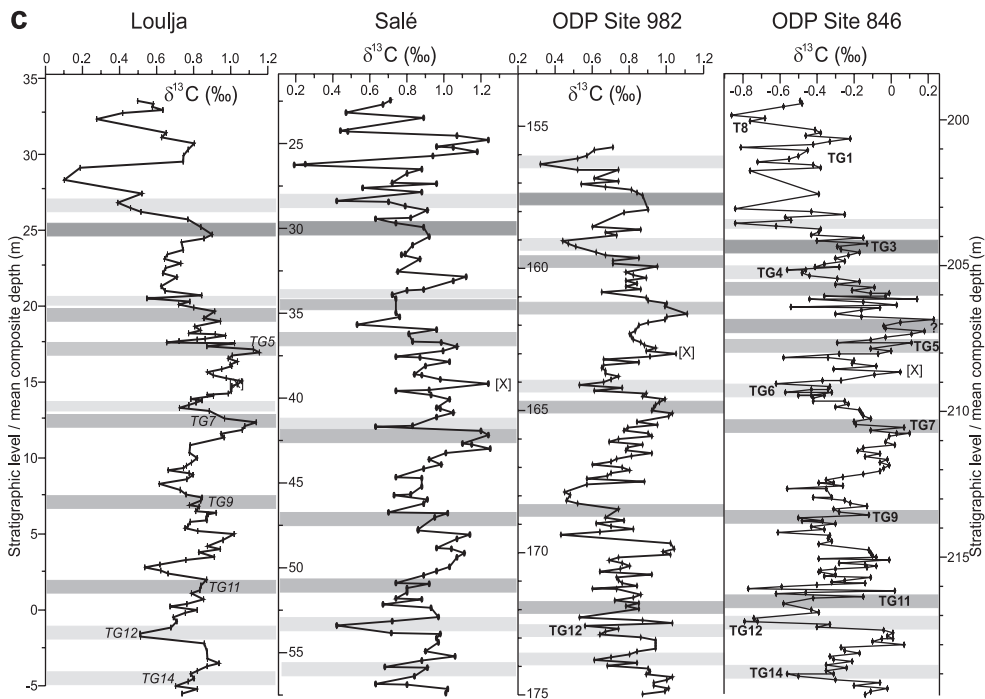
The absolute carbon isotope values are very similar for Loulja, Salé, and ODP Site 982 but the values at Site 846 are considerably lower. This difference can best be explained by  $\delta^{13}\text{C}$  aging of Pacific deep water (see, e.g., Ruddiman, 2001). However, the overall pattern of all records is quite similar suggesting that whole-ocean processes (e.g., terrestrial-marine carbon transfer) control it.

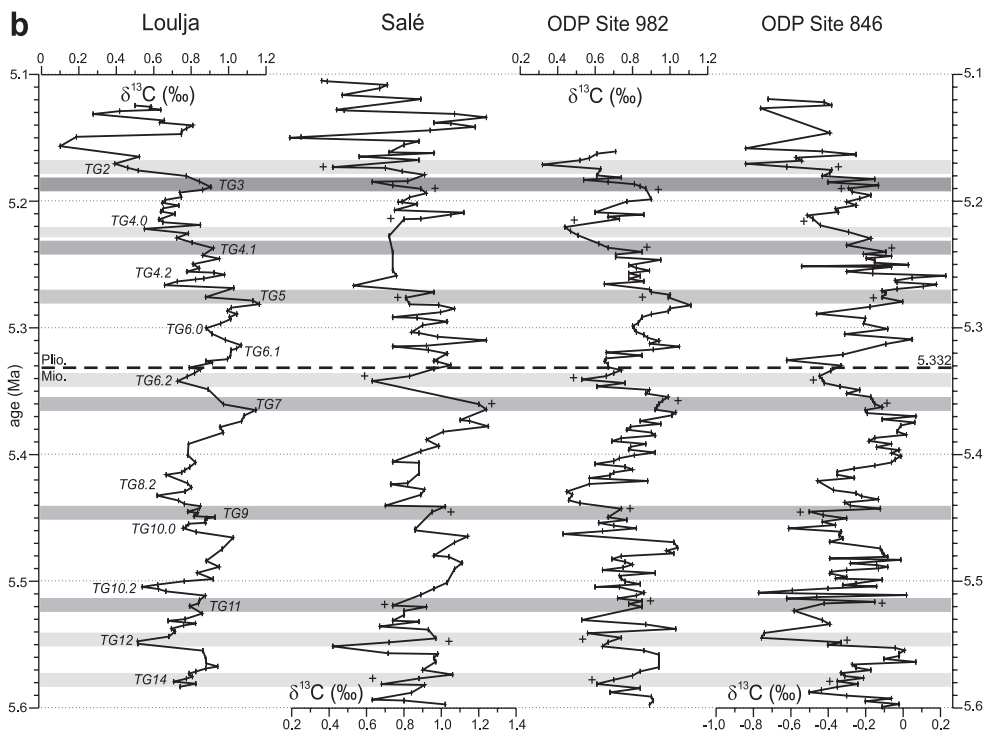
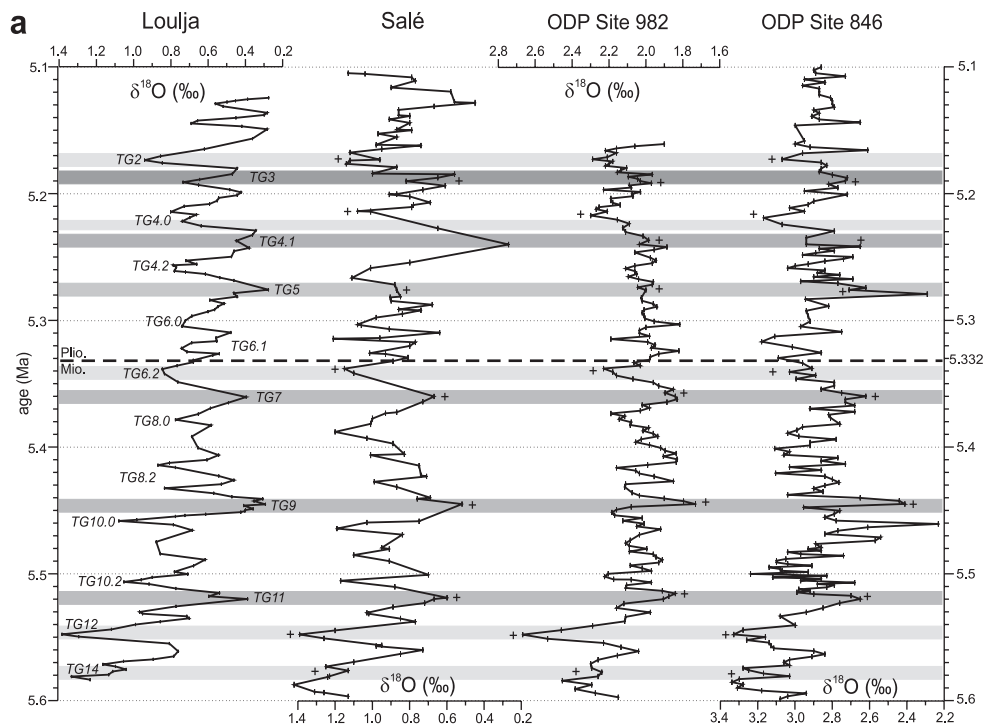
### 5.8.3 Miocene-Pliocene boundary

Irrespective whether the low-amplitude  $\delta^{18}\text{O}$  minimum at 5.315 Ma in the Loulja-A record corresponds to TG5, it is clear that the M-P boundary coincides with the very beginning of a minor shift to lighter values that, as far as the obliquity component is concerned, leads to the low-amplitude  $\delta^{18}\text{O}$  minimum at 5.315 Ma. This transition (“deglaciation”) is interrupted by a precession-controlled shift to heavier values in  $\delta^{18}\text{O}$  but it is unclear whether this precession component is also present in the  $\delta^{18}\text{O}$  records from the open ocean. Such a presence may suggest

*Figure 5.10.* (see next page) Comparison in the depth domain and time domain between the (a-b)  $\delta^{18}\text{O}$  and (c-d)  $\delta^{13}\text{C}$  records of Loulja-A, Salé, and ODP Sites 846 and 982. Light grey bands mark correlations based on glacial stages; dark grey bands indicate correlations based on interglacial stages. Correlations are based on characteristic patterns in either  $\delta^{18}\text{O}$  or  $\delta^{13}\text{C}$  in the depth domain. The original stages defined by Shackleton et al. (1995b) are denoted in boldface next to the Site 846 record. Stages in boldface next to the record of Site 982 denote stage designations of Hodell et al. (2001), while stages in italics denote stage designations that result from our correlations. Question mark in the dark grey band in the Site 846  $\delta^{13}\text{C}$  record indicates alternative option for TG5 based on the correlation with maximum  $\delta^{13}\text{C}$  values from other records. The Salé record of Hodell et al. (1994) was redated by Hodell et al. (2001) using the same tuned age model as developed for ODP Site 982, which is based on the La90(1,1) solution. The original age model for ODP Site 846 (Shackleton et al., 1995b) is based on the Be91 solution and was revised by Shackleton et al. (1999) using the La93(1,1) solution.







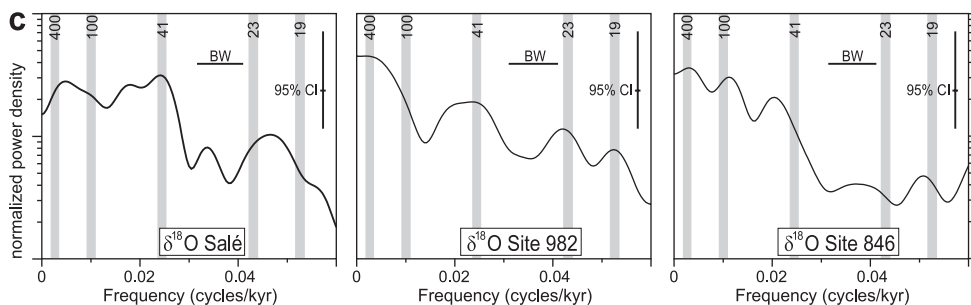


Figure 5.11. Comparison between the (a)  $\delta^{18}\text{O}$  and (b)  $\delta^{13}\text{C}$  time series of Loulja-A, Salé, and ODP Sites 846 and 982 after adopting revised age models based on control points (indicated by crosses) from Loulja-A. c) Resulting power spectra for  $\delta^{18}\text{O}$ ; note the relatively strong power in the (23-19 kyr) precession band. In each spectral panel the horizontal bar denotes the band width (BW) that is 0.0093 for Salé, 0.0101 for Site 982, and 0.0097 for Site 846. Vertical bar denotes the 95% confidence interval (CI).

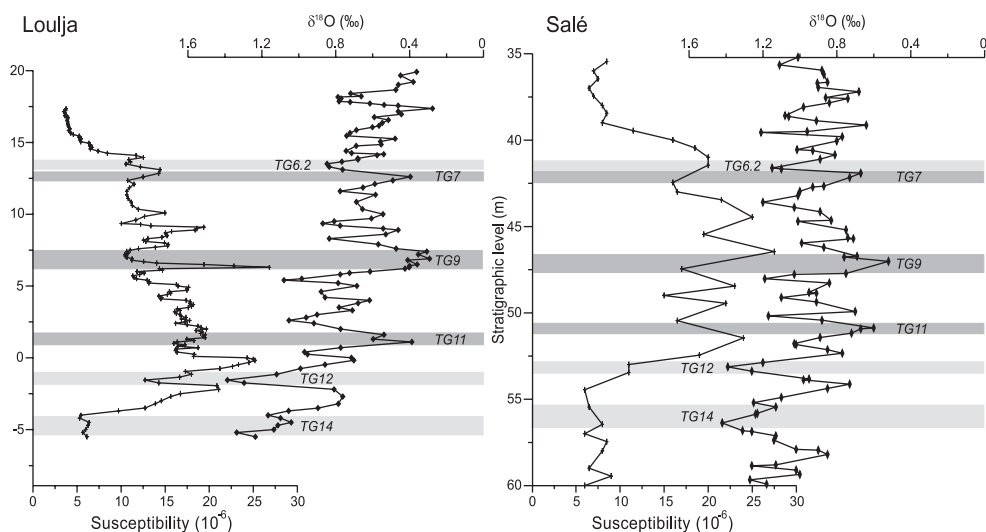


Figure 5.12. Comparison between the magnetic susceptibility of dehydrated samples (note difference from Figure 5.2) and benthic  $\delta^{18}\text{O}$  records from Loulja-A (partial section III) and from Salé (data from Hodell et al., 1994).

a precession component in the glacial cyclicity, i.e. similar to the precession signal between TG14 and TG9 and for instance between TG32 and TG28 (i.e., TG30) and between C3An.18O.14 (codification of Hodell et al., 1994) and C3An.18O.10 (i.e., 12) at Ain el Beida (Van der Laan et al., 2005). On the other hand, at Loulja-A, it can also easily be related to the dominantly precession-controlled regional climate oscillations that underlie the colour and PC-1 cyclicity.

Close inspection of the isotope record of Site 846 in fact indicates that the M-P boundary coincides with an extra obliquity-controlled and very weak interglacial between TG7 and TG5 and that TG5 represents an interglacial stage some 50 kyr younger than the M-P boundary (see paragraph 5.8.1; Figs. 5.10 and 5.11; Table 5.3). Comparison with our record further suggests that the actual Site 846 peak  $\delta^{18}\text{O}$  values reached in TG5 may represent outliers because such

exceptionally light values are found neither in our record nor in other records spanning the boundary (Hodell et al., 1994, 2001).

All this indicates that glacio-eustatic sea level rise (deglaciation) played only a minor role, if at all, in the basal Pliocene flooding of the Mediterranean. Probably, factors that are more important were extensional tectonics and/or ongoing headward erosion of an initially restricted connection between the Atlantic and Mediterranean. The latter situation may already have played a role during deposition of the Upper Evaporites in the Mediterranean with Atlantic waters intermittently entering the Mediterranean, thereby increasing seawater salinities.

The M-P boundary is formally defined at the base of the deep marine Trubi marls overlying the Upper Evaporites and Arenazzolo Formation of the Messinian at Eraclea Minoa (Van Couvering et al., 2000). This level marks the onset of open marine conditions in the Mediterranean following the Messinian salinity crisis (Hsü et al., 1973; Cita, 1975; Hilgen and Langereis, 1993; Iaccarino et al., 1999). This level was selected mainly for historical reasons but the possibly unconformable nature of the formation boundary in combination with the abrupt transition from nonmarine to fully marine conditions makes it in principle less suitable. Suc et al. (1997), recognizing the problem of the possible unconformable character of the contact, proposed to define the M-P boundary near Salé, some 5 km northwest of Ain el Beida, at the stratigraphic level that corresponds with the base of oxygen isotope stage TG5. The isotope shift was supposed to correspond with the base of the Trubi reflecting the marked deglaciation held responsible for the Pliocene flooding of the Mediterranean at that time. The proposal was considered less favourable because the level was only indicated in the Salé drill core but not in any existing outcrop.

Our results show that the M-P boundary is positioned at 13.90 m in the middle of LA<sub>R</sub>-11 in section Loulja-A in an open marine succession located just outside the Mediterranean. Hence it might be preferable to designate Loulja-A as an auxiliary stratotype section for the M-P boundary. Our results also indicate however that the boundary does not coincide with TG5.

#### 5.8.4 Upper Evaporites

The stepwise shift to lighter values between TG12 and TG9 marks a more dramatic deglaciation than TG5 (e.g., Shackleton et al., 1995b). An important implication of the revised age model of Shackleton et al. (1999) is that the onset of the Upper Evaporites (UE) following the main desiccation phase of the Mediterranean is linked to the glacio-eustatic sea level rise associated with the deglaciation manifested in particular by the TG12 to TG11 transition. The number of 7/8 sedimentary cycles observed in the UE and correlative units throughout the Mediterranean (Vai, 1997; Krijgsman et al., 2001; Fortuin and Krijgsman, 2003) is consistent with such a scenario in case these cycles are precession-controlled (Fig. 5.13). Alternative options start from an obliquity control for the UE cyclicity (Vai, 1997); this interpretation is inconsistent with linking the beginning of the UE to the TG12 to TG9 deglaciation. It further is not in agreement with a precession control for the evaporite cycles of the Lower Evaporites (LE) although the distinction between a precession or obliquity control on the UE cyclicity becomes problematical in view of the hiatus of ~100 kyr inferred between the LE and UE according to the precession scenario (Krijgsman et al., 1999, 2001).

There are indications in the literature that the Mediterranean was not fully isolated from the world ocean during deposition of the UE but that marine incursions may have occurred. The gypsum cycles of the UE in the Eraclea Minoa section (Caltanissetta Basin, Sicily) display a facies evolution from fine-grained laminar gypsum at the base of each cycle to selenites at the top, accompanied by increasing strontium values indicating increasing salinity conditions (Rosell

et al., 1998). Partly backed-up by these data, Schreiber (1997) claimed a distinctly marine origin of the gypsum in this section alternating with non-marine beds and concludes that a connection with the open ocean existed throughout the MSC. In addition, Londeix (2004) interpreted the intercalated clays of Eraclea Minoa with dinocyst assemblages to be indicative of a shallow marine environment with occasionally hypersaline conditions and river influxes. However, according to Taberner et al. (2004) previous interpretations of the geochemical and biological markers from the Eraclea Minoa UE, supposedly indicative of a marine contribution, need reconsideration. Recycling of older Messinian evaporites may offer an alternative explanation for the observed isotopic composition of the sulphates. Nevertheless, Flecker et al. (2002) argued that neither the observed Sr isotopic offsets from ocean values nor the high salinities during evaporite precipitation require total isolation of the Mediterranean from the world ocean.

Also Clauzon et al. (1996) considered marginal basins (including Eraclea Minoa) in the Mediterranean to have received Atlantic waters during deposition of the LE and UE, although their age model differs from the age model we prefer. From the uppermost Messinian of the Nijar Basin in SE Spain, Fortuin and Krijgsman (2003) reported marine microfaunas and suggested that short-lived connections with the Atlantic Ocean could have existed during periods of high sea level although reworking could not be excluded. Aguirre and Sánchez-Almazo (2004) are much more explicit by stating that the planktonic foraminiferal faunas from the Messinian post-evaporitic beds in the Nijar Basin are not reworked but represent *in situ* faunas. The latter would imply that open marine conditions already existed in the western Mediterranean area during the latest Messinian. Nevertheless, the arguments put forward by Aguirre and Sánchez-Almazo (2004) concerning the sometimes excellent preservation and the absence of reworked older faunas do by no means exclude reworking. Even on Cyprus, Rouchy et al. (2001) claim to have found authentic marine faunas in the local equivalent of the UE/Lago Mare, indicative of the persistence of marine influences. Müller (1990) mentioned that assemblages of low diversity and smaller sized calcareous nannofossils and planktonic foraminifera are found in the uppermost Messinian of the Tyrrhenian Sea, while Castradori (1998) observed anomalous nannofossil assemblages in the same interval in the Alboran, Balearic, and Levantine basins. From the latter basin and from the Mediterranean Ridge south of Crete, Spezzaferri et al. (1998) ascribed the presence of beds with planktonic foraminifera to an Atlantic origin, a conclusion that was shared, although with more caution, by Iaccarino and Bossio (1999) for sediments of the uppermost Messinian in the Balearic Basin. Iaccarino et al. (1999) stated that periodic spill-overs into the (western) Mediterranean occurred at the end of the Messinian, related to eustatic sea level changes.

The latter would favour an obliquity control because of the dominant obliquity forcing of glacial cyclicity and hence glacio-eustatic sea level change during the latest Miocene and Pliocene. Nevertheless, it is evident that the benthic isotope records reveal a well-defined precession signal in addition to obliquity in this interval, suggesting that precession exerted an additional control on glacial cyclicity and sea level in the interval between TG12 and TG5, i.e., the time that the UE were formed according to our preferred precession scenario. However, the precession control may also stem from precession-induced changes in regional climate. Such changes are also held responsible for the formation of gypsum cycles in the LE, i.e., between 5.96 and 5.59 Ma when obliquity-induced glacial cycles and associated sea level changes were operative as well (Krijgsman et al., 1999).

Finally, it is remarkable that the Upper Evaporites according to the preferred precession scenario correspond exactly with the interval marked by peak magnetic susceptibility values in the Loulja-A section and the Salé drill core (Fig. 5.12). In addition, this peak interval corresponds

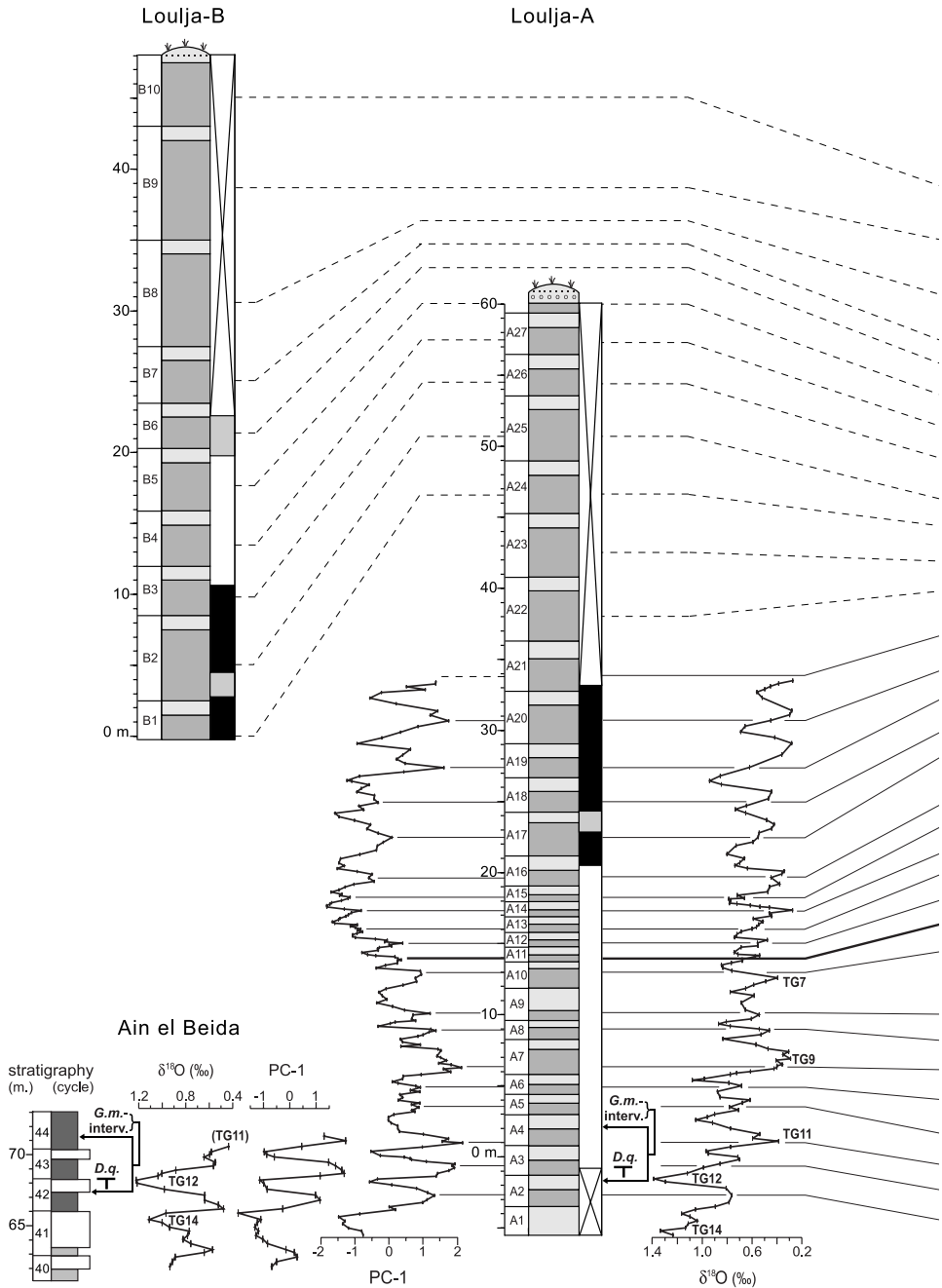
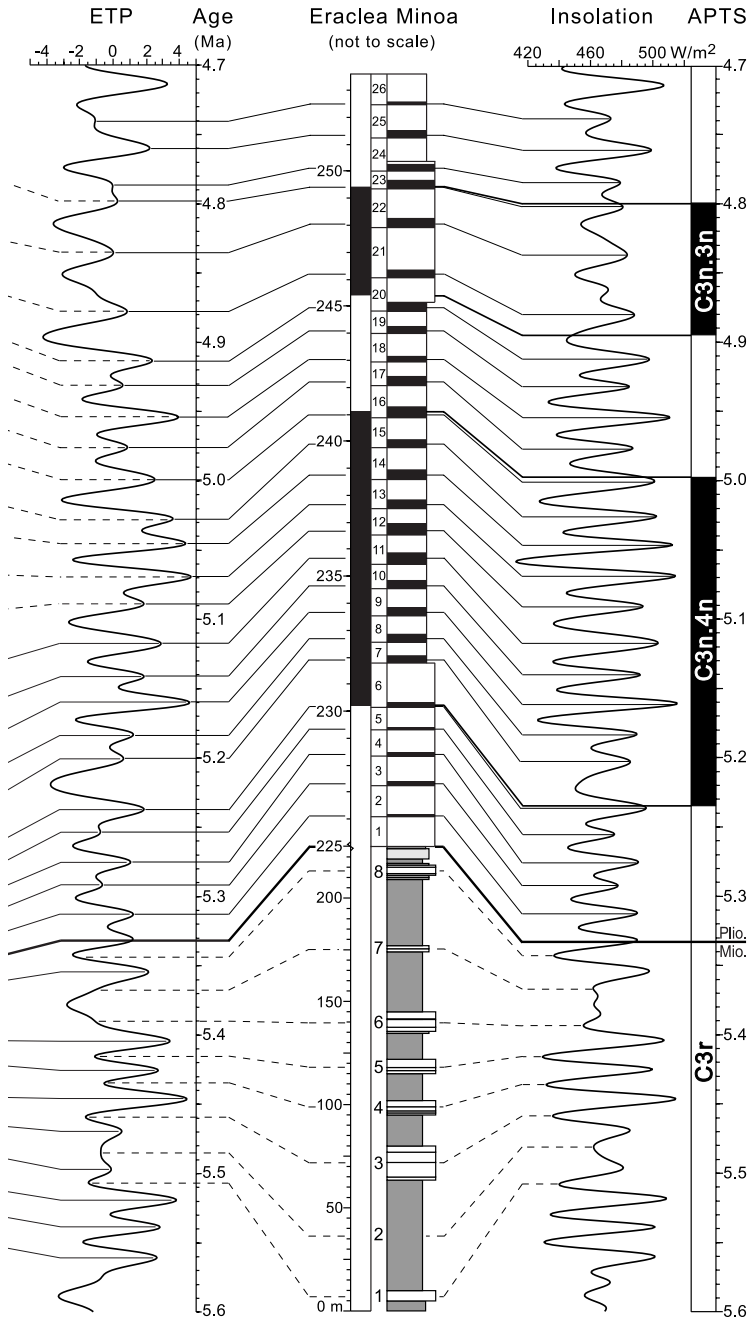


Figure 5.13. Cyclostratigraphic correlations of the Loulja-A and Loulja-B sections (for key, see caption to Figure 5.2) to the Upper Evaporites and Trubi marls in the Eraclea Minoa section on Sicily, Italy (note scale change at the Miocene-Pliocene boundary). Eraclea Minoa tuning is partly based on the work of Lourens et al. (1996). Correlations of the PC-1 and  $\delta^{18}\text{O}$  records between the basal part of Loulja-A and the uppermost part of Ain el





Beida (Krijgsman et al., 2004; Van der Laan et al., 2005; E. Van der Laan, unpublished data, 2003) are also shown. Isotope stages are numbered following the codification scheme of Shackleton et al. (1995b); see caption to Figure 5.9 for further explanation.

to the 400-kyr eccentricity maximum around 5.45 Ma. The latter might explain our peak interval because magnetic susceptibility maxima are reached in reddish layers (Fig. 5.2) and the most prominent reddish layers are associated with enhanced precession amplitudes related to maximum eccentricity. Such an explanation does hold for the elemental data of PC-1, which clearly mimic the eccentricity modulation of the precession amplitude (see paragraph 5.7.1 and Figure 5.5). However, in contrast to PC-1, magnetic susceptibility values remain low in sections Loulja-A and Loulja-B, i.e., during the next 400-kyr eccentricity maximum. Furthermore it does not explain why the marked decrease in magnetic susceptibility (Fig. 5.2) does not follow the precession/eccentricity pattern but coincides with the Miocene-Pliocene boundary and thus with the top of the Upper Evaporites and the Pliocene flooding of the Mediterranean. At present, a sound explanation for this apparent linkage between the magnetic susceptibility peak interval and the Upper Evaporites is lacking.

### 5.8.5 Deglaciation interval

Also the biostratigraphic record of *Globorotalia miotumida*/*Globorotalia menardii* has some bearing on (the termination of) the late Messinian interval marked by the occurrence of distinct glacials. The warm-water species *G. menardii* and *Neogloboquadrina humerosa* represent subtropical faunal elements, which occur together with species typical of the eastern boundary current fauna association. Remarkably enough, the short interval with *G. menardii* corresponds exactly with the major shift in  $d^{18}O$  to lighter values between oxygen isotope stages TG12 and TG11 that marks the end of the characteristic interval with prominent obliquity-controlled glacial cycles of the late Messinian. The short distribution range of this warm water species is consistent with the deglaciation step inferred from the isotope data. This deglaciation step coincides with the increase in eccentricity following the distinct eccentricity minimum around 5.6 Ma. Stage TG10 corresponds with the next (100 kyr) eccentricity minimum around 5.48 Ma and the (second) deglaciation step from TG10 to TG9 with the subsequent increase in eccentricity just prior to 5.45 Ma. This coincidence suggests that eccentricity may have played a role in terminating the series of prominent glacial cycles in the late Messinian.

### 5.8.6 Glacial cycles and regional climate oscillations

At Loulja-A the PC-1 and sedimentary cycle records show a dominant precession-related signal, which suggests a regional low-latitude climate origin for these variations (Van der Laan et al., 2005). The 23-kyr component in  $\delta^{13}C$  is rather weak and is only present in intervals when enhanced precession amplitudes are reached at times of eccentricity maxima. This 23-kyr signal is essentially in phase with precession, with minima in  $\delta^{13}C$  corresponding to maxima in precession (see also Figure 5.8). The 23-kyr signal in  $\delta^{13}C$  may be explained by enhanced surface water productivity, but a planktonic isotope record is needed to support this interpretation. The enhanced productivity might be a consequence of better vertical mixing of the water column due to colder and hence denser surface waters during summer at times of precession maxima. In addition, precession-induced changes in wind-stress and hence upwelling may have played a role. Alternatively, it may signal variations in the storage of carbon between the terrestrial and marine domain on precession time scales, although obliquity- and eccentricity-related variations in  $\delta^{13}C$  seem to be more important here.

Cross-spectral analysis in addition revealed a weak 41-kyr component in PC-1 that is significantly coherent and essentially in phase with obliquity. This obliquity signal, which was also observed in the older Oued Akrech section (F.J. Hilgen, unpublished data, 2000), most likely

reflects a direct response of regional climate to obliquity as suggested by Mediterranean sapropel patterns (Hilgen et al., 2000). Contrary to expectation, no significant lag is observed between the obliquity component in  $\delta^{18}\text{O}$  and PC-1, despite the fact that the 41-kyr component in  $\delta^{18}\text{O}$  is much stronger than in PC-1 and supposedly reflects glacial cyclicity in addition to regional climate change. Consequently, no distinction can be made between an early response group and a (glacial controlled) late response group reflecting ice volume and related ice sheet response (compare Imbrie et al., 1992). Similarly, the identical and in-phase relation between the 23-kyr components in PC-1,  $\delta^{18}\text{O}$ , and precession does not rule out a precession-induced ice volume signal in  $\delta^{18}\text{O}$ . The latter is actually suggested by the precession signal found in benthic  $\delta^{18}\text{O}$  records from the open ocean (Fig. 5.11c).

Although a separate 41-kyr peak is lacking in the  $\delta^{13}\text{C}$  spectrum, an inverse covariance with  $\delta^{18}\text{O}$  is clearly recognized in the interval older than  $\sim 5.3$  Ma. This inverse correlation is confirmed by the in-phase relationship between the 41-kyr  $\delta^{13}\text{C}$  filter and obliquity up to at least 5.22 Ma (see paragraph 5.7.4). It is furthermore interpreted as to mainly reflect glacial-interglacial cycles: during glacials (enriched  $\delta^{18}\text{O}$  values), overall lighter  $\delta^{13}\text{C}$  values are recorded in the marine realm due to increased storage of  $^{13}\text{C}$ -depleted terrestrial-derived carbon in oceanic reservoirs (Shackleton, 1977; Ruddiman, 2001). Alternatively, enhanced productivity linked to a strengthening in wind regimes inferred for glacial periods, causing better vertical mixing through the water column, could have caused the lighter  $\delta^{13}\text{C}$  values. However, after TG9 ( $\sim 5.45$  Ma), obliquity-induced changes in  $\delta^{13}\text{C}$  become less distinct and longer-term variations with a period of  $\sim 100$  kyr start to dominate. The  $\sim 100$ -kyr band-pass filter reveals an in-phase relationship with short-term eccentricity whereby  $\delta^{13}\text{C}$  minima coincide with eccentricity maxima (see Figure 5.8). Only the interval of relatively depleted  $\delta^{13}\text{C}$  values between 5.23 and 5.18 Ma causes the  $\sim 100$ -kyr  $\delta^{13}\text{C}$  filter to slightly run out of phase with eccentricity.

## 5.9 Conclusions

The Loulja-A section contains a well-tuned, continuous open marine succession straddling the M-P boundary in the Bou Regreg area that can be correlated cyclostratigraphically in detail to the Mediterranean. In addition, the section provides a detailed history of glacial cyclicity through its high-resolution and high-quality benthic oxygen isotope record.

The M-P boundary does not coincide with a major deglaciation as previously assumed but with the beginning of a relatively minor shift to lighter values in  $\delta^{18}\text{O}$ . This shift does not coincide with marine isotope stage TG5 but actually corresponds to an extra (weak) obliquity-controlled cycle in between TG7 and TG5. On the other hand, the onset of the Upper Evaporites in the Mediterranean marked by hyposaline conditions coincides with the major deglaciation step between TG12 and TG11, suggesting that the associated sea level rise might at least be partly responsible for the onset of possibly (marginally) marine conditions following the main desiccation phase.

The section is perfectly suitable to act as auxiliary-boundary stratotype for the M-P boundary as formally defined at the base of the deep marine Trubi marls in the Eraclea Minoa section on Sicily, i.e., at the level that marks the definitive opening of the Atlantic-Mediterranean connection and the basal Pliocene flooding of the Mediterranean following the Messinian salinity crisis.

## Acknowledgements

Nadia Barhoun from Université Hassan II Mohammedia, Casablanca, and Helmut Willems and Katarzyna Bison from Bremen University are kindly thanked for discussions and their invaluable assistance in the field. Mohamed Dahmani and Mohamed Haddane of the Geology Division of the Ministry of Energy and Mines at Rabat are kindly acknowledged for their cooperation and permission to carry out the fieldwork in Morocco. The manuscript benefited from Cor Langereis' critical review of the paleomagnetic part. We are grateful to David Hodell and an anonymous reviewer for their valuable comments and suggestions, which greatly improved an earlier version of the manuscript. Geert Ittmann and Gerrit van 't Veld are thanked for washing the samples, Arnold van Dijk for the isotope analyses, and Helen de Waard for the ICP-OES measurements. Douwe van Hinsbergen generously provided the paleobathymetric data.

This work was conducted under the programme of the Netherlands Research School of Sedimentary Geology (NSG) and the Vening Meinesz Research School of Geodynamics (VMSG). The Netherlands Research Centre for Integrated Solid Earth Science (ISES) provided funds for sampling campaigns.

## References

- Aguirre, J., Sánchez-Almazo, I.M., 2004. The Messinian post-evaporitic deposits of the Gafares area (Almeria-Nijar basin, SE Spain). A new view of the "Lago-Mare" facies. *Sedimentary Geology* 168, 71-95. doi:10.1016/j.sedgeo.2004.03.004.
- Backman, J., Raffi, I., 1997. Calibration of Miocene nannofossil events to orbitally-tuned cyclostratigraphies from Ceara Rise. *Proceedings of the Ocean Drilling Program, Scientific Results* 154, 83-100. doi:10.2973/odp.proc.sr.154.101.1997.
- Benson, R.H., Rakic-El Bied, K., 1996. The Bou Regreg section, Morocco: Proposed Global Boundary Stratotype Section and Point of the Pliocene. *Notes et Mémoires du Service Géologique du Maroc* 383, 51-150.
- Benson, R.H., Rakic-El Bied, K., Bonaduce, G., 1991. An important current reversal (influx) in the Rifian corridor (Morocco) at the Tortonian-Messinian boundary: the end of Tethys Ocean. *Paleoceanography* 6, 165-192. doi:10.1029/90PA00756.
- Benson, R.H., Hayek, L.A.C., Hodell, D.A., Rakic-El Bied, K., 1995. Extending the climatic precession curve back into the late Miocene by signature template comparison. *Paleoceanography* 10 (1), 5-20. doi:10.1029/94PA02539.
- Bramlette, M.N., Sullivan, F.R., 1961. Coccolithophoreids and related nanoplankton of the early Tertiary in California. *Micropaleontology* 7(2), 129-188.
- Castradori, D., 1998. Calcareous nannofossils in the basal Zanclean of the Eastern Mediterranean Sea: remarks on paleoceanography and sapropel formation. *Proceedings of the Ocean Drilling Program, Scientific Results* 160, 113-124. doi:10.2973/odp.proc.sr.160.005.1998.
- Cita, M.B., 1975. The Miocene-Pliocene boundary: History and definition. In: Saito, T., Burckle, L. (Eds.), *Late Neogene Epoch Boundaries*, *Micropaleontology, Spec. 1*, pp. 1-30.
- Clauzon, G., Suc, J.P., Gautier, F., Berger, A., Loutre, M.F., 1996. Alternate interpretation of the Messinian salinity crisis: Controversy resolved? *Geology* 24, 363-366. doi:10.1130/0091-7613(1996)024<0363: AIOTMS>2.3.CO;2.

- Di Stefano, E., Sprovieri, R., Scarantino, S., 1996. Chronology of biostratigraphic events at the base of the Pliocene. *Palaeopelagos* 6, 401-414.
- Driever, B.W.M., 1988. Calcareous nannofossil biostratigraphy and paleoenvironmental interpretation of the Mediterranean Pliocene. *Utrecht Micropaleontological Bulletins* 36, pp. 1-248.
- Flecker, R., De Villiers, S., Ellam, R.M., 2002. Modelling the effect of evaporation on the salinity-<sup>87</sup>Sr/<sup>86</sup>Sr relationship in modern and ancient marginal-marine systems: the Mediterranean Messinian Salinity Crisis. *Earth and Planetary Science Letters* 203, 221-233. doi:10.1016/S0012-821X(02)00848-8.
- Fortuin, A.R., Krijgsman, W., 2003. The Messinian of the Nijar Basin (SE Spain): sedimentation, depositional environments and paleogeographic evolution. *Sedimentary Geology* 160, 213-242. doi:10.1016/S0037-0738(02)00377-9.
- Hilgen, F.J., 1991. Extension of the astronomically calibrated (polarity) time scale to the Miocene-Pliocene boundary. *Earth and Planetary Science Letters* 107, 349-368. doi:10.1016/0012-821X(91)90082-S.
- Hilgen, F.J., Langereis, C.G., 1993. A critical evaluation of the Miocene/Pliocene boundary as defined in the Mediterranean. *Earth and Planetary Science Letters* 118, 167-179. doi:10.1016/0012-821X(93)90166-7.
- Hilgen, F.J., Bissoli, L., Iaccarino, S.M., Krijgsman, W., Negri, A., Villa, G., 2000 Integrated stratigraphy and astrochronology of the Messinian GSSP at Oued Akrech (atlantic Morocco). *Earth and Planetary Science Letters* 182, 237-251. doi:10.1016/0012-821X(91)90082-S.
- Hodell, D.A., Benson, R.H., Kennett, J.P., Rakic-El Bied, K., 1989. Stable isotope stratigraphy of latest Miocene sequences in northwest Morocco: the Bou Regreg section. *Paleoceanography* 4, 467-482. doi:10.1029/89PA00550.
- Hodell, D.A., Benson, R.H., Kent, D.V., Boersma, A., Rakic-El Bied, K., 1994. Magnetostratigraphic, biostratigraphic, and stable isotope stratigraphy of an Upper Miocene drill core from the Salé Briqueterie (northwest Morocco): A high-resolution chronology for the Messinian stage. *Paleoceanography* 9, 835-855. doi:10.1029/94PA01838.
- Hodell, D.A., Curtis, J.H., Sierro, F.J., Raymo, M.E., 2001. Correlation of late Miocene to early Pliocene sequences between the Mediterranean and North Atlantic. *Paleoceanography* 16, 164-178. doi:10.1029/1999PA000487.
- Hrouda, F., 1994. A technique for the measurement of thermal changes of magnetic susceptibility of weakly magnetic rocks by the CS-2 apparatus and KLY-2 Kappabridge. *Geophysical Journal International* 118 (3), 604-612. doi:10.1111/j.1365-246X.1994.tb03987.x.
- Hsü, K.J., Cita, M.B., Ryan, W.B.F., 1973. The origin of the Mediterranean evaporites. *Initial Reports of the Deep Sea Drilling Project* 42, 1203-1231. doi:10.2973/dsdp.proc.13.143.1973.
- Iaccarino, S.M., Bossio, A., 1999. Paleoenvironment of uppermost Messinian sequences in the Western Mediterranean (Sites 974, 975, and 978). *Proceedings of the Ocean Drilling Program, Scientific Results* 161, 529-541. doi:10.2973/odp.proc.sr.161.246.1999.
- Iaccarino, S.M., Castradori, D., Cita, M.B., Di Stefano, E., Gaboardi, S., McKenzie, J.A., Spezzaferri, S., Sprovieri, R., 1999. The Miocene-Pliocene boundary and the significance of the earliest Pliocene flooding in the Mediterranean. *Memorie della Societa Geologica Italiana* 54, 109-131.
- Imbrie, J., Hays, J.D., Martinson, D.G., McIntyre, A., Mix, A.C., Morley, J.J., Pisias, N.G., Prell, W.L., Shackleton, N.J., 1984. The orbital theory of Pleistocene climate: Support from a

- revised chronology of the marine  $\delta^{18}\text{O}$  record. In: Berger, A., Imbrie, J., Hays, J.D., Kukla, G., Saltzman, B. (Eds.), *Milankovitch and Climate*, NATO ASI Series 126, pp. 269-305.
- Imbrie, J., Boyle, E.A., Clemens, S.C., Duffy, A., Howard, W.R., Kukla, G., Kutzbach, J., Martinson, D.G., McIntyre, A., Mix, A.C., Molino, B., Morley, J.J., Peterson, L.C., Pisias, N.G., Prell, W.L., Raymo, M.E., Shackleton, N.J., Toggweiler, J.R., 1992. On the structure and origin of major glaciation cycles. 1. Linear responses to Milankovitch forcing. *Paleoceanography* 7, 701-738. doi:10.1029/92PA02253.
- Krijgsman, W., Hilgen, F.J., Raffi, I., Sierro, F.J., Wilson, D.S., 1999. Chronology, causes and progression of the Messinian salinity crisis. *Nature* 400, 652-655. doi:10.1038/23231.
- Krijgsman, W., Fortuin, A.R., Hilgen, F.J., Roep, Th.B., Sierro, F.J., 2001. Astrochronology for the Messinian Sorbas Basin (SE Spain) and orbital (precessional) forcing for evaporite cyclicity. *Sedimentary Geology* 140, 43-60. doi:10.1016/S0037-0738(00)00171-8.
- Krijgsman, W., Gaboardi, S., Hilgen, F.J., Iaccarino, S.M., De Kaenel, E., Van der Laan, E., 2004. Revised astrochronology for the Ain el Beida section (Atlantic Morocco): No glacio-eustatic control for the onset of the Messinian Salinity Crisis. *Stratigraphy* 1 (1), 87-101.
- Laskar, J., Robutel, P., Joutel, F., Gastineau, M., Correia, A., Levrard, B., 2004. A long-term numerical solution for the insolation quantities of the Earth. *Astronomy and Astrophysics* 428 (1), 261-285. doi: 10.1051/0004-6361:20041335.
- Londeix, L., 2004. Synthetic Messinian dinoflagellate cyst record from Sicily. 4<sup>th</sup> International Congress Environment and Identity in the Mediterranean: the Messinian Salinity Crisis revisited, Università di Corsica Pasquale Paoli, Corte, France, Abstracts, 57.
- Lourens, L.J., Hilgen, F.J., Zachariasse, W.J., Van Hoof, A.A.M., Antonarakou, A., Vergnaud-Grazzini, C., 1996. Evaluation of the Pliocene to early Pleistocene astronomical time scale. *Paleoceanography* 11, 391-413. doi:10.1029/96PA01125.
- Lourens, L.J., Hilgen, F.J., Laskar, J., Shackleton, N.J., Wilson, D., 2004. The Neogene Period. In: Gradstein, F.M., Ogg, J.G., Smith, A.G. (Eds.), *A geologic time scale 2004*. Cambridge University Press, Cambridge, pp. 409-440.
- McFadden, P.L., McElhinny, M.W., 1988. The combined analysis of remagnetization circles and direct observations in paleomagnetism. *Earth and Planetary Science Letters* 87, 161-172. doi:10.1016/0012-821X(88)90072-6.
- McKenzie, J.A., Spezzaferri, S., Isern, A., 1999. The Miocene/Pliocene boundary in the Mediterranean and Bahamas: implications for a global flooding event in the earliest Pliocene. *Memorie della Società Geologica Italiana* 54, 93-108.
- Millies-Lacroix, A., 1974. Carte géotechnique de la région de Rabat. Editions du Service Géologique du Maroc, Notes et Mémoires 238.
- Müller, C., 1990. Nannoplankton biostratigraphy and paleoenvironmental interpretations from the Tyrrhenian Sea, ODP Leg 107 (western Mediterranean). *Proceedings of the Ocean Drilling Program, Scientific Results* 107, 495-511. doi:10.2973/odp.proc.sr.107.146.1990.
- Paillard, D.L., Labeyrie, L., Yiou, P., 1996. Macintosh program performs time-series analysis. *Eos, Transactions AGU* 77, 379. doi:10.1029/96EO00259.
- Raffi, I., Backman, J., Rio, D., 1998. Evolutionary trends of tropical calcareous nannofossils in the late Neogene. *Marine Micropaleontology* 35, 17-41. doi:10.1016/S0377-8398(98)00014-0.
- Raymo, M.E., Ruddiman, W.F., Backman, J., Clement, B.M., Martinson, D.G., 1989. Late Pliocene variation in northern hemisphere ice sheets and North Atlantic deepwater circulation. *Paleoceanography* 4, 413-446. doi:10.1029/PA004i004p00413.

- Rio, D., Channell, J.E.T., Bertoldi, R., Poli, M.S., Vergerio, P.P., Raffi, I., Sprovieri, R., Thunell, R.C., 1997. Pliocene sapropels in the northern Adriatic area: chronology and paleoenvironmental significance. *Palaeogeography, Palaeoclimatology, Palaeoecology* 135, 1-25. doi:10.1016/S0031-0182(97)00027-8.
- Rosell, L., Orti, F., Kasprzyk, A., Playa, E., Peryt, T.M., 1998. Strontium geochemistry of Miocene primary gypsum; Messinian of southeastern Spain and Sicily and Badenian of Poland. *Journal of Sedimentary Research, Section A: Sedimentary Petrology and Processes* 68 (1), 63-79.
- Rouchy, J.M., Orszag-Sperber, F., Blanc-Valleron, M.-M., Pierre, C., Rivière, M., Combourieu-Nebout, N., Panayides, I., 2001. Paleoenvironmental changes at the Messinian-Pliocene boundary in the eastern Mediterranean (southern Cyprus basins): significance of the Messinian Lago-Mare. *Sedimentary Geology* 145, 93-117. doi:10.1016/S0037-0738(01)00126-9.
- Ruddiman, W.F., 2001. *Earth's climate: past and future*. W.H. Freeman and Company, New York, U.S.A. 465 p.
- Ruddiman, W.F., Raymo, M.E., McIntyre, A., 1986. Matuyama 41,000-year cycles: North Atlantic Ocean and northern hemisphere ice sheets. *Earth and Planetary Science Letters* 80, 117-129. doi:10.1016/0012-821X(86)90024-5.
- Schreiber, B.C., 1997. Messinian and younger deposition in the southern Caltanissetta Basin: Stop 5, Eraclea Minoa. In: Grasso, M., Lentini, F. (Eds.), *Neogene basins of the Mediterranean region: controls and correlation in space and time*. Excursion guidebook of the Interim Colloquium R.C.M.N.S., 4-9 November 1997. Università di Catania, Istituto di Geologia e Geofisica, Catania, Italy, pp. 50-55.
- Shackleton, N.J., 1977. Carbon-13 in *Uvigerina*: tropical rainforest history and the equatorial Pacific carbonate dissolution cycles. In: Andersen, N.R., and Malahoff, A. (eds.), *The Fate Of Fossil Fuel CO<sub>2</sub> in the Oceans* (Plenum, New York), 401-427.
- Shackleton, N.J., Crowhurst, S., Hagelberg, T., Pisias, N.G., Schneider, D.A., 1995a. A new Late Neogene time scale: application to leg 138 sites. *Proceedings of the Ocean Drilling Program, Scientific Results* 138, 73-101. doi:10.2973/odp.proc.sr.138.106.1995.
- Shackleton, N.J., Hall, M.A., Pate, D., 1995b. Pliocene stable isotope stratigraphy of Site 846. *Proceedings of the Ocean Drilling Program, Scientific Results* 138, 337-355. doi:10.2973/odp.proc.sr.138.117.1995.
- Shackleton, N.J., Pälike, H., Loutre, M.-F., 1999. Improved astronomically tuned timescales for the late Neogene. *Journal of Conference Abstracts (EUG)* 4 (1), 235.
- Spezzaferri, S., Cita, M.B., McKenzie, J.A., 1998. The Miocene/Pliocene boundary in the Eastern Mediterranean: results from Sites 967 and 969. *Proceedings of the Ocean Drilling Program, Scientific Results* 160, 9-28. doi:10.2973/odp.proc.sr.160.026.1998.
- Suc, J.P., Clauzon, G., Gautier, F., 1997. The Miocene/Pliocene boundary; present and future. In: Montanari, A., Odin, G.S., Coccioni, R. (Eds.), *Miocene stratigraphy; an integrated approach*, *Developments in Palaeontology and Stratigraphy*, 15. Elsevier, Amsterdam, pp. 149-154. doi:10.1016/S0920-5446(06)80014-2.
- Taberner, C., Rouchy, J.M., Pueyo, J.J., Thirlwall, M., 2004. Origin of solutes and evaporite deposition at the end of the Messinian Salinity Crisis. The onset of "Lago Mare" sedimentation. 4<sup>th</sup> International Congress Environment and Identity in the Mediterranean: the Messinian Salinity Crisis revisited, Università di Corsica Pasquale Paoli, Corte, France, Abstracts, 83.

- Tiedemann, R., Sarnthein, M., Shackleton, N.J., 1994. Astronomical timescale for the Pliocene Atlantic  $\delta^{18}\text{O}$  and dust flux records of Ocean Drilling Program Site 659. *Paleoceanography* 9, 619-638. doi:10.1029/94PA00208.
- Vai, G.B., 1997. Cyclostratigraphic estimate of the Messinian Stage duration. In: Montanari, A., Odin, G.S., Coccioni, R. (Eds.), *Miocene stratigraphy; an integrated approach*, *Developments in Palaeontology and Stratigraphy*, 15. Elsevier, Amsterdam, pp. 463-476. doi:10.1016/S0920-5446(06)80035-X.
- Van Couvering, J.A., Castradori, D., Cita, M.B., Hilgen, F.J., Rio, D., 2000. The base of the Zanclean Stage and of the Pliocene Series. *Episodes* 23 (3), 179-187.
- Van der Laan, E., Gaboardi, S., Hilgen, F.J., Lourens, L.J., 2005. Regional climate and glacial control on high-resolution oxygen isotope records from Ain El Beida (latest Miocene, NW Morocco): A cyclostratigraphic analysis in the depth and time domain. *Paleoceanography* 20, doi 10.1029/2003PA000995
- Van Hinsbergen, D.J.J., Kouwenhoven, T.J., Van der Zwaan, G.J., 2005. Paleobathymetry in the backstripping procedure: distinguishing between tectonic and climatic effects on depth estimates. *Palaeogeography, Palaeoclimatology, Palaeoecology* 221 (3-4), 245-265. doi:10.1016/j.palaeo.2005.02.013.
- Vidal, L., Bickert, T., Wefer, G., Roehl, U., 2002. Late Miocene stable isotope stratigraphy of SE Atlantic ODP Site 1085; relation to Messinian events. *Marine Geology* 180 (1-4), 71-85. doi:10.1016/S0025-3227(01)00206-7.
- Zijderveld, J.D.A., 1967. A.c. demagnetization of rocks: analysis of results. In: Collinson, D.W., Creer, K.M., Runcorn, S.K. (Eds.), *Methods in palaeomagnetism*. Elsevier, Amsterdam, pp. 254-286.



# The Messinian salinity crisis from the Atlantic to the Eastern Paratethys

---

This chapter is partly co-authored by M. Mărunțeanu (section 6.2) and H. Brinkhuis (section 6.3). Other parts (of sections 6.4 and 6.5) are published in: Hilgen, F.J., Kuiper, K.F., Krijgsman, W., Snel, E., Van der Laan, E., 2007. Astronomical tuning as the basis for high resolution chronostratigraphy: the intricate history of the Messinian Salinity Crisis. *Stratigraphy* 4, 231-238.

## Synopsis

The Messinian salinity crisis (MSC) strongly affected the environmental evolution of the Mediterranean and Paratethys basins. Deteriorating connections with the Atlantic Ocean during its successive stages caused a variable degree of isolation and influenced basin configuration and sedimentation. The mechanisms that triggered the onset and conclusion of the MSC can be expressed in terms of both tectonic and climatic control. In order to assess the relative importance of these forcing factors, a detailed MSC age model is constructed. Furthermore, an attempt is made to determine to what extent separation from the world ocean occurred and whether marine conditions in the two basins persisted.

The previous chapters encompassed the MSC, or time-equivalent, interval as recorded in sections located either outside the Mediterranean (chapters 2 and 5) or within the Mediterranean, yet in a relatively low resolution (chapters 3 and 4). In contrast, this concluding chapter covers in general continuously exposed 'classic' sections from southern Spain (Sorbas and Nijar basins), through northern Italy (Vena del Gesso Basin) and Sicily (Caltanissetta Basin) to Greece (Ionian Islands and Crete). Calcareous nannofossils and organic-walled palynomorphs, including dinoflagellate cysts, have been studied from samples taken there in the Lower Evaporite and Upper Evaporite (Lago Mare) formations. Additionally, a number of samples from areas surveyed before, the Dacic Basin in the Romanian part of the Eastern Paratethys (chapter 2) and the Orphanic Gulf and Strimon Basin in the Greek Northern Aegean (chapter 3), were selected for palynological analyses. Astronomical age calibration of the Mediterranean key sections then results in a high-resolution chronology of the sequence of events characterizing the MSC. This interval is henceforth compared to Atlantic records of the stable oxygen isotope composition of benthic foraminiferal shells (chapter 5), presenting climate shifts and glacial stages on a 10-100 kyr-scale, and of magnetic susceptibility reflecting lithological and paleoenvironmental variations.

It appears that, superimposed on a continuing tectonic closure of the Atlantic gateway(s), eccentricity-modulated climatic control was involved in the transition to, if not in the 5.96 Ma onset of, the MSC and strongly influenced the subsequent timing of the actual isolation and desiccation of the Mediterranean. This second event corresponds to glacial stages TG14 and TG12, between 5.59 and 5.55 Ma; the following onset of the Upper Evaporites at 5.54 Ma coincides with the transition to (a precursor of) interglacial stage TG11. Conversely, the end of the MSC and the associated Pliocene flooding of the Mediterranean at 5.33 Ma are not related to deglaciation but

most likely to a combination of geodynamic and (tectonically forced) erosional processes near the western end of the Mediterranean.

The combined occurrences of marine dinoflagellate cysts and (low-diversity) nannofossil assemblages in confined stratigraphic intervals within both the Lower and Upper Evaporites suggest intermittent influxes of oceanic water into the Mediterranean. However, absence of chronostratigraphic markers in both fossil groups inhibits the exclusion of an element of reworking in the Upper Evaporites. The strontium isotope ratios and foraminiferal records of this interval and the susceptibility records of its Atlantic time-equivalent indicate that the Mediterranean was indeed isolated from the open ocean during the deposition of the Upper Evaporites. This conclusion is in agreement with biostratigraphic and paleoenvironmental results from the Aegean and Paratethys.

## 6.1 Sections and sampling

A selection of Mediterranean sections is described in geographical order from west to east (Fig. 6.1). For biostratigraphic analyses, sampling concentrated on the Lower and Upper Evaporites (Decima and Wezel, 1971; Krijgsman et al., 1999b; CIESM, 2008), the partly corresponding Lago Mare interval (Ruggieri, 1967; Hsü et al., 1978; Orszag-Sperber, 2006), or time-equivalent upper Messinian successions (Figs. 6.2 and 6.3).

### 6.1.1 Spain

Thick gypsum and limestone beds characterize outcrops of Messinian evaporites in the Sorbas Basin, SE Spain (Figs. 6.1 and 6.2). These evaporites are collectively referred to as the Yesares Member (Ruegg, 1964; Krijgsman et al., 2001). The unit is visible in the Los Molinos section, which reveals fourteen gypsum or (towards the top) evaporitic limestone beds, interlayered by calcareous pelitic laminites. The nearby Rio de Aguas section covers a relatively well-developed lateral equivalent of the upper nine evaporite cycles of the Yesares Member, topped by coastal sandstones, calcarenites, and conglomerates, and shelf mudstones of the Sorbas Member. Below the Yesares Member, a transitional unit of clays and limestones, best exposed in the Perales-C

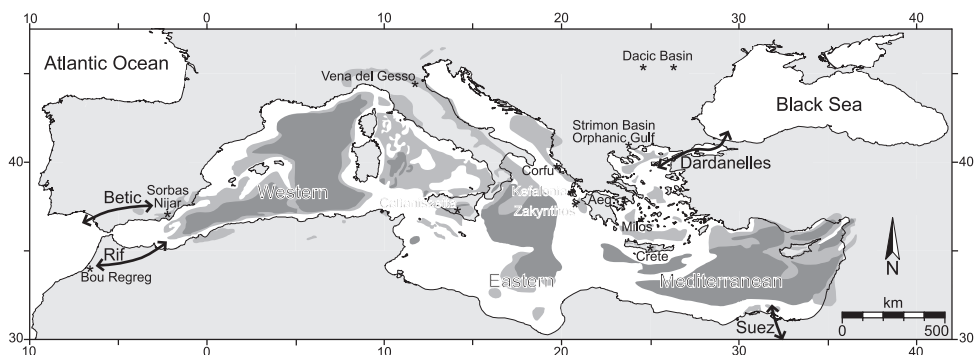


Figure 6.1. Map of the circum-Mediterranean area with locations of the studied sections (\*). Messinian gypsum (light shading) and halite (dark) distribution: modified from Rouchy and Caruso (2006). Mediterranean gateways (double arrows): after Vasiliev et al. (2004).

section, conformably separates the evaporites from the underlying cyclically bedded marls, sapropels, and diatomites of the Abad Member (Sierro et al., 2001). Samples were taken from the clays below gypsum/limestone beds 3–12 in the Los Molinos section.

Eight cycles of erosional, continental sediments constitute the younger Zorreras Member in the central part of the same basin (Martín-Suárez et al., 2000; Krijgsman et al., 2001). This unit overlies the Sorbas Member sandstones with an abrupt but conformable contact. In its type section, light- (yellow-) coloured silts and sandy clays of the Zorreras Member represent the wetter phase of the sedimentary cycles. They change into lagoonal marly chalks in cycles 1 and 5. Relatively dry intervals of red-coloured clastics are intercalated (Fig. 6.3). Samples from the upper four cycles were examined.

In the central part of the adjacent Nijar Basin, the Feos Formation, which is similarly composed of eight cycles of alternating wet and dry periods, is suggested to be the time-equivalent of the Zorreras Member (Fortuin and Krijgsman, 2003; see Aguirre and Sánchez-Almazo, 2004, who considered the Feos Formation to include alternating Sorbas- and Zorreras-type of facies, for a different interpretation of this stratigraphic scheme). Feos cycles consist of an alternation of ‘Lago Mare’-type marly to chalky sediments with silty to sandy laminites and either gypsum/gypsum-rich sandstone beds (in the lower half of the formation) or continental clay and conglomerate beds (in the upper half). Samples were taken from the first cycle and from the top part of the Feos-E section, and from correlative levels in the Castellones (Feos-D of Fortuin and Krijgsman, 2003) and El Argamason sections (Fig. 6.3).

### 6.1.2 Italy

The Vena del Gesso gypsum body (Photo 6.1) of the homonymous basin constitutes the Gessoso-Solfifera Formation and hence the evaporitic interval of the Messinian in the Northern Apennines (Vai, 1997; Krijgsman et al., 1999a). The onset of the evaporites is well exposed in the Cava Li Monti section of the Monticino Quarry, which shows the transitional interval with the underlying pre-evaporitic Tortonian and lower Messinian so-called euxinic shales (Fig. 6.2). Sampling was limited to the interval around the first ‘Calcare di Base’ limestone beds, between 6 and 9 m, and to the clay in between the two gypsum beds. In the nearby Anic Quarry at Monte Tondo, the entire evaporite sequence is exposed, consisting of sixteen alternating gypsum beds and laminites, of which the laminated clays of cycles 2–14 were sampled.

The Colombacci Formation comprises the uppermost continuation of the Messinian sediments in the Vena del Gesso Basin, unconformably overlying the Gessoso-Solfifera Formation. As in the Spanish post-gypsum deposits, eight climatic cycles are recognised in this Lago Mare interval (Bertini, 1994; Vai, 1997; Krijgsman et al., 1999a). These include brackish water marls and clays, sands, and conglomerates; six cycles contain characteristic ‘Colombacci’ beds of white evaporitic limestone (Fig. 6.3; see Roveri and Manzi (2006) and Roveri et al. (2008b) for an alternative stratigraphic interpretation). Samples were taken in the Cusercoli and Gualdo sections, from cycle 4 upwards into the overlying marine marls of the basal Pliocene.

The Miocene-Pliocene Eraclea Minoa section, boundary-stratotype of the Zanclean stage (Van Couvering et al., 2000), is exposed along the shoreline cliffs of Eraclea Minoa in the Caltanissetta Basin on Sicily (Photo 6.2). The upper part of the gypsiferous Gessoso Solfifera (the Upper Evaporites of Sicily), sandy Arenazzolo, and Pliocene calcareous Trubi formations are exposed (a.o.: Decima and Wezel, 1971; Decima and Sprovieri, 1973; Schreiber, 1997; Bonaduce and Sgarrella, 1999; Manzi et al., 2009). Sampling of the first, gypsiferous, interval mainly focussed on the shallow water clays and diatomites underlying the five highest gypsum beds. The strata

beneath the uppermost gypsum bed as well as the overlying non-marine Arenazzolo sands and open marine Trubi carbonates were sampled in a more continuous way (Fig. 6.3).

### 6.1.3 Greece

The Kalamaki Beach section on Zakynthos' southern coast comprises Messinian shallow water marls and clays, with six evaporite beds in between, which are overlain by Zanclean carbonates (Braune et al., 1973; Pierre et al., 2006; Van Hinsbergen et al., 2006). Twenty samples were taken from the marls and clays; the Miocene-Pliocene transitional interval was sampled in detail (Fig. 6.3). On the neighbouring Ionian Islands to the north, the upper Messinian and Zanclean were sampled in the Akros Liakas and Kedros-Sgourou sections on Kefalonia and in the Agios Stefanos section on Corfu (Braune et al., 1973; Pierre et al., 2006; Van Hinsbergen et al., 2006). Along the road from Agia Varvara to Panasos, at the northern margin of the Messara Basin in the south-central part of Crete, a short section (4.7 m) is exposed recording one complete cycle of upper Messinian gypsum (Lower Evaporites: Zachariasse et al., 2008). It consists of laminated clays in between two beds of gypsum, from which five samples were taken.

## 6.2 Calcareous nannofossils

### 6.2.1 Method

Samples were cut and rinsed to remove the weathered surface and to prevent contamination. Standard preparation techniques of Bramlette and Sullivan (1961) were used, supplemented by filtering the samples with a 36- $\mu\text{m}$  sieve. Smear slides were examined under a light microscope using transmitted and cross-polarized light at 1250 $\times$  magnification. Zonal assignments of the nannofossil content follow the Mediterranean MNN zonal scheme (after Raffi and Rio, 1979) incorporating updates by Raffi et al. (2003) and Lourens et al. (2004).

### 6.2.2 Results

Assignments of the assemblages listed below do not always correspond to the MNN zonation of the time interval to which the fossiliferous beds belong (Table 6.1). Reworking and/or the absence of biomarker species may cause interpretations that are too old, as seen in some of the Strimon and Orphanic Gulf sections where lithology and the foraminiferal record suggested chronostratigraphic positions different from the age-ranges of the accompanying nannofossils (Snel et al., 2006b-chapter 3: Fig. 3.7). For instance, the important marker *Nicklithus amplificus*, the last occurrence of which at 6.0-5.94 Ma defines the MNN11c-MNN12 transition (Lourens et al., 2004), was not found in any sample from the (pre-) MSC interval. Hence, for reasons of simplicity, the labelling of MNN zones in Table 6.1 conforms to the ages of the sample levels presented in paragraph 6.4.

#### *Spain*

Sorbas Basin (Yesares Member) samples from the clays of gypsum bed 3 and from below the gypsum of cycles 7 and 12 in Los Molinos contain rare calcareous nannofossils. In the laminated clay below gypsum bed 6 (sample AQ\_5, at 72 m), a relatively rich and diverse flora is present that nonetheless lacks *Discoaster* species or other biostratigraphic markers. Small reticulofenestrids and *Sphenolithus abies* dominate the assemblages of these four samples, while the other samples (as those from the Zorreras Member) do not contain nannofossils. Pre-Pliocene sediments from

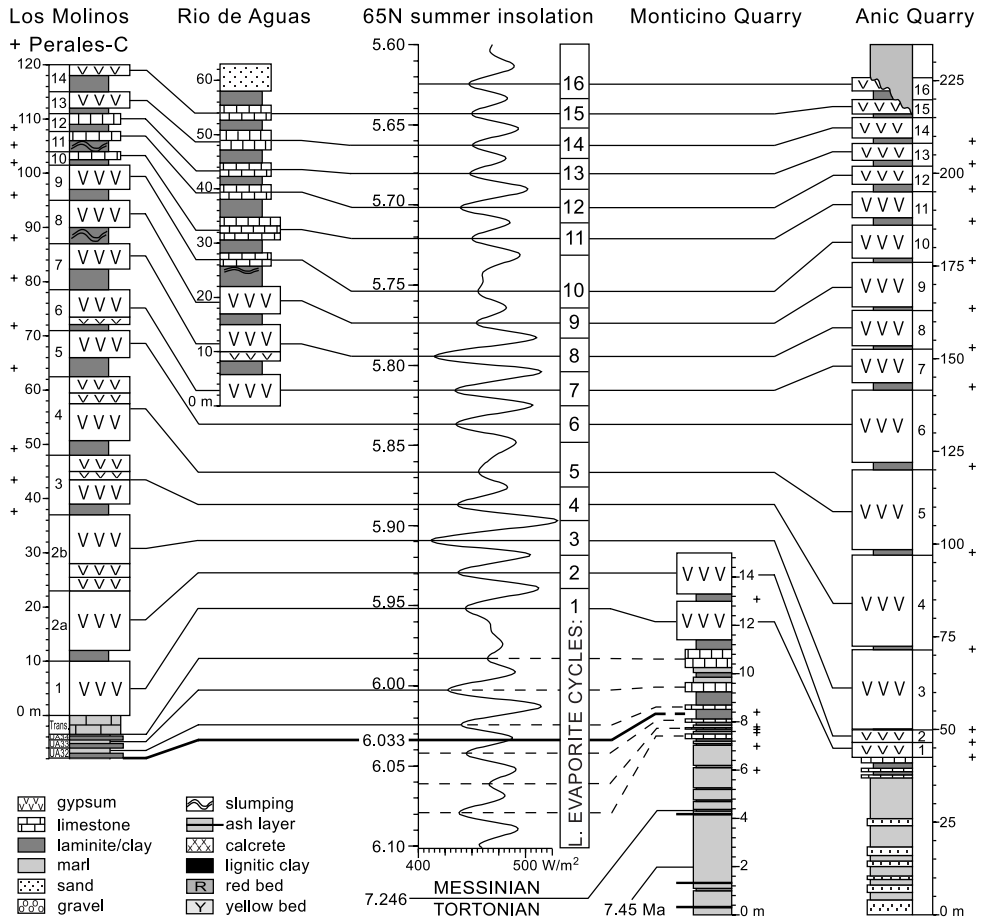


Figure 6.2. Astronomical age calibration (modified from Krijgsman et al., 2001) of Lower Evaporite sections to the 65°N summer insolation time series of the La2004 solution (Laskar et al., 2004). Left: the top of the Abad Member in the Perales-C section and the Yesares Member in the Los Molinos and Rio de Aguas sections in the Sorbas Basin (SE Spain: Krijgsman et al., 2001; Sierro et al., 2001). Right: the euxinic shales and Gessoso-Solfifera Formation in the Cava Li Monti section of the Monticino Quarry and in the Anic Quarry at Monte Tondo in the Vena del Gesso Basin (N Italy: Krijgsman et al., 1999a). The six 'Calcare di Base' limestone cycles below the Vena del Gesso evaporites in the Monticino Quarry are tentatively tuned (dashed correlation lines). Ages for the *Catapsydrax parvulus* LO (7.45 Ma), the Tortonian-Messinian boundary (7.246 Ma), and the base of Chron C3r (bold line at 6.033 Ma) are from Lourens et al. (2004). Sample levels are indicated with '+'.

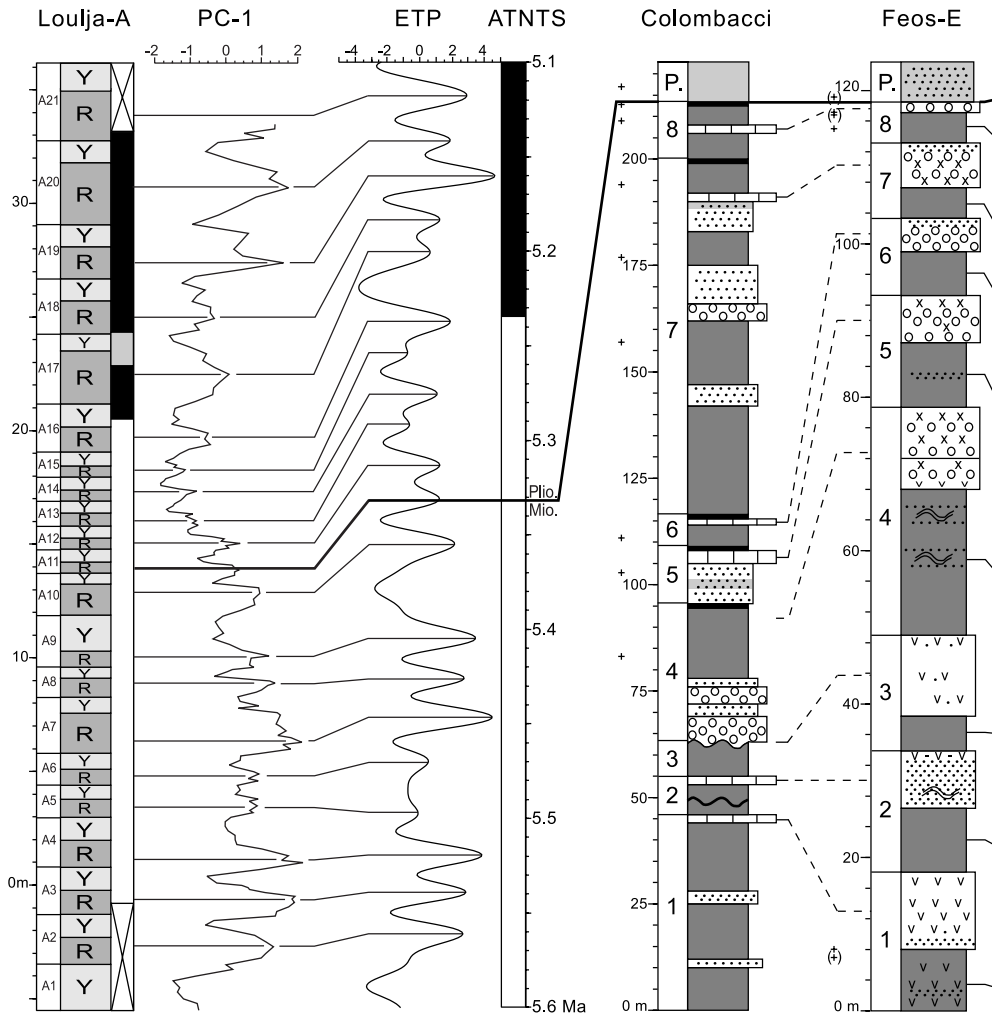
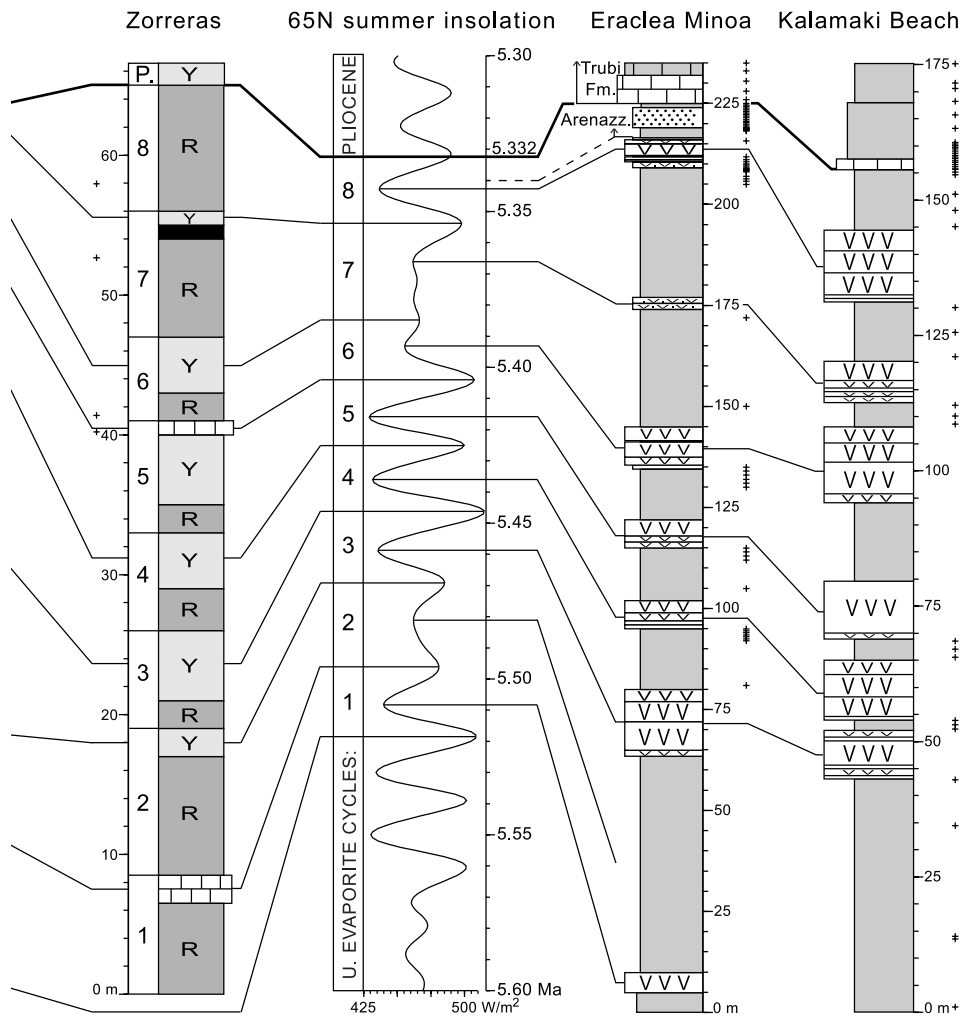


Figure 6.3. Astronomical age calibration of Upper Evaporite and Lago Mare sections to the 65°N summer insolation time series of the La2004 solution (Laskar et al., 2004) and comparison to the Loulja-A section in the Bou Regreg area (Atlantic coast, Morocco: Van der Laan et al., 2006-chapter 5), showing tuning of colour cycles and PC-1 (first principal component of geochemical element data) record to the ETP (normalized eccentricity, tilt, and precession) time series of the La2004 solution (Laskar et al., 2004) and the ATNTS2004 (Lourens et al., 2004). The Colombacci Formation comprises the combined Cusercoli and Gualdo sections in the Vena del Gesso Basin (N Italy; modified from Vai, 1997); the Feos Formation in section 'E' in the Nijar Basin (SE Spain) is after Fortuin and Krijgsman (2003); the type section of the Zorreras Member in the adjacent Sorbas Basin is after Krijgsman et al. (2001); the lower part of the Eraclea Minoa section in the Caltanissetta Basin on Sicily (S Italy) is after Schreiber (1997); the Kalamaki Beach section on Zakynthos (W Greece) is after Braune et al. (1973). Sample levels are indicated with '+'; samples between brackets (+) are from the Castellones (section Feos-D; Fortuin and Krijgsman, 2003) and El Argamason localities in Nijar, from levels that correlate to those indicated in section Feos-E. For lithology key, see Figure 6.2.



the Nijar Basin (Feos Formation) yielded samples containing in general few and poorly preserved long ranging nannofossils. At 7 m, in the fish-bearing laminitic marl of the first cycle of Fortuin and Krijgsman (2003), a richer and diversified assemblage typical for the uppermost Miocene was found including *Reticulofenestra rotaria* and *Triquetrorhabdulus rugosus*, but also *Braarudosphaera bigelowii* and reworked elements from the lower Miocene.

### Italy

Samples from the Monticino Quarry (Vena del Gesso Basin) contain nannofossil assemblages including *Discoaster berggrenii*, *D. quinquaramus*, *Helicosphaera stalis*, and *Reticulofenestra rotaria* up to the 7.8 m-level, assignable to Zone MNN11. Non-diagnostic low-diversity assemblages with small reticulofenestrads and sphenoliths are present at 8.4 m and, in the Anic Quarry section, below the 13<sup>th</sup> gypsum bed. The other samples do not contain nannofossils. The Colombacci Formation produced samples relatively rich in nannofossils, including reworked specimens and

*Micrantholithus vesper*. They do not contain marker species except for *Discoaster icarus*, in cycle 7 at 157 m, known from Zone NN12a in open ocean records (Perch-Nielsen, 1985) and also from older stratigraphic levels in the Ain el Beida section corresponding to Zone NN11b (Krijgsman et al., 2004).

In the samples from the Gessoso Solfifera and Arenazzolo formations of the Eraclea Minoa section, assemblages are generally poor and represented by long ranging species that can be regarded as reworked. Rare specimens of *Discoaster quinqueramus*, observed at 92 m and 133 m, and *Reticulofenestra rotaria*, present at 81, 92, and 134 m, are assignable to Zone MNN11. The very rich MNN12-assemblages found throughout the overlying Trubi Formation constitute a noticeable contrast. However, in samples from below the gypsum beds of cycle 6 (particularly at 135 m) and cycle 8, other rich and diverse assemblages were observed, containing *Braarudosphaera bigelowii* and *Micrantholithus vesper*, two species tolerant to hyposaline conditions (Bartol et al., 2008). Samples in the Arenazzolo Formation mainly contain reworked Cretaceous, Paleogene, and older Neogene nannofossils, if any. At 219 and 221 m, species of a.o. *Discoaster*, *Helicosphaera*, and *Reticulofenestra* occur and few older reworked specimens; at 223 m, only reticulofenestrids are relatively common. On the contrary, the very top of the Arenazzolo sands (225 m) already contains a distinctively rich assemblage with abundant *Discoaster* and *Scyphosphaera*, which can only be explained by burrowing. Samples from the Trubi marls are richer still and floral assemblages include many species of *Amaurolithus*.

#### Greece

Kalamaki Beach samples from the Upper Evaporite beds on Zakynthos scarcely contain nannofossils, in contrast to the Trubi-like lowermost Pliocene limestones on top. Only the lower two samples (at 1 and 13.5 m; Fig. 6.3) yielded relatively rich assemblages with *Amaurolithus delicatus*, *A. primus*, and *Discoaster quinqueramus*, indicative of Zone MNN11b-c or MNN12. Similarly, pre-Pliocene samples of the sections on Kefalonia and Corfu produced in general poor and low-diversity assemblages. Exceptions were found in the lower part of the Akros Liakas section, where floras consist of (a.o.) many specimens of *Discoaster brouweri* (only in the lowermost sample, together with rare *Amaurolithus delicatus*), *Helicosphaera* spp., and *Pontosphaera discopora*. Higher, towards the evaporites, nannofossils become increasingly scarce, apart from the smaller reticulofenestrids. Marine clays below the gypsum of the Kedros-Sgourou section contain *Amaurolithus delicatus* and *Discoaster quinqueramus*, denoting the Messinian (Zones MNN11b-c to MNN12). Notably, in four of the samples from the Agia Varvara section on Crete, equally rich nannofossil assemblages as in sample AQ\_5 from the Los Molinos section in the Sorbas Basin were found, similarly dominated by small reticulofenestrid species and *Sphenolithus abies*.

## 6.3 Organic-walled microfossils

### 6.3.1 Palynological processing and counting

Organic-walled microfossils were extracted for analysis using standard palynological processing techniques at the Laboratory of Palaeobotany and Palynology at the Utrecht University. From the samples, ~5 cm<sup>3</sup> was processed involving an initial treatment in hydrochloric acid (10%) to dissolve carbonates, followed by a treatment of hydrofluoric acid (38%) to dissolve silicates. After each acid step, samples were washed two times by decanting after 24 hours of settling and filling up with distilled water. The hydrofluoric step included two hours shaking at ~250 rpm and adding



30% hydrochloric acid to remove fluoride gels. Then, samples were repeatedly washed in distilled water and finally sieved through a 15- $\mu\text{m}$  nylon mesh sieve. To break up clumps of residue, the sample was placed in an ultrasonic bath for a maximum of 5 min after the first sieving. The residue remaining on the sieve was transferred to a glass tube. The tubes were centrifuged for 5 min at 2000 rpm and the excess amount of water was removed. For slide preparation, residues were transferred to vials and glycerine water was added. The residue was homogenized, no colouring was added, a droplet of each residue was mounted on a slide adding glycerine jelly, and the mixture was stirred and sealed with nail varnish. Two slides per sample were prepared.

For semi-quantitative analysis, slides were randomly counted to ~100 palynomorphs, and then to ~100 organic-walled dinoflagellate cysts (dinocysts), where possible. When dealing with low yields, counting was stopped after two slides at this stage. Dinocysts were counted at species level, whereas other palynomorphs were counted in broad categories: bisaccate pollen, other pollen, spores, inner linings of foraminifers (if > 3 chambers), remains of chlorophyte algae such as *Pediastrum* spp., and acritarchs. Dinocysts usually dominate aquatic palynomorphs. Cyst taxonomy follows that cited in Williams (1998).

### 6.3.2 Palynomorphs and dinocysts

A semi-quantitative overview of palynomorph and dinocyst distribution is given in Table 6.2. Samples selected for palynological analysis were recovered from sections in the Vena del Gesso Basin (Anic Quarry), Sicily (Eraclea Minoa), and Zakynthos (Kalamaki Beach). In addition, suitable samples from previously studied localities in the Orphanic Gulf and Strimon Basin areas in northern Greece (sections “Rema Marmara” (Photo 6.3), Kavala Road West (Photo 6.4), and Myrini (Photo 6.5); Snel et al., 2006b-chapter 3) and in the Dacic Basin in Romania (Bădislava (Photo 6.6) and Valea Vacii (Photo 6.7); Snel et al., 2006a-chapter 2) were prepared and re-examined for palynomorphs and dinocysts. Recovery of palynomorphs is quite variable. Dinocysts are in most cases the most prominent aquatic palynomorphs, while sporomorphs, notably bisaccate pollen, generally dominate samples. Some samples yield only poorly preserved palynomorphs; prolonged exposure to oxic conditions probably hampered significant accumulation of organic matter, dinocysts, in these cases.

In essence, the dinocyst assemblages fall into two categories: (I) a fresh to brackish water assemblage in the three Dacic and Strimon Basin samples, or (II) relatively open marine, normal salinity assemblages, with an important input of typical hypersaline lagoonal taxa. Taxa associated with assemblage I are, e.g., *Galeacysta etrusca*, *Spiniferites cruciformis* s.l., and *Gonyaulacysta apiculata*. Previous studies have shown the latter two to be essentially fresh water species (Kouli et al., 2001). *G. etrusca* is known to dominate the Italian Lago Mare facies (Corradini and Biffi, 1988; Bertini et al., 1995; Bertini, 2006). The sample from the Myrini section (Strimon Basin) also contains long ranging ‘normal marine’ species of *Spiniferites* and *Operculodinium*. In combination with *G. etrusca*, this indicates brackish to normal marine conditions.

Long ranging representatives of *Impagidinium*, *Lingulodinium*, *Spiniferites*, and *Operculodinium* generally dominate the ‘open marine’ assemblages (II). Notably species of *Impagidinium* are known to be typical for offshore, oligotrophic, oceanic, and warm conditions, while also the other taxa are definitively of open marine character (Marret and Zonneveld, 2003). In some cases, the above taxa are joined by species indicative for lagoonal, subtropical to tropical hypersaline settings (e.g., *Homotryblum* spp. and *Operculodinium israelianum*; Marret and Zonneveld, 2003; Dybkjær, 2004). This aspect indicates the influence of such settings, and may indicate proximity to the coastline.









## 6.4 Age model

Climatically induced sedimentary cyclicity in most of the Lower and Upper Evaporite sections enables astronomical age calibration of individual beds. This results in the cyclostratigraphic correlation diagrams and orbital tuning presented in Figures 6.2 and 6.3.

### 6.4.1 Lower Evaporites

The evaporites of the Yesares Member in the Sorbas Basin are considered time-equivalent of the major part of the Lower Evaporite unit of the central Mediterranean Gessoso-Solfifera Formation (Clauzon et al., 1996; Krijgsman et al., 2001). Regular cyclic bedding likely implies precession-dominated astronomical forcing and permits good age control in both the Sorbas Basin and the Vena del Gesso Basin. According to Krijgsman et al. (1999b), evaporite beds represent relatively dry periods and correspond to precession maxima and thus to insolation minima. Following a low-amplitude insolation interval, which corresponds to the transitional unit at the top of the Abad marls in the Perales-C section of the Sorbas Basin (Sierro et al., 2001), the onset of evaporite deposition is inferred to concur with the relatively high-amplitude insolation minimum at ~5.96 Ma (cycle 1; Fig. 6.2). In the Los Molinos section, the second ('double') gypsum bed incorporates one extra precession cycle, which results in a preferred tuning that is slightly different from the Krijgsman et al. (2001) solution. The transition towards relatively reduced amplitudes of the insolation minima, from cycle 9 (Rio de Aguas section) or 10 onward, roughly relates to the change from thick gypsum beds to thinner evaporitic limestone beds in the Sorbas Basin sections, and to the reduction in thickness of the gypsum beds in the Vena del Gesso Basin. Likewise, the basal carbonates below the gypsum in the Monticino Quarry can be cautiously tied to insolation minima (Fig. 6.2), as they occupy the same position within the sedimentary cycles as the gypsum beds (Krijgsman et al., 1999a).

### 6.4.2 Upper Evaporites

Cyclostratigraphy of the Upper Evaporite and Lago Mare interval has been pioneered by Hilgen et al. (1995), Vai (1997), Krijgsman et al. (1999a, 2001), Roveri and Manzi (2006), Roveri et al. (2008b), and Manzi et al. (2009). Up to eight (or ten, according to the last three papers) sedimentary cycles of inferred precessional origin, predominantly characterized by gypsum and/or brackish water deposits, partly fill the gap between the Lower Evaporites and the base of the Pliocene. Obliquity-controlled cyclicity, an option suggested by Vai (1997), would require a 320 kyr time span for the Upper Evaporites and therefore imply their onset at 5.65 Ma. This also would be in conflict with the precession scenarios for the Lower Evaporites and Atlantic counterparts in the sections of Ain el Beida and Loulja (Krijgsman et al., 2004; Van der Laan et al., 2005, 2006-chapter 5, in prep.). An intra-Messinian hiatus, appearing as a Mediterranean-wide erosional surface related to the desiccation event (e.g., Cita and Ryan, 1978; Clauzon et al., 1996), separates the two evaporite units and should account for the remaining time.

As discussed by Krijgsman et al. (2001), the lighter coloured, wet-phase intervals of the Zorreras section in the Sorbas Basin represent insolation maxima. Figure 6.3 shows a possible astronomical tuning that correlates these yellow beds to insolation maxima one younger than in Krijgsman et al. (2001). This alternative option is preferred because it includes the 5.35 Ma insolation maximum and reveals a better fit between the pattern in cycles 2-6 of relatively thick yellow beds (cycles 3 and 5) and corresponding high-amplitude peaks of maximum insolation.

Age calibration of the cycles of the Feos Formation in the Nijar Basin is equally based on the assumption of a conformable and abrupt change of the upper Messinian continental sediments

into the marine basal Pliocene (Fortuin and Krijgsman, 2003). The pattern of eight dry- and wet-phase intervals of coarse clastic beds and 'Lago Mare' laminites can thus be correlated to peak values of, respectively, minimum and maximum insolation from 5.52 Ma upwards. Notably, the weakly developed 5.48 Ma minimum and the relatively high-amplitude maximum at ~5.45 Ma match well with the reduced thickness of the bed that represents the dry-phase of cycle 2 and the, in contrast, exceptionally thick bed that represents the wet-phase of cycle 4. According to Aguirre and Sánchez-Almazo (2004), alternating marine and continental deposits of the post-evaporitic unit gradually replace the gypsum beds of the Yesares Member. These authors defined the boundary between the two Messinian units at the top of the last primary-precipitated gypsum, which resulted in an older age than the 5.60-5.54 Ma of the Yesares-Feos formation boundary of Fortuin and Krijgsman (2003).

Cyclicity in the Colombacci Formation of the Vena del Gesso Basin presents a far less regular pattern in contrast to its Spanish counterpart. The tectonically active setting (Roveri et al., 2003) clearly influenced deposition of the Lago Mare sequence. Correlation lines in Figure 6.3 between the individual beds of the two basins should consequently be regarded as merely indicative. The phase relation seems straightforward though, implying that 'dry', evaporitic Colombacci limestones alternating with 'wet' black marls correspond to insolation minima and maxima, respectively. Roveri and Manzi (2006) suggested, however, that cyclicity in the Colombacci Formation is not precession-controlled and that the locally underlying Tetto Formation corresponds to the post-evaporitic Lago Mare interval as well, which would strongly reduce the duration of the Colombacci Formation. Furthermore, the base of the Arenazzolo Formation, calibrated in the Eraclea Minoa section at 5.34 Ma (Fig. 6.3; see also Manzi et al., 2009), corresponds in their view to the base of the Colombacci Formation. In the chronostratigraphic scheme in CIESM (2008; p. 79), however, the authors used a broader definition for the Arenazzolo Formation: upwards from gypsum bed 6 in the Eraclea Minoa section (at ~140 m; Fig. 6.3). As in Roveri et al. (2008b), they correlated the lower boundaries of the Arenazzolo and Colombacci formations to the 5.42 Ma insolation minimum, thus diminishing the otherwise drastic difference (Fig. 6.4).

The pattern of gypsum beds in this Sicilian section and in the Kalamaki Beach section on Zakynthos, the latter equally assigned to the Upper Evaporites by Van Hinsbergen et al. (2006), are to a certain extent similar. There is a distinct group of well-developed gypsum beds, labelled 3-6 in Figure 6.3, preceded by a thick clay unit (and, below that, the first gypsum bed in the Eraclea Minoa section) and followed by the relatively thin gypsum bed of cycle 7 and then again by a final thicker one. This pattern of evaporites resembles the sequence of high- and low-amplitude minimum values of the insolation cycles from 5.51 Ma upwards. Hence, the group of gypsum beds 3-6 may correlate to the group of four relatively thin reddish beds in Zorerras cycles 3-6. Decima and Sprovieri (1973) reported the presence of yet another gypsum bed in drilled wells, stratigraphically below the outcrop of the Eraclea Minoa section but still above the salts from the Lower Evaporite unit. CIESM (2008) and Manzi et al. (2009) also mentioned an additional thin bed of banded selenite at the base of the Sicilian upper unit. This extra evaporite bed could have an age of 5.53 Ma, in agreement with the age model of CIESM (2008) and Manzi et al. (2009), which nevertheless starts from a correlation of the younger cycles that is different from Figure 6.3. These last two solutions are presented in Figure 6.4, where the same cycle numbers are maintained for the same gypsum beds. Alternatively (not shown), the lowermost evaporite could correspond to cycle '1', thereby leaving the start of the Upper Evaporites unchanged at 5.51 Ma. The first gypsum bed in the section itself, at 5-10 m, would consequently correspond to cycle '2' at 5.48 Ma.

Section + sample	Level (m)	Age (Ma)	Dinoflagellate taxa																								
			Dinocysts	Acritarchs	Bisaccate pollen	Other pollen	Spores	Foram linings	Pediastrum spp.	Reworked M-P	Achomosphaera cf. andalusiensis	Galeacysta etrusca	Gonyaulacysta apiculata	Spiniferites cruciformis s.l.	Tectatodinium psilatum	Cleistosphaeridium placacanthum	Homotryblium spp.	Hystrioholoporia spp.	Impagidinium spp.	Lingulodinium machaerophorum	Operculodinium centrocarpum s.l.	Operculodinium israelianum	Operculodinium janduchenei	Spiniferites ramosus cpx.	Other dinocysts		
<b>Anic Quarry (Vena del Gesso)</b>																											
AC 3	50	5.92 (F2)	X	P	D	C	C														X						
AC 10	177	5.765 (*)	X	P	D	C	C														X			X			
<b>Eraclea Minoa (Caltanissetta)</b>																											
EM-UE 5.0	130	5.40 (F3)	P	P	D	C	C	P													F	F	P	P	F	F	
EM-UE 7.3	207	5.35 (*)	P	P	D	C	C														P	F	P	P	F	X	
EM 3	208.2	5.35 (*)	C	P	D	C	P												D	P	P	C			C	X	
EM 20	219.1	5.34 (*)	C	P	D	C	P												D	P	P	C			C		
EM 21	219.4	5.34 (*)	C	P	A	C	P												C	P	P	C			D		
EN 29	222.6	5.335 (*)	A	P	A	C	P												C	P	P	C			C		
EM 35	225	5.333 (*)	A	P	A	C	P		P										P	P	P	C	P	C	C	X	
<b>Kalamaki Beach (Zakynthos)</b>																											
KB 2	13.5	~5.5 (F3)	C	P	D	P	P	P													P	C	C	C	D	X	
<b>"Rema Marmara" (Orph. Gulf)</b>																											
ST 58	40	~6.0 (C3)	P	P	D	C	C	P													P	P			D		
ST 44	101	~5.33 (*)	P	P	D	C	C	P													P	P			D		
ST 47	110	~5.3 (*)	P	P	D	C	C	P											P	P	P	P			D		
ST 51	119	~5.25 (*)	P	P	D	C	C	P													P	D	P		C		
<b>Kavala Road West (Orph. Gulf)</b>																											
ST 75	151.5	~5.25 (C3)	P	P	D	C	C	P													P	P	P	P	C	X	
<b>Myrini (Strimon Basin)</b>																											
MY 1	0.01	6-5.3 (C3)	P	P	D	C	C				C											P			P		
<b>Badislava (Dacic Basin)</b>																											
BV 158	64.2	~5.6 (C2)	C	F	D	C	C	P	F		D	P	C														
<b>Valea Vacii (Dacic Basin)</b>																											
VA 28.2	80.75	~5.8 (C2)	D	F	A	P	P	F	C	P	A	A	A	P							P						

Table 6.2. Semi-quantitative distribution of organic-walled palynomorphs and dinoflagellate cysts. Lightly shaded species are fresh to brackish water (hyposaline) dinoflagellates; dark shading denotes relatively open marine (normal saline) and lagoonal (hypersaline) taxa. Key: X = rare (< 1%), P = present (< 2%), F = frequent (< 15%), C = common (< 25%), A = abundant (< 50%), D = dominant (> 50%). Ages are inferred from stratigraphic positions in Figure 6.2 (F2), Figure 6.3 (F3), Snel et al. (2006a-chapter 2) (C2), and Snel et al. (2006b-chapter 3) (C3).

## 6.5 Oxygen isotope and magnetic susceptibility records

The improved dating of the Mediterranean sections allows detailed comparison of the successive phases of the MSC to the stable oxygen isotope and initial bulk magnetic susceptibility records from the Atlantic Ocean (Krijgsman et al., 2004; Van der Laan et al., 2006-chapter 5, in prep.). In this way, Figure 6.4 shows the inferred relation between astronomically controlled late Messinian



climate changes recorded outside the Mediterranean and Mediterranean paleoenvironmental events.

### 6.5.1 Atlantic reference sections

The Loulja composite section of the Bou Regreg area (Photo 6.8) on the Atlantic coast of northern Morocco contains an open marine record of latest Messinian (and earliest Zanclean) age, in which lithology is dominated by astronomically controlled cyclicity. The geochemical parameter PC-1 clearly reflects the cyclic variability of the lithological record and enables a straightforward tuning to the nearly identical ETP curve (Fig. 6.3). The benthic oxygen isotope ( $\delta^{18}\text{O}$ ) record from section Loulja-A (Photo 6.9) and the partly overlapping, older Ain el Beida section (Photo 6.8) reveals a similar resemblance with the astronomical curves as visualised by ETP and  $65^\circ\text{N}$  summer insolation (Fig. 6.4). This benthic  $\delta^{18}\text{O}$  record is interpreted to largely reflect glacial history, with heavy values corresponding to cold, glacial periods (Zachos et al., 2001). Note that not only obliquity-controlled variations may drive global ice volume-related shifts in oxygen isotope values. The evident precession component in the data from the Bou Regreg area probably reflects both precession-controlled fluctuations in ice volume, as indicated by other Atlantic Ocean records, as well as a local or regional bottom-water temperature signal (Van der Laan et al., 2006-chapter 5).

The single noteworthy exception to the excellent fit with the astronomical forcing is the striking decrease in the Ain el Beida  $\delta^{18}\text{O}$  record just above glacial stage TG32, coinciding with the onset of the MSC (Krijgsman et al., 2004). Recalibration of the less distinct cycles in this interval of reduced insolation amplitudes, related to a 100-kyr eccentricity minimum (Fig. 6.4), may solve this 10-kyr discrepancy and a remarkable peak in sedimentation rate (Van der Laan et al., 2005). In that case, a (minor) glacio-eustatic sea level lowering, expressed by the relatively heavy  $\delta^{18}\text{O}$  values at 36 m, may have contributed to the formation of the first evaporite, as it corresponds to the 5.96 Ma minimum in ETP. This would oppose the interpretations of Hodell et al. (2001), Krijgsman et al. (2004), and Van der Laan et al. (2005), however, and it should be realized that shifting lithological cycles up by one precession cycle would cause other tuning problems, as mentioned by Van der Laan et al. (2005). In fact, short-term non-cyclic events in multiple proxy records characterize the 6.0-5.95 Ma interval (Van der Laan, in prep.). The transitional interval between the marine marls and evaporites in the Sorbas Basin (Sierro et al. (2001) represents an additional expression of this same interval of minimum eccentricity, when the influence of regional tectonic activity on the sedimentary record was perhaps more significant than astronomical forcing.

Studies in and at both ends of the Rifian Corridor (Fig. 6.1; Krijgsman et al., 1999c; Barbieri and Ori, 2000; Van Assen et al., 2006) hint at tectonic closure of this southern entrance of the Mediterranean culminating just prior to 6 Ma, which restricted the basin and facilitated land-faunal exchange between Africa and Europe. At 6.07 Ma, synchronous with this transition at the Atlantic gateway, a tectonically controlled facies change occurred in the intramontane basins of NW Greece (Steenbrink et al., 2006). These last authors cautiously linked a series of similar semi-parallel trends in the depositional environments of the continental and marine realm to the interplay of tectonics and orbital forcing, specifically the influence of the 400-kyr eccentricity cycle. Another general aspect, shared by continental and marine deposits alike, is lithological cyclicity at various scales: millennial-scale sub-Milankovitch cycles, those controlled by precession periods, and 100- to 400-kyr eccentricity cycles. Examples are found, e.g., in the Greek marl/lignite complexes (Steenbrink et al., 2006) and in the Italian Upper Evaporite sections, where higher-frequency cycles within the individual gypsum beds may be attributed to solar fluctuations (Manzi et al., 2009). The open marine marl rhythmites of the Bou Regreg composites clearly

show eccentricity-induced bundles of darker beds and, similarly, the whole MSC succession in the Mediterranean can be regarded as one large evaporite sequence that is subdivided in eccentricity-scale clusters of gypsum beds (Fig. 6.4).

### 6.5.2 Lower Evaporites

As observed before, the first nine or ten thicker gypsum beds of the Lower Evaporites between 5.96 and 5.75 Ma correspond to the interval of relatively enhanced insolation minima that are related to the two 100-kyr eccentricity maxima (and the minimum in between) during the 400-kyr eccentricity maximum around 5.85 Ma (Fig. 6.4). In the Sorbas Basin, the replacement of thick gypsum by thin limestone in beds 10–12 of the Los Molinos section and upwards from evaporite bed 9 in the Rio de Aguas section (Fig. 6.2), approximately appears to follow the relatively heavy  $\delta^{18}\text{O}$  values related to glacial stages TG22 and TG20. The effect of climatic forcing on bed thickness, being consistent with the correlation shown in Figure 6.2, may however be diluted by the general shallowing-up trend caused by sedimentary infill and a tectonically controlled reduction of the rate of relative sea level rise (Roveri and Manzi, 2006).

TG20, the most prominent glacial stage of the latest Miocene in the record from ODP Site 928, fails as a candidate for the Messinian desiccation event (Hodell et al., 2001). Coeval with the 5.75 Ma minimum of the 100-kyr eccentricity cycle, it predates the estimated time of the drawdown by 160 kyr (Krijgsman et al., 1999b). At 5.75 Ma, the Atlantic–Mediterranean gateway, its location being unknown (CIESM, 2008), may still have been too deep to cause complete isolation of the Mediterranean. Apparently, gradual or stepwise sea level drops and rises, recorded by in-/decreasing  $\delta^{18}\text{O}$  values, merely provided a modification effect superimposed on larger-scale tectonic trends and only affected the depositional environment of the Mediterranean once the required boundary conditions were met. Hodell et al. (2001) stated that small glacio-eustatic changes may have been important when the Atlantic–Mediterranean gateway became very shallow, which seems more appropriate for the second half of the MSC following the 5.59 Ma eccentricity minimum (Krijgsman and Meijer, 2008).

### 6.5.3 Mediterranean desiccation

The corresponding upper part of the Moroccan isotope record is characterized by heavy  $\delta^{18}\text{O}$  values of glacial stages TG 14 and TG12 dated at 5.59 and 5.55 Ma, reaching a peak of 1.4 ‰ in samples from the Loulja-A section, followed by a stepwise decrease to average values of ~0.6 ‰ before the end of the Messinian (Fig. 6.4). This climate pattern fits remarkably well with the sequence of events in the Mediterranean from the end of the Lower Evaporite interval onward. Hodell et al. (2001) presented in their North Atlantic record the two prominent stages TG14 and TG12 as a possible cause for sea level lowering, subsequently leading to the concluding isolation and drawdown of the Mediterranean. This desiccation event was estimated to have taken place between 5.59 and 5.50 Ma, calculated by using the average 21.7 kyr precession period and assuming the existence of a seventeenth Lower Evaporite cycle (Krijgsman et al., 1999b). In fact, that potential evaporite bed may have been deposited in the Vena del Gesso Basin at 5.60 Ma, thus reaching the same time-stratigraphic level as the highest cycle of the combined Yesares and Sorbas members in the Sorbas Basin (Krijgsman et al., 2001). In that case, incision after the glacio-eustatic controlled sea level drop associated with the severe glacial stage TG14 at 5.59 Ma probably erased it.

Ongoing intra-Messinian tectonic activity (Vai, 1997; Steenbrink et al., 2006; CIESM, 2008) may have exerted an indirect influence on the Mediterranean desiccation event. Vice versa, removal

of the supporting water body from instable slopes could have triggered gravitational collapse of the margins after the final deposition of the Lower Evaporites, as for example in northern Italy (Roveri et al., 2003; Roveri and Manzi, 2006; Roveri et al., 2008b), and may have affected the stability of the orogenic wedge (DeCelles and Cavazza, 1995). On the other hand, desiccation was suggested to play a role in isostatic rebound processes (Norman and Chase, 1986) and would have led to a decreasing basin gradient, consequently contributing to increasing slope stability (Govers et al., 2009).

#### 6.5.4 Upper Evaporites

As much as the drawdown and accompanying erosional phase may be related to the cold TG14-TG12 interval, the succeeding start of the Upper Evaporite series appears to concur with the next major deglaciation event. When indeed the Upper Evaporites cover a time span of only eight precession cycles (Vai, 1997; Krijgsman et al., 2001; Fortuin and Krijgsman, 2003) and when they are deposited directly before the Miocene-Pliocene boundary, then their onset is synchronous with the TG11 interglacial at 5.52 Ma (Hodell et al., 2001; Krijgsman et al., 2004). However, incorporating the extra evaporite bed of the Eraclea Minoa section (Decima and Sprovieri, 1973; CIESM, 2008; Manzi et al., 2009), the local start of the Upper Evaporites there likely corresponds to the previous interglacial at 5.54 Ma, directly after stage TG12 and just before the small  $\delta^{18}\text{O}$  peak labelled '0' (Fig. 6.4). In that case, the erosional gap between the Lower and Upper Evaporite units may be closer to only 50 kyr.

The relative magnitude pattern of maximum  $\delta^{18}\text{O}$  values from 5.52 Ma onward is generally matching the sequence of corresponding insolation minima, and therefore equally comparable to lithological cyclicity. In the Eraclea Minoa section, for example, the thicknesses of evaporite beds 1, 3-6, and 8 visibly resemble the relative amplitudes of the corresponding insolation minima; with the exception of cycles 6 and 7, this also holds for the pattern in the isotope curve (Figs. 6.3 and 6.4). In line with the correlation in paragraph 6.4, the lithology of the Feos-E section seems to reflect the less developed isotope extremes that correspond to two consecutive 100-kyr eccentricity minima. The 19 m thick 'Lago Mare' interval between evaporitic/continental beds of Feos cycles 3 and 4, caused by tectonic instability (Fortuin and Krijgsman, 2003) and resulting in this extra thick cycle, coincides with interglacial stage TG9 (Fig. 6.4). This step at 5.45 Ma, from intermediate to relatively low peak values of  $\delta^{18}\text{O}$ , corresponds to a reduction of the gypsum content in those beds of the Feos-E section that represent the dry-phase of the climatic cycle. Similarly, the distinctive lithologies of cycles 7 and 8 in the Zorreras and Eraclea Minoa sections could be related to the 5.38 Ma eccentricity minimum and subsequent interglacial stage TG7, although the studied sections (Fig. 6.3) lack a uniform expression of this interval and of the stronger TG9 interglacial. Another sedimentary break in the upper unit of the MSC, observed in sections along the Apennine foredeep (Roveri and Manzi, 2006), divides the Lago Mare sequence into the Tetto and Colombacci formations. This regional-scale unconformity and the associated widespread onset of hyposaline conditions have a recalibrated age of 5.42 Ma (CIESM, 2008; Roveri et al., 2008b), which is ~30 kyr after stage TG9 and therefore apparently unrelated to climatic forcing.

To conclude, the relation of global ice volume and sea level with the end of both the Messinian stage and the salinity crisis has been discussed by Hodell et al. (2001) and Van der Laan et al. (2006-chapter 5). Clearly, no indication for a direct link can be found in the  $\delta^{18}\text{O}$  records. This conclusion favours piracy of Atlantic waters through regressive fluvial erosion near the present-day Strait of Gibraltar (Loget and Van Den Driessche, 2006) and/or a tectonic cause for the Pliocene flooding of the Mediterranean (Govers, 2009).

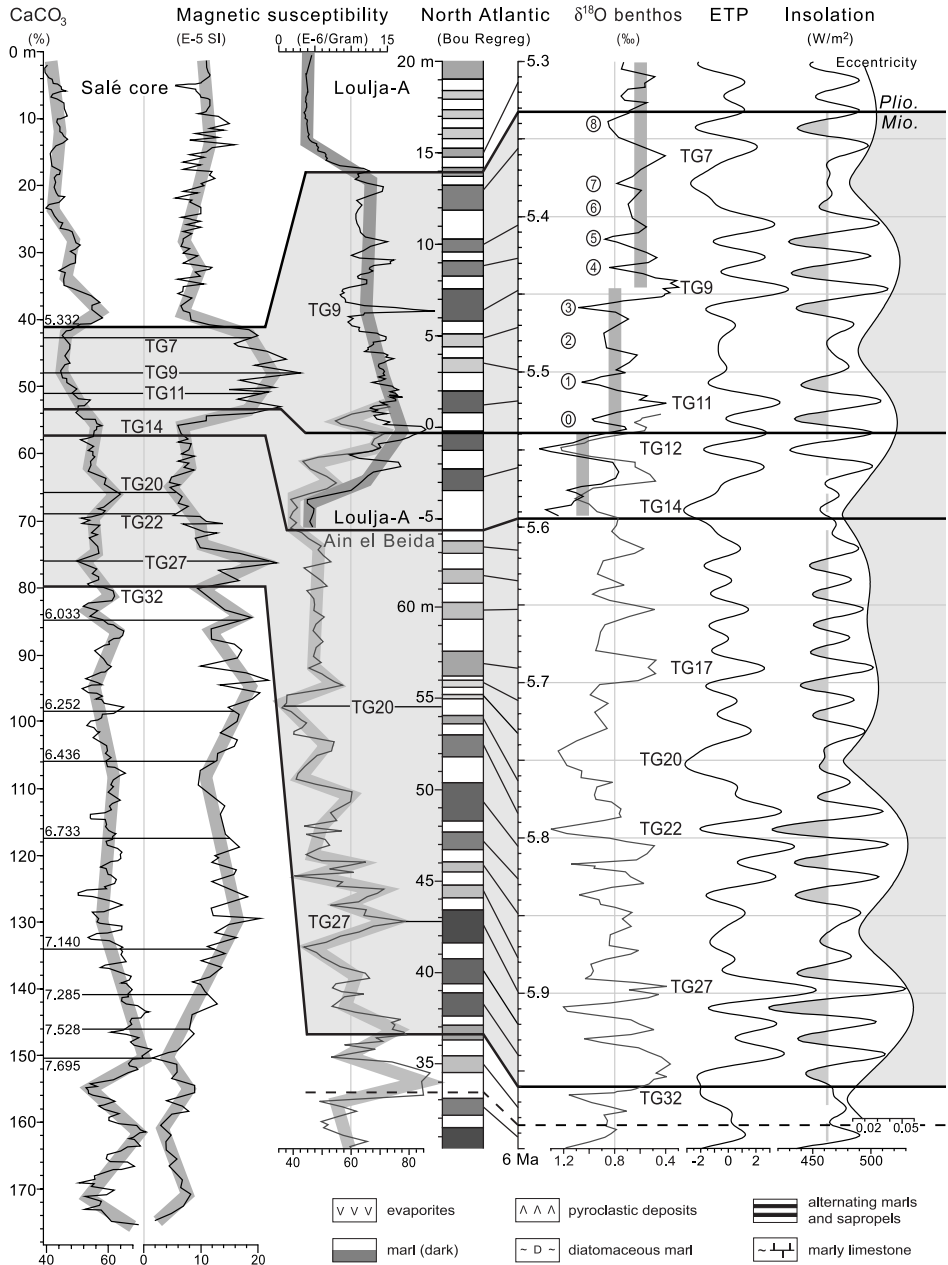
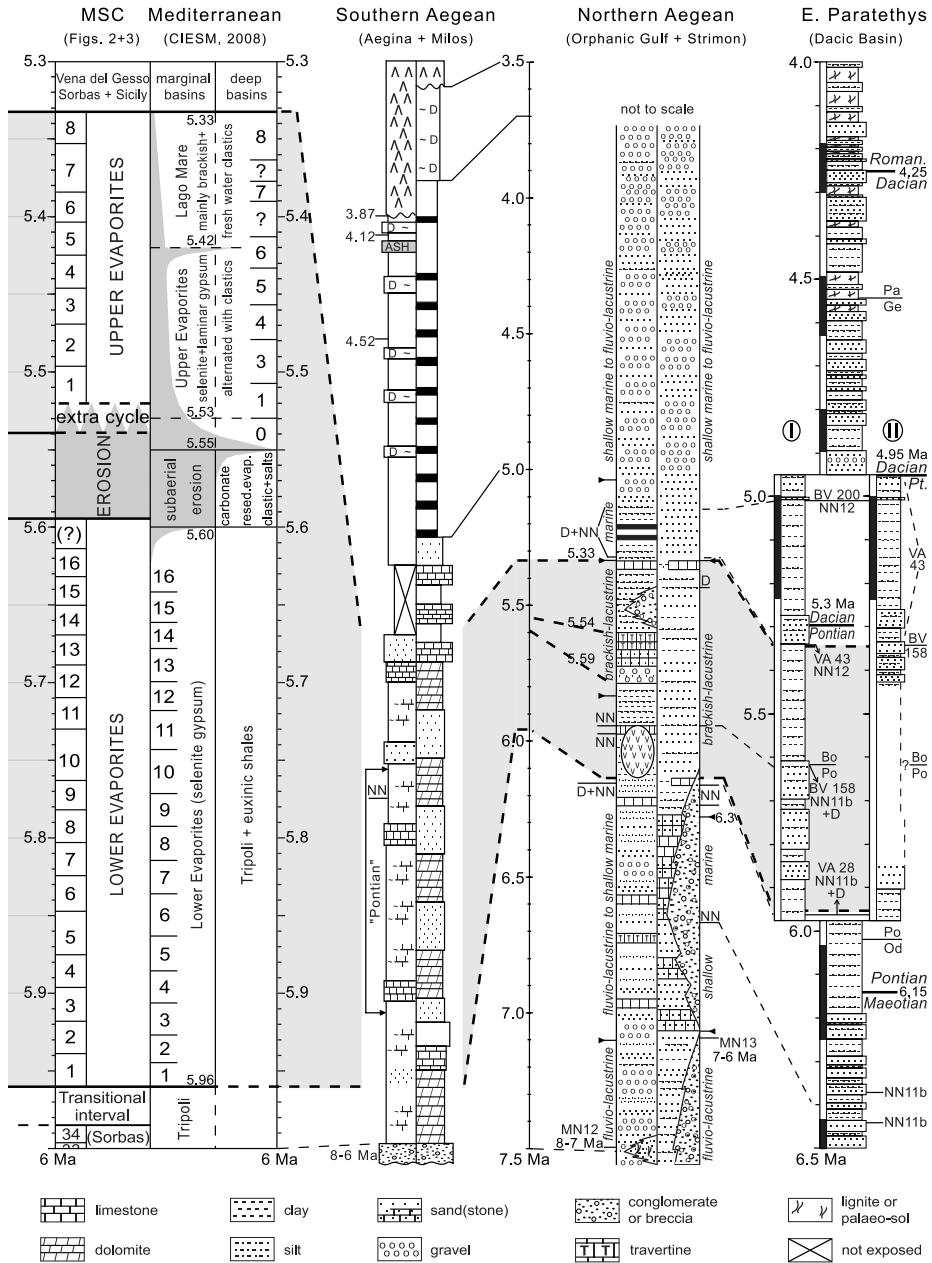


Figure 6.4. Chronology of Messinian salinity crisis (MSC) events in the Mediterranean (from Figs. 6.2, 6.3, and CIESM, 2008) in relation to  $\delta^{18}\text{O}$ , magnetic susceptibility, and carbonate records of the Bou Regreg sections (Atlantic coast, Morocco; Loulja-A: modified from Van der Laan et al., 2006-chapter 5; Ain el Beida: Van der Laan et al., 2005, in prep.; Salé: Hodell et al., 1994, with approximate positions of magnetic polarity reversals and marine isotope (TG) stages from Lourens et al., 2004, and Van der Laan et al., 2005, 2006-chapter 5; grey bars indicate averages) and compared to stratigraphic composite sections from the Aegean (Southern: Van Hinsbergen et al., 2004-chapter 4; Northern: Snel et al., 2006b-chapter 3) and Eastern Paratethys (modified from Snel et al.,



2006a-chapter 2). TG stages are according to the codification scheme of Shackleton et al. (1995). ETP, insolation, and eccentricity time series are from Laskar et al. (2004). Magnetic polarity reversals in the Dacic Basin composite section follow the ATNTS2004 (Lourens et al., 2004). 'D' and 'NN' indicate dinocyst and nannofossil levels. Also indicated are the inferred positions of boundaries between regional (sub) stages Od(essian), Po(rtferrian), Bo(sphorian), Ge(tian), Pa(rscovian), and Pontian (Pt). VA and BV refer to samples in sections Valea Vacii and Badislava. Note variable time and depth scales.

### 6.5.5 Magnetic susceptibility

The initial bulk magnetic susceptibility ( $\chi_{in}$ ) record of the Ain el Beida section is closely related to lithological variability and largely follows the 100-kyr eccentricity cycle (Van der Laan et al., in prep.). Low average  $\chi_{in}$ -values characterize the record from 6.3 to 6.0 Ma and between 5.85 and 5.55 Ma, while the intermediate interval displays high values, which at 5.9 Ma correspond to interglacial stage TG27; minimum values concur with glacial stages TG20 and TG14 during two 100-kyr eccentricity minima (Fig. 6.4). The top part, overlapping with the base of the Loulja-A record, reveals a rising trend that begins at 5.58 Ma and is most pronounced at 5.54 Ma, during the deglaciation after stage TG12. Marked deviations from the climatic trend occur especially at 5.99-5.98 Ma and at 5.96 Ma, around the (transition to the) base of the Lower Evaporites, at what time  $\chi_{in}$  reaches extreme magnitudes. The 5.99 Ma peak coincides with the base of the Sorbas Basin transitional interval and follows a strong negative shift of planktonic  $\delta^{13}C$  values at 6.0 Ma. Noticed by Van der Laan et al. (in prep.), this preliminary event may be caused by a sudden decrease of Mediterranean outflow water during the final closure of the Rifian Corridor (Benson et al., 1991; Krijgsman et al., 1999c).

As mentioned by Van der Laan et al. (2006-chapter 5), the record of the younger Loulja-A section shows a series of peak  $\chi_{in}$ -values nicely corresponding to the interval of the Mediterranean desiccation and succeeding Upper Evaporites. High values commence at the interglacial after stage TG14, reaching maxima of over  $20 \cdot 10^{-6}$  SI units per gram of untreated sediment (25% higher in dehydrated samples) between stages TG12 and TG11, coeval with the earliest optional onset of the Upper Evaporite at 5.54 Ma, and culminate at the base of the Pliocene. The spike at 6.3 m, in a thin layer relatively rich in Li, K, Fe, Ni, Zn, and Y (unpublished data, E. van der Laan), coincides with stage TG9. Low values of less than  $6 \cdot 10^{-6}$  SI units prevail from the base of the Pliocene upwards for at least another 400 kyr, covered in the Loulja-B section, making the anomalous values from the Upper Evaporite interval even more exceptional. These results resemble those from the parallel Salé drill core (Hodell et al., 1994; Photo 6.8c), where the highest  $\chi_{in}$ -values also occur during the Upper Evaporite interval (Fig. 6.4).

Possibly, analogous to the ~6 Ma event, circulation west of its then probably blocked entrance changed again during this sharply confined period of Mediterranean isolation, resulting in yet another relative increase of the magnetic mineral content in the sediment supply of the Bou Regreg area. It is conceivable that, following the restoration of Atlantic-Mediterranean water exchange at 5.33 Ma, renewed dilution suppressed the astronomically controlled  $\chi_{in}$ -signal again. Hodell et al. (1994) rejected variable dilution by nonmagnetic carbonate, claiming it showed only a very weak inverse correlation with carbonate content, and instead proposed a change in concentration or type of magnetic mineral within the terrigenous fraction, through diagenesis, as a possible cause for the low  $\chi_{in}$ -values in the 0-40, 55-75, and 150-175 m intervals. Nevertheless, trends are in general anti-parallel and, for example, a sudden (moderate) increase of the carbonate content across the Miocene-Pliocene boundary clearly concurs with the decrease of  $\chi_{in}$ -values. Van der Laan et al. (in prep.) demonstrate that the variations in the  $\chi_{in}$ -record of the Ain el Beida section related to the dominantly precession-controlled colour cycles are inversely related to the variations in carbonate content, and argued that increased terrigenous input causes a dilution of the carbonate signal. In addition, unless the diagenesis was somehow related to the changes in circulation, it would be quite a coincidence if local diagenesis twice affected all three Bou Regreg locations simultaneously, sparing exactly the 5.6-5.3 Ma interval. Alternatively, intensified mineral-laden runoff due to a temporarily wetter climate in the source region concurring with the 400-kyr eccentricity maximum around 5.45 Ma, which Rouchy and Caruso (2006) concluded for

the circum-Mediterranean peripheral mountain areas (see also Steenbrink et al., 2006), could have led to the high values in the Moroccan records. This would explain why the interval with higher  $\chi_{in}$ -values corresponds to the interval marked by the occurrence of thicker and more prominent reddish layers between 5.57 and 5.35 Ma. However, this provides no explanation why  $\chi_{in}$ -values remain high during this entire interval (i.e. including several 100-kyr eccentricity minima) and drop relatively abrupt across the Miocene-Pliocene boundary, partly independent of precession amplitude. Moreover, they remain low in the succeeding 400-kyr eccentricity maximum, contrary to the strongly sinusoidal PC-1 record (Fig. 6.3).

## 6.6 Biostratigraphic and paleoenvironmental considerations

### 6.6.1 Lower Evaporites

The erratic presence of low diversity nannofossil assemblages and rare cysts of open marine dinoflagellate species generally characterizes the fossil content of the Lower Evaporite samples. In the lower part of this interval in the Sorbas Basin and on Crete, relatively rich but oligospecific nannofossil assemblages are preserved (samples AQ5 and Gr 12.544; Table 6.1). This is consistent with the expected conditions in a restricted marine environment and in line with earlier faunal and floral observations from samples between the evaporite beds (Landini and Sorbini, 1989; Bertini et al., 1998; Saint-Martin et al., 2000; Goubert et al., 2001).

The cyclostratigraphically calibrated ages of two relatively diverse assemblages from the Sorbas Basin, estimated at 5.825 Ma and 5.805 Ma, coincide with the two high-amplitude insolation peaks and relatively light values in the open ocean  $\delta^{18}\text{O}$  record just before the prominent glacial stage TG22 (Fig. 6.4). Interestingly, the uppermost nannofossil-bearing level from the Sorbas Basin (sample AQ11) and the one in the Lower Evaporites of the Vena del Gesso Basin (sample AC 13) both correspond to the interglacial stage TG17 at 5.69 Ma. Furthermore, according to Bertini (2006), the only relatively diverse dinocyst assemblage in the latter location is present below the fourth gypsum bed, which concurs with the pronounced 5.9 Ma insolation maximum and stage TG27. I conclude, therefore, that the influx of normal marine water sufficiently increased during these stronger interglacials (and higher sea levels), thus overruling the concomitant influence of precession-controlled, relatively wet regional climate conditions, to give rise to slightly more favourable conditions for nanoplankton or dinoflagellate floras (Bertini et al., 1998) at least half way across the Mediterranean. This is in support of continuous or repetitive replenishment of this basin with normal marine water from the Atlantic, possibly even from the Indian Ocean via the Suez area (Fig. 6.1; Vai, 1997), which was required in any case to form the kilometre-thick Lower Evaporite deposits (Hsü et al., 1973; Krijgsman et al., 1999b; Meijer, 2006). In fact, Krijgsman and Meijer (2008) demonstrated that Atlantic-Mediterranean water exchange must have persisted across a relatively deep sill during the Lower Evaporite interval. Strontium isotope ratios of Lower Evaporite sediments provide additional evidence: these are similar to oceanic values and indicative of Atlantic water influx (Flecker and Ellam, 2006).

### 6.6.2 Upper Evaporites

Nannofossil assemblages from the Upper Evaporite and Lago Mare interval, although richer and more diverse than in the Lower Evaporites, are still overall poorer and less diverse than in the overlying Pliocene, and often include reworked Cretaceous to Neogene taxa. For instance in the samples of the Nijar and Caltanissetta basins, the occasional presence of *Reticulofenestra rotaria*

(top at 5.99 Ma, Lourens et al., 2004) is indicative of reworking. *Discoaster quinqueramus* (top at 5.537 Ma, Van der Laan et al., 2006-chapter 5) can be regarded as in situ in the Zakynthos and Kefalonia samples, in view of its age range, but its appearance in the younger levels of the Upper Evaporites in the Eraclea Minoa section (Table 6.1; Clauzon et al., 2005) probably originates from reworking as well.

Nevertheless, the occurrence of low-salinity indicators *Braarudosphaera bigelowii* and/or *Micrantholithus vesper* in samples from the Colombacci and Eraclea Minoa sections seems to reflect a brackish 'Lago Mare'-type environment, alternating on a precession scale with hypersaline conditions corresponding to the gypsum intervals of the latter locality. Ostracod studies by Bonaduce and Sgarrella (1999), for example, demonstrated such salinity fluctuations throughout the Upper Evaporites. However, only a few of the nannoplankton pentoliths are present and always together with normal marine species. Besides, also in stratigraphically adjacent sample levels of the Eraclea Minoa section, some dinoflagellate species are associated with rather hypersaline settings (Tables 6.1 and 6.2). In samples from the top part of the Upper Evaporites, directly below and above the gypsum of cycle 8, the high-salinity tolerating taxon *Homotryblum* even dominates the dinocyst assemblages, an observation shared with Londeix et al. (2007) and interpreted by these authors to indicate (only) a temporary tendency of basin restriction. At the base of this uppermost evaporite and in particular in the succeeding Arenazzolo sands, they additionally observed a second peak interval of the, in contrast, low-salinity species *Galeacysta etrusca*.

Based on the nannofossil data of this study alone, unambiguous evidence for a stressed marine environment, as the occasional dominance of floral assemblages by small reticulofenestrads and sphenoliths in the Lower Evaporites and in other (Sicilian) Upper Evaporite sections (Rouchy and Caruso, 2006; Wade and Bown, 2006) suggests, is lacking. Conversely, the presence of relatively rich floras, as in the basal samples from the Feos and Kalamaki Beach sections and in limited intervals below the gypsum beds of the Eraclea Minoa section (at ~5.5, 5.4, and 5.35 Ma, i.e.), should still be regarded with caution. Since dinocyst results from these intervals at first sight reflect marine conditions as well, a similar scenario as for the Lower Evaporites, involving continuous or repeated connections of the Mediterranean with the Atlantic Ocean, may seem likely. In contradiction, planktonic foraminifers from the Upper Evaporites of the Eraclea Minoa section exclusively are reworked late Tortonian to earliest Messinian faunas (pers. comm. F.J. Hilgen, 2002), which discredits the suggested in situ character of the other marine microfossils. The presence of fossil fish remains in the Lago Mare interval led Carnevale et al. (2008) to conclude that the marine refilling of the Mediterranean occurred well before the end of the Messinian. In contrast, the brackish-lacustrine paleoenvironmental indications of other (micro)fossil groups show that reworking is again possible (Roveri et al., 2008b), also since some of these fish taxa were found in the Lower Evaporites as well (Landini and Sorbini, 1989).

Concerning the problem of distinguishing between reworked and in situ fauna/flora, the discussion in Roveri et al. (2008a) on the Colombacci Formation in the Maccarone section, a lateral equivalent of the Vena del Gesso Basin sections, is illuminating and confirms the reworked origin of marine faunas in the upper Messinian unit (see also Roveri et al., 2008b; their Fig. 9). The authors furthermore argue that diversified nannofossil assemblages in this interval show a considerable degree of reworking and differ significantly from the richer Zanclean floras. Indeed, in the Maccarone section as well as in the Cusercoli and Gualdo sections of the Vena del Gesso Basin, the exclusive occurrence of *Triquetrorhabdulus rugosus* in Colombacci Formation samples and the marked presence of *Amaurolithus delicatus* in Early Pliocene beds are evident (Table 6.1). Moreover, the simultaneous *Scyphosphaera* proliferation in the latter two Vena del Gesso Basin



sections and in the Eraclea Minoa and Kalamaki Beach sections at the beginning of the Pliocene denotes the true restoration of the Mediterranean-Atlantic connection. Dinocyst results from the Maccarone section, similar to the Eraclea Minoa record, support this conclusion (Bertini, 2006). The post-evaporitic upper Messinian beds (Upper Evaporites) contain poorly diversified, non-diagnostic and clearly reworked marine taxa, dominated by the *Spiniferites ramosus* group and *Operculodinium* spp. (compare Table 6.2), which are followed by a low-salinity interval with *Galeacysta etrusca* that, at the base of the Pliocene, abruptly gives way to a highly diverse and rich assemblage consisting of open marine species. In addition, this biotic resemblance of the Arenazzolo and Colombacci formations in the Eraclea Minoa and Maccarone sections is an argument in favour of the Roveri and Manzi (2006) age model, if the onset of the hyposaline *G. etrusca* event in the Lago Mare interval has a chronostratigraphic implication and is not just a locally controlled paleoenvironmental phenomenon.

Pierre et al. (2006) put forward that all upper Messinian deposits along a Mediterranean transect similar to that presented here (Fig. 6.1) are devoid of autochthonous marine microfossils. The strata are either barren or contain reworked planktonic foraminifers (see also Rouchy et al., 2007), which is in stark contrast to the normal marine beds of the lowermost Pliocene. This demonstrates a rapid, basin-wide isochronous replacement of the continental or brackish Lago Mare environment at the end of the MSC through the inflow of Atlantic water at 5.33 Ma (Hsü et al., 1973, 1978; Iaccarino et al., 1999; Orszag-Sperber, 2006; Roveri et al., 2008b; Ryan, 2009). A comparable trend is followed by the Mediterranean strontium isotope ratios, which show maximum divergence from the oceanic curve in Upper Evaporite and Lago Mare sediments and return to oceanic values in the Pliocene (Flecker and Ellam, 2006). I therefore conclude that the presence of nannofossils and marine dinocysts in the Colombacci Formation and consequently in all other Upper Evaporite and Lago Mare deposits probably does not indicate in situ marine conditions, but should be explained by reworking or perseverance of floras in an isolated basin.

## 6.7 Constraints from the Aegean and Paratethys

### 6.7.1 Southern Aegean

On Aegina and Milos (Photos 6.10 and 6.11), an open marine environment existed only after ~5 Ma as a result of rapid subsidence (Van Hinsbergen et al., 2004-chapter 4). The sporadic nannofossil content of older, Miocene and lowermost Pliocene sediments consists of a small number of long ranging Neogene species. Messinian samples from Aegina do not contain nannofossils, except for two contiguous assemblages in a brackish water succession, part of which Rögl et al. (1991) described as the “Pontian” interval (Fig. 6.4; Photos 6.10b-c). One consists of only very small reticulofenestrads, which indicates stressed conditions; the other is slightly more diverse but, reminiscent of the Lower Evaporite assemblages of the Sorbas Basin and Crete, still dominated by small forms of *Reticulofenestra* and *Sphenolithus abies* (Rögl et al., 1991). The shallow, brackish water interval may at first glance appear to correspond to the Upper Evaporite and Lago Mare unit, which seems plausible considering the similarly shallow and hyposaline environmental character. In the Aegean, on the other hand, such predominantly non-marine conditions were not restricted to the youngest part of the MSC alone, as the age of ~6.3 Ma for the base of the brackish water Choumnikon Formation in the Strimon Basin illustrates (Snel et al., 2006b-chapter 3). Besides, Rögl et al. (1991) arrived at a more specific Portaferrian (middle Pontian) assignment for

the Aegina deposits, by means of its ostracod content, implying an age of ~6-5.6 Ma (Snel et al., 2006a-chapter 2).

However, the occurrence of *Ceratolithus acutus*, claimed by Rögl et al. (1991), would determine a maximum age of 5.35 Ma (Lourens et al., 2004), but this observation is disputable too (see also Roveri et al., 2008a), since ceratoliths and other biostratigraphic markers in general are often absent in latest Messinian records, especially in impoverished stress floras like this one. When present in the Upper Evaporite or Lago Mare interval, and therefore possibly reworked if not residual, these species are usually associated with rich and diversified nannofossil assemblages (Table 6.1). In a comparably marginal setting in the Northern Aegean, for example, *C. acutus* itself only appeared in rich and diversified assemblages from two Orphanic Gulf sections after the Early Pliocene re-establishment of open marine conditions (Snel et al., 2006b-chapter 3). It was found in a single sample from the Dacic Basin in the Eastern Paratethys, again in a relatively diverse assemblage in presumably the basal part of the Pliocene (Snel et al., 2006a-chapter 2). Rather than this Pliocene alternative (Clauzon et al., 2005), and in view of their typical oligospecific character, I prefer an age-assignment of the presumably in situ nannofossil assemblages and enclosing stratigraphic interval on Aegina to the Lower Evaporites, hence supporting the assignment of Rögl et al. (1991), but disregarding their *C. acutus* observation.

The Upper Evaporite interval, deposited when lowered Mediterranean water levels caused erosion of the margins, may thus be missing or discontinuously represented there. A more accurate correlation of the non- to shallow marine lower strata on Aegina and Milos to the MSC interval in other Mediterranean areas remains therefore difficult. Despite the regional consistency of the most obvious paleoenvironmental change, represented by the abrupt transition to open marine Pliocene successions, the relative sea level changes recorded on Aegina and Milos had a tectonic cause post-dating the 5.33 Ma flooding event (Van Hinsbergen et al., 2004-chapter 4).

### 6.7.2 Northern Aegean

Dinocysts from two Orphanic Gulf sections indicate normal marine conditions, but these palynomorphs are present in levels that probably are either older than ~6 Ma or younger than 5.33 Ma (Table 6.2). Nannofossils from the intermediate MSC interval are limited to a few samples from the top of a gypsum unit recorded in nearby sections (Fig. 6.4; Photo 6.12), which nevertheless contain remarkably diverse assemblages including *Amaurolithus* and *Discoaster* species. This leaves a largely non-marine interval for the remaining uppermost Messinian in the Orphanic Gulf area, apart from the stratigraphically inconclusive upper part of lateral subsection II of “Rema Marmara” (Snel et al., 2006b-chapter 3; Photo 6.3c).

The only sample with dinocysts having an age that corresponds to the MSC, comes from the bordering Strimon Basin (Photo 6.5), where nannofossils are virtually absent in beds younger than 6 Ma. The poorly diversified assemblage mainly consists of *Galeacysta etrusca*, resembling the dinocyst content of the Lago Mare interval in the Maccarone and Eraclea Minoa sections (Bertini, 2006; Londeix et al., 2007). This is in agreement with its position in the brackish water succession of the Choumnikon Formation beneath shallow marine Pliocene beds. The MSC interval is entirely represented by this non-marine unit in the presently landlocked and – relative to the Orphanic Gulf – probably also during the late Messinian and early Zanclean more marginal Strimon Basin. Earlier marine conditions, marked by the Dafni Formation, are confined in this basin to the first half of the Messinian. The later intra-MSC desiccation event between 5.59 and 5.54 Ma, probably recorded in the Orphanic Gulf area (Fig. 6.4), had no apparent effect on the Strimon Basin stratigraphy, where no unconformity was observed within the brackish

water Choumnikon Formation nor below the overlying shallow marine Pliocene (Snel et al., 2006b-chapter 3).

Moreover, instead of flooding a hitherto empty basin (Clauzon et al., 1996), the Miocene-Pliocene boundary in these shallow, marginal basins in the Northern Aegean corresponds rather to a changeover from brackish to marine conditions: a scenario that has been envisaged for the entire Mediterranean (Iaccarino and Bossio, 1999; Roveri and Manzi, 2006; Rouchy et al., 2007). However, Ryan (2009) argued that the main lake/sea water body in the central parts of the Mediterranean, as opposed to some marginal basins, never reached its pre-desiccation level until after the Pliocene flooding. This conclusion questions the possibility of migration of marine organisms from the Atlantic Ocean into the Mediterranean and Paratethys satellite basins.

### 6.7.3 Eastern Paratethys

On the other hand, Clauzon et al. (2005) concluded that the MSC, and the desiccation event in particular, left the central part of the Dacic Basin in the Eastern Paratethys unaffected. They consequently interpreted this location as a perched lake setting with continuous sedimentation throughout the Miocene-Pliocene boundary interval, possibly fed by the Danube (Gillet et al., 2007). Fresh to brackish water dinoflagellate assemblages, including the prominently present *Galeacysta etrusca*, dominate two middle Pontian (Portaferrian) samples from this area (VA 28, BV 158; Table 6.2). Excluding the very rare presence of small benthos in sample VA 28, appearing together with scarce marine dinocysts, foraminifers are absent in all seven sections studied (Snel et al., 2006a-chapter 2). In contrast, nannofossils constitute one rich and diverse assemblage (VA 28) and a second, poorer but still diversified assemblage (BV 158), in itself indicative of normal marine conditions. Two younger assemblages from these localities, of late Pontian (Bosphorian; VA 43) and early Dacian (Getian; BV 200) age, are similarly diverse, thereby feeding the suggestion that marine incursions occasionally reached the otherwise non-marine basin during the latest Miocene and earliest Pliocene. Clauzon et al. (2005) recovered nannofossils and dinocysts from time-equivalent strata in nearby sections and arrived at the same conclusion.

This interpretation is problematic for the two levels that correlate to the MSC interval. Age-diagnostic marker species of *Amaurolithus* and *Discoaster*, which are present in Portaferrian samples VA 28 and BV 158 and in assemblages associated with the Orphanic Gulf evaporites, are generally absent in Lower Evaporite samples of other Mediterranean sections, where in situ (stressed) marine assemblages reveal a lower diversity instead (Table 6.1). It is hard to envision how relatively rich nannoplankton floras, reaching the more remote Aegean and Paratethys, bypassed unfavourable conditions in the Mediterranean without leaving a comparable record. Furthermore, the dinocyst assemblages from the same two samples do not reflect marine conditions, as opposed to those in Mediterranean samples (Table 6.2), but rather reflect the regional lacustrine conditions. Taking the stratigraphic range of *A. delicatus* into account (from 7.22 Ma; Lourens et al., 2004), reworking of marine Maeotian sediments containing nannofossils (MăruŃeanu and Papaianopol, 1998) in a non-marine environment could explain the co-occurrences of nannofossil species denoting Zone NN11 and predominantly fresh to brackish water dinocysts in the Pontian. According to Stoica et al. (2007) and their ostracod biochronology (unpublished data, M. Stoica), the upper Maeotian and lower and middle Pontian are all missing in the Bădislava section. Hence, we find upper Pontian (Bosphorian) directly on top of middle Maeotian deposits and reworking of nannofossils.

However, the nannofossil assemblages with NN12 markers in uppermost Pontian and Dacian samples (VA 43 and BV 200) require a different provenance. In keeping with the uncertainty limits of the chronostratigraphic scheme of Snel et al. (2006a-chapter 2), these latter levels with

possibly in situ marine floras may correlate to the lower Pliocene. Similarly, if reworking was not involved, the older Portaferrian level (VA 28) may have an age predating the onset of the Lower Evaporites, whereas the sample at the Portaferrian-Bosphorion boundary (BV 158) may be ~5.6 Ma or older, consistent with the hypothesis of an interval of Mediterranean isolation between 5.59 and 5.33 Ma (Fig. 6.4).

Orszag-Sperber (2006) rightly drew attention to discrepancies with the age model of Vasiliev et al. (2004), who arrived at ages of  $5.9 \pm 0.1$  Ma and  $4.9 \pm 0.1$  Ma for the lower and upper boundaries of the Pontian stage in the eastern Carpathian foredeep, respectively. These authors subsequently calibrated the Pontian boundaries in the southern Carpathian foredeep at 5.8 and 4.8 Ma, partly based on data from the Bădislava section (Vasiliev et al., 2005). Variable interpretations of the (local) appearances and development of mollusc taxa, used for stage boundary definitions, mainly led to the different solutions of Vasiliev et al. (2005) and Snel et al. (2006a-chapter 2). Firstly, the Maeotian-Pontian boundary interval, recorded in other sections in a normal polarity zone (Snel et al., 2006a-chapter 2), is incomplete in the Bădislava section, since the lower Pontian (Odessian) substage is not represented there (pers. comm. I. Papaianopol, 1998). Stoica et al. (2007) confirmed this observation and furthermore concluded, as mentioned above, that the Portaferrian was missing as well, resulting in a Maeotian-Bosphorion contact and leaving a potential ~1 Myr gap that may encompass a substantial part of the Messinian. Secondly, they emphasized that the Pontian-Dacian boundary is difficult to determine, because the Bosphorion and Getian mollusc assemblages show a gradual transition. On the other hand, their data from the eastern Carpathian foredeep are in excellent agreement with the 4.8 Ma for the Pontian-Dacian boundary. Furthermore, unpublished results, including detailed ostracod biochronology in the eastern Carpathian foredeep and the Black Sea (pers. comm. W. Krijgsman, 2009), show an age for the Maeotian-Pontian boundary at the normal to reversed polarity reversal from chron C3An.1n to C3r at 6.033 Ma (Lourens et al., 2004). Also Snel et al. (2006a-chapter 2) initially assumed an age of  $4.95 \pm 0.05$  Ma for the Pontian-Dacian boundary (option II; Fig. 6.4), recognised at 364 m in the same Bădislava section (pers. comm. I. Papaianopol, 1996). Re-evaluation of the biostratigraphy (pers. comm. R. Macalet, 2000), acknowledged by I. Papaianopol (pers. comm., 2000), subsequently led to the published position of 135 m for this boundary (option I; Fig. 6.4).

Irrespective of the nomenclature, the unambiguous magnetostratigraphic results of both research groups provide similar ages for the higher stratigraphic levels in the Bădislava section. The uppermost level with nannofossils, being characteristic of Zone NN12 and having an estimated age of ~5 Ma (BV 200), would be designated in option II to the uppermost Pontian, instead of Dacian (option I). In accordance with Stoica et al. (2007) and adopting a Bosphorion age for the major part of the Bădislava section (option II), sample level BV 158 could alternatively have a much younger age than the ~5.6 Ma of Snel et al. (2006a-chapter 2). Considering this alternative, the sandy sediments of the lower 150 m of the section may represent less time than the next, relatively fine-grained, 200 m interval that incorporates the normal polarity Thvera chron with a duration of 238 kyr (Lourens et al., 2004). The nannofossils at 64 m in BV 158 then may correspond to the 5.33 Ma Pliocene flooding (Fig. 6.4). Specimens of the Zone NN11 marker species *Discoaster quinqueramus* appeared in the earliest Pliocene samples from the “Rema Marmara” section in the Orphanic Gulf area, there considered to be reworked (Snel et al., 2006b-chapter 3). The presence of *D. cf. D. quinqueramus* in sample BV 158 may similarly be explained by reworking, which in that case would probably be the case for the entire assemblage, or it may be considered as an incorrect observation, to be consistent with option II. The Bosphorion clays with NN12 nannofossils (VA

43), tentatively placed at 5.33 Ma near the top of the Pontian stage (option I), consequently may have a slightly younger age as well, up to 4.95 Ma.

In the early and middle Pontian (the latter corresponding partly to the Lower Evaporite interval), for what time Rögl et al. (1991) still proposed Aegean-Paratethys connections, marine ingressions thus possibly caused nannoplankton appearances on Aegina and in the Orphanic Gulf area. This would support the scenario of a filled Mediterranean prior to 5.59 Ma. During the Upper Evaporite interval, isolation from the open ocean would occur, subsequently resulting in a desiccation event in parts of the Paratethys as well (Hsü and Giovanoli, 1979; Clauzon et al., 2005; Gillet, 2007). In line with option II (Fig. 6.4), a longer isolation interval of the Paratethys, or at least of the central part of the Dacic Basin, cannot be excluded. In consideration of the different nature of the Northern Aegean and Dacic Basin nannofossil assemblages with respect to those from Aegina and from assumed contemporaneous proper Lower Evaporite samples, reworking may explain coincidental observations in samples from the former two areas that are approximately time-equivalent to the MSC. Nevertheless, both the earlier and later occurrence of NN11 and NN12 nannofossils in strata in the Dacic Basin that correlate to the (early) Messinian and Zanclean, respectively, necessitate in my opinion a gateway through the Dardanelles (Fig. 6.1) or to the west of this area (Clauzon et al., 2005; CIESM, 2008).

## 6.8 Conclusions

In summary, a combination of (long-term) tectonic closure of the Atlantic gateway and astronomically controlled climate changes led to stepwise isolation of the Mediterranean from the open ocean and culminated in the MSC. Detailed comparison of Atlantic benthic stable oxygen isotope records and of Mediterranean evaporite successions using high-resolution tuned age models reveals that the onset of the MSC at ~5.96 Ma, marked by the base of the Lower Evaporites, is predominantly related to regional tectonics and less to glacio-eustatic control. However, this transition also corresponds to the end of a 100- and 400-kyr eccentricity minimum, suggesting an additional control by the influence of the precession-eccentricity combination on regional climate. Marine dinocysts and (oligospecific) nannofossil assemblages present in between gypsum beds of the precession-controlled Lower Evaporites cycles indicate restricted though full basin conditions and ongoing replenishment with oceanic water. Progressive tectonic isolation of the Mediterranean in combination with glacio-eustatic sea level lowering associated with the major glacial stages TG14 and TG12, at 5.59 and 5.54 Ma, resulted in a basin-wide desiccation event. Related to the subsequent TG11 interglacial, depositional processes in the Mediterranean resumed, while eccentricity and superimposed precession-modulated climate changes continued to control sedimentary cyclicity. Microfossils and strontium isotope data from this Upper Evaporite and Lago Mare interval and time-equivalent susceptibility records from the adjacent part of the Atlantic signify that the Mediterranean remained an isolated basin, probably periodically subdivided and with reduced or fluctuating water level and salinity. Finally, the abrupt restoration of open marine conditions, illustrated by an isochronous invasion of rich and highly diverse microfaunas and (nannoplankton) floras, determined the end of the MSC at 5.33 Ma. Erosion and/or geodynamic activity in the Gibraltar area rather than a glacio-eustatic sea level rise caused this Pliocene flooding event.

The effects of the MSC phases of isolation and desiccation on marginal Mediterranean basins were variable. Shallow areas in the Southern Aegean experienced a marine flooding caused by

regional tectonics well after the beginning of the Pliocene. A brackish water paleoenvironment dominated the Northern Aegean Strimon Basin from 6.3 Ma onward, whereas a 'standard' MSC sequence of evaporites and non-marine deposits is present along the Orphanic Gulf. The Miocene-Pliocene boundary is marked in both areas by a rapid salinity change with water levels remaining presumably constant. Influxes of marine water intermittently reached the Eastern Paratethys in the early Messinian and in the Pliocene. During the (second half of the) MSC, this brackish to lacustrine realm was isolated from the open ocean.

## Acknowledgements

Frits Hilgen, Wout Krijgsman, Jan-Willem Zachariasse, and Johan Meulenkamp are kindly thanked for their helpful comments and for critically reviewing (much) earlier versions of the manuscript. Anne Fortuin, Frits Hilgen, Wout Krijgsman, Jan-Willem Zachariasse, Douwe van Hinsbergen, Rink Kruk, and Frans Bronneberg are gratefully acknowledged for skilful sampling efforts in the Sorbas, Nijar, and Vena del Gesso basins, and on Sicily, Corfu, Kefalonia, Zakynthos, and Crete. Geert Ittmann, Gerrit van 't Veld, Ankie van Steenbergen, Jan van Tongeren, and Natasja Welters are kindly thanked for their invaluable expertise and assistance with foraminifer, nannofossil, and dinocyst sample and slide preparation. Marjolein Boonstra, Tom Mullender, Piet-Jan Verplak, Wil den Hartog, Tom van Hinte, Douwe van Hinsbergen, Rink Kruk, Kees Hordijk, and Hemmo Abels generously provided logistical and technical support.

This work was initially conducted under the programme of the Netherlands Research School of Sedimentary Geology (NSG). The Netherlands Research Centre for Integrated Solid Earth Science (ISES) provided funds for visiting research fellowships.

## References

- Aguirre, J., Sánchez-Almazo, I.M., 2004. The Messinian post-evaporitic deposits of the Gafares area (Almeria-Nijar basin, SE Spain). A new view of the "Lago-Mare" facies. *Sedimentary Geology* 168, 71-95. doi:10.1016/j.sedgeo.2004.03.004.
- Barbieri, R., Ori, G.G., 2000. Neogene palaeoenvironmental evolution in the Atlantic side of the Rifian Corridor (Morocco). *Palaeogeography, Palaeoclimatology, Palaeoecology* 163, 1-31. doi:10.1016/S0031-0182(00)00100-0.
- Bartol, M., Pavšič, J., Dobnikar, M., Bernasconi, S.M., 2008. Unusual *Braarudosphaera bigelowii* and *Micrantholithus vesper* enrichment in the Early Miocene sediments from the Slovenian Corridor, a seaway linking the Central Paratethys and the Mediterranean. *Palaeogeography, Palaeoclimatology, Palaeoecology* 267, 77-88. doi:10.1016/j.palaeo.2008.06.005.
- Benda, L., Jonkers, H.A., Meulenkamp, J.E., Steffens, P., 1979. Biostratigraphic correlations in the Eastern Mediterranean Neogene: 4. Marine microfossils, sporomorphs and radiometric data from the lower Pliocene of Aghios Thomas, Aegina, Greece. *Newsletters on Stratigraphy* 8, 61-69.
- Benson, R.H., Rakic-El Bied, K., Bonaduce, G., 1991. An important current reversal (influx) in the Rifian corridor (Morocco) at the Tortonian-Messinian boundary: the end of Tethys Ocean. *Paleoceanography* 6, 165-192. doi:10.1029/90PA00756.

- Bertini, A., 1994. Messinian-Zanclean vegetation and climate in North-Central Italy. *Historical Biology* 9, 3-10. doi: 10.1080/10292389409380483.
- Bertini, A., 2006. The Northern Apennines palynological record as a contribute for the reconstruction of the Messinian palaeoenvironments. *Sedimentary Geology* 188-189, 235-258. doi:10.1016/j.sedgeo.2006.03.007.
- Bertini, A., Corradini, D., Suc, J.-P., 1995. On *Galeacysta Etrusca* and the connections between the Mediterranean and the Paratethys (abstracts of the X<sup>th</sup> RCMNS Congress, Bucharest). *Romanian Journal of Stratigraphy* 76 (Suppl. 7, vol. 1), 141-142.
- Bertini, A., Londeix, L., Maniscalco, R., Di Stefano, A., Suc, J.-P., Clauzon, G., Gautier, F., Grasso, M., 1998. Paleobiological evidence of depositional conditions in the Salt Member, Gessoso-Solfifera Formation (Messinian, Upper Miocene) of Sicily. *Micropaleontology* 44 (4), 413-433.
- Bonaduce, G., Sgarrella, F., 1999. Paleocological interpretation of the latest Messinian sediments from southern Sicily (Italy). *Memorie della Società Geologica Italiana* 54, 83-91.
- Bramlette, M.N., Sullivan, F.R., 1961. Coccolithophorids and related nannoplankton of the early Tertiary in California. *Micropaleontology* 7 (2), 129-188.
- Braune, K., Fabricius, F., Heimann, K.O., 1973. Sedimentation and facies of Late Miocene strata on Cephalonia (Ionian Islands, Greece). In: Drooger, C.W., Broekman, J.A., Hageman, J., Hantelmann, J.J., Marks, J., Meulenkamp, J.E., Schmidt, R.R. (Eds.), *Messinian Events in the Mediterranean*, Volume Geodynamics Scientific Report 7, *Verhandelingen van de Koninklijke Nederlandse Akademie van Wetenschappen*, Utrecht, pp. 192-201.
- Carnevale, G., Longinelli, A., Caputo, D., Barbieri, M., Landini, W., 2008. Did the Mediterranean marine reflooding precede the Mio-Pliocene boundary? Paleontological and geochemical evidence from upper Messinian sequences of Tuscany, Italy. *Palaeogeography, Palaeoclimatology, Palaeoecology* 257, 81-105. doi:10.1016/j.palaeo.2007.09.005.
- CIESM, 2008. The Messinian Salinity Crisis from mega-deposits to microbiology – A consensus report. In: Briand, F. (Ed.), *CIESM Workshop Monographs* 33, Monaco, pp. 1-168.
- Cita, M.B., Ryan, W.B.F., 1978. Messinian erosional surfaces in the Mediterranean. *Marine Geology* 27, 193-366. doi:10.1016/0025-3227(78)90031-2.
- Clauzon, G., Suc, J.-P., Gautier, F., Berger, A., Loutre, M.-F., 1996. Alternate interpretation of the Messinian salinity crisis: Controversy resolved? *Geology* 24 (4), 363-366. doi:10.1130/0091-7613(1996)024<0363: AIOTMS>2.3.CO;2.
- Clauzon, G., Suc, J.-P., Popescu, S.-M., Mărușeanu, M., Rubino, J.-L., Marinescu, F., Melinte, M.C., (2005). Influence of Mediterranean sea-level changes on the Dacic Basin (Eastern Paratethys) during the late Neogene: the Mediterranean Lago Mare facies deciphered. *Basin Research* 17, 437-462. doi:10.1111/j.1365-2117.2005.00269.x.
- Corradini, D., Biffi, U., 1988. Étude des Dinokystes à la limite Messinien-Pliocène dans la coupe Cava Serredi, Toscane, Italie. *Bulletin des Centres de Recherches Exploration-Production Elf-Aquitane* 12 (1), 221-236.
- DeCelles, P.G., Cavazza, W., 1995. Upper Messinian conglomerates in Calabria, southern Italy: Response to orogenic wedge adjustment following Mediterranean sea-level changes. *Geology* 23, 775-778. doi:10.1130/0091-7613(1995)023<0775:UMCICS>2.3.CO;2.
- Decima, A., Sprovieri, R., 1973. Comments on Late Messinian microfaunas in several sections from Sicily. In: Drooger, C.W., Broekman, J.A., Hageman, J., Hantelmann, J.J., Marks, J., Meulenkamp, J.E., Schmidt, R.R. (Eds.), *Messinian Events in the Mediterranean*, Volume

- Geodynamics Scientific Report 7, Verhandelingen van de Koninklijke Nederlandse Akademie van Wetenschappen, Utrecht, pp. 229-234.
- Decima, A, Wezel, F.C., 1971. Osservazioni sulle evaporiti messiniane della Sicilia centro-meridionale. *Rivista Mineralogica Siciliana* anno 22 (nn. 130-132), 172-187.
- Dybkjær, K., 2004. Morphological and abundance variations in *Homotryblidium*-cyst assemblages related to depositional environments; uppermost Oligocene-Lower Miocene, Jylland, Denmark. *Palaeogeography, Palaeoclimatology, Palaeoecology* 206, 41-58. doi:10.1016/j.palaeo.2003.12.021.
- Flecker, R., Ellam, R.M., 2006. Identifying Late Miocene episodes of connection and isolation in the Mediterranean-Paratethys realm using Sr isotopes. *Sedimentary Geology* 188-189, 189-203. doi:10.1016/j.sedgeo.2006.03.005.
- Fortuin, A.R., Krijgsman, W., 2003. The Messinian of the Nijar Basin (SE Spain): sedimentation, depositional environments and paleogeographic evolution. *Sedimentary Geology* 160, 213-242. doi:10.1016/S0037-0738(02)00377-9.
- Gillet, H., Lericolais, G., Réhault, J.-P., 2007. Messinian event in the Black Sea: Evidence of a Messinian erosional surface. *Marine Geology* 244, 142-165. doi:10.1016/j.margeo.2007.06.004.
- Goubert, E., Néraudeau, D., Rouchy, J.M., Lacour, D., 2001. Foraminiferal record of environmental changes; Messinian of the Los Yesos area (Sorbas Basin, SE Spain). *Palaeogeography, Palaeoclimatology, Palaeoecology* 175, 61-78. doi:10.1016/S0031-0182(01)00386-8.
- Govers, R., 2009. Choking the Mediterranean to dehydration: The Messinian salinity crisis. *Geology* 37, 167-170. doi:10.1130/G25141A.1.
- Govers, R., Meijer, P., Krijgsman, W., 2009. Regional isostatic response to Messinian Salinity Crisis events. *Tectonophysics* 463, 109-129. doi:10.1016/j.tecto.2008.09.026.
- Hilgen, F.J., Krijgsman, W., Langereis, C.G., Lourens, L.J., Santarelli, A., Zachariasse, W.J., 1995. Extending the astronomical (polarity) time scale into the Miocene. *Earth and Planetary Science Letters* 136, 495-510. doi:10.1016/0012-821X(95)00207-S.
- Hodell, D.A., Benson, R.H., Kent, D.V., Boersma, A., Rakic-El Bied, K., 1994. Magnetostratigraphic, biostratigraphic, and stable isotope stratigraphy of an Upper Miocene drill core from the Salé Briqueterie (northwest Morocco): A high-resolution chronology for the Messinian stage. *Paleoceanography* 9, 835-855. doi:10.1029/94PA01838.
- Hodell, D.A., Curtis, J.H., Sierro, F.J., Raymo, M.E., 2001. Correlation of late Miocene to early Pliocene sequences between the Mediterranean and North Atlantic. *Paleoceanography* 16 (2), 164-178. doi:10.1029/1999PA000487.
- Hsü, K.J., Giovanoli, F., 1979. Messinian event in the Black Sea. *Palaeogeography, Palaeoclimatology, Palaeoecology* 29, 75-93. doi:10.1016/0031-0182(79)90075-0.
- Hsü, K.J., Cita, M.B., Ryan, W.B.F., 1973. The origin of the Mediterranean evaporites. *Initial Reports of the Deep Sea Drilling Project* 42, 1203-1231. doi:10.2973/dsdp.proc.13.143.1973.
- Hsü, K.J., Montadert, L., Bernouilli, D., Cita, M.B., Erickson, A., Garrison, R.E., Kidd, R.B., Mélières, F., Müller, C., Wright, R., 1978. History of the Mediterranean salinity crisis. *Initial Reports of the Deep Sea Drilling Project* 42, 1053-1078. doi:10.2973/dsdp.proc.42-1.155.1978.
- Iaccarino, S.M., Castradori, D., Cita, M.B., Di Stefano, E., Gaboardi, S., McKenzie, J.A., Spezzaferri, S., Sprovieri, R., 1999. The Miocene-Pliocene boundary and the significance of



- the earliest Pliocene flooding in the Mediterranean. *Memorie della Società Geologica Italiana* 54, 109-131.
- Kouli, K., Brinkhuis, H., Dale, B., 2001. *Spiniferites cruciformis*: a fresh water dinoflagellate cyst? *Review of Palaeobotany and Palynology* 113, 273-286. doi:10.1016/S0034-6667(00)00064-6.
- Krijgsman, W., Meijer, P.Th., 2008. Depositional environments of the Mediterranean “Lower Evaporites” of the Messinian salinity crisis: Constraints from quantitative analyses. *Marine Geology* 253, 73-81. doi:10.1016/j.margeo.2008.04.010.
- Krijgsman, W., Hilgen, F.J., Marabini, S., Vai, G.B., 1999a. New paleomagnetic and cyclostratigraphic age constraints on the Messinian of the Northern Apennines (Vena del Gesso Basin, Italy). *Memorie della Società Geologica Italiana* 54, 25-33.
- Krijgsman, W., Hilgen, F.J., Raffi, I., Sierro, F.J., Wilson, D.S., 1999b. Chronology, causes and progression of the Messinian salinity crisis. *Nature* 400, 652-655. doi:10.1038/23231.
- Krijgsman, W., Langereis, C.G., Zachariasse, W.J., Boccaletti, M., Moratti, G., Gelati, R., Iaccarino, S.M., Papani, G., Villa, G., 1999c. Late Neogene evolution of the Taza-Guercif basin (Rifian Corridor, Morocco) and implications for the Messinian salinity crisis, *Marine Geology* 153, 147-160. doi:10.1016/S0025-3227(98)00084-X.
- Krijgsman, W., Fortuin, A.R., Hilgen, F.J., Sierro, F.J., 2001. Astrochronology for the Messinian Sorbas Basin (SE Spain) and orbital (precessional) forcing for evaporite cyclicity. *Sedimentary Geology* 140 (1-2), 43-60. doi:10.1016/S0037-0738(00)00171-8.
- Krijgsman, W., Gaboardi, S., Hilgen, F.J., Iaccarino, S.M., De Kaenel, E., Van der Laan, E., 2004. Revised astrochronology for the Ain el Beida section (Atlantic Morocco): No glacio-eustatic control for the onset of the Messinian Salinity Crisis. *Stratigraphy* 1 (1), 87-101.
- Landini, W., Sorbini, F., 1989. Ichthyofauna of the evaporitic Messinian in the Romagna and Marche regions. *Bollettino della Società Paleontologica Italiana* 28 (2-3), 287-293.
- Laskar, J., Robutel, P., Joutel, F., Gastineau, M., Correia, A., Levrard, B., 2004. A long-term numerical solution for the insolation quantities of the Earth. *Astronomy and Astrophysics* 428 (1), 261-285. doi: 10.1051/0004-6361:20041335.
- Loget, N., Van Den Driessche, J., 2006. On the origin of the Strait of Gibraltar. *Sedimentary Geology* 188-189, 341-356. doi:10.1016/j.sedgeo.2006.03.012.
- Londeix, L., Benzakour, M., Suc, J.-P., Turon, J.-L., 2007. Messinian palaeoenvironments and hydrology in Sicily (Italy): The dinoflagellate cyst record. *Geobios* 40, 233-250. doi:10.1016/j.geobios.2006.12.001.
- Lourens, L.J., Hilgen, F.J., Zachariasse, W.J., Van Hoof, A.A.M., Antonarakou, A., Vergnaud-Grazzini, C., 1996. Evaluation of the Pliocene to early Pleistocene astronomical time scale. *Paleoceanography* 11, 391-413. doi:10.1029/96PA01125.
- Lourens, L.J., Hilgen, F.J., Laskar, J., Shackleton, N.J., Wilson, D., 2004. The Neogene Period. In: Gradstein, F.M., Ogg, J.G., Smith, A.G. (Eds.), *A geologic time scale 2004*. Cambridge University Press, Cambridge, pp. 409-440.
- Manzi, V., Lugli, S., Roveri, M., Schreiber, B.C., 2009. A new facies model for the Upper Gypsum of Sicily (Italy): chronological and palaeoenvironmental constraints for the Messinian salinity crisis in the Mediterranean. *Sedimentology* 56 (7), 1937-1960. doi:10.1111/j.1365-3091.2009.01063.x.
- Marret, F., Zonneveld, K., 2003. Atlas of modern organic-walled dinoflagellate cyst distribution. *Review of Palaeobotany and Palynology* 125, 1-200. doi:10.1016/S0034-6667(02)00229-4.

- Martín-Suárez, E., Freudenthal, M., Krijgsman, W., Fortuin, A.R., 2000. On the age of the continental deposits of the Zorreras Member (Sorbas Basin, SE Spain). *Geobios* 33 (4), 505-512. doi:10.1016/S0016-6995(00)80084-4.
- Mărunțeanu, M., Papaianopol, I., 1998. Mediterranean calcareous nannoplankton in the Dacic Basin. *Romanian Journal of Stratigraphy* 78, 115-121.
- Meijer, P.Th., 2006. A box model of the blocked-outflow scenario for the Messinian Salinity Crisis. *Earth and Planetary Science Letters* 248, 471-479. doi:10.1016/j.epsl.2006.06.013.
- Norman, S.E., Chase, C.G., 1986. Uplift of the shores of the western Mediterranean due to Messinian desiccation and flexural isostasy. *Nature* 322, 450-451. doi:10.1038/322450a0.
- Orszag-Sperber, F., 2006. Changing perspectives in the concept of “Lago-Mare” in Mediterranean Late Miocene evolution. *Sedimentary Geology* 188-189, 259-277. doi:10.1016/j.sedgeo.2006.03.008.
- Perch-Nielsen, K., 1985. Cenozoic calcareous nannofossils. In: Bolli, H.M., Saunders, J.B., Perch-Nielsen, K. (Eds.), *Plankton Stratigraphy*, Cambridge University Press, Cambridge, pp. 427-554.
- Pierre, C., Caruso, A., Blanc-Valleron, M.-M., Rouchy, J.M., Orszag-Sperber, F., 2006. Reconstruction of the paleoenvironmental changes around the Miocene-Pliocene boundary along a West-East transect across the Mediterranean. *Sedimentary Geology* 188-189, 319-340. doi:10.1016/j.sedgeo.2006.03.011.
- Raffi, I., Rio, D., 1979. Calcareous nannofossil biostratigraphy of DSDP Site 132, Leg 13 (Tyrrhenian Sea, Western Mediterranean). *Rivista Italiana di Paleontologia e Stratigrafia* 85, 127-172.
- Raffi, I., Mozzato, C., Fornaciari, E., Hilgen, F.J., Rio, D., 2003. Late Miocene calcareous nannofossil biostratigraphy and astrobiochronology for the Mediterranean region. *Micropaleontology* 49 (1), 1-26. doi:10.2113/49.1.1.
- Rögl, F., Bernor, R.L., Dermitzakis, M.D., Müller, C., Stancheva, M., 1991. On the Pontian Correlation in the Aegean (Aegina Island). *Newsletters on Stratigraphy* 24, 137-158.
- Rouchy, J.M., Caruso, A., 2006. The Messinian salinity crisis in the Mediterranean basin: A reassessment of the data and an integrated scenario. *Sedimentary Geology* 188-189, 35-67. doi:10.1016/j.sedgeo.2006.02.005.
- Rouchy, J.M., Caruso, A., Pierre, C., Blanc-Valleron, M.-M., Bassetti, M.A., 2007. The end of the Messinian salinity crisis: Evidence from the Chelif Basin (Algeria). *Palaeogeography, Palaeoclimatology, Palaeoecology* 254, 386-417. doi:10.1016/j.palaeo.2007.06.015.
- Roveri, M., Manzi, V., 2006. The Messinian salinity crisis: Looking for a new paradigm? *Palaeogeography, Palaeoclimatology, Palaeoecology* 238, 386-398. doi:10.1016/j.palaeo.2006.03.036.
- Roveri, M., Manzi, V., Ricci-Lucchi, F., Rogleli, S., 2003. Sedimentary and tectonic evolution of the Vena del Gesso Basin (Northern Apennines, Italy); implications for the onset of the Messinian salinity crisis. *Geological Society of America Bulletin* 115 (4), 387-405. doi:10.1130/0016-7606(2003)115<0387: SATEOT>2.0.CO;2.
- Roveri, M., Bertini, A., Cipollari, P., Cosentino, D., Di Stefano, A., Florindo, F., Gennari, R., Gliozzi, E., Grossi, F., Iaccarino, S., Lugli, S., Manzi, V., 2008a. Comment on “Earliest Zanclean age for the Colombacci and uppermost Di Tetto formations of the “latest Messinian” northern Apennines: New palaeoenvironmental data from the Maccarone section (Marche Province, Italy)” by Popescu et al. (2007), *Geobios* 40 (359-373). *Geobios* 41, 669-675. doi:10.1016/j.geobios.2008.01.002.

- Roveri, M., Bertini, A., Cosentino, D., Di Stefano, A., Gennari, R., Gliozzi, E., Grossi, F., Iaccarino, S., Lugli, S., Manzi, V., Taviani, M., 2008b. A high-resolution stratigraphic framework for the latest Messinian events in the Mediterranean area. *Stratigraphy* 5 (3-4), 323-342.
- Ruegg, G.J.H., 1964. Geologische onderzoeken in het bekken van Sorbas, S.E. Spanje. Internal Report Geological Institute, University of Amsterdam, 67 pp.
- Ruggieri, G., 1967. The Miocene and later evolution of the Mediterranean sea. In: Adams, C.G., Ager, D.V. (Eds.), *Aspects of Tethyan biogeography*. Systematics Association Publication 7, Oxford, U.K., pp. 283-290.
- Ryan, W.B.F., 2009. Decoding the Messinian salinity crisis. *Sedimentology* 56 (1), 95-136. doi:10.1111/j.1365-3091.2008.01031.x.
- Saint-Martin, J.-P., Néraudeau, D., Lauriat-Rage, A., Goubert, E., Secrétan, S., Babinot, J.-F., Boukli-Hacene, S., Pouyet, S., Lacour, D., Pestrea, S., Conesa, G., 2000. La faune interstratifiée dans les gypses messiniens de Los Yesos (bassin de Sorbas, SE Espagne): implications. *Geobios* 33 (5), 637-648.
- Schreiber, B.C., 1997. Messinian and younger deposition in the southern Caltanissetta Basin: Stop 5, Eraclea Minoa. In: Grasso, M., Lentini, F. (Eds.), *Neogene basins of the Mediterranean region: controls and correlation in space and time*. Excursion guidebook of the Interim Colloquium R.C.M.N.S., 4-9 November 1997. Università di Catania, Istituto di Geologia e Geofisica, Catania, Italy, pp. 50-55.
- Shackleton, N.J., Hall, M.A., Pate, D., 1995. Pliocene stable isotope stratigraphy of Site 846. *Proceedings of the Ocean Drilling Program, Scientific Results* 138, 337-355. doi:10.2973/odp.proc.sr.138.117.1995.
- Sierro, F.J., Hilgen, F.J., Krijgsman, W., Flores, J.A., 2001. The Abad composite (SE Spain): A Mediterranean and global reference section for the Messinian. *Palaeogeography, Palaeoclimatology, Palaeoecology* 168, 141-169. doi:10.1016/S0031-0182(00)00253-4.
- Snel, E., Mărunțeanu, M., Măcalet, R., Meulenkamp, J.E., Van Vugt, N., 2006a. Late Miocene to Early Pliocene chronostratigraphic framework for the Dacic Basin, Romania. *Palaeogeography, Palaeoclimatology, Palaeoecology* 238, 107-124. doi:10.1016/j.palaeo.2006.03.021.
- Snel, E., Mărunțeanu, M., Meulenkamp, J.E., 2006b. Calcareous nannofossil biostratigraphy and magnetostratigraphy of the Upper Miocene and Lower Pliocene of the Northern Aegean (Orphanic Gulf-Strimon Basin areas), Greece. *Palaeogeography, Palaeoclimatology, Palaeoecology* 238, 125-150. doi:10.1016/j.palaeo.2006.03.022.
- Steenbrink, J., Hilgen, F.J., Krijgsman, W., Wijbrans, J.R., Meulenkamp, J.E., 2006. Late Miocene to Early Pliocene depositional history of the intramontane Florina-Ptolemais-Servia Basin, NW Greece: Interplay between orbital forcing and tectonics. *Palaeogeography, Palaeoclimatology, Palaeoecology* 238, 151-178. doi:10.1016/j.palaeo.2006.03.023.
- Stoica, M., Lazăr, I., Vasilev, I., Krijgsman, W., 2007. Mollusc assemblages of the Pontian and Dacian deposits from the Topolog-Argeș area (southern Carpathian foredeep-Romania). *Geobios* 40, 391-405. doi:10.1016/j.geobios.2006.11.004.
- Vai, G.B., 1997. Cyclostratigraphic estimate of the Messinian Stage duration. In: Montanari, A., Odin, G.S., Coccioni, R. (Eds.), *Miocene stratigraphy; an integrated approach*, *Developments in Palaeontology and Stratigraphy*, 15. Elsevier, Amsterdam, pp. 463-476. doi:10.1016/S0920-5446(06)80035-X.

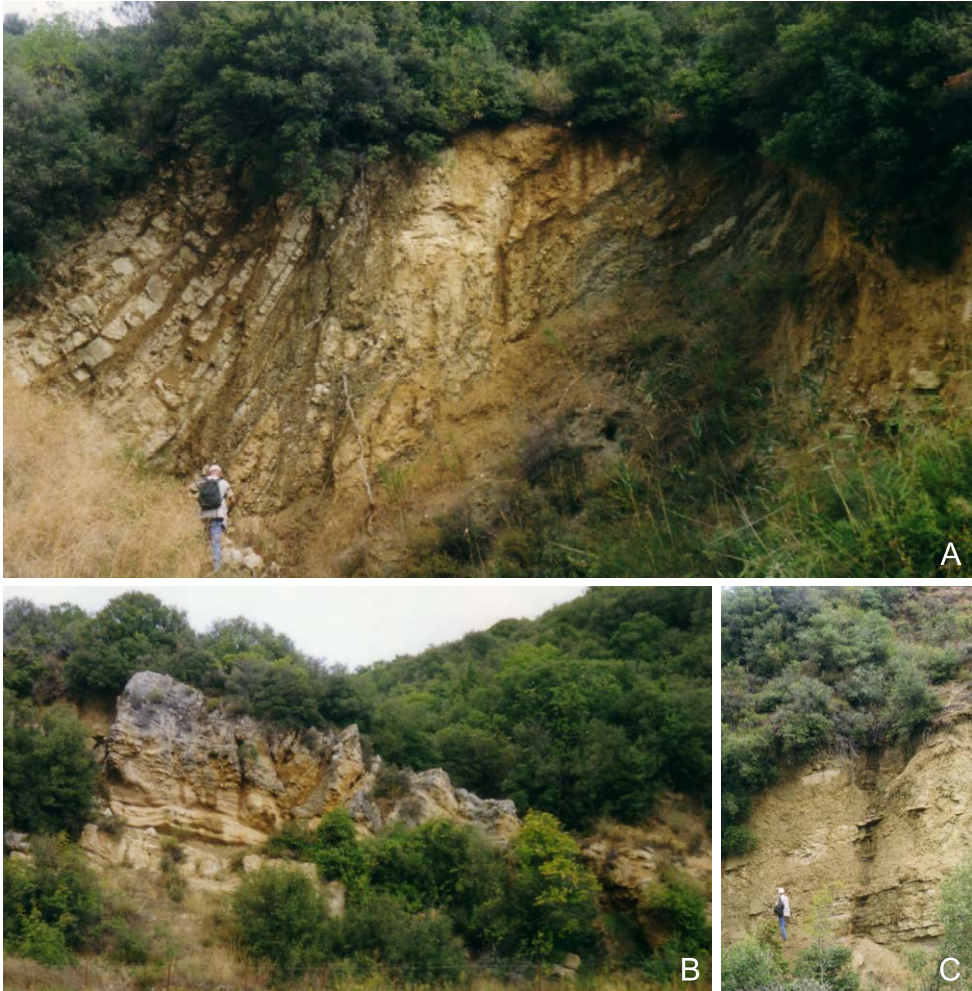
- Van Assen, E., Kuiper, K.F., Barhoun, N., Krijgsman, W., Sierro, F.J., 2006. Messinian astrochronology of the Melilla Basin: Stepwise restriction of the Mediterranean-Atlantic connection through Morocco. *Palaeogeography, Palaeoclimatology, Palaeoecology* 238, 15-31. doi:10.1016/j.palaeo.2006.03.014.
- Van Couvering, J.A., Castradori, D., Cita, M.B., Hilgen, F.J., Rio, D., 2000. The base of the Zanclean Stage and of the Pliocene Series. *Episodes* 23 (3), 179-187.
- Van der Laan, E., Gaboardi, S., Hilgen, F.J., Lourens, L.J., 2005. Regional climate and glacial control on high-resolution oxygen isotope records from Ain el Beida (latest Miocene, northwest Morocco): A cyclostratigraphic analysis in the depth and time domain. *Paleoceanography* 20, PA1001, doi:10.1029/2003PA000995.
- Van der Laan, E., Snel, E., De Kaenel, E., Hilgen, F.J., Krijgsman, W., 2006. No major deglaciation across the Miocene-Pliocene boundary: integrated stratigraphy and astronomical tuning of the Loulja sections (Bou Regreg area, NW Morocco). *Paleoceanography* 21, PA3011, doi:10.1029/2005PA001193.
- Van der Laan, E., Hilgen, F.J., Lourens, L.J., De Kaenel, E., Gaboardi, S., Iaccarino, S.M., in preparation. Astronomical forcing of Northwest African climate during the Messinian (6.5-5.5 Ma).
- Van Hinsbergen, D.J.J., Snel, E., Garstman, S.A., Mărunțeanu, M., Langereis, C.G., Wortel, M.J.R., Meulenkaamp, J.E., 2004. Vertical motions in the Aegean volcanic arc: evidence for rapid subsidence preceding volcanic activity on Milos and Aegina. *Marine Geology* 209, 329-345. doi:10.1016/j.margeo.2004.06.006.
- Van Hinsbergen, D.J.J., Van der Meer, D.G., Zachariasse, W.J., Meulenkaamp, J.E., 2006. Deformation of western Greece during Neogene clockwise rotation and collision with Apulia. *International Journal of Earth Sciences* 95 (3), 463-490. doi:10.1007/s00531-005-0047-5.
- Vasiliev, I., Krijgsman, W., Langereis, C.G., Panaiotu, C.E., Mațenco, L., Bertotti, G., 2004. Towards an astrochronological framework for the eastern Paratethys Mio-Pliocene sedimentary sequences of the Focșani basin (Romania). *Earth and Planetary Science Letters* 227, 231-247. doi:10.1016/j.epsl.2004.09.012.
- Vasiliev, I., Krijgsman, W., Stoica, M., Langereis, C.G., 2005. Mio-Pliocene magnetostratigraphy in the southern Carpathian foredeep and Mediterranean-Paratethys correlations. *Terra Nova* 17, 376-384. doi:10.1111/j.1365-3121.2005.00624.x.
- Wade, B.S., Bown, P.R., 2006. Calcareous nannofossils in extreme environments: The Messinian Salinity Crisis, Polemi Basin, Cyprus. *Palaeogeography, Palaeoclimatology, Palaeoecology* 233, 271-286. doi:10.1016/j.palaeo.2005.10.007.
- Williams, R.W., 1998. Dinium-Alpha; a chronostratigraphical range, morphology and photomicrography database builder for dinoflagellate cyst taxa. *Review of Palaeobotany and Palynology* 103 (1-2), 45-57. doi:10.1016/S0034-6667(98)00025-6.
- Zachariasse, W.J., Van Hinsbergen, D.J.J., Fortuin, A.R., 2008. Mass wasting and uplift on Crete and Karpathos during the early Pliocene related to initiation of south Aegean left-lateral, strike-slip tectonics. *Geological Society of America Bulletin* 120 (7/8), 976-993. doi:10.1130/B26175.1.
- Zachos, J., Pagani, M., Sloan, L., Thomas, E., Billups, K., 2001. Trends, rhythms, and aberrations in global climate 65 Ma to present. *Science* 292, 686-693. doi:10.1126/science.1059412.



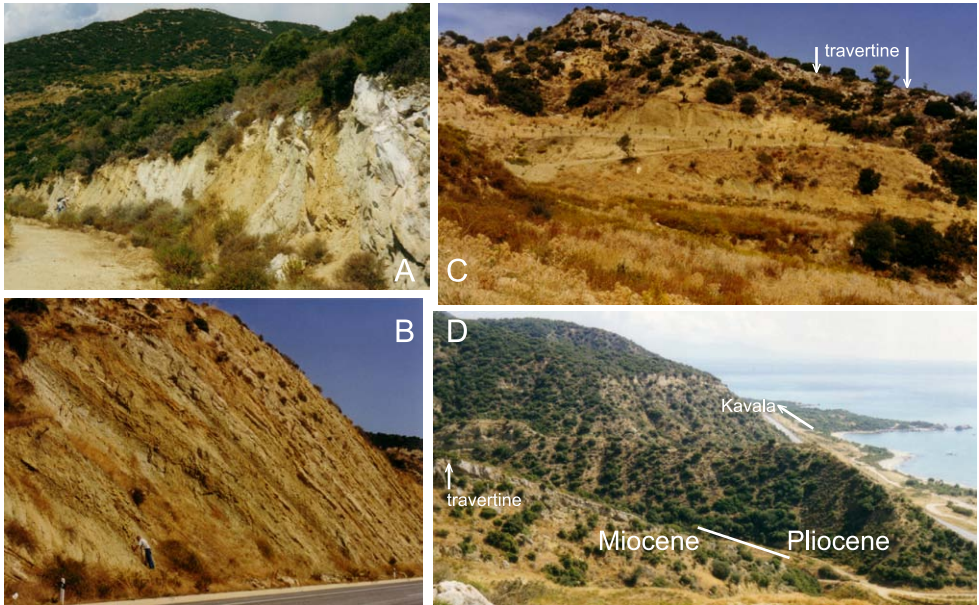
*Photo 6.1.* Gessoso-Solfifera Formation (Lower Evaporites) of the Vena del Gesso Basin at the Monte del Casino in the Northern Apennines east of Tossignano, near Imola (Romagna, Italy).



*Photo 6.2.* Miocene-Pliocene boundary interval at the western edge of the village of Eraclea Minoa (Sicily, Italy).



*Photo 6.3.* a) Middle part of subsection I of “Rema Marmara” (Orphanic Gulf area, Greece: chapter 3). Sheared shallow marine marl, sand and carbonate beds. b) Travertine and sandstone at the base of subsection II. c) Sandy top part of subsection II.



*Photo 6.4.* a, b) Lower part of section Kavala Road West along the coastal road between Thessaloniki and Kavala (Orphanic Gulf area, Greece: chapter 3). c) Dip-slope on top of a conglomerate-sandstone-travertine bed that is suggested to represent the desiccation phase of the MSC. d) Miocene-Pliocene boundary interval in the upper part of the section.



*Photo 6.5.* Section Myrini (Strimon Basin, Greece: chapter 3) left of the bridge. At the hilltop, shallow marine sands and gravels cover laminated diatomaceous brackish water clays and silts of the Choumnikon Formation.



Photo 6.6. a) Upper part of section Bădislava (Dacic Basin, Romania: chapter 2). b) Blue clays in the lower part.



Photo 6.7. Portaeferrian sandy clays in the upper part of section Valea Vacii (Dacic Basin, Romania: chapter 2).



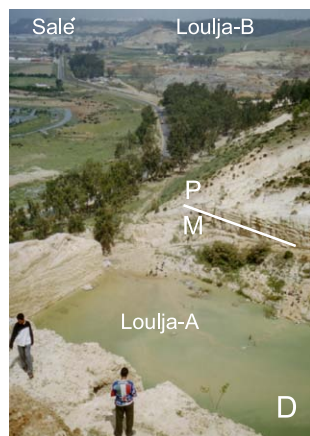
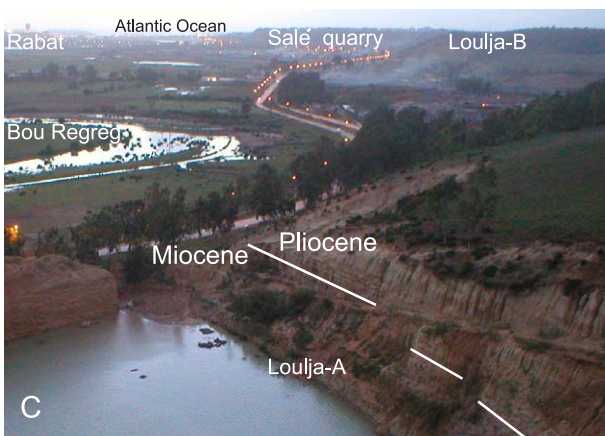
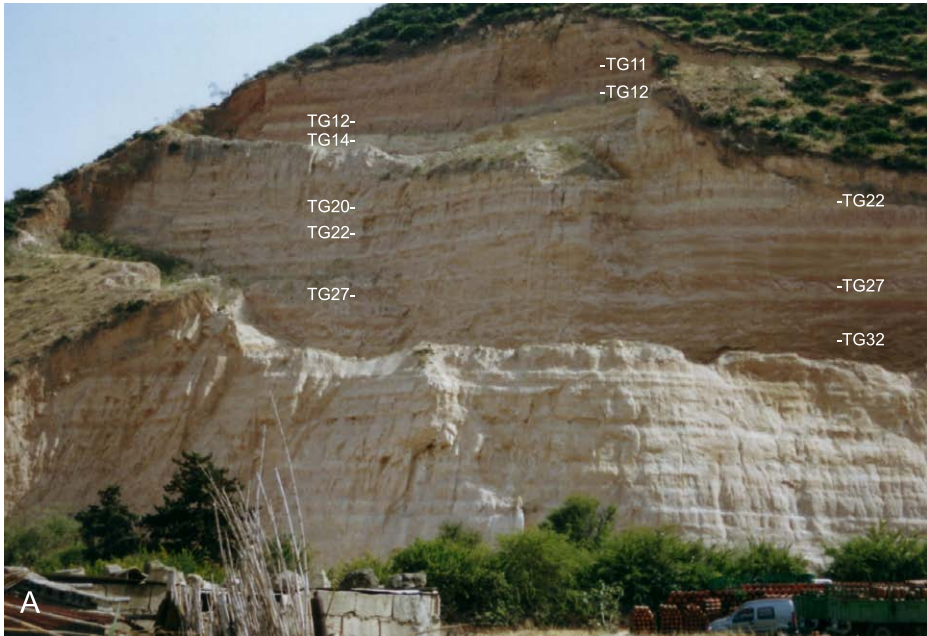


Photo 6.8. a) Section Ain el Beida (Bou Regreg area, Morocco: chapter 5). TG (inter)glacial stages as in Figure 6.4. b) The Bou Regreg valley, seen towards the southeast. c, d) The lower Bou Regreg valley, towards the Atlantic.



Photo 6.9. a) Miocene-Pliocene boundary interval in partial section I of Loulja-A (Bou Regreg area, Morocco: chapter 5). Interglacial TG stages as in Figure 6.4. b) Loulja-A, partial section II. c-g) Loulja-A, partial section III.

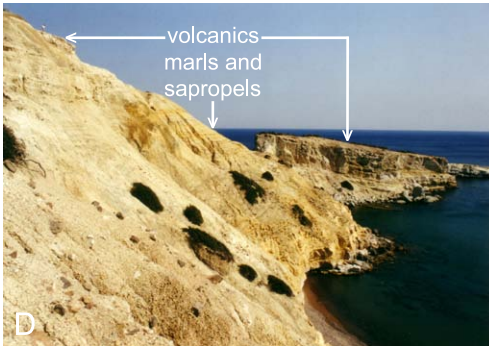


*Photo 6.10.* a-d) Section Souvala (Aegina island, Greece: chapter 4). Messinian lacustrine and brackish water marls, marly limestones and sands. e) Former section Aghios Thomas. Olive terraces cover a lower Pliocene marl-diatomite sequence. The andesite breccia on top of the hill was dated at 3.87 Ma (Benda et al., 1979).

*Photo 6.11.* (see page 180) a) View to the west from Cape Kipos (Milos island, Greece: chapter 4). Outcrops of lower Pliocene marine sediments along the south coast of Milos. b) Tilted blocks of upper Miocene continental to shallow marine strata at the east side of Cape Kipos, seen from Provatas beach. c) Detail of the west side of Cape Kipos. d-g) Cape Akrotiraki. Cyclic lower Pliocene marine marls and sapropels cover intercalations of (upper Miocene) lacustrine limestones, shallow marine hardgrounds, slumped marls, sandstones, and limestones (g).

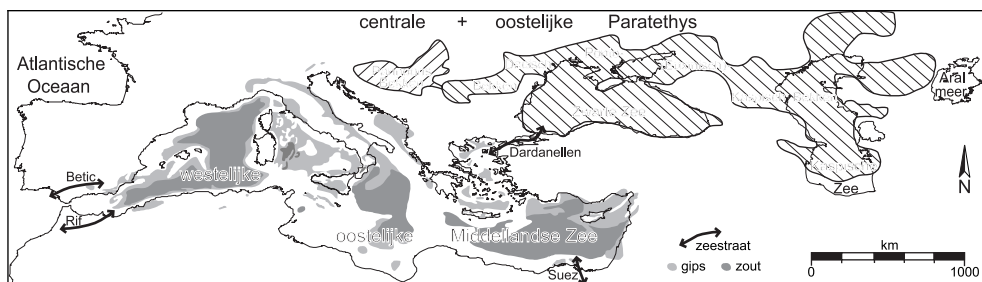


*Photo 6.12.* Subsection II near the village of Akropotamos (Orphanic Gulf area, Greece: chapter 3).



# Samenvatting

Tijdens het Messinien (7,246 tot 5,332 miljoen jaar geleden), aan het einde van het Miocene tijdvak, onderging het gebied dat wordt ingenomen door de huidige Middellandse Zee (zie kaart) ingrijpende milieuveranderingen. Gedurende deze relatief korte periode werden zeeverbindingen met de Atlantische Oceaan stapsgewijs vernauwd en vervolgens helemaal afgesloten, werden dikke pakketten evaporieten afgezet (in totaal ongeveer 1 miljoen kubieke kilometer) en, nadat het waterniveau enkele kilometers was gezakt, werd het Mediterrane Bekken weer gedeeltelijk opgevuld met niet-marien water. Een snelle instroom van zeewater door de Straat van Gibraltar aan het begin van het Pliocen herstelde het mariene milieu en leidde uiteindelijk tot de huidige land-zee verdeling. Aanwijzingen voor deze reeks gebeurtenissen werden geleverd door waarnemingen aan ontsluitingen op land, waarin – ingebed tussen oudere en jongere sedimenten met de overblijfselen van micro-organismen die wijzen op een diep marien milieu – opeenvolgende evaporietlagen van kalk, gips en zout en daar bovenop afzettingen met brakwater fossielen te zien waren. Het begrip “saliniteitscrisis van het Messinien” (hierna afgekort als MSC) werd in 1960 ingevoerd om voornoemde veranderingen aan te duiden. Het idee van een afgesloten en opgedroogde Middellandse Zee, enigszins vergelijkbaar met moderne zoutmeren (zoals de Salinas Grandes in Argentinië: zie foto), kreeg toenemende aanhang na de vondst van enorme gips- en zoutafzettingen in de bodem van de Middellandse Zee (zie kaart) tijdens een campagne van het Deep Sea Drilling Project in 1970. Talloze en dikwijls uiteenlopende modellen poogden vervolgens de oorzaak hiervan te verklaren. De evaporietlagen uit het Messinien zijn onder te verdelen in een onderste en een bovenste eenheid, waarvan de precieze ouderdommen en het afzettingsmilieu tot op de dag van vandaag betwist worden. De onderste evaporiet eenheid werd afgezet ten tijde van de eerste, mariene fase van de MSC (5,96 tot 5,59 miljoen jaar geleden), terwijl de bovenste evaporiet eenheid beschouwd kan worden als vertegenwoordiger van de continentale, ondiep water omstandigheden die overheersten tijdens en na de periode van erosie ten gevolge van het droogvallen van de Middellandse Zee gedurende de complete afsluiting van de verbinding met de Atlantische Oceaan. Dit jongste interval (ongeveer 5,50 tot 5,33 miljoen jaar geleden) wordt tevens aangeduid met de term “Lago Mare”, daar waar het gekenmerkt is door het voorkomen van zoet- en brakwater fauna in niet-mariene lagen op en tussen de gipslagen van de bovenste evaporieten. De afzettingsomstandigheden beneden de zeespiegel vertoonden waarschijnlijk enige gelijkenis met het brakwatermilieu van de huidige, door neerslag en rivieren gevoede Kaspische Zee. Dit afgesloten bekken is een van de restanten van de uitgestrekte binnenzee, de zogenaamde





Paratethys (zie kaart), die zich gedurende de MSC ten noordoosten van de Middellandse Zee bevond. De Paratethys vormde de andere geïsoleerde watermassa die, samen met een voorloper van de Middellandse Zee, ooit deel uitmaakte van de Tethys Oceaan tussen Eurazië en de Afrikaanse en Indische continenten.

Dit proefschrift geeft de resultaten weer van het promotieonderzoek naar 'Mediterrane doorgangen', uitgevoerd in het kader van het multidisciplinaire onderzoeksprogramma 'Mediterranean Neogene depositional environments: modelling, validation and perspectives', een samenwerking van het Geodynamisch Onderzoeksinstituut (GOI) en het Instituut voor Paleomilieu en Paleoklimaat Utrecht (IPPU) van de Faculteit Aardwetenschappen van de Universiteit Utrecht en het Department of Geosciences van de Pennsylvania State University. Het hoofdonderwerp van dit programma was om de oorsprong en de ruimte-/tijdsverdeling te doorgronden van Mioocene opeenvolgingen van zwarte kleisteen (sapropel) en evaporiet in en rondom het Middellandse Zeegebied, in termen van de gezamenlijke effecten van geodynamische en milieu-gerelateerde (klimatologische, oceanografische) processen in het botsingsgebied van de Afrikaanse en Euraziatische platen. Oorspronkelijk waren drie benaderingswijzen voorzien, welke zich vertaalden in een tijd-stratigrafische en tektonostratigrafische, een numerieke modellering en een milieu-onderzoekscomponent. Het doel van de laatste component had betrekking op gedetailleerde analyses van het effect van tektoniek en door klimaat (zeespiegel) gestuurde gebeurtenissen op bekkenconfiguratie en sedimentatie. Het onderhavige promotieonderzoek, bijdragend aan de milieucomponent, was gericht op de respons van paleoceanografie en milieu van het circum-Mediterrane gebied op verslechterende Atlantisch-Mediterrane en intra-Mediterrane verbindingen en op de herhaaldelijke opening van (mariene) doorgangen tussen de Middellandse

Zee en de Paratethys voorafgaand aan, gedurende en na de MSC. Het onderzoek concentreerde zich vooral op geïntegreerde stratigrafische analyses van boven Miocene en onder Pliocene opeenvolgingen in (a) het Dacische Bekken van de oostelijke Paratethys (in Roemenië), (b) gebieden langs de Orfanische Golf en in het Strimon Bekken in het noordelijke Egeïsche deel en Aegina en Milos in het zuidelijke Egeïsche deel van de Middellandse Zee (in Griekenland) en (c) het aan de Atlantische kant van de Middellandse Zee liggende Bou Regreg gebied (in Marokko). Daarnaast werden cyclostratigrafische en biostratigrafische analyses verricht aan daadwerkelijke MSC eenheden binnen Spaanse, Italiaanse en Griekse randbekkens van de Middellandse Zee.

Om de tijdsbepaling van Mediterrane-Paratethys verbindingen in de periode van de MSC te kunnen duiden, is een gedetailleerde correlatie van laat Neogene Paratethys etages met die van het Middellandse Zeegebied onontbeerlijk. Dit kan verwezenlijkt worden door middel van het opstellen van chronostratigrafische kaders aan weerszijden van de noordoostelijke verbinding. Voorafgaande en vergelijkbare studies in de oostelijke Paratethys hebben in dit verband de mogelijkheden aangetoond van cyclostratigrafisch en magnetostratigrafisch onderzoek aan het Mioceen en Pliocene. **Hoofdstuk 2** geeft de magnetostratigrafische en biostratigrafische resultaten weer van bemonstering van boven Miocene en onder Pliocene sedimenten langs de noordrand van het Dacische Bekken (Roemenië) in de jaren 1996 tot en met 1999. Voor de regionale etages van dit deel van de oostelijke Paratethys, die bepaald worden aan de hand van de verschijning en ontwikkeling van zoet- en brakwater mollusken, zijn ouderdommen verkregen tussen 6,5 en 4,0 miljoen jaar geleden. De ouderdom van de Meotien-Pontien grens kan worden gesteld op ~6,15 miljoen jaar en die van de Pontien-Dacien grens op ~5,3 miljoen jaar, zodat de etage van het Pontien samenvalt met de bovenste helft van het Messinien en daarmee de MSC omvat. De Odessien-Portaferrien en de Portaferrien-Bosphorien subetage grenzen zijn geschat op ~6,0 en ~5,6 miljoen jaar, respectievelijk. De subetage grens tussen het onder Dacien (Getien) en het boven Dacien (Parscovien) kan worden gedateerd op ~4,55 miljoen jaar, terwijl de Dacien-Romanien etage grens een ouderdom krijgt van ~4,25 miljoen jaar. Een alternatieve correlatie van de normale polariteitsintervallen in de Lupoia sectie naar oudere subchrons in de astronomische polariteit tijdschaal levert respectievelijke ouderdommen van ~4,83 en ~4,58 miljoen jaar voor deze laatste twee grenzen. Het voorkomen van fossielen van kalkig nannoplankton in het midden en boven Pontien en in het onder Dacien, met geschatte leeftijden van 5,9 tot 5 miljoen jaar, is een aanwijzing voor kortstondige influxen van marien (Atlantisch) water via de Middellandse Zee in de Paratethys, wat betekent dat de periode van afsluiting van deze bekkens tijdens de MSC beperkt zou zijn gebleven tot het interval van de bovenste evaporieten en de Lago Mare. N.B.: aanvullende gegevens en recente inzichten met betrekking tot dit onderwerp en de chronostratigrafie van het Dacisch Bekken hebben tot andere conclusies geleid dan hier en in het volgende hoofdstuk vermeld; zie hiervoor hoofdstuk 6.

In **hoofdstuk 3** worden de resultaten besproken van drie veldwerkcampagnes langs de Orfanische Golf en in het Strimon Bekken in het noordelijk Egeïsch gebied (Griekenland) in 1998-2000. Dit onderzoeksgebied bevindt zich aan de voormalige rand van de oostelijke Paratethys en heeft mogelijk deel uitgemaakt van de noordoostelijke verbinding tussen de Middellandse en Zwarte Zee. Biostratigrafische, lithostratigrafische en paleomagnetische gegevens maken correlaties met het Mediterrane Neogeen mogelijk en suggereren dat de afzettingen een tijdspanne beslaan tussen 7,5 en 5 miljoen jaar geleden. De overgang van de ondiep mariene Dafni Formatie naar de lacustriene-brakwater Choumnikon Formatie in het Strimon Bekken wordt geschat op 6,3 miljoen jaar, wat vergelijkbaar is met de ouderdom van de Meotien-Pontien grens in het Dacische Bekken. In het aangrenzende gebied van de Orfanische Golf vormen ondiep mariene klastische

afzettingen en gipslagen, gevolgd door een fluvio-lacustriene brak-/zoetwater eenheid, het lokale equivalent van de Choumnikon Formatie. De evaporieten worden gecorreleerd met de onderste evaporiet eenheid van het Middellandse Zeegebied, 5,96-5,59 miljoen jaar geleden, terwijl een wijdverbreide markeringslaag van travertijn in de jongere, niet-mariene eenheid wordt gezien als een weerspiegeling van het droogvallen van de Middellandse Zee tussen 5,59 en 5,5 miljoen jaar geleden. De Mioceen-Pliocene grens, in het Strimon Bekken vertegenwoordigd door een kortstondige ondiep mariene onderbreking van de fluvio-lacustriene condities, wordt in het gebied langs de Orfanische Golf gemarkeerd door een overgang naar open mariene omstandigheden in een dan al relatief diep bekken. Fossielen van kalkig nannoplankton zijn her en der aanwezig in boven Mioceen strata, voornamelijk in de ondiep mariene intervallen. Echter, hun voorkomen langs de Orfanische Golf voorafgaand aan de eerste verschijning van foraminiferen aan de veronderstelde basis van het Pliocene behoeft nadere verklaring en kan duiden op omwerking van oudere afzettingen van Messinien ouderdom of op de sporadische instroom van oceaan water aan het einde van de MSC.

**Hoofdstuk 4**, reeds verschenen in het proefschrift van Douwe van Hinsbergen, handelt over Mioceen en Pliocene continentale en mariene opeenvolgingen (6,0 tot 3,5 miljoen jaar oud) en daarop liggende vulkanische sedimenten op de zuid-Egeïsche eilanden van Milos en Aegina in Griekenland. Deze eilanden werden gevormd door Plio-Pleistoceen vulkanisme dat samenviel met laat-orogeen extensie in het Egeïsch gebied. Reconstructie van de vroeg Pliocene paleobathymetrische geschiedenis maakt gebruik van de verhouding tussen planktonische en bentonische foraminiferen en van een ouderdomsmodel dat gebaseerd is op geïntegreerde biostratigrafie, magnetostratigrafie en cyclostratigrafie. Het blijkt dat een snelle regionale bodemdaling tot wel 1 kilometer heeft plaats gevonden, waarschijnlijk samenhangend met de grootschalige extensie in het zuidelijk Egeïsch gebied 1 tot 1,5 miljoen jaar voorafgaand aan het begin van vulkanisme. De bodemdaling veroorzaakte een relatieve zeespiegelstijging vanaf 5 miljoen jaar geleden, dus ~300.000 jaar na het einde van de MSC. De afwisselend fluviaatiele, brakke en ondiep mariene sedimenten uit het boven Mioceen en onderste Pliocene van Milos en Aegina vertegenwoordigen mogelijk het paleomilieu van een drempel gebied tussen de werkelijke Middellandse Zee en het aangrenzende deel van het Egeïsch gebied, dat tijdens de MSC wellicht te ondiep was om de opeenvolgende gebeurtenissen van droogvallen en volstromen vast te kunnen leggen. Alhoewel extensie van de Egeïsche lithosfeer niet direct het smelten van de onderliggende mantel veroorzaakte, bepaalde deze waarschijnlijk wel het moment waarop het vulkanisme begon en maakte het omhooggaan van magma mogelijk door het vormen van uitzettingsscheuren. De diepte van de onderschuivende plaat onder het Egeïsch gebied was waarschijnlijk bepalend voor het smelten en daarmee voor de ligging van de vulkanische centra.

Onderzoek uitgevoerd in het Melilla Bekken, in het westen van het Middellandse Zeegebied, toonde de stapsgewijze vernauwing van de Rif-straat aan, die de voorbode betekende voor de MSC. Deze poort vormde samen met de Betische straat de westelijke verbinding met de Atlantische Oceaan voor de uiteindelijke opening van de moderne straat van Gibraltar op de Mioceen-Pliocene grens. Om een correlatie van het eigenlijke MSC interval met het geologisch archief van de open oceaan te kunnen maken, moesten de boven Mioceen referentie secties van Oued Akrech en Ain el Beida in het Bou Regreg gebied aan de Atlantische kant van de Rif-straat naar boven toe uitgebreid worden, over het Mio-Pliocene grensinterval heen. **Hoofdstuk 5**, tevens opgenomen in het proefschrift van Erwin van der Laan, presenteert de twee veelbelovende secties van Loulja, die geselecteerd werden voor een geïntegreerd, stratigrafisch onderzoek met een hoge resolutie. De combinatie van de door precessie gestuurde cycliciteit van sectie Loulja-A



(5,59 tot 5,12 miljoen jaar oud), die ondubbelzinnige astronomische datering mogelijk maakt, en een uitstekende benthonische stabiele isotopen record maken een gedetailleerde vergelijking van de glaciële geschiedenis met paleomilieu gebeurtenissen in de Middellandse Zee mogelijk. Als gevolg hiervan kan de sectie als een alternatief dienen voor de stratotype sectie van de Mioceen-Pliocene grens in Eraclea Minoa op Sicilië. Het blijkt dat deze grens samenvalt met een kleine, aan precessie gerelateerde verschuiving naar lichtere  $\delta^{18}\text{O}$  waarden tussen de isotopen etages TG7 en TG5. Het volstromen van de Middellandse Zee aan het einde van de MSC heeft daarom niets te maken met een grootschalige glacio-eustatische zeespiegelstijging, maar waarschijnlijker met tektoniek of stroomopwaartse fluviaatiele erosie. Een eerdere, grote deglaciatie fase tussen etages TG12 en TG11 komt overeen met het begin van afzetting van de bovenste evaporiet eenheid, na het droogvallen van de Middellandse Zee tijdens het hoogtepunt van de MSC.

Het samenvattende **hoofdstuk 6**, tenslotte, behandelt opeenvolgingen van de Mediterrane onderste en bovenste evaporiet eenheid (Lago Mare) in de Sorbas en Nijar bekkens van Spanje, in de Vena del Gesso en Caltanissetta bekkens van Italië en op Kreta en de Ionische eilanden in Griekenland. Regionale, door precessie gestuurde klimaatsschommelingen bepaalden de cycliciteit van de evaporieten. Analyses van fossielen van kalkig nannoplankton en dinoflagellaat cysten met een organische wand in cyclostratigrafisch gedateerde monsters uit deze en andere ontsluitingen langs de Orfanische Golf en in het Strimon en Dacische bekken tonen aan dat een continue of herhaaldelijke instroom plaats vond van Atlantisch water (in ieder geval) in het Middellandse Zeegebied tijdens de periode van afzetting van de onderste evaporieten (5,96 tot 5,59 miljoen jaar geleden). Aan de andere kant, en in overeenstemming met de interpretatie van magnetische susceptibiliteit gegevens uit het Bou Regreg gebied (Atlantische kust, Marokko), waren de Middellandse Zee en de daarin uitmondende oostelijke Paratethys geïsoleerd gedurende de intra-Messinien periode van droogvallen en het daaropvolgende bovenste evaporiet interval (5,59 tot 5,33 miljoen jaar geleden). Deze bevindingen komen overeen met conclusies van strontium isotopenonderzoek en andere aanwijzingen in de literatuur over mariene microfossielen. Om de oorzaken van de opeenvolgende MSC gebeurtenissen samen te vatten: de aanzet tot de MSC (5,96 miljoen jaar geleden) had geen directe glacio-eustatische oorsprong, maar was het resultaat van het klimatologische effect van de eccentriciteitscyclus gesuperponeerd op de regionale tektonische tendens van vernauwing van de westelijke toegang tot de Middellandse Zee; de in het oog springende glaciële etages TG14 en TG12 bepaalden in hoge mate de fase van isolatie en droogvallen (5,59 tot 5,55 miljoen jaar geleden), waarna het Mediterrane bekken weer gedeeltelijk volliep tijdens de deglaciatie die met etage TG11 samenhangt; het uiteindelijke volledig volstromen aan het begin van het Pliocene (5,33 miljoen jaar geleden), dat het einde betekende van de MSC en tot de terugkeer van open mariene omstandigheden leidde, is waarschijnlijk eerder gerelateerd aan geodynamische en/of erosieprocessen dan aan glacio-eustatie.

# Acknowledgements

---

Highly enjoyable and carefree field-holidays, assisting Cor, Nicole, and Joris (the ‘night mayor’ of Ptolemaida) in exotic Greek coal mines and Charon, Nicole and Davide on the island of Rhodes, and paleobotany research under the cheerful supervision of Wolfram and Rike persuaded me to apply for a PhD-position. At the time of the IT-hype, 1998, this was the easy part. My initial promotors Cor and Johan, successive promotor Bert, supervisors Wout, Tanja, Jan-Willem, Mariana (my scientific mother), Henk B, Ankie, Natasja, and of course co-promotor Frits, generations of roommates – Willy at the Fort, and Tom vH & Wil, Douwe & Rink, and paranympths Kees (the troubleshooter) & Hemmo at ‘the other side’ –, and the indispensable support from Hans (in Serres), Piet-Jan, Tom M, Henk M, Geert, Gerrit, Marjolein, Ronald, Roy, Arnold, Helen, Luc, Ton, Jan, Giovanni, Frans (Sicily), Stefan, Rob, Koenraad, Anne, and Eric guided me through the next decade.

Abroad, preferably at diner tables, or elsewhere in the field (euphemism for roadside or rubbish dump) and in various (ministry, police, university) offices, I have had the privilege to meet and enjoy the pleasant company and selfless help – besides of those already mentioned – of Rachel, Gheorghe, Maria, Sorin, Radu, Rodica, Nadia, Mohamed D, Mohamed H, Erwin (fellow Loulja veteran), Katarzyna, Helmut, Frank, Esther, Klaudia, Constantin (the best ambassador from Greece) and Danae, George, Frosso, Maria, Yiannis, Silvia, Francisco (both kind members of the reading committee, together with Poppe and again Cor), Jean-Pierre and Speranța-Maria, Jelle, ...

Thanks also to the many people that created a relaxed atmosphere on the third floor of the Earth Sciences building (including lunch-manager Wilma, Hayfaa, ...) and at the Fort Hoofddijk (Dave, Geert, Mark, ...). For doing the same in the real world, like at home, I am grateful to Christine, friends, and family and appreciate their encouragement and patience.

# Curriculum Vitae

---

Erik Snel werd geboren te Antwerpen op 5 april 1974. Na het volgen van onderwijs aan de Openbare Lagere School – later OBS – Buten de Poorte in Goedereede en de Gemeentelijke Scholengemeenschap Helinium – voorheen Rijksscholengemeenschap – in Hellevoetsluis behaalde hij het Atheneum diploma op 12 juni 1992. De in datzelfde jaar begonnen studie Geologie aan de (toen) Rijksuniversiteit te Utrecht werd afgesloten met het doctoraal examen in de hoofdrichting Sedimentaire Geologie/Geochemie op 27 april 1998. Van 1 augustus 1998 tot 1 mei 2003 en van 1 april tot 1 augustus 2004 was hij aangesteld als assistent in opleiding (AIO) bij de projectgroep Stratigrafie en Paleontologie van de faculteit Aardwetenschappen, respectievelijk Geowetenschappen. Op 1 juli 2003 trad hij in dienst als expeditiemedewerker bij TPG – nu TNT – Post in Zeist.



Photos by N. van Vugt and E. van der Laan

